UCLA
UCLA Electronic Theses and Dissertations

Title
Seismic Performance and Design of Steel Plate Shear Walls with Low Yield Point Steel Infill Plates

Permalink
https://escholarship.org/uc/item/697856gp

Author
Zirakian, Tadeh

Publication Date
2013

Peer reviewed|Thesis/dissertation

eScholarship.org Powered by the California Digital Library
University of California

UNIVERSITY OF CALIFORNIA

Los Angeles

Seismic Performance and Design of Steel Plate Shear Walls with Low Yield Point Steel Infill Plates

A dissertation submitted in partial satisfaction of the requirements for the degree Doctor of Philosophy in Civil Engineering

by

Tadeh Zirakian

2013

© Copyright by

Tadeh Zirakian

2013

ABSTRACT OF THE DISSERTATION

Seismic Performance and Design of

Steel Plate Shear Walls

with Low Yield Point Steel Infill Plates

by

Tadeh Zirakian

Doctor of Philosophy in Civil Engineering

University of California, Los Angeles, 2013

Professor Jian Zhang, Chair

Steel plate shear walls (SPSWs) have been frequently used as the primary or part of the primary lateral force-resisting system in design of low-, medium-, and high-rise buildings. Their application has been based on two different design philosophies as well as detailing strategies. Stiffened and/or stocky-web SPSWs with improved buckling stability and high seismic performance have been mostly used in Japan, which is one of the pioneering countries in design and application of these systems. Unstiffened and slender-web SPSWs with relatively lower buckling and energy dissipation capacities, on the other hand, have been deemed as a rather economical alternative and accordingly widely used in the United States and Canada. Development and use of low yield point (LYP) steel with considerably low yield stress and high elongation capacity provides the possibility to combine merits of these two distinctive design strategies, and consequently result in rather cost-effective and high-performing SPSW systems.

Although some reported studies have demonstrated the advantages of LYP steel shear walls, various aspects of structural and seismic characteristics of these systems have not been investigated thoroughly. In particular, the linkage between structural specifications and seismic performance and pathway to performance-based design of these systems are largely undeveloped. Hence, systematic investigations are required to facilitate the seismic design and prevalent application of such promising lateral force-resisting and energy dissipating systems.

The main objectives of this research are to evaluate the structural behavior and seismic performance of unstiffened LYP steel shear wall systems in a rather comprehensive manner. To achieve these objectives, element-level investigations on steel plates, component-level investigations on SPSW panels, and system-level investigations on multi-story steel frame-shear wall structures are performed in a hierarchical and systematic manner.

Through detailed element- and component-level investigations, it is shown that employment of LYP steel infill plates in SPSW systems facilitates the design and effectively improves the buckling stability, serviceability, and energy absorption capacity of such lateral force-resisting systems. Some practical design tools and recommendations are also provided through analytical and numerical studies. In system-level investigations, the effectiveness of use of LYP steel material in design and retrofit construction is demonstrated through nonlinear time-history analysis as well as seismic response and performance assessment of multi-story structures subjected to earthquake ground motions representing various hazard levels. Ultimately, the fragility methodology is utilized by developing appropriate fragility functions for probabilistic seismic performance and vulnerability assessment of structures designed and retrofitted with conventional and LYP steel infill plates. The results of this study are indicative of relatively lower damage probability and superior seismic performance of LYP steel shear wall systems.

The dissertation of Tadeh Zirakian is approved.

Jiann-Wen Woody Ju

Ertugrul Taciroglu

Christopher S. Lynch

Jian Zhang, Committee Chair

University of California, Los Angeles

2013

To my loving parents

Grish & Mary

for their endless
love, support, and patience…

TABLE OF CONTENTS

ABSTRACT OF THE DISSERTATION ii
COMMITTEE APPROVAL iv
DEDICATION v
TABLE OF CONTENTS vi
LIST OF FIGURES ix
LIST OF TABLES xiii
ACKNOWLEDGMENTS xv
VITA xvi

1. INTRODUCTION 1
   1.1 General 1
   1.2 Applications 2
   1.3 Wall Types 4
   1.4 Advantages, Disadvantages and Limitations 7
   1.5 Scope and Objectives 9
   1.6 Organization 11

2. PAST RESEARCH AND RECENT DEVELOPMENTS 14
   2.1 General 14
   2.2 Development of Analytical Modeling Techniques of SPSW Systems 15
   2.3 Prior Analytical and Experimental Research on SPSWs 20
   2.4 Recent Developments 25
   2.5 Low Yield Point Steel 30

3. BEHAVIOR AND DESIGN OF SPSW SYSTEMS 33
   3.1 General 33
   3.2 Fundamental Mechanics of Unstiffened SPSWs 33
   3.3 NEHRP Recommended Provisions (FEMA 450) 39
   3.4 AISC 341 Seismic Provisions 41
   3.5 Performance-Based Design 44

4. STUDY OF BUCKLING, YIELDING, AND CYCLIC BEHAVIORS OF STEEL SHEAR PANELS 48
   4.1 Introduction 48
   4.2 Determination of Limiting Plate Thickness 49
   4.3 Finite Element Analysis and Discussion of Results 54
      4.3.1 Elastic Buckling Analysis and Convergence Studies 54
      4.3.2 Nonlinear Buckling Analysis 56
      4.3.3 Cyclic Analysis of Plates with Two and Four Restrained Edges 62
   4.4 Effects of Use of LYP Steel and Aspect Ratio on Limiting Plate Thickness 65
   4.5 Buckling of Plates and Application of Extrapolation Techniques 67
   4.6 Determination of Limiting Shear Panel Thickness in SPSW Systems 70

4.7 Concluding Remarks 77

5. STUDY OF MONOTONIC AND CYCLIC BEHAVIORS OF SPSWS WITH LYP STEEL INFILL PLATES 79
5.1 Introduction 79
5.2 Design and Properties of SPSW Models 80
5.3 Finite Element Modeling and Analysis 81
5.4 Advantages of Use of LYP Steel Infill Plates in SPSW Systems 83
5.5 Performance of SPSWs with Slender, Moderate, and Stocky LYP Steel Infill Plates 90
5.6 Modified Plate-Frame Interaction Model for SPSWs with Moderate and Stocky Infill Plates 95
5.7 Concluding Remarks 105

6. STUDY ON SEISMIC DESIGN AND STRUCTURAL PERFORMANCE OF SPSWS WITH LYP STEEL INFILL PLATES 107
6.1 Introduction 107
6.2 Design of SPSW Models 108
6.3 Finite Element Modeling and Verification 111
6.4 Strength, Stiffness, and Cyclic Performances of Code-Designed SPSW Models 113
6.5 Design Considerations and Structural Performance 118
6.5.1 Diagonal Tension Field and Angle of Inclination 118
6.5.2 Performance of Reduced Beam Section (RBS) Connections 120
6.5.3 Performance of Panel Zones 123
6.5.4 Lateral Bracing of Frame Members 126
6.6 Prediction of SPSW Behavior Using Modified PFI Method 128
6.7 Concluding Remarks 131

7. STUDY ON SEISMIC RETROFIT OF STRUCTURES USING SPSW SYSTEMS AND LYP STEEL MATERIAL 134
7.1 Introduction 134
7.2 Design and Properties of Structural Systems 135
7.3 Finite Element Modeling and Verification 141
7.4 Modal Analysis and Elastic Behavior 149
7.5 Nonlinear Time-History Analysis and Selection of Ground Motions 154
7.6 Nonlinear Time-History Analysis Results 157
7.6.1 Story and Interstory Drift Ratios 157
7.6.2 Story Acceleration 164
7.6.3 Base Shear 168
7.6.4 Base Moment 171
7.6.5 VBE Axial Loads at Column Bases 173
7.6.6 Web Plate Ductility Ratio and Energy Dissipation Mechanism 175
7.7 Concluding Remarks 181

8. PROBABILISTIC ASSESSMENT OF SEISMIC RETROFIT OF STRUCTURES USING FRAGILITY FUNCTION METHOD 184
8.1 Introduction 184

8.2 Fragility Function Methodology ……. 186
8.3 Specifications and Modeling of Structural Systems ……... 188
8.3.1 Selected Structural Systems ……..……..... 188
8.3.2 Finite Element Modeling and Analysis ……..... 189
8.3.3 Ground Motion Suite ……..……... 189
8.3.4 Seismic Response of Structural Models …… 191
8.4 Fragility Analysis of Structural Systems …….…… 194
8.4.1 Selection of Appropriate EDP-IM Data Pairs ……... 194
8.4.2 Determination of Lognormal Distribution Parameters …….. 200
8.4.3 Considered Damage and Repair States ……. 203
8.4.4 Fragility Curves of Structural Models ……..……. 205
8.5 Discussion of Results …….. 209
8.6 Concluding Remarks ……... 213

9. SUMMARY, CONCLUSIONS, AND FUTURE WORK ……. 216
9.1 Summary ……..……..... 216
9.2 Conclusions ……..……..... 218
9.3 Recommendations for Future Work …… 222

References ……...……...……..……... 225

LIST OF FIGURES

Fig. 1.1 A typical SPSW system …… 1
Fig. 1.2 SPSW configurations and applications in Japan (Sabelli and Bruneau, 2006) …… 3
Fig. 1.3 Application of SPSW systems in United States (Sabelli and Bruneau, 2006) ……. 4
Fig. 1.4 Typical SPSW systems (Sabelli and Bruneau, 2006) ……... 4
Fig. 1.5 SPSWs with composite shear panels (Astaneh-Asl, 2002) …….. 6
Fig. 1.6 SPSWs with steel slit walls (Hitaka and Matsui, 2003) ……... 6

Fig. 2.1 Hysteresis model proposed by Mimura and Akiyama (1977) …….. 15
Fig. 2.2 Multi-strip model proposed by Thorburn et al. (1983) ……. 16
Fig. 2.3 Equivalent brace model proposed by Thorburn et al. (1983) ……... 16
Fig. 2.4 Diagonal strip model proposed by Elgaaly et al. (1993) …….. 17
Fig. 2.5 Multi-angle strip model proposed by Rezai (1999) …….. 17
Fig. 2.6 Plate-frame interaction method proposed by Sabouri-Ghomi et al. (2005) …….. 18
Fig. 2.7 Modified strip model proposed by Shishkin et al. (2009) …… 19
Fig. 2.8 Examples of finite element models ……... 20
Fig. 2.9 Single-story SPSW specimens tested by Lubell et al. (2000) …….. 21
Fig. 2.10 Buckled LYP steel panels of SPSW specimens tested by Tsai and Lin (2005) …. 22
Fig. 2.11 Deformations of SPSW specimens at ultimate stage tested by Chen and Jhang (2006) ……. 23
Fig. 2.12 Buckling-yielding and deformations of SPSWs tested by Chen and Jhang (2011) 24
Fig. 2.13 Various SPSW configurations tested by Bruneau and his research associates ….. 26
Fig. 2.14 SPSW systems with beam-attached infill plates ……. 27
Fig. 2.15 Recommended SPSW fragility functions by Baldvins et al. (2012) …….. 29
Fig. 2.16 Stress-strain curves of the LYP steel (Yamaguchi et al., 1998) ……. 31

Fig. 3.1 Idealized steel shear wall behavior ……... 33
Fig. 3.2 Braced frame and stiffened plate girder analogies (Sabelli and Bruneau, 2006) …. 34
Fig. 3.3 Free-body diagrams of the web plate and boundary elements in SPSWs (Sabelli and Bruneau, 2006) …….. 36
Fig. 3.4 Details of stresses imposed on SPSW boundary frame members (Sabelli and Bruneau, 2006) ……. 38
Fig. 3.5 Performance limit states in Ghosh et al.'s (2009) proposed PBD method ……... 46
Fig. 3.6 Selected yield mechanisms in Bayat's (2010) proposed PBD method ……. 47

Fig. 4.1 Plates under different in-plane loading conditions ……... 50
Fig. 4.2 Plate under combined shear and compressive loads as per Chen et al. (2009) …… 51
Fig. 4.3 Plate support conditions …… 54
Fig. 4.4 Convergence study and validity of results …… 55
Fig. 4.5 Typical first buckling mode shapes …….. 56
Fig. 4.6 Load vs. out-of-plane displacement curves of plates …… 58
Fig. 4.7 Load vs. in-plane lateral displacement curves of plates ……... 59
Fig. 4.8 von Mises stress contour plots at ultimate strengths of various plates: external 61

face (left) and internal face (right) ……...
Fig. 4.9 Cyclic loading and hysteresis behaviors of plates with two and four clamped edges ……. 63
Fig. 4.10 Cumulative dissipated energy ……. 64
Fig. 4.11 Out-of-plane displacement contour plots of PL 3000×3000×14.0 at 8.00 mm in-plane lateral displacement …….. 65
Fig. 4.12 Effect of use of LYP steel on the required limiting plate thickness ……... 66
Fig. 4.13 Effect of aspect ratio on the required limiting plate thickness ……... 67
Fig. 4.14 Data points and application of the extrapolation techniques …….. 68
Fig. 4.15 Typical Southwell, Massey, and Modified Plots (Model P20) ……... 69
Fig. 4.16 Material properties of the steel used in SPSWs …….. 72
Fig. 4.17 SPSW finite element model validation by Lubell's (1997) test results …….. 72
Fig. 4.18 SPSW finite element model validation by Chen and Jhang's (2006) test results ... 73
Fig. 4.19 Finite element models and buckling mode shapes of SPSWs …… 73
Fig. 4.20 Simultaneous geometrical buckling and material yielding of SPSW models with exact limiting plate thicknesses …….. 76
Fig. 4.21 Geometrical buckling and material yielding of SPSW models with limiting plate thicknesses corresponding to clamped support condition …….. 77

Fig. 5.1 Finite element models ……... 81
Fig. 5.2 Material properties of the steel used in SPSWs …… 82
Fig. 5.3 Behavior of SPSW2 model with various infill plate thicknesses and steel types …. 85
Fig. 5.4 Structural strength and behavior ……... 87
Fig. 5.5 Stiffness performance ……... 87
Fig. 5.6 von Mises stress contour plots of SPSW2 model with various infill plate thicknesses and steel types at 0.01 and 0.02 drift ratios ……... 88
Fig. 5.7 Comparison of the developed column axial loads …… 89
Fig. 5.8 Comparison of the hysteretic behaviors ……... 89
Fig. 5.9 Buckling stability of SPSWs with various infill plate slenderness ratios ……. 91
Fig. 5.10 Load-drift ratio curves of SPSWs with various infill plate slenderness ratios …... 91
Fig. 5.11 Stiffness-drift ratio curves of SPSWs with various infill plate thicknesses ……... 91
Fig. 5.12 von Mises stress contour plot of SPSW4 model at 0.03 drift ratio ……. 91
Fig. 5.13 Hysteresis curves of the LYP steel shear wall models with various infill plate slenderness ratios …… 93
Fig. 5.14 Cumulative dissipated energy at various cycles ……. 93
Fig. 5.15 Comparison with Chen and Jhang's (2006) experimental results …….. 98
Fig. 5.16 Comparison with Tsai and Lin's (2005) experimental results …… 98
Fig. 5.17 Buckling and yielding behavior of the modeled experimental SPSW specimens .. 101
Fig. 5.18 Comparison of the modified PFI model predictions with numerical results of Lubell's (1997) SPSW2 specimen model …….. 102
Fig. 5.19 Comparison of the modified PFI model predictions with numerical results of Chen and Jhang's (2006) specimen no. 1 model …… 102
Fig. 5.20 Comparison of the modified PFI model predictions with numerical results of full-scale and code-designed SPSW models with various aspect ratios and under lateral load …….. 103

Fig. 6.1 Consideration of compressive load ……... 109

Fig. 6.2 Finite element models ……... 112
Fig. 6.3 Monotonic behaviors of SPSW models …… 114
Fig. 6.4 Cyclic behaviors of SPSW models ……... 115
Fig. 6.5 Normalized responses of SPSW models for different aspect ratios ……. 117
Fig. 6.6 Angle of inclination of the principal tensile stresses developed in the infill plate of SPSW2 model at 0.03 drift ratio …….. 119
Fig. 6.7 von Mises stress (MPa) contour plots at 0.05 drift ratio ……... 121
Fig. 6.8 Frame out-of-plane displacement (mm) contour plots at 0.05 drift ratio ……. 121
Fig. 6.9 Web local instability at the RBS portion of the upper beam …… 122
Fig. 6.10 Performance of upper left and right panel zones in SPSW1 model ……... 124
Fig. 6.11 Performance of upper left and right panel zones in SPSW2 model ……... 124
Fig. 6.12 Performance of upper left and right panel zones in SPSW3 model ……... 125
Fig. 6.13 Performance of SPSW3 model with and without beam midspan lateral brace ….. 127
Fig. 6.14 Out-of-plane displacements at mid-length of SPSW3 model without beam lateral brace ……... 127
Fig. 6.15 Deformation modes in SPSWs with fixed joints …… 129
Fig. 6.16 Comparison of the modified PFI model predictions with numerical results of full-scale and code-designed SPSW models with various aspect ratios and under gravity and lateral loads ……. 130

Fig. 7.1 Floor plan and elevation for the modified Los Angeles 9-story SAC building model …… 136
Fig. 7.2 Evaluation of buckling and yielding behavior of web plates in the structural models …….. 140
Fig. 7.3 Bare frame and wall-frame structural models …….. 141
Fig. 7.4 Modeling details and results for Lubell's (1997) SPSW2 specimen …… 144
Fig. 7.5 Modeling details and results for Chen and Jhang's (2006) specimen no. 1 ……. 145
Fig. 7.6 Modeling details and results for Park et al.'s (2007) SC2T specimen ……. 146
Fig. 7.7 Modeling details and results for a 3D finite element slender-web SPSW model …. 147
Fig. 7.8 Modeling details and results for a 3D finite element stocky-web SPSW model ….. 148
Fig. 7.9 Mode shapes of MRF model ……. 149
Fig. 7.10 Mode shapes of GF-CSPSW model ……... 149
Fig. 7.11 Initial stiffnesses of the considered structural models …… 153
Fig. 7.12 Time histories of selected Los Angeles ground motions for seismic performance evaluation ……... 156
Fig. 7.13 Maximum story and interstory drift ratios induced by three sample ground motions ……... 158
Fig. 7.14 Maximum story and interstory drift ratios induced by the considered ground motions ……... 159
Fig. 7.15 Variations of seismic-induced peak story and interstory drift ratios due to retrofit of structures using SPSW systems and LYP steel material ……... 161
Fig. 7.16 Comparison of 9th story drift ratio time histories of MRF, GF-CSPSW, and GF-LYPSPSW2 models ……. 163
Fig. 7.17 Maximum story accelerations induced by the considered ground motions …… 165
Fig. 7.18 Variations of seismic-induced peak floor accelerations due to retrofit of structures using SPSW systems and LYP steel material …… 166
Fig. 7.19 Comparison of 9th story acceleration time histories of MRF, GF-CSPSW, and 167

GF-LYPSPSW2 models …….
Fig. 7.20 Variations of seismic-induced normalized maximum base shear demands due to retrofit of structures using SPSW systems and LYP steel material ……... 169
Fig. 7.21 Comparison of base shear time histories of MRF, GF-CSPSW, and GF-LYPSPSW2 models ……. 170
Fig. 7.22 Variations of seismic-induced normalized maximum base moment demands due to retrofit of structures using SPSW systems and LYP steel material ……... 171
Fig. 7.23 Comparison of base moment time histories of MRF, GF-CSPSW, and GF-LYPSPSW2 models ……. 172
Fig. 7.24 Variations of seismic-induced normalized maximum VBE axial load demands at column bases due to retrofit of SPSWs using LYP steel material ……. 174
Fig. 7.25 Average web plate ductility ratios of GF-CSPSW and GF-LYPSPSW2 models .. 177
Fig. 7.26 Strain energy contour plots for MRF, GF-CSPSW (frame only), and GF-LYPSPSW2 (frame only) models at the end of application of LA28 ground motion showing the plastification zones in beam/HBE and column/VBE frame members ……. 179
Fig. 7.27 Deformed shapes (×15) of MRF, GF-CSPSW, and GF-LYPSPSW2 models at the end of application of LA28 ground motion …….. 180

Fig. 8.1 Characteristics of selected earthquake records for probabilistic seismic demand analysis ……. 191
Fig. 8.2 Average PIDR (%) and PFA (g) values for MRF, GF-CSPSW, and GF-LYPSPSW2 models ……... 193
Fig. 8.3 Relationship between ln[*EDP* = *PIDR*] and ln[*IM* = *PGV* (m/s)] …… 196
Fig. 8.4 Relationship between ln[*EDP* = *PFA* (g)] and ln[*IM* = *PGV* (m/s)] …… 197
Fig. 8.5 Relationship between ln[*EDP* = *PIDR*] and ln[*IM* = *PGA* (g)] …… 198
Fig. 8.6 Relationship between ln[*EDP* = *PFA* (g)] and ln[*IM* = *PGA* (g)] …… 199
Fig. 8.7 Selected *EDP-IM* data sets and the corresponding power trendlines for MRF, GF-CSPSW, and GF-LYPSPSW2 models ……... 202
Fig. 8.8 Fragility curves for predicting the probability of reaching or exceeding the damage states of MRF and repair states of GF-CSPSW and GF-LYPSPSW2 structural systems ……. 206
Fig. 8.9 Fragility curves for predicting the probability of reaching or exceeding the nonstructural damage states for drift-sensitive components of buildings …… 207
Fig. 8.10 Fragility curves for predicting the probability of reaching or exceeding the nonstructural damage states for acceleration-sensitive components/contents of buildings ……. 208
Fig. 8.11 Schematic illustration of the PEER-developed performance-based earthquake engineering methodology adopted in this study (Baker and Cornell, 2006) …….. 209
Fig. 8.12 Median values of PGA from the fragility curves for the damage/repair states of structural systems ……... 210
Fig. 8.13 Median values of PGA from the fragility curves for the damage states of nonstructural drift-sensitive components ……... 211
Fig. 8.14 Median values of PGA from the fragility curves for the damage states of nonstructural acceleration-sensitive components/contents …… 212

LIST OF TABLES

Table 2.1 Mechanical properties of LYP steel products (Yamaguchi et al., 1998) ……... 31

Table 4.1 Specifications of plate models ……... 53
Table 4.2 Theoretical and numerical elastic buckling loads of plates ……... 55
Table 4.3 Comparison of theoretical and numerical results of first yield point properties ... 60
Table 4.4 Theoretical and extrapolated buckling loads of moderate plates …….. 70
Table 4.5 Specifications of code-designed SPSW models …… 71
Table 4.6 Elastic buckling loads of plates under different edge support conditions ……. 74
Table 4.7 Limiting thicknesses of plates under pure shear with various edge conditions … 76

Table 5.1 Properties of the code-designed SPSW models ……. 80
Table 5.2 Loading protocol ……... 89
Table 5.3 Stiffness, strength, and energy dissipation characteristics of SPSW models …… 94
Table 5.4 Results of calculations for determining the limiting plate thicknesses of the experimental SPSW specimens ……. 99
Table 5.5 Considered numerical models of tested SPSW specimens …… 100
Table 5.6 Material properties of the modeled experimental SPSW specimens ……. 100

Table 6.1 Comparison of theoretically-predicted and exact limiting plate thicknesses …… 110
Table 6.2 HBE, VBE, and infill plate cross-sectional and geometrical properties of SPSWs ……... 110
Table 6.3 Cyclic loading protocol ……. 113
Table 6.4 Numerically- and analytically-obtained values for the angle of inclination ……. 119

Table 7.1 Properties of the moment-resisting and gravity frames (pre-Northridge design) from the Los Angeles 9-story SAC building model and SPSW structure …… 137
Table 7.2 Design parameters for SPSWs ……... 138
Table 7.3 Considered structural models …… 139
Table 7.4 Story seismic and lumped masses ……. 142
Table 7.5 Periods of the considered structural models …….. 151
Table 7.6 Percentage variations in initial stiffness and period …….. 153
Table 7.7 Rayleigh damping coefficients determined using the 1st and 5th modal frequencies and 2% damping ratio …… 154
Table 7.8 Details of selected Los Angeles ground motions for seismic performance evaluation …….. 155
Table 7.9 Peak story drift ratios (%) of the structural models induced by ground motions .. 160
Table 7.10 Peak interstory drift ratios (%) of the structural models induced by ground motions …… 160
Table 7.11 Peak floor accelerations (g) of the structural models induced by ground motions …… 166
Table 7.12 Normalized maximum base shear demands (V_b/W_s) of the structural models induced by ground motions ……. 168

Table 7.13 Normalized maximum base moment demands ($M_b/(W_s \times H_t) \times 100$) of the structural models induced by ground motions …… 171
Table 7.14 Normalized maximum VBE axial load demands ($P_{VBE-base}/P_y$) at column bases of the SPSW models induced by ground motions ……... 174
Table 7.15 Maximum web plate ductility ratios of GF-CSPSW and GF-LYPSPSW2 models ……. 176

Table 8.1 Details of selected Los Angeles ground motions for probabilistic seismic demand analysis …… 190
Table 8.2 Summary of ground motion intensity measure and seismic response parameter values ……..... 193
Table 8.3 R^2 values obtained from linear regression of ln[*EDP*] and ln[*IM*] variables …… 199
Table 8.4 Regression coefficients, standard deviation, and functional relation for selected *EDP-IM* data sets …….. 201
Table 8.5 HAZUS-MH MR5 (2010) interstory drift ratios of structural damage states for high-rise steel moment frames with high-code design level ……. 204
Table 8.6 Baldvins et al.'s (2012) recommended story drift ratios of structural repair states for SPSWs that meet certain seismic criteria …….. 204
Table 8.7 HAZUS-MH MR5 (2010) interstory drift ratios of nonstructural damage states for drift-sensitive components of all building types …….. 205
Table 8.8 HAZUS-MH MR5 (2010) peak floor accelerations of nonstructural damage states for acceleration-sensitive components/contents of all building types with high-code design level ……... 205

ACKNOWLEDGMENTS

First and foremost, my deepest acknowledgement is given to my Lord and Savior, JESUS CHRIST *The Only Answer*, for His mercy, plan, and giving me strength to overcome various challenges and difficulties, and achieve my educational goals.

Next, I want to express my boundless gratefulness to my parents and family for their endless love and continual prayers, support as well as encouragement throughout my studies.

I would like to offer my utmost gratitude to my academic advisor, Prof. Jian Zhang, for her precious and continual guidance, support, and encouragement during the course of my graduate studies at UCLA. Also, I wish to extend my wholehearted and profound appreciation to the members of my doctoral committee, Prof. Jiann-Wen Woody Ju, Prof. Ertugrul Taciroglu, and Prof. Christopher S. Lynch, who have taught me invaluable lessons and always provided me with their great and precious support.

My special thanks go to Prof. Qiuhong Zhao from Tianjin University in China, Prof. Carlos Estuardo Ventura from The University of British Columbia in Canada, Prof. Sheng-Jin Chen from National Taiwan University of Science and Technology in Taiwan, Dr. Chyuan Jhang from the Sinotech Engineering Consultants in Taiwan, and Dr. In-Rak Choi from the Research Institute of Industrial Science and Technology in South Korea, for their great and precious support in providing me with experimental data and details.

Finally, I would like to thank all my friends, fellow students, researchers, and professionals from all over the world, who supported me with their helpful and constructive comments, ideas, and feedback regarding various aspects of this research work.

VITA

EDUCATION

- M.Sc. in Structural Engineering, Urmia University, Iran (2003-2005)
- B.Sc. in Civil Engineering, Azad University - Urmia Branch, Iran (1998-2002)

TEACHING AND RESEARCH ACTIVITIES (SELECTED)

- Graduate Research and Teaching Assistant, Department of Civil and Environmental Engineering, University of California, Los Angeles, U.S.A. (2009-2013)
- Lecturer, Department of Civil Engineering, California State Polytechnic University, Pomona, U.S.A. (2012-2013)
- Graduate Research and Teaching Assistant, Department of Civil and Environmental Engineering, University of California, Irvine, U.S.A. (2007-2009)
- Graduate Teaching Assistant, Department of Civil Engineering, Azad University - Urmia Branch, Iran (2004-2005)
- Graduate Research Assistant, Department of Civil Engineering, Urmia University, Iran (2003-2005)

HONORS AND AWARDS (SELECTED)

- UCLA Outstanding Civil Engineering Ph.D. Award, CA, U.S.A. (2012-2013)
- UCLA Graduate Division, Fellowship Award, CA, U.S.A. (2010-2013)
- ASCE-IECC'5 Conference Best Student Paper Award, Irvine, CA, U.S.A. (2008)
- Urmia University, Highest G.P.A. of Graduates, Top Student, Urmia, Iran (2005)
- Azad University - Urmia Branch, Highest G.P.A. of Graduates, Top Student, Urmia, Iran (2002)

PROFESSIONAL ACTIVITIES (SELECTED)

- Journal Paper Reviewer: The Structural Design of Tall and Special Buildings; Ain Shams Engineering Journal; Structural Engineering and Mechanics, An international Journal; Steel and Composite Structures, An International Journal; Journal of Civil Engineering and Architecture; Mathematical Problems in Engineering; World Applied Sciences Journal
- Conference Paper Reviewer: CSCE 2007 Annual General Meeting & Conference, Canada

JOURNAL PUBLICATIONS (SELECTED)

Zirakian T. (2008). "*Lateral-Distortional Buckling of I-Beams and the Extrapolation Techniques*", Journal of Constructional Steel Research, 64(1), 1-11.

Zirakian T. (2008). "*Elastic Distortional Buckling of Doubly Symmetric I-Shaped Flexural Members with Slender Webs*", Thin-Walled Structures, 46(5), 466-475.

Zirakian T. (2010). "*On the Application of the Extrapolation Techniques in Elastic Buckling*", Journal of Constructional Steel Research, 66(3), 335-341.

Zirakian T. and Zhang J. (2012). "*Elastic Distortional Buckling of Singly Symmetric I-Shaped Flexural Members with Slender Webs*", International Journal of Structural Stability and Dynamics, 12(2), 359-376.

Zhang J. and Zirakian T. (2013). "*Buckling and Yielding Behavior of Unstiffened Slender, Moderate, and Stocky Low Yield Point Steel Plates*". (To Be Submitted)

Zirakian T. and Zhang J. (2013). "*Structural Behavior of Shear Wall Systems with Unstiffened Slender, Moderate, and Stocky Low Yield Point Steel Infill Plates*". (To Be Submitted)

Zirakian T. and Zhang J. (2013). "*Seismic Design and Behavior of Low Yield Point Steel Plate Shear Walls*". (To Be Submitted)

Zhang J. and Zirakian T. (2013). "*Study on Seismic Retrofit of Structures Using Steel Plate Shear Wall Systems and Low Yield Point Steel Material*". (Under Preparation)

Zhang J. and Zirakian T. (2013). "*Probabilistic Assessment of Seismic Retrofit of Structures by SPSW Systems and LYP Steel Material Using Fragility Function Method*". (Under Preparation)

CONFERENCE PRESENTATIONS (SELECTED)

Zirakian T. (2007). "*Elastic Distortional Buckling Analysis of Steel I-Beams Using CUFSM*", Proc., 2007 Annual Conference of the Canadian Society for Civil Engineering (CSCE), Yellowknife, Northwest Territories, Canada.

Zirakian T. (2008). "*Elastic Lateral-Distortional Buckling of Doubly Symmetric I-Beams: The 2005 AISC Specification*", ASCE 5th International Engineering and Construction Conference, University of California, Irvine, U.S.A.

Zirakian T. (2010). "*Further Results on the Application of the Extrapolation Techniques*", 2010 International Colloquium on Stability and Ductility of Steel Structures, Rio de Janeiro, Brazil.

Zirakian T. and Zhang J. (2010). "*Elastic Lateral-Distortional Buckling of Singly Symmetric I-Beams: The 2005 AISC Specification*", 2010 International Colloquium on Stability and Ductility of Steel Structures, Rio de Janeiro, Brazil.

Zirakian T. (2011). "*On the Application of the Meck Plot in Elastic Buckling*", ASCE Conference Proceedings of the 2011 Structures Congress, Las Vegas, Nevada, U.S.A.

Zirakian T. and Zhang J. (2012). "*Modified PFI Model for SPSWs with Moderate and Stocky LYP Steel Infill Plates*", Joint SSRC Annual Stability and AISC Steel Conference, Grapevine, Texas, U.S.A.

Zirakian T. and Zhang J. (2012). "*Structural Performance of SPSWs with Unstiffened Slender, Moderate, and Stocky LYP Steel Infill Plates*", 15th World Conference of Earthquake Engineering, Lisbon, Portugal.

Zirakian T. and Zhang J. (2013). "*Study on Seismic Design and Performance of SPSWs with Unstiffened LYP Steel Infill Plates*", 2013 Conference of the ASCE Engineering Mechanics Institute, Northwestern University, Evanston, Illinois, U.S.A.

Zirakian T. and Zhang J. (2013). "*Assessment of Seismic Behavior of Structures Retrofitted with Conventional and LYP Steel Infill Plates Using the Fragility Function Method*", 2013 Conference of the ASCE Engineering Mechanics Institute, Northwestern University, Evanston, Illinois, U.S.A.

Zhang J. and Zirakian T. (2013). "*Dynamic Response of Structures Retrofitted with SPSW Systems and LYP Steel Material*", 10th U.S. National Conference on Earthquake Engineering, Anchorage, Alaska, U.S.A. (To Be Submitted)

1. INTRODUCTION

1.1 General

Rigid frames, shear walls, and braced frames are three typical types of structural systems which are used to resist the lateral loads and limit the drift in buildings. Among the lateral force-resisting systems, steel plate shear walls (SPSWs) are relatively new systems which offer many advantages over other systems in terms of cost, performance, and ease of design. As shown in Fig. 1.1, a typical SPSW system consists of a steel infill plate, two vertical boundary elements (VBEs), i.e. columns, and two horizontal boundary elements (HBEs), i.e. beams.

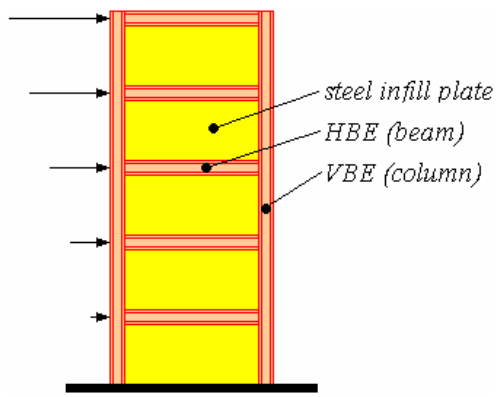

Fig. 1.1 A typical SPSW system

SPSWs have been in use since the 1970s, and a proliferation of research work has been undertaken to improve the performance and design of these lateral force-resisting systems. Based on structural and economical considerations, SPSWs have been generally designed with either heavily-stiffened and/or thick plates, or unstiffened thin plates.

Application of low yield point (LYP) steel infill plates has been recently shown in a number of studies to result in ductile SPSW systems with improved stiffening, damping, and

serviceability characteristics. Considering the various advantages of use of LYP steel infill plates in SPSWs and limited number of studies on this subject, more research is required to identify the structural characteristics and evaluate the seismic performance of LYP steel shear wall systems. Hence, the main objective of this research program is to perform a rather comprehensive and systematic study on the structural behavior and seismic performance of SPSWs employing unstiffened LYP steel infill plates.

1.2 Applications

Since 1970s, SPSWs have been used as the primary and/or part of the primary lateral force-resisting system in a number of buildings ranging from single-family residential to high-rise construction mainly in highly-seismic areas in Japan and North America. Initially, and during 1970s, stiffened SPSWs were used in Japan in new construction and in the United States for seismic retrofit of the existing and construction of new buildings. Later on, in 1980s and 90s, unstiffened steel shear walls were used in buildings in the United States and Canada (Astaneh-Asl, 2000).

In Japan, various types of SPSW configurations including stiffened steel plates (Fig. 1.2(a)) and specially-detailed shear yielding plates/elements (Fig. 1.2(b)), have been introduced and used, some of which may not be the SPSW in the sense considered in North America. Examples of SPSW buildings with stiffened infill plates include the Nippon Steel Building (Fig. 1.2(c)) in Tokyo built in the 1970s, and also the 35-story Kobe City Hall Tower in Kobe constructed in 1988 (Fig. 1.2(d)) which resisted the 1995 Kobe earthquake with minor damage (Astaneh-Asl, 2000).

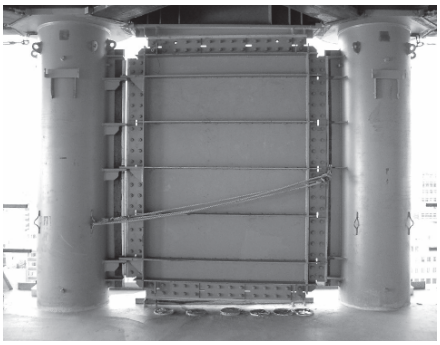

(a) SPSW with stiffened infill plate

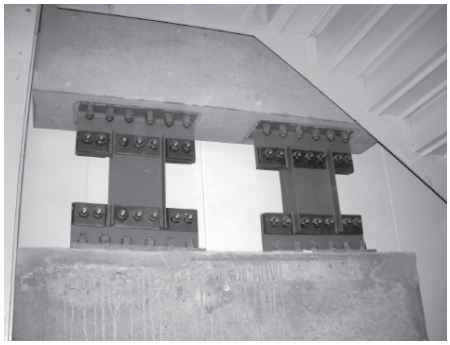

(b) Shear yielding plates/elements

(c) Nippon Steel Building

(d) Kobe City Hall Tower

Fig. 1.2 SPSW configurations and applications in Japan (Sabelli and Bruneau, 2006)

Following the development of LYP steel by Nippon Steel in Japan, some LYP steel shear wall projects included LYP plates to dissipate energy (Yamaguchi et al., 1998). The Saitama Wide-Area Joint Agency Buildings, 31 and 26 stories, provide an example of implementation of a stiffened SPSW with LYP100 steel. In these structures, thicknesses of plates varied from 25 to 6 mm (1 to 1/4 in.) along the height of the building, with panels of up to 4.5×3.0 m (15×10 ft) in size (Sabelli and Bruneau, 2006).

In early applications of SPSWs in United States, shear walls were designed with relatively closely-spaced horizontal and vertical stiffeners to prevent buckling of the plate, and used for seismic retrofit of low and medium-rise existing structures. However, the current North American practice is to use unstiffened plates, since considering today's construction and labor costs in North America, welding stiffeners to steel wall are costly and time-consuming and the

research undertaken in recent years has indicated that the steel plate alone, without stiffeners, performs in a very ductile, desirable, and efficient manner. Fig. 1.3 shows some of the buildings with such SPSW systems.

SPSW systems have been used in other countries such as Canada, Mexico, etc. as well. In particular, since the early 1980s, unstiffened SPSWs have been used in Canada, as these were the types of SPSWs on which Canadian research focused.

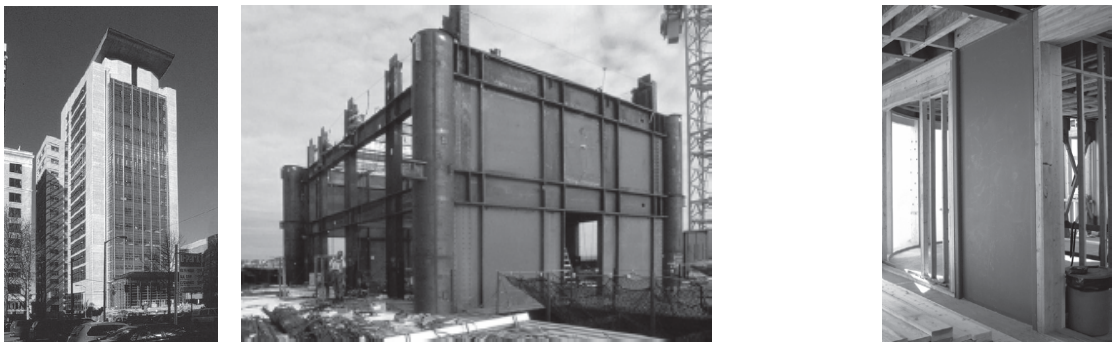

(a) U.S. Federal Courthouse, Seattle, WA

(b) Four-story residence in San Francisco, CA

Fig. 1.3 Application of SPSW systems in United States (Sabelli and Bruneau, 2006)

1.3 Wall Types

In building construction, SPSWs have been mostly designed with unstiffened and stiffened infill plates as shown in Figs. 1.4(a) and (b), respectively.

(a) Unstiffened infill plates

(b) Stiffened infill plates

Fig. 1.4 Typical SPSW systems (Sabelli and Bruneau, 2006)

Unstiffened and slender-web SPSWs have been the most popular type used in the United States and Canada. Such SPSW systems have negligible compression strength and thus, shear buckling occurs at low levels of loading. Hence, the main disadvantage of such systems is the premature buckling of the compression zone of the wall, which results in reduced shear strength, stiffness, and energy dissipation capacity (Zhao and Astaneh-Asl, 2004). Nonetheless, extensive research work in Canada undertaken by Kulak, Thorburn, Driver, Grondin, and others has resulted in development of a design methodology to utilize the post-buckling capacity of the web plates and the usefulness of a web plate has not been limited to its buckling capacity.

Stiffeners are primarily provided to increase the buckling strength of infill plates in SPSWs. In fact, stiffeners limit the plate out-of-plane deflections, increase their elastic buckling strength, and extend yielding throughout the plate (Alinia and Sarraf Shirazi, 2009). Sufficient stiffening will permit the web plate to achieve its full plastic strength and avoid overall buckling.

Another approach to mitigate most disadvantages of unstiffened and slender-web shear walls is to employ composite infill plates in which the steel infill plate is connected to thin concrete panels on one or both sides, as shown in Fig. 1.5. The concrete wall restrains the steel plate and prevents its buckling before it yields. In addition, the reinforced concrete wall provides sound and temperature insulation as well as fire proofing to steel shear walls (Astaneh-Asl, 2002). Composite shear walls have been used in buildings in recent years even though not as frequently as the unstiffened and stiffened shear walls. As shown in Fig. 1.5, composite shear walls may be of either traditional or innovative type. In an innovative system, as proposed by Astaneh-Asl (2002), there is a gap between the concrete wall and the boundary frame elements to prevent the concrete wall from engaging in resisting the lateral forces too early during small and moderate

earthquakes, otherwise the concrete wall is seriously damaged and can not prevent the plate buckling.

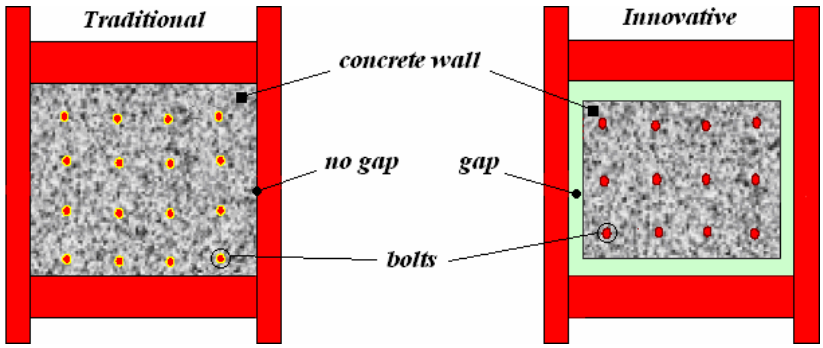

Fig. 1.5 SPSWs with composite shear panels (Astaneh-Asl, 2002)

In addition to the aforementioned typical systems, SPSWs with other configurations have also been introduced and used in some limited cases. Hitaka and Matsui (2003) introduced a new type of SPSW which relies on ductile flexural deformations provided by the numerous slits slotted in the panel, without the need for heavy transverse stiffening (Fig. 1.6). The slit wall features include ductile and stable behavior, independent adjustment of strength and stiffness by changing the slit configuration, simple fabrication and installation, and compactness so that the wall need not occupy the full beam span. On this basis, three buildings ranging from 7 to 19 stories and incorporating steel slit walls have been constructed in Japan (Hitaka and Matsui, 2003).

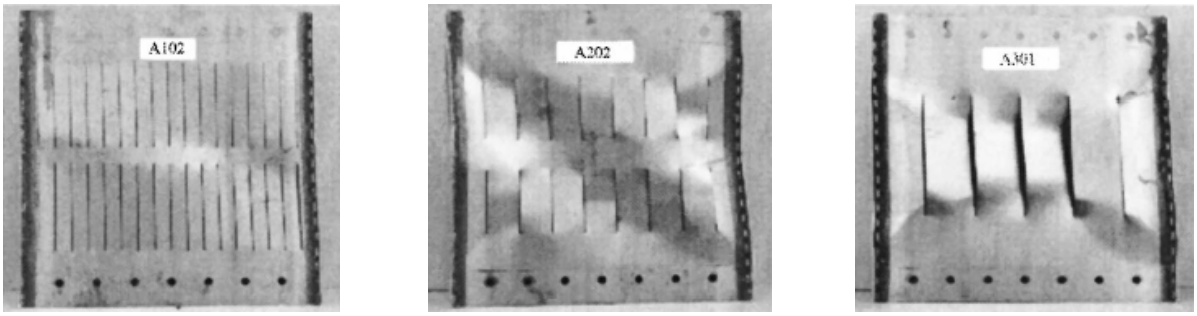

Fig. 1.6 SPSWs with steel slit walls (Hitaka and Matsui, 2003)

SPSWs with corrugated, e.g. Mo and Perng (2000) and Berman and Bruneau (2003), as well as perforated, e.g. Roberts and Sabouri-Ghomi (1992), infill plates have also been studied. Moreover, Xue and Lu (1994), Pirmoz (2010), and others considered a novel configuration of SPSWs in which the infill plates are only attached to the beams and consequently the whole tension field force applied on the columns is removed. Although this system has not been sufficiently investigated, the preliminary results indicate that "beam-attached" SPSWs have promising potential to reduce the overall system demand on the vertical boundary members.

1.4 Advantages, Disadvantages and Limitations

Some of the key advantages of using SPSW systems to resist lateral loads are as following:

- **Small Wall Thickness:** Due to this property and from architectural standpoint, compared to equivalent reinforced concrete shear walls SPSWs occupy much less area of the floor plan, especially in high-rise buildings.
- **Reduced Building Weight:** SPSWs are much lighter than reinforced concrete shear walls. This property can result in less weight to be carried by the columns and foundations as well as less seismic load due to reduced mass of the structure.
- **Fast Construction:** Not only SPSWs are fast to erect, but also there is no curing period. Further, it has been noted (Seilie and Hooper, 2005) that the erection of the SPSW is much easier than that of the special concentrically braced frames.
- **Ease of Construction:** Shop-welded field-bolted elements can make SPSWs more efficient than the traditional systems. SPSWs can also be very practical and efficient for cold regions where concrete construction may not be economical under very low temperatures.

- **High Stiffness and Strength:** Due to their relatively high initial stiffness, SPSWs can effectively limit the drift. Also, due to their high stiffness and strength, shorter bays may be used in construction, which can result in greater flexibility for use of the space.
- **High Ductility and Energy Dissipation Capacity:** Past research shows that properly-designed and detailed SPSWs are very ductile and can have relatively large energy dissipation capability.
- **Tested System:** Some buildings with SPSW systems have undergone significant earthquake ground shaking in the past, and have survived with insignificant structural damage (Astaneh-Asl, 2000).

In spite of considerable advantages of the SPSW systems, according to Seilie and Hooper (2005) they may also have some disadvantages as noted in the following:

- **Lower Stiffness due to Flexural Flexibility:** Compared to the reinforced concrete shear walls, SPSWs are usually more flexible primarily due to their flexural flexibility, which has to be properly addressed in design of tall buildings.
- **Construction Sequence:** Excessive initial compressive force may delay the development of tension-field action in SPSWs. So, it is important that the construction sequence be designed to avoid excessive compression in the panel. For instance, in the U.S. Federal Courthouse project, the welding of the plate splice connections was delayed until most of the dead load deformation occurred in order to relieve the pre-compression within the SPSW panel.

- **New System:** Due to unfamiliarity with such a relatively new lateral force-resisting system, a contractor may typically estimate a high erected cost. This may be solved by engaging the contractor early in the design phase.

In addition to the above-mentioned advantages and disadvantages of SPSWs, there may be some limitations in use of such systems in practice. Although this system is viable for both small and large structures, according to Sabelli and Bruneau (2006) aspects of the design vary with building size. For instance, compliance with some design requirements of AISC 341 for seismic design may be more difficult or at least more tedious than typical detailing practice for smaller structures. As another example, SPSW bays with long horizontal proportions may be needed in taller buildings to control the drift. However, because of lack of research and knowledge on the behavior of SPSWs with both shorter and longer bays, use of such systems may be restricted.

1.5 Scope and Objectives

SPSWs, in general, have been utilized based on two different design philosophies and detailing strategies. Stiffened and/or stocky-web SPSWs with high structural and seismic performance have been mostly designed and used in Japan. Unstiffened and slender-web SPSWs with relatively lower buckling and energy dissipation capacities, on the other hand, have been deemed as a rather economical alternative and accordingly widely used in the United States and Canada. Development and use of LYP steel with exclusive material properties for seismic applications nowadays makes it possible to take advantage of merits of the two design strategies and consequently design relatively cost-effective SPSW systems with improved buckling stability, serviceability, and energy absorption capacity. Nevertheless, in order to promote and encourage the employment of LYP steel shear wall systems in practice, a thorough and sound

understanding of their structural characteristics and seismic performance is crucial which, of course, requires detailed and systematic theoretical as well as experimental investigations.

Despite some experimental and numerical studies on the behavior of LYP steel shear walls, the structural and seismic characteristics of these systems have not been fully explored and still lots of questions and concerns regarding various aspects of application of such lateral force-resisting systems remain unaddressed. It is also important to note that currently LYP steel is only produced in a limited number of countries such as Japan and China, and it is believed that sufficient research and broad knowledge on structural characteristics and effective practical application of LYP steel material in lateral force-resisting and energy dissipating systems will, in turn, result in mass production and economical use of such efficient steel material in other parts of the world, especially in the United States.

On this basis, this research aims at reaching a deep understanding of behavioral characteristics of unstiffened SPSW systems employing LYP steel infill plates through detailed element-, component-, and system-level investigations on their structural behavior and seismic performance using analytical, numerical, and probabilistic approaches. It also intends to provide effective and practical design tools and recommendations for efficient design and application of LYP steel shear wall systems. The major tasks of this comprehensive research program are summarized in the following:

1. **Element-Level Investigations on Steel Plates:** Analytical and numerical studies on determination of limiting thicknesses corresponding to simultaneous buckling and yielding of steel plates. Evaluation of buckling, yielding, and hysteresis behaviors of LYP steel plates. Assessment of effects of using LYP steel and plate aspect ratio on limiting thickness.

2. **Component-Level Investigations on SPSW Panels:** Study on behaviors of code-designed SPSWs with slender, moderate, and stocky LYP steel infill plates via nonlinear pushover and cyclic analyses. Evaluation of advantages of using LYP steel infill plates in design and retrofit of SPSW systems. Development and verification of a modified plate-frame interaction (PFI) model for predicting the behaviors of SPSWs with low yielding and high bucking capacities. Evaluation of effectiveness of some AISC 341 code-specified design requirements and recommendations.
3. **System-Level Investigations on Multi-Story SPSW Frames:** Selection and verification of an efficient modeling approach for representing the behavior of SPSWs employed in multi-story structures. Seismic response and performance assessment of code-designed and retrofitted structures employing conventional and LYP steel infill plates via nonlinear time-history analyses.
4. **Probabilistic Seismic Vulnerability Assessment Using Fragility Function Method:** Determination of proper engineering demand parameter (EDP) and seismic intensity measure (IM) pairs with less variation and good linear correlation. Development of structural and nonstructural fragility functions by considering appropriate damage and repair states. Probabilistic seismic performance and vulnerability assessment of code-designed and retrofitted SPSW frames through fragility analyses.

1.6 Organization

This dissertation includes a total of 9 chapters in order to address the key issues and achieve the considered objectives of this research presented in the previous section.

A general description of SPSW systems along with the motivations and objectives of this research are provided in Chapter 1.

Chapter 2 includes a survey of the past analytical and experimental research and recent developments on the analysis, design, and application of SPSW systems as well as production and properties of the LYP steel material.

Chapter 3 provides a general discussion of the fundamental mechanics of unstiffened SPSWs, and also addresses the AISC 341 code-specified design requirements as well as performance-based design of SPSW systems.

In Chapter 4, element-level investigations on the buckling, yielding, and cyclic behaviors of steel plates are presented. This chapter also focuses on the determination of the limiting thickness corresponding to concurrent geometrical buckling and material yielding of steel plates, which serves as the guiding parameter quantifying the behavior of steel plates.

Chapter 5 presents component-level studies on the pushover and cyclic behaviors of SPSWs with slender, moderate, and stocky infill plates. In this chapter, a modified PFI method is also proposed and its efficiency in predicting the behaviors of SPSWs with moderate and stocky infill plates is evaluated.

In Chapter 6, component-level investigations are continued by evaluating the structural behavior and performance of further sophisticated LYP steel shear walls designed for high-seismic applications. Accordingly, the effectiveness of some AISC 341 code design requirements and recommendations are evaluated through detailed numerical simulations.

Chapter 7 includes system-level investigations on the seismic response assessment of multi-story SPSW frames under the action of earthquake ground motions. The effectiveness of the strip model in representing the behaviors of SPSWs with various buckling and yielding behaviors is

primarily evaluated. Subsequently, the seismic performances of code-designed and retrofitted SPSW frames with conventional and LYP steel infill plates are investigated by considering various seismic response parameters from nonlinear dynamic analyses.

In Chapter 8, the seismic performance and vulnerability of code-designed and retrofitted structures employing SPSW systems and LYP steel material are evaluated through probabilistic seismic demand analysis (PSDA) method by developing appropriate fragility functions.

Ultimately, Chapter 9 provides the major findings and conclusions of this research along with the recommendations for the future work.

2. PAST RESEARCH AND RECENT DEVELOPMENTS

2.1 General

Early designs for SPSWs were based on the premise that out-of-plane buckling constituted the limit of usefulness of the infill plates. To prevent buckling, either stiffeners were needed or the plate had to be relatively thick in order to fulfill this philosophy (Kulak et al., 2001). In addition, it was demonstrated (Takahashi et al., 1973) that substantial stiffening of a plate could increase the energy dissipation capacity of the system under cyclic loading, which was, of course, accompanied by enhanced construction costs.

On the other hand, Wagner (1931) showed that buckling did not necessarily represent the limit of useful behavior and that there was considerable post-buckling strength in an unstiffened shear panel. Consideration of the post-buckling strength of plates was accepted in the design of plate girder webs based largely on the work of Basler (1961). The appropriateness of post-buckling stiffness and strength characteristics of SPSW to resist lateral loads was analytically predicted by Thorburn et al. (1983) and experimentally confirmed by Timler and Kulak (1983). Thus, the key research on unstiffened SPSWs was performed in the 1980s and since then such SPSW systems have been studied and widely used particularly in the United States and Canada.

In recent years, LYP steel plates have been developed in Japan and used successfully in steel shear wall systems in some projects. It has been demonstrated in Japan that LYP steel can be used in energy dissipating elements of a structure (Astaneh-Asl, 2000). Recent studies have also shown that LYP steel shear walls with improved structural and hysteretic characteristics can be effectively utilized as the primary and/or part of the primary lateral force-resisting and energy dissipating systems in buildings.

This chapter presents a brief summary of the prior and recent theoretical and experimental investigations as well as developments on the application and performance of SPSW systems, in particular, those with LYP steel infill plates.

2.2 Development of Analytical Modeling Techniques of SPSW Systems

This section deals with analytical research which includes theoretical works primarily focusing on the behavioral aspects of the SPSW. In fact, the main purpose of the analytical works has been to facilitate the analysis and design of SPSW systems without introducing much complexity.

Hysteresis Model. This method was developed by Mimura and Akiyama (1977) through some experimental and analytical studies, as shown in Fig. 2.1. In the figure, Q is the lateral load applied to the panel and δ is the resulting lateral displacement. The proposed model was validated through tests on small-scale simply supported stiffened plate girders subjected to a single cyclic point load at midspan.

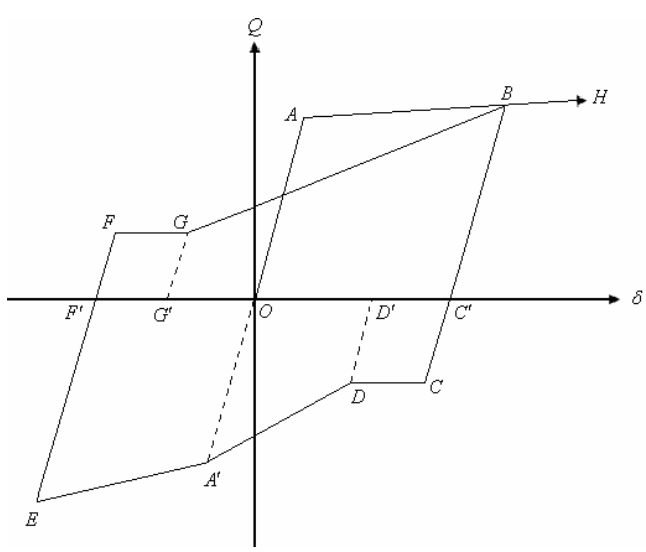

Fig. 2.1 Hysteresis model proposed by Mimura and Akiyama (1977)

Multi-Strip Model. Thorburn et al. (1983) developed a simple analytical model, so-called "multi-strip model", to study the shear behavior of thin unstiffened SPSW systems, based on the diagonal tension-field theory proposed by Wagner (1931) and modified later by other researchers. In this model, as shown in Fig. 2.2, action of the tension field was modeled by a series of pin-ended inclined tension-only members, which were oriented parallel to the direction of the tension field. Each strip was assigned an area equal to the width of the strip times the plate thickness. The angle of tension field (α) was obtained using the principle of least work. The boundary beams were assumed to be infinitely rigid and pin-connected to the columns, while the boundary columns were assigned to actual stiffnesses. Thorburn et al. (1983) also derived an expression of the angle of tension field for steel shear wall with rigid beam-to-column connections. This model was validated through some cyclic load tests conducted by Timler and Kulak (1983), and these researchers modified the angle of inclination of the principal tensile direction which was originally proposed by Thorburn et al. (1983). The multi-strip modeling technique, with minor variations, remains the most commonly-used idealization for analysis and design of the SPSW systems as yet (Ghosh and Kharmale, 2010).

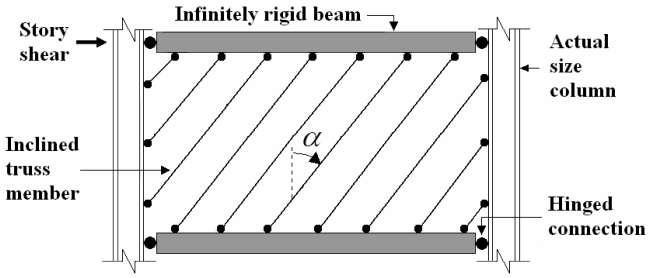

Fig. 2.2 Multi-strip model proposed by Thorburn et al. (1983)

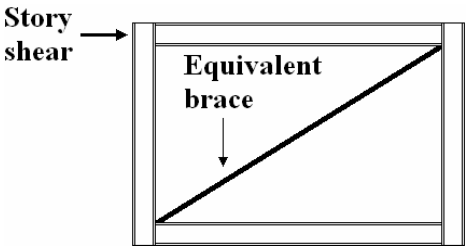

Fig. 2.3 Equivalent brace model proposed by Thorburn et al. (1983)

Equivalent Brace Model. Thorburn et al. (1983) also developed a Pratt truss model (Fig. 2.3) for the analysis of the thin steel shear wall, known as "equivalent (story) brace model", in which

stiffness of the infill plate is equal to that derived from the multi-strip model of the panel. In spite of relative simplicity of this model, the multi-strip modeling technique is preferred by most users since its results are of relatively higher accuracy.

Cross (Diagonal) Strip Model. This model was developed by Elgaaly et al. (1993) to predict the hysteretic behavior of SPSWs. As shown in Fig. 2.4, the cross truss members are used to model the tension-field action in opposite directions during cyclic load reversals and a hysteretic stress-strain relationship for these truss members was developed based on test results. Although this modeling technique is a little more computation intensive compared to the multi-strip technique, for obvious advantages it has gained acceptance over the years, particularly for nonlinear response/time-history analyses of SPSW systems (Ghosh and Kharmale, 2010).

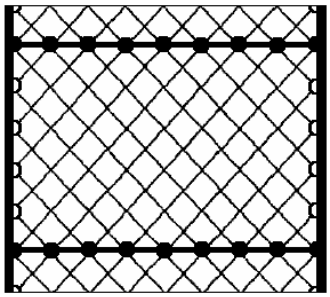

Fig. 2.4 Diagonal strip model proposed by Elgaaly et al. (1993)

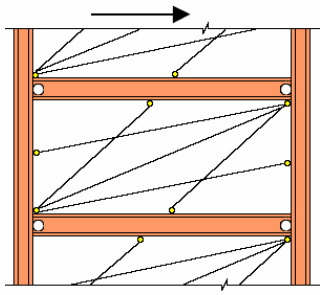

Fig. 2.5 Multi-angle strip model proposed by Rezai (1999)

Multi-Angle Strip Model. Based on experimental studies conducted in the University of British Columbia, it was found that the angle of the tension strips in steel shear wall was closer to vertical at the corners and more horizontal around the mid-point of the plate, which was primarily related to the interaction of the infill plate and boundary elements (Rezai, 1999). On this basis and in order to overcome this deficiency of the multi-strip model, Rezai (1999) proposed a “multi-angle strip model” as shown in Fig. 2.5, and also presented the respective

equations for calculating the cross-sectional area of each strip. As seen in Fig. 2.5, the five strips oriented at various angles, account for the variation in the angle of tension field across the panel. In spite of reasonable predictions of this model, the model was found to be conservative in predicting the ultimate capacity, besides being a complex one to handle without any significant gain in accuracy when compared to the multi-strip model (Ghosh and Kharmale, 2010).

Plate-Frame Interaction (PFI) Model. This general modeling technique was developed by Sabouri-Ghomi et al. (2005) to analyze and design SPSW systems with different configurations. In this method, the behaviors of the infill plate and boundary frame are considered separately, and the interaction of these structural components is taken into account, as shown in Fig. 2.6. Hence, it was named as the "plate-frame interaction" model. This modeling technique was also modified to include the effect of overturning moments on the steel shear wall response. The accuracy of this method has been verified through comparison with experimental and numerical results and good agreement has been observed for the stiffness and strength of the SPSW systems (Ghosh and Kharmale, 2010).

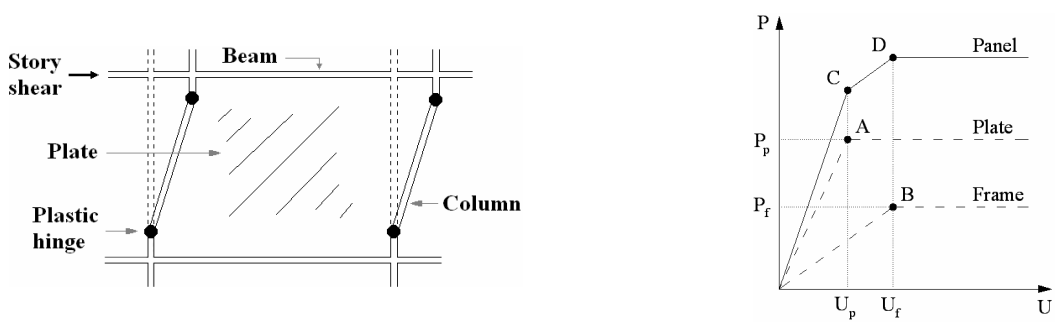

(a) Plate and frame idealization **(b)** Components of PFI method

Fig. 2.6 Plate-frame interaction method proposed by Sabouri-Ghomi et al. (2005)

Modified Strip Model. The multi-strip model originally developed by Thorburn et al. (1983) neglected the pre-buckling compression resistance of infill panel. Later on, Driver et al. (1997)

found that the original model underestimated both elastic stiffness and ultimate capacity of the SPSW, since it neglected the small contribution from the compression diagonal (pre-buckling) to the strength and stiffness of the infill panel. Also, it did not account for the gradual strength degradation of SPSW system at large inelastic displacement cycles. In order to overcome these deficiencies, Shishkin et al. (2009) refined the original multi-strip model primarily to achieve an accurate representation of yielding and eventual deterioration of the wall, although moderate improvements in initial stiffness predictions were also made. The modified strip model is shown in Fig. 2.7. The modified model incorporates bilinear flexural hinges positioned at the edges of the frame panel zones, bilinear axial hinges in the tension strips, a simplified method of spacing the strips, a diagonal compression strut with a bilinear axial hinge to represent phenomena present in a continuous plate that are not captured by discrete strips, and a conservative deterioration behavior that simulates experimentally observed tearing of the infill plate under extreme cyclic loading. This model was validated using three SPSW specimens with different properties and configurations (Shishkin et al., 2005 and 2009).

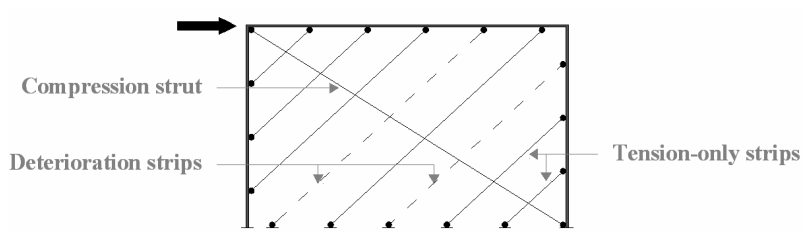

Fig. 2.7 Modified strip model proposed by Shishkin et al. (2009)

Finite Element Model. Over the past 20 years, finite element approach has been adopted by various researchers to study the structural behavior of SPSW systems. This modeling technique has various advantages in terms of simulating the actual physical behavior of a structural system, albeit at the cost of being highly computation intensive. Two examples of SPSW finite element

models are shown in Fig. 2.8. In spite of considerable advantages of finite element modeling, it is much more complex in comparison with the other analytical modeling techniques such as the strip models. In any case, despite its complexity, finite element approach is considered as a great tool for research.

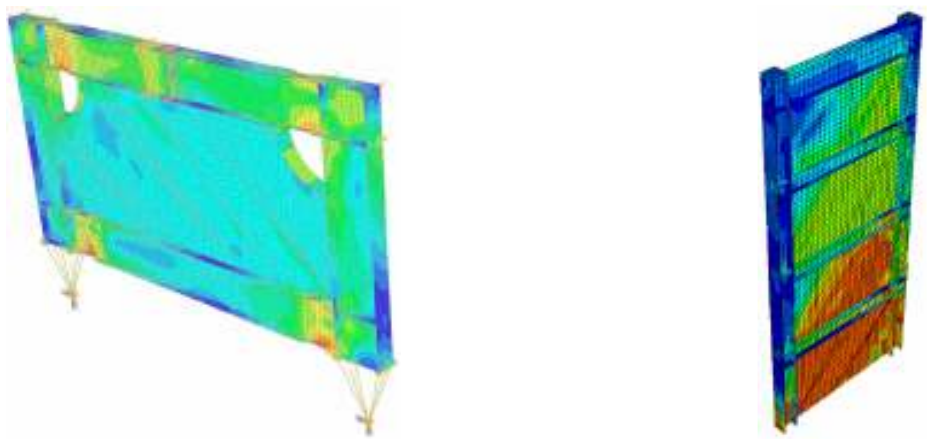

(a) Vian et al. (2009a) **(b)** Habashi and Alinia (2010)

Fig. 2.8 Examples of finite element models

2.3 Prior Analytical and Experimental Research on SPSWs

Analytical and experimental studies have been carried out on SPSWs increasingly over the last forty years. The experimental research has covered the static, quasi-static cyclic, and dynamic tests of both stiffened and unstiffened SPSWs from single to multi-story and from small to large-scale specimens with various configurations. Kharrazi (2005), Sabelli and Bruneau (2006), and Ghosh and Kharmale (2010) provide summaries of the experimental studies on the behavior and performance of SPSW systems. It is notable that SPSWs with LYP steel infill plates have only been studied during the past decade or so and most of such research work has been done quite lately. This section summarizes some outstanding research works, especially those on LYP steel shear walls.

At the University of British Columbia, Lubell et al. (2000) conducted a series of tests consisting of two single-story (shown in Fig. 2.9) and one four-story specimens with unstiffened, thin, and hot-rolled steel infill plates subjected to quasi-static cyclic loads. The results and findings of this study demonstrated that SPSWs exhibit many desirable characteristics such as good displacement ductility capacity and stable hysteresis behavior with desirable energy dissipation for structures in areas of high seismic risk. The results of this experimental study have been used by many researchers and are also used in the current study to validate the finite element modeling.

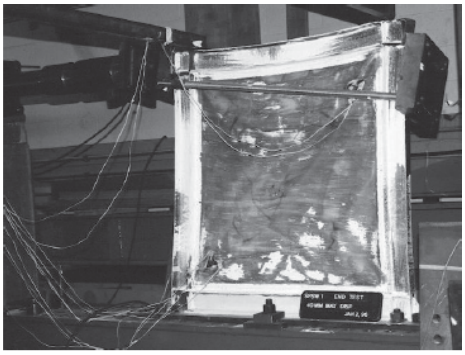

(a) SPSW1 (Sabelli and Bruneau, 2006)

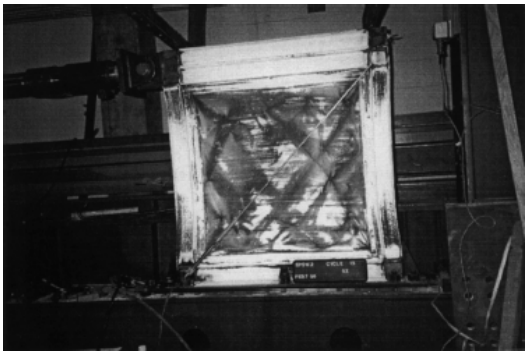

(b) SPSW2 (Lubell et al., 2000)

Fig. 2.9 Single-story SPSW specimens tested by Lubell et al. (2000)

Nakashima and his research associates (1995a and 1995b) reported experimental and analytical studies on the hysteretic behavior of shear panels made of LYP steel material. They compared the behavior of LYP steel shear panels with that of conventional mild steel shear panels and demonstrated the superior performance of shear panels made of LYP steel material with significant strain-hardening under load reversals.

Bruneau and Bhagwagar (2002) performed nonlinear inelastic analyses in order to study the seismic retrofit of steel frames using LYP steel infill plates and concluded that LYP steel does behave slightly better than standard constructional grade steel under extreme seismic conditions

but at the cost of some extra material. In addition, as a result of some nonlinear dynamic analyses, De Matteis et al. (2003) showed that LYP steel shear panels act as efficient stiffening and damping devices which are capable of strongly enhancing the seismic performance of steel frames. As well, they supply a large source of energy dissipation, which results in limiting the plastic deformation demand to the primary structure.

Vian and Bruneau (2004) reported an experimental study on SPSWs with LYP steel infill panels and reduced beam sections (RBS) at the beam-ends. They found that lower yield strength of the tested panels resulted in earlier onset of energy dissipation by the panel as compared to the available hot-rolled plate, and concluded that LYP steel shear walls are viable option for use in resistance of lateral loads imparted on a structure during seismic excitation. In another paper, Tsai and Lin (2005) evaluated the results of test of three SPSW specimens with stiffened and unstiffened LYP steel infill plates and RBS connections, as shown in Fig. 2.10. The tested specimens exhibited improved buckling stability, serviceability, and energy dissipation capacity.

(a) Specimen S **(b)** Specimen 2T **(c)** Specimen 3T

Fig. 2.10 Buckled LYP steel panels of SPSW specimens tested by Tsai and Lin (2005)

Chen and Jhang (2006) conducted a series of experimental studies to examine the stiffness, strength, deformation capacity, and energy dissipation capacity of five LYP steel shear walls under cyclic loading. As reported, all of the specimens failed after significant inelastic tension-

field action which occurred concurrent with large story drift deformation. Fig. 2.11 shows the typical deformation pattern in two specimens after the testing. This study demonstrated that LYP steel shear wall system has excellent deformation capacity, and its ultimate story drift angle can be as large as 3-6%. Also, the experimental findings indicated that LYP steel shear wall system is able to provide good post-yield stiffness, strength and energy dissipation capacity.

(a) Specimen no. 1 with unstiffened infill plate

(b) Specimen no. 5 with stiffened infill plate and simple beam-to-column connections

Fig. 2.11 Deformations of SPSW specimens at ultimate stage tested by Chen and Jhang (2006)

Lashgari (2009) presented a finite element study and investigated the stiffness, strength, deformation capacity, and energy dissipation capacity of SPSWs with LYP steel infill plates. In this study, it was found that decreasing of plate width-to-thickness ratio, while all dimensions are kept constant, does not increase the initial stiffness and ultimate strength of the SPSW significantly, but results in considerable increase in energy dissipation capacity of the system. Lashgari concluded that with proper design, the LYP steel shear wall is able to yield at low force levels and dissipate energy via plastic deformation.

Lately, Mistakidis (2010) investigated the behaviors of LYP and ordinary steel shear walls used for improving the seismic performances of new and existing structures, via nonlinear finite element analyses. Some of the advantages of use of LYP steel relative to the ordinary steel were shown and also some characteristics of the plate-frame interaction in SPSW systems were addressed in this study in the light of use of LYP steel material.

Most recently, Chen and Jhang (2011) reported another series of experimental studies on inelastic shear buckling behavior, stiffness, strength, deformation, and energy dissipation characteristics of single and multi-story LYP steel plate shear walls under monotonic and cyclic loadings. As shown in Fig. 2.12(a), SPSW specimens with LYP steel infill plates underwent early yielding and inelastic buckling. Buckled and deformed shapes of the stiffened and unstiffened LYP steel shear wall specimens are also shown in Figs. 2.12(b) through 2.12(d). It was reported that excellent deformation and energy dissipation capacity were obtained for all specimens tested, and the LYP steel plate shear wall system is able to exceed 5% of storey drift angle under lateral force.

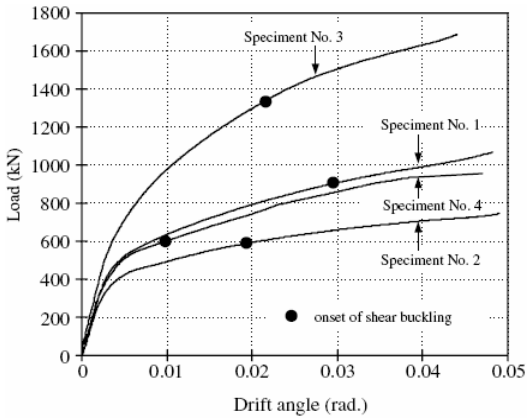

(a) Buckling and yielding behavior

(b) Buckling of unstiffened specimen

(c) Buckling of stiffened specimen

(d) Deformation of multi-story specimen

Fig. 2.12 Buckling-yielding and deformations of SPSWs tested by Chen and Jhang (2011)

2.4 Recent Developments

In recent years, considerable research on various aspects of analysis, design, and application of SPSW systems has been carried out in different countries around the world, such as United States, Canada, Japan, Iran, Taiwan, United Kingdom, Korea, India, China, and Turkey. In addition to the research publications, some studies have also been reported which focus more on engineering practice. Some of the recent significant developments in research and application of steel shear wall systems are summarized in this section.

Some approaches have been introduced and investigated by Bruneau and his research associates, e.g. Berman and Bruneau (2003), Vian and Bruneau (2004), and Vian et al. (2009b), in order to decrease the strength and stiffness of the shear panel for consequently reducing the burden on the horizontal and vertical boundary members as well as the foundation demands, which include: i) use of light-gauge, cold-rolled, and LYP steel for infill plate (Fig. 2.13(a)), ii) placement of a pattern of perforations in the infill plate (Fig. 2.13(b)), iii) use of RBS connections at the ends of HBE members (Fig. 2.13(c)), and iv) use of steel panels with reinforced cut-out corners (Fig. 2.13(d)).

The lower yield strength of the infill plates can result in a reduced stiffness and earlier onset of energy dissipation by the panel as compared to currently available hot-rolled plates. The special perforated panel SPSW specimens with multiple regularly spaced holes have already exhibited ductile behavior during testing and are viable alternative to solid panel SPSWs which not only allow utility access through the panel but also alleviate stiffness and over-strength concerns using conventional hot-rolled plates. In addition, RBS connection is an effective detail for SPSW anchor beams which can control boundary frame yielding during a significant earthquake. Finally, the cut-out reinforced corner configuration appears to be a design option that

may allow a designer the option of sizing for a solid panel infill, but still have the benefit of access through the wall for utilities. Based on the experimental findings, some of these approaches have been recently incorporated in the AISC 341-10 (2010) design code.

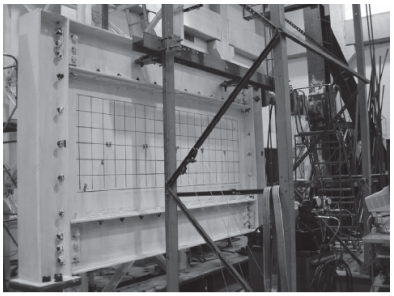

(a) Light-gauge SPSW
(Berman and Bruneau, 2003)

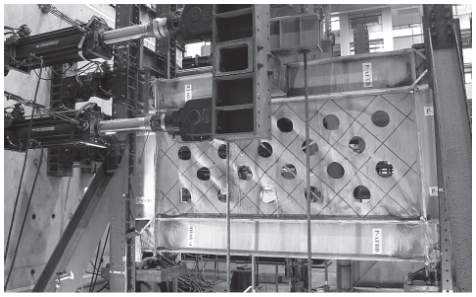

(b) Perforated panel SPSW
(Vian and Bruneau, 2004)

(c) SPSW with RBS connections
(Vian et al., 2009b)

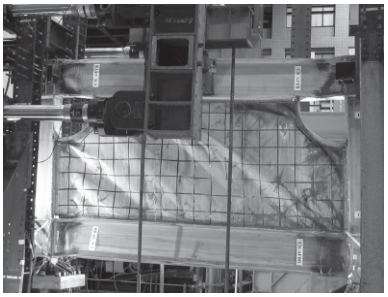

(d) SPSW with reinforced cut-out corners
(Vian and Bruneau, 2004)

Fig. 2.13 Various SPSW configurations tested by Bruneau and his research associates

In addition to the prior research on beam-attached and/or semi-supported steel shear walls, recent investigations on the design and performance of these systems have been accompanied by consideration and testing of new configurations. Fig. 2.14 shows two examples of such SPSWs studied by Kurata et al. (2012) and Jahanpour et al. (2012). As seen in the figures, in the proposed configurations, a plate with surrounding (secondary) boundary elements is installed at the middle of the bay, separate from the primary columns. The reported studies have shown the favorable behavior of such systems.

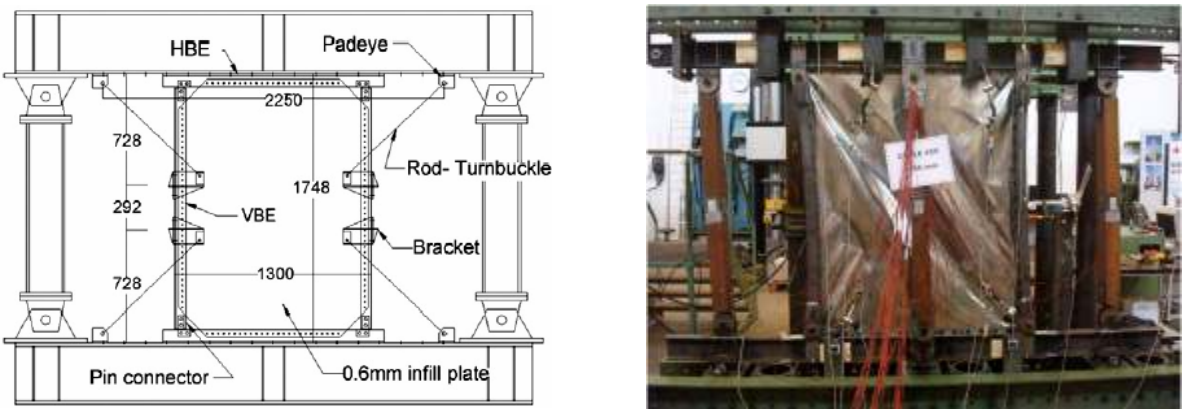

(a) SPSW tested by Kurata et al. (2012) **(b)** SPSW tested by Jahanpour et al. (2012)

Fig. 2.14 SPSW systems with beam-attached infill plates

As a result of considerable advancements in modeling techniques as well as computational mechanics in recent years, several studies on the seismic behavior of multi-story SPSWs and/or structures employing SPSW systems have been reported through detailed nonlinear response history (dynamic) analyses of 2D and 3D structural models. Some reported studies exemplary of such improvements are as follows. Kurban and Topkaya (2009b) performed a numerical study to evaluate the response modification, ductility reduction, over-strength, and displacement amplification factors for several SPSWs with various configurations and properties. Bhowmick et al. (2009b) studied the nonlinear seismic responses of some multi-story SPSWs by considering the strain rate and *P*-delta effects. Berman (2011) also reported a study on the seismic behavior of a suite of code-designed SPSWs using nonlinear response history analysis for ground motions representing different hazard levels. Such numerical studies have led to a better understanding of seismic performance of the SPSW systems.

Lately, the earthquake resistant design of structural systems has been gradually moving from simplified force-based deterministic design methods towards performance-based design techniques, with emphasis on better characterization of structural damage and on proper accounting for uncertainties involved in the design process (Ghosh et al., 2009). Accordingly, the

structural engineering community must have performance-based design procedures for SPSWs to ensure that they can meet multiple performance objectives in an efficient and economical manner (Berman et al., 2008). Hence, initial steps have been recently taken by researchers towards performance-based seismic design of SPSW systems.

Berman et al. (2010) and Baldvins et al. (2012) reported studies in which experimental data were collected for SPSW specimens from various test programs and analyzed in order to generate appropriate fragility functions for SPSWs. Fragility functions are deemed the basis for performance-based earthquake engineering, which are used to link structural and/or nonstructural damage with a structural response parameter such as story drift and/or story acceleration (Berman et al., 2010). The following twelve damage states were developed for SPSWs as a result of analysis of the collected experimental data:

- DS 1: Elastic Web Plate Buckling
- DS 2: Web Plate Yielding
- DS 3: Residual Web Plate Buckling
- DS 4: HBE and/or VBE Yielding
- DS 5: Initial VBE Local Buckling
- DS 6: Initial HBE Local Buckling
- DS 7: VBE Local Buckling Requiring Repair
- DS 8: HBE Local Buckling Requiring Repair
- DS 9: Web Plate Tearing/Cracking
- DS 10: VBE Cracking
- DS 11: HBE and HBE-to-VBE Connection Cracking
- DS 12: Connection and/or Boundary Frame Failure

These damage states were then used as a basis for identifying a series of repair states that describe repair activities required to approximately restore a SPSW to pre-earthquake strength and stiffness. Consequently, the damage states were consolidated into five final repair states, as listed below:

- RS 1: Cosmetic Repair
- RS 2: Replace Web Plate
- RS 3: VBE Repair
- RS 4: HBE and Connection Repair
- RS 5: Replace Boundary Elements or Frame

The fragility curves shown in Fig. 2.15 were finally generated for each repair state. Included in the figures are also the discrete fragility functions defined by the raw experimental data. As shown in Figs. 2.15(a) and (b), fragility curves have been generated for both seismically and nonseismically designed SPSWs. Moreover, as seen, no fragility curves were developed for RS4 due to lack of experimental data.

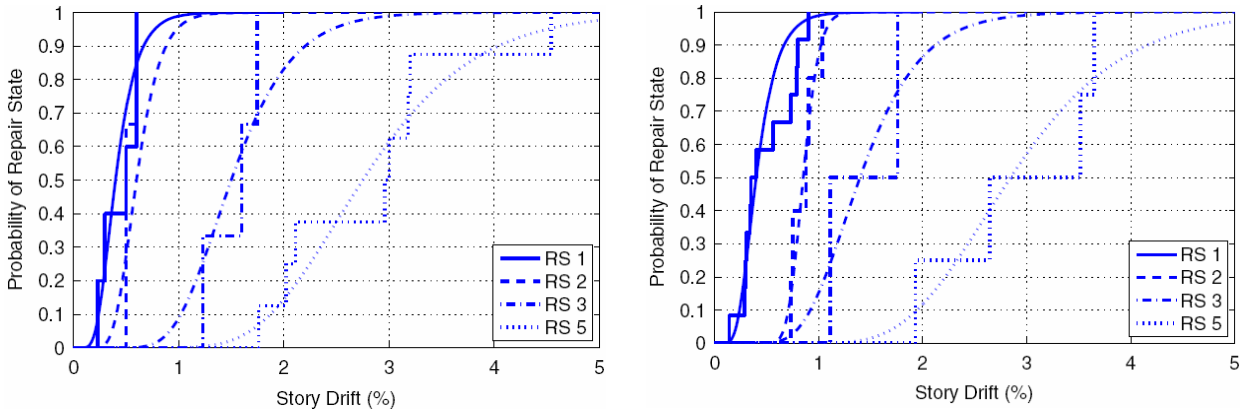

(a) SPSWs meeting certain seismic design criteria **(b)** Nonseismic design

Fig. 2.15 Recommended SPSW fragility functions by Baldvins et al. (2012)

In addition to the development of fragility functions, Ghosh et al. (2009) and Bayat (2010) has also proposed two distinct performance-based design methods for SPSW systems, whose applicability have been verified as well. Further details on these methods will be provided in Chapter 3.

2.5 Low Yield Point Steel

Vibration of buildings due to earthquake and/or wind loads can be reduced by two major methods, including i) adjusting the stiffness, and ii) improving the damping performance. Improving the damping performance of a building means fitting the building with a mechanism that artificially absorbs vibration energy, and LYP steel has been shown to be one of the most efficient damping materials (Saeki et al., 1998). Considering the main objectives of this research on the seismic performance and design of SPSWs with LYP steel infill plates, an introduction to the development and properties of LYP steel material is provided in this section.

After the 1995 Kobe earthquake in Japan, the design philosophy of structures started to switch from the conventional design to the design of seismic control structures with seismic control devices to absorb the seismic energy in a further efficient and economical manner. Nippon Steel Corporation was the first to conduct studies on seismic control structures and develop a new steel product for this application. Considering the need for workable and weldable steel products with excellent elongation as well as low cycle fatigue characteristics in devices undergoing great repeated deformations in the plastic region, LYP100 and LYP235 steel material were produced by the Nippon Steel Corporation, whose mechanical properties are given in Table 2.1. The two types of LYP steel products were developed to provide the designers with some freedom in selecting the design strength in seismic control devices. Moreover, the characteristic

of the chemical composition is that both of the LYP steels have a composition system that is nearly pure iron with very negligible carbon and alloy elements (Yamaguchi et al., 1998).

Table 2.1 Mechanical properties of LYP steel products (Yamaguchi et al., 1998)

Steel type	Yield point (MPa)	0.2% offset proof stress (MPa)	Tensile strength (MPa)	Elongation at fracture (%)
LYP100	-	80-120	200-300	≥50%
LYP235	215-245	-	300-400	≥40%

The stress-strain curves of the LYP steel along with other steel products are shown in Fig. 2.16. As seen in the figure, pure iron and LYP235 steel show clear yield points, whereas LYP100 steel shows no yield point and is low in yield strength. The yield elongation of LYP235 steel is much greater than that of SS400. Additionally, LYP steel and pure iron possess great elongation capacities.

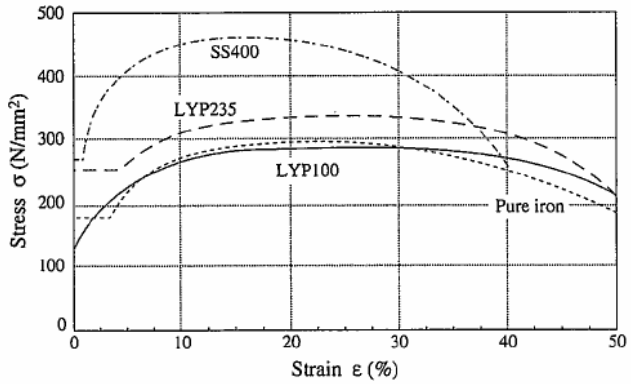

Fig. 2.16 Stress-strain curves of the LYP steel (Yamaguchi et al., 1998)

It is notable that yield strength of LYP100 steel is about one-third of the conventional structural steel such as ASTM A36 steel. Its elongation properties can exceed 40% which is more than two times of the conventional structural steel. In addition, the LYP steel possesses low yield ratio, i.e. the ratio between yield stress to ultimate stress, which is only 0.34. With such a low

yield ratio, the structure is able to redistribute the plastic stress and provide a larger inelastic zone (Chen and Jhang, 2006).

The characteristics of the base materials that affect the performance of seismic control devices using LYP steel include hysteresis characteristics, strain-rate effect, and the characteristic of low cycle fatigue since in an earthquake, the damper is repeatedly exposed to high plastic strain. Yamaguchi et al. (1998) and Saeki et al. (1998) addressed the above-mentioned characteristics and demonstrated the advantages of application of LYP steel as compared to the conventional steel material.

3. BEHAVIOR AND DESIGN OF SPSW SYSTEMS

3.1 General

This chapter provides a discussion of the behavior and design of SPSW systems. A general discussion is first made on the fundamental mechanics of unstiffened SPSWs. Design requirements and recommendations incorporated in the American standards including the FEMA 450 (2004) recommended guidelines and AISC 341 provisions for seismic design of SPSW systems are subsequently reviewed. Ultimately, performance-based seismic design of SPSW systems, as a new and efficient design methodology, is discussed.

3.2 Fundamental Mechanics of Unstiffened SPSWs

SPSWs resist lateral loads primarily through diagonal tension in the web plate and overturning forces in the adjoining columns. This behavior is demonstrated in Fig. 3.1. Web plates in such lateral force-resisting systems may be categorized in accordance with their ability to resist buckling. Unstiffened steel shear walls are the commonly-used type, which possess negligible compression strength and therefore undergo early geometrical buckling. Such systems indeed resist lateral loads through the tension field developed in the post-buckling stage.

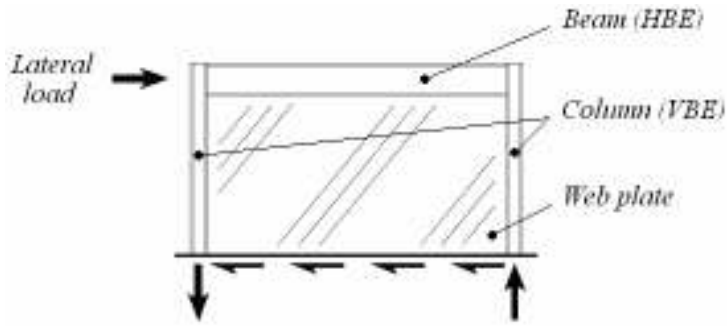

Fig. 3.1 Idealized steel shear wall behavior

This behavior is analogous to that of a braced frame as well as a stiffened plate girder. As shown in Fig. 3.2(a), in a braced frame, the braces only resist tension, the overturning forces are resisted by the columns, and the beams serve to transfer the horizontal component of the force in the brace. As well, in a plate girder, tension-field action in the web is transmitted through the transverse stiffeners, as shown in Fig. 3.2(b).

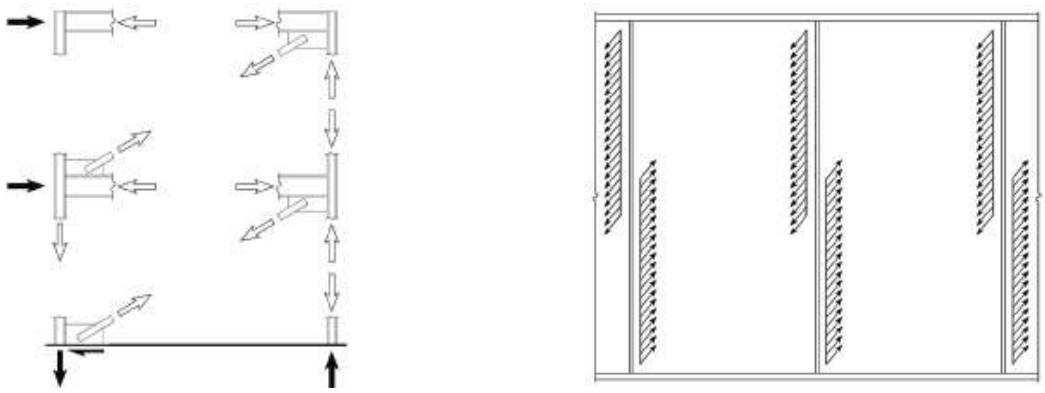

(a) Braced frame **(b)** Stiffened plate girder

Fig. 3.2 Braced frame and stiffened plate girder analogies (Sabelli and Bruneau, 2006)

It should be noted that the mechanics of SPSW behavior are distinct from both tension-only bracing and plate girders, since these are insufficient for capturing many of the aspects of SPSW behavior that must be understood in order to design the system. In SPSW systems, web plates work almost entirely in tension, the beams and columns that constitute the frame around the web plates are designed differently from the frame members of tension-only bracing, and from the flanges and stiffeners of plate girders. Hence, both of these analogies are conceptually valid, and only useful in developing a general understanding of SPSW behavior (Sabelli and Bruneau, 2006).

In a steel shear wall, the tension in the web plate acts along the length of the boundary frame members, so that large inward forces can be exerted on the horizontal and vertical boundary

frame members. Hence, the boundary frame members are designed to resist web-plate tension forces through flexure. These forces act inward on the steel shear wall at an angle determined from the frame and member section geometrical properties.

The effect of the inward forces acting on the beam in a SPSW is typically counteracted to a large degree by similar tensile forces in the web plate of the adjacent story, although these are often of different magnitudes. However, such counteracting tensile forces are not present at the top and foundation beams of a SPSW, and the design of these horizontal boundary members must include consideration of the inward forces. Thus, these members at the top story and at the foundation of a steel shear wall are typically deep with sufficient strength to anchor the tension in the web plates. Fig. 3.3 illustrates the free-body diagrams of the steel shear wall and boundary frame members, and shows the effects of web-plate tension.

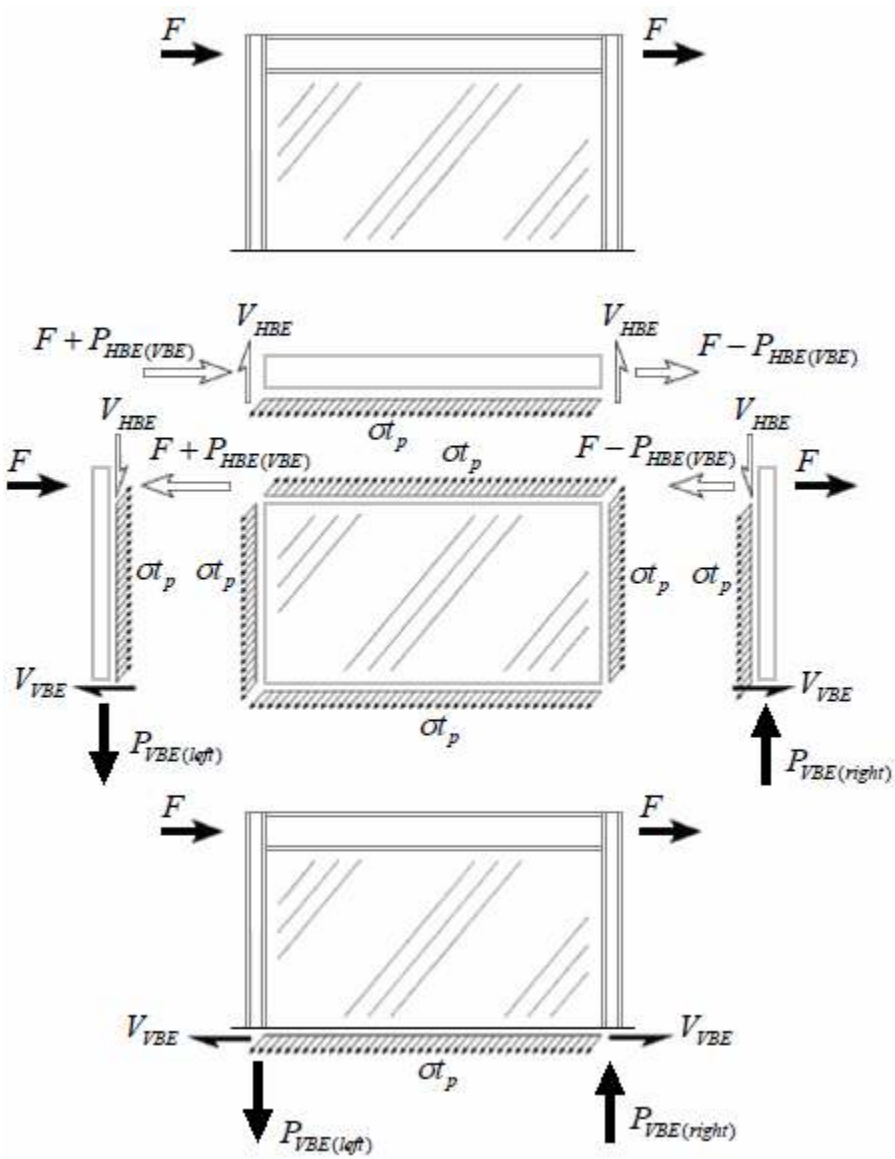

Fig. 3.3 Free-body diagrams of the web plate and boundary elements in SPSWs (Sabelli and Bruneau, 2006)

The symbols in Fig. 3.3 are as follows:

F = the applied lateral force on the wall,

$P_{HBE(VBE)}$ = the axial force applied at the end of HBE due to web-plate tension on the VBE,

P_{VBE} = the axial force reaction of the VBE,

V_{HBE} = the shear reaction of the HBE due to the web-plate tension,

V_{VBE} = the shear reaction of the VBE due to the web-plate tension,

t_p = web-plate thickness, and

σ = web-plate tension stress.

In high-seismic design of steel shear walls, it is assumed that lateral loads will be sufficient to cause tension yielding of the web plate along its full height. Thus, the web plate forces are uniform, as shown in Fig 3.3 (Sabelli and Bruneau, 2006).

As it is seen in Fig. 3.3, the tensile forces in the web plate induce flexure in the columns, in addition to the axial forces due to overturning of the wall. Therefore, in order to develop a uniform tension across the web plate and also let the web plate develop its full tension strength at the vertical interfaces with the columns, the vertical boundary frame members need to have sufficient transverse stiffness.

In addition, from Fig. 3.3 it is evident that the inward flexure of the columns is resisted by the beams at the top and bottom of the vertical boundary frame members segment. Therefore, the beams are required to resist significant compression in conjunction with the flexural forces induced by tension in the web plates.

In Fig. 3.3, it is also observed that the force at the upper-right connection is the difference between the collector force (F) and the inward reaction from the vertical boundary frame member ($P_{HBE(VBE)}$). In some conditions this will be in tension, in others it will be in compression. It is typically in tension at the top story and at levels at which the web-plate thickness is reduced by a large percentage, while in compression elsewhere. At the vertical

boundary frame member in tension, the connection is in compression and the two components are additive.

Consideration of rigid beam-to-column connections in a SPSW system will introduce additional flexural forces in the boundary frame members, which should be taken into consideration in the design of the horizontal and vertical boundary frame members.

The tension stress in the web plate is used, in conjunction with gravity loads, to define the required strength of the boundary frame members. To achieve this, the diagonal tension stress in the web plate is decomposed. Fig. 3.4 shows the stresses acting on the vertical and horizontal interfaces of the web plate. In this analysis of stresses, it is assumed that the web plate is in pure tension and that no shear or compression stresses exist on sections cut in the direction of the tension stress (Sabelli and Bruneau, 2006).

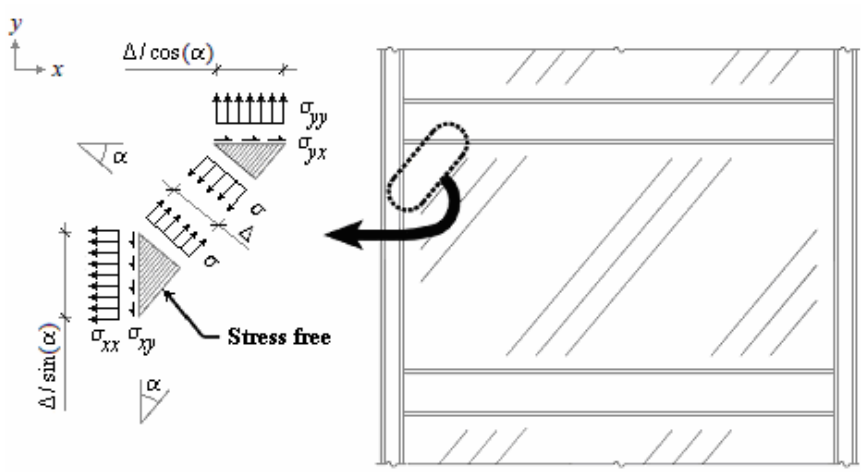

Fig. 3.4 Details of stresses imposed on SPSW boundary frame members (Sabelli and Bruneau, 2006)

Following symbols are used in Fig. 3.4:

α = angle of tension stress (measured from vertical),

Δ = width of web-plate segment under consideration,

σ_{yy} = principal stress at horizontal boundary,

σ_{yx} = shear stress at horizontal boundary,

σ_{xx} = principal stress at vertical boundary, and

σ_{xy} = shear stress at vertical boundary.

The interface stresses, i.e. σ_{yy}, σ_{yx}, σ_{xx}, and σ_{xy}, are functions of both the web-plate tension stress and the angle of tension in the web plate, equations of which are derived from statics using trigonometric functions, and presented in the following.

$$\sigma_{yy} = \sigma \cos^2(\alpha) \tag{3.1}$$

$$\sigma_{yx} = \sigma \sin(\alpha)\cos(\alpha) = \frac{1}{2}\sigma \sin(2\alpha) \tag{3.2}$$

$$\sigma_{xx} = \sigma \sin^2(\alpha) \tag{3.3}$$

$$\sigma_{xy} = \sigma \sin(\alpha)\cos(\alpha) = \frac{1}{2}\sigma \sin(2\alpha) \tag{3.4}$$

In order to apply these equations, it is necessary to determine the angle of tension stress in the web plate. The relative equation of this angle was originally derived by Thorburn et al. (1983) and later on modified by other researchers, which will be presented later in this chapter while reviewing the codified design requirements.

3.3 NEHRP Recommended Provisions (FEMA 450)

Canadian standard CAN/CSA-S16, Limit States Design of Steel Structures (CAN/CSA S16-01, 2001), has included specifications for the design of SPSWs since 1994. Similar provisions

were subsequently included in the American standard FEMA 450, NEHRP Recommended Provisions for Seismic Regulations for New Buildings and Other Structures, for the first time in 2004, in which steel shear walls are denoted as Special Steel Plate Walls (SSPWs).

FEMA 450 (2004) provides design coefficients and factors for various types of seismic-force-resisting systems, including special and composite steel shear wall systems. Accordingly, seismic response modification coefficient, R, is recommended to be taken as 7 and 6½ for respective special and composite steel shear walls. The seismic response modification coefficient reflects the degree of inelastic response expected for design-level ground motions, as well as the ductility capacity of the system. Thus, SSPWs, permitted to be designed using a value of $R = 7$, are expected to sustain multiple cycles of significant inelastic response when subjected to design-level ground motion.

According to FEMA 450 (2004), SSPWs are expected to withstand significant inelastic deformations in the webs when subjected to the forces resulting from the motions of the design earthquake. In fact, the slender unstiffened steel infill plates connected to surrounding horizontal and vertical boundary elements are designed to yield and behave in a ductile hysteretic manner during earthquakes. Also, it is noted that FEMA 450 (2004) recognizes the use of special highly ductile low yield steel having specified minimum yield in the range of 82.7 to 227.5 MPa (12 to 33 ksi) for the web plates in SSPWs.

The HBEs and VBEs adjacent to the webs shall be designed per capacity design principles to remain essentially elastic under the maximum forces that can be generated by the fully yielded webs, except that plastic hinging at the ends of HBEs is permitted. Plastic hinging at the ends of HBEs is needed to develop the plastic collapse mechanism of the system, whereas plastic hinging in the middle of HBEs, which could partly prevent yielding of the webs, is deemed

undesirable. Also, all HBEs are expected to be rigidly connected to the VBEs with moment-resisting connections able to develop the expected plastic moment of the HBEs.

Considering the similarity between FEMA 450 and AISC 341 specifications and also the focus of the current study on AISC 341 seismic provisions, the specified design requirements and recommendations are discussed in further detail in the next section.

3.4 AISC 341 Seismic Provisions

In this section, the steel shear wall seismic design provisions included in the AISC 341-05 (2005) and AISC 341-10 (2010), mostly pertaining to the subject of the current research are reviewed. It should be noted that in AISC 341, "unstiffened" and "slender-web" steel shear walls, denoted as Special Plate Shear Walls (SPSWs), are considered as the basis for the SPSW system and addressed accordingly.

Provisions for seismic design of SPSW systems were initially included in AISC 341 in 2005, which were pretty similar to those included in FEMA 450 (2004). However, in the newer version of AISC 341, i.e. AISC 341-10 (2010), these seismic provisions have been reorganized and modified in some cases. These changes have been made based on recent research works as well as the experiences gained from design of such systems, in order for further clarification of several identified aspects of the design methodology and also for efficient design of SPSW systems. In a paper, Sabelli et al. (2008) discussed the proposed changes in the seismic provisions for inclusion in AISC 341-10 (2010).

On the basis of the specifications of AISC 341-10 (2010), code-designed SPSWs are expected to provide significant inelastic deformation capacity primarily through web plate yielding and as plastic-hinge formation in the ends of HBEs. It is time and again noted that

boundary frame members in SPSWs are designed according to capacity design principles, with plate yielding providing the "fuse". In addition, webs in SPSWs shall not be considered as resisting gravity forces. HBE, VBE and intermediate boundary elements shall satisfy the ductility requirements specified for "highly ductile members", since these are anticipated to undergo significant plastic rotation (more than 0.02 rad.).

The panel design shear strength, ϕV_n (LRFD), according to the limit state of shear yielding, is determined as follows:

$$V_n = 0.42\sigma_{yp} t_p l \sin 2\alpha \tag{3.5}$$

where, $\phi = 0.90$ (LRFD), σ_{yp} is the yield stress of the infill plate, and l is the length of infill plate (clear distance between column flanges). It is noted that plastic shear strength of a panel is given by $0.50(R_y \sigma_{yp}) t_p l \sin 2\alpha$ (see Eq. (3.2)), and the nominal strength (Eq. (3.5)) is obtained by dividing this value by a system over-strength factor taken as 1.2 for steel shear walls. In the aforementioned equation, R_y is the ratio of the expected plate yield stress to the specified minimum plate yield stress, σ_{yp}. Angle of web yielding/inclination (α), which is measured relative to the vertical, can be determined by

$$\tan^4 \alpha = \frac{1 + \dfrac{t_p l_s}{2A_c}}{1 + t_p h_s \left(\dfrac{1}{A_b} + \dfrac{h_s^3}{360 I_c l_s} \right)} \tag{3.6}$$

in which, l_s is the distance between VBE centerlines, A_c is the cross-sectional area of a VBE, h_s is the distance between HBE centerlines, A_b is the cross-sectional area of a HBE, and I_c is the

moment of inertia of a VBE taken perpendicular to the direction of the web plate line. It has been demonstrated (Dastfan and Driver, 2008) that the strength of a code-designed SPSW is not substantially sensitive to the angle of inclination, and that using a single value of 40° throughout the design will generally lead to slightly conservative results.

In AISC 341-05 (2005), only VBEs were required to satisfy a certain stiffness requirement, while in AISC 341-10 (2010), both VBEs and HBEs shall meet stiffness requirements. Accordingly, VBEs shall have moments of inertia (I_c) about an axis taken perpendicular to the plane of the web, that

$$I_c \geq 0.0031 t_p h_s^4 / l_s \,, \tag{3.7}$$

and HBEs shall have moments of inertia (I_b) about an axis taken perpendicular to the plane of the web, that

$$I_b \geq 0.0031 \Delta t_p l_s^4 / h_s \,, \tag{3.8}$$

where Δt_p is the difference in web plate thicknesses above and below the horizontal boundary frame element.

Providing the stability of SPSW boundary elements is necessary for proper performance of the system. In order to fulfill this requirement, AISC 341-10 (2010) design provisions stipulate that HBEs shall be laterally braced to meet the requirements for “moderately ductile members”. As defined, moderately ductile members are expected to undergo moderate plastic rotation (0.02 rad. or less) under the design earthquake. In addition, all intersections of HBE and VBE must be braced to ensure stability of the entire panel.

In AISC 341-10 (2010) no lower and upper bounds are specified for the panel aspect ratio, l_s/h_s, while FEMA 450 (2004) and AISC 341-05 (2005) provisions limited the SPSW applicability to wall panels having aspect ratios of $0.8 < l_s/h_s \leq 2.5$.

Ultimately, in addition to the six subsections included in AISC 341-10 (2010) that follow the typical pattern, there is a newly-added section which addresses the design of two variations on the SPSW system including web plates with regular layout of circular perforations and reinforced corner cut-outs, which is of course out of scope of this research.

3.5 Performance-Based Design

Performance-based design (PBD) is a novel design methodology which offers many advantages over current code-based design methodologies. It considers the uncertainties in hazard demand and structural capacity, reliability of existing structures against future hazards, and accounts for the nonlinear and inelastic structural response. Furthermore, this design methodology can enable the engineers to balance between costs and benefits in design and construction of structures.

According to the capacity-design requirements of AISC 341, the seismic design of SPSW is based on confining ductility demands to the web plates and plastic hinges in the HBE at the VBE face. In a capacity-design method, boundary elements are designed for forces corresponding to the expected strength of the web plate. However, SPSWs have significant inelastic deformation capacity which is not utilized properly using the elastic force-based or even the capacity design provisions, available in current seismic design codes and guidelines that only implicitly incorporate this deformation capacity. In the performance-based seismic design methodology, the inelastic behavior of a lateral force-resisting system is directly and properly taken into

consideration by using pre-selected target drift and yield mechanism as key performance limit states.

In PBD methodology, performance objectives must be identified and a procedure for reliably achieving those objectives for various levels of seismic hazard must be developed. Since SPSW systems are inherently dual systems (infill plates within moment-resisting frames), yielding in different elements can be used as performance objectives for various levels of seismic demand (Berman et al., 2008). According to Berman et al. (2008), in order to develop PBD procedures for SPSWs, a full account of failure modes for conventional and innovative SPSW configurations must be taken primarily. Then, the design approach must establish a yielding hierarchy and balance the more desirable yielding mechanisms, e.g. web plates and then beams followed by columns, while restricting undesirable mechanisms from forming, e.g. beam buckling, plate tearing, etc.

One of the few developed PBD methods is an inelastic displacement-based design procedure propounded by Ghosh et al. (2009) for SPSWs with pin-connected beams. In this method, the design formulation considers the inelastic energy demand on a structural system, which is equated with the inelastic work done through the plastic deformations for a monotonic loading up to the target drift. In fact, this design procedure is based on selected "target inelastic drift" and "yield mechanism", as shown in Fig. 3.5, in which θ_p is the target plastic drift based on an assumed yield drift (θ_y), F_i is the portion of the seismic base shear induced at *i*-th level, and M_{pc} is the base column moment capacity. In development of this method, it is considered that all steel plates reach their plastic shear capacity and that plastic hinges form at both the column bases. In addition, it is also assumed that the plates and the column bases become fully plastic simultaneously, and the story drift ratios are uniform along the height of the building.

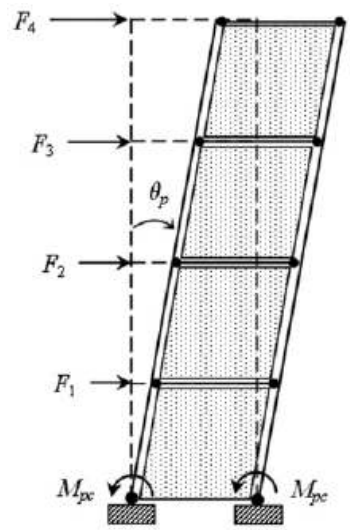

Fig. 3.5 Performance limit states in Ghosh et al.'s (2009) proposed PBD method

Ghosh et al. (2009) provided a design flowchart giving the individual design steps. They also applied this method to the design of four-story steel frame structures with different steel panel aspect ratios and showed that this method is able to achieve the target displacement ductility quite satisfactorily. However, it was concluded that this method requires further validation and modification in order to improve its applicability and performance.

A second performance-based plastic design method for SPSWs with pinned and moment-resisting HBE-to-VBE connections was recently proposed by Bayat (2010), which is similarly based on the work-energy concept. In this method, the design base shear is obtained using the "target drift" and "yield mechanism" as the main design criteria. Using the performance-based plastic design lateral force distribution, the web plates are then designed by plastic design method. After sizing of the web plates, the HBE and VBE are designed by following the capacity design procedure. The selected yield mechanisms for SPSW systems with pinned as well as moment-resisting HBE-to-VBE connections are shown in Figs. 3.6(a) and (b), respectively, in which Δp is the plastic deflection at the top story.

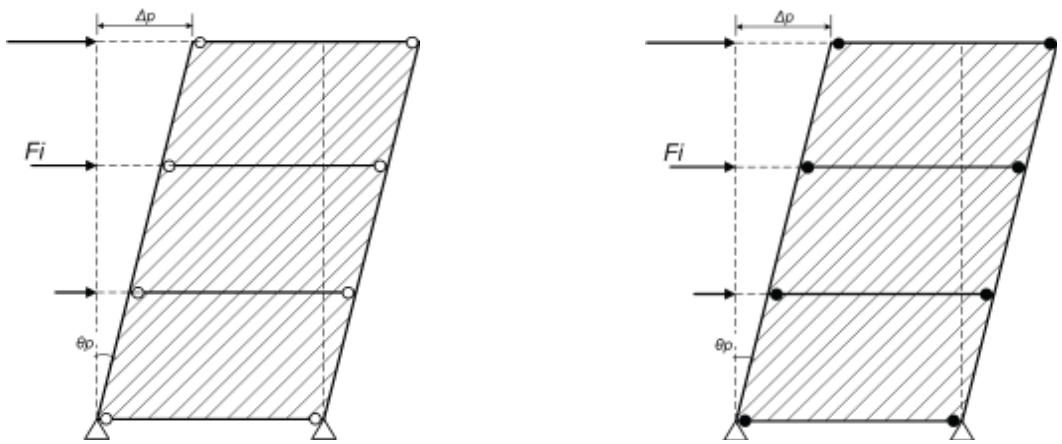

(a) Pinned HBE-to-VBE connection *(all plates become fully yielded)*

(b) Moment-resisting HBE-to-VBE connection *(all plates and HBE ends become fully yielded)*

Fig. 3.6 Selected yield mechanisms in Bayat's (2010) proposed PBD method

This method was applied in design of a 4-story SPSW frame, and it was shown that the proposed performance-based plastic design procedure works very well for design of these systems. Also, the PBD-designed frames showed improved performance compared to the code-designed SPSW frame. According to Bayat (2010), the PBD procedure can be extended to the design of coupled SPSW and dual lateral force-resisting systems in the next step of research.

In spite of the reported studies and design procedures proposed for the performance-based seismic design of SPSW systems, as noted in Chapters 2 and 3, much research work is still required to develop reliable PBD guidelines and codified design provisions for such efficient lateral force-resisting systems. Furthermore, it is important to note that performance-based seismic design and evaluation requires fragility functions to enable engineers to predict the damage state of a structure following an earthquake as well as the economic impact of repairing the structure (Lowes and Li, 2009). Hence, application of the fragility methodology, as adopted in this research, is believed to provide the engineers with powerful design tools in performance-based earthquake engineering.

4. STUDY OF BUCKLING, YIELDING, AND CYCLIC BEHAVIORS OF STEEL SHEAR PANELS

4.1 Introduction

Structural stability and performance of steel plates are characterized by geometrical buckling and material yielding, which are two independent phenomena that may interact with each other. Based on the material and geometrical properties, material yielding may occur either before or after or even at the same time as buckling (Alinia et al., 2009).

Based on their slenderness parameter as well as buckling and yielding behavior, steel plates may be quantitatively and qualitatively divided into slender, moderate, and stocky categories. Slender plates undergo elastic buckling and then yield in post-buckling stage. These type of plates have low buckling capacity and large post-buckling reserve. Stocky plates, on the other hand, yield first and then undergo inelastic buckling and have some post-yield reserve, while moderate plates undergo simultaneous buckling and yielding, and neither have post-buckling nor post-yield reserves (Gheitasi and Alinia, 2010).

From point of view of their application in SPSW systems and also by considering their buckling and yielding behavior, thin and thick plates offer essentially disparate structural and economical characteristics. Thin plates are economically viable components; however, they possess relatively low buckling strength and weak energy absorption as well as serviceability characteristics. Thick plates, on the other hand, have comparatively higher buckling as well as energy dissipation capacities and improved serviceability characteristics, while economically are considered to be disadvantageous. Nowadays, use of LYP steel plates with extremely low yield strength as well as high ductility and elongation properties makes it possible to somewhat

balance between structural and economical considerations and consequently design relatively cost-effective SPSWs with high buckling and energy dissipation capacities and also improved serviceability characteristics. LYP steel shear panels may indeed undergo early material yielding followed by inelastic geometrical buckling. Such efficient stiffening and damping components have been demonstrated to be quite favorable based on their superior characteristics and performance.

In order for efficient design and application of LYP steel shear panels, it is important to determine the limiting thickness corresponding to simultaneous geometrical buckling and material yielding. In fact, this is believed to consequently serve as an effective parameter in seismic design of infill plates as the primary lateral force-resisting and energy dissipating components in SPSW systems. On this basis, the limiting thicknesses of LYP steel plates with various support and loading conditions are determined theoretically in this chapter, which is, in turn, followed by numerical verification of the theoretical predictions. In addition, advantages of use of LYP steel as compared to the conventional steel are also addressed along with other case studies. Ultimately, the limiting plate thicknesses in SPSW systems are determined and the accuracy of the results is verified via nonlinear finite element analyses.

4.2 Determination of Limiting Plate Thickness

Theoretical determination of the limiting thicknesses of simply supported and clamped plates subjected to shear and/or compressive loads is discussed in this section. Fig. 4.1 shows flat plates under pure shear, pure and uniform compression as well as combination of the two in-plane loadings, where l and h are the respective length and height of the plates.

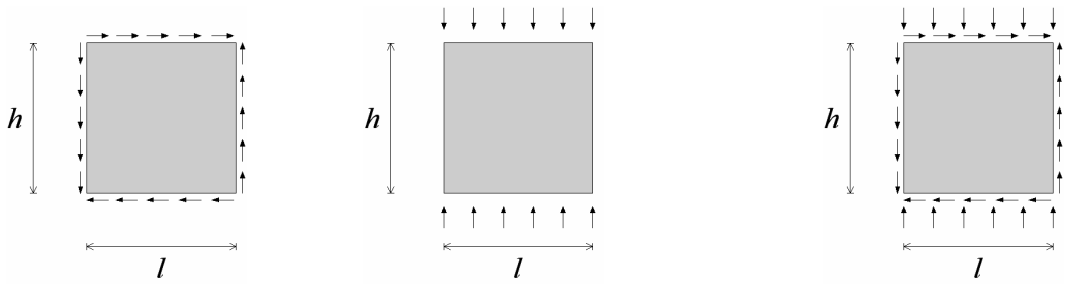

(a) Pure shear **(b)** Pure compression **(c)** Combined shear and compression

Fig. 4.1 Plates under different in-plane loading conditions

The critical stress of rectangular plates under the action of shearing stresses uniformly distributed along the edges (Fig. 4.1(a)) is given by

$$\tau_{cr} = \frac{k_s \pi^2 E}{12(1-\nu^2)} \times \left(\frac{t_p}{b}\right)^2 \tag{4.1}$$

where, E and ν are Young's modulus and Poisson's ratio, respectively, t_p is the plate thickness, and k_s is the elastic shear buckling coefficient which is $k_s = 5.34 + 4.0/(a/b)^2$ for simple and $k_s = 8.98 + 5.6/(a/b)^2$ for clamped support conditions. It should be noted that $a = \max(l, h)$ and $b = \min(l, h)$.

The critical stress of rectangular plates uniformly compressed in one direction (Fig. 4.1(b)) is also expressed by

$$\sigma_{cr} = \frac{k_c \pi^2 E}{12(1-\nu^2)} \times \left(\frac{t_p}{l}\right)^2 . \tag{4.2}$$

k_c in Eq. (4.2) can be determined from the figures and tables presented in stability books for various support conditions, e.g. Timoshenko and Gere (1961) and Brush and Almroth (1975). However, for simply supported plates $k_c = [(ml/h) + (h/ml)]^2$ may also be applied, in which m is the wavelength parameter.

Chen et al. (2009) developed a concise formula (Eq. (4.3)) for the critical buckling stresses of simply supported rectangular plates under combined biaxial compression and shear, as shown in Fig. 4.2.

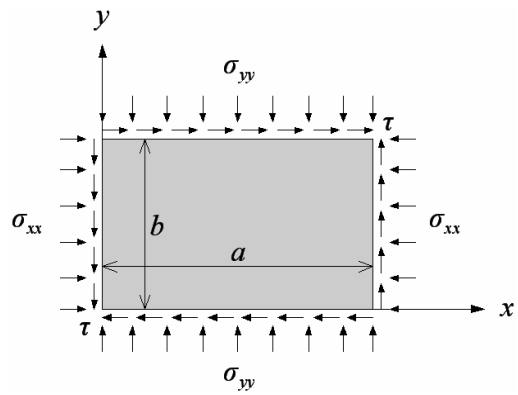

Fig. 4.2 Plate under combined shear and compressive loads as per Chen et al. (2009)

$$\left(\frac{\sigma_{xx}}{\sigma_{xx,cr}}\right)^{\alpha}+\left(\frac{\sigma_{yy}}{\sigma_{yy,cr}}\right)^{\beta}+\left(\frac{\tau}{\tau_{cr}}\right)^{\gamma}=1.0 \tag{4.3}$$

In the above interaction equation, $\alpha=1$, $\gamma=2$,

$$\beta=\begin{cases}1, & 1\le a/b\le\sqrt{2}\\ (a/b)^{\left(1-(\tau/\tau_{cr})^2\right)}, & a/b>\sqrt{2}\end{cases}, \tag{4.4}$$

and $\sigma_{xx,cr}$, $\sigma_{yy,cr}$, and τ_{cr} are the respective critical stresses for pure compression in *x*-direction, pure compression in *y*-direction, and pure shear, which can be determined by using the classical equations.

Concurrent geometrical-material bifurcation will occur when the plate critical shear stress is equal to the plate shear yield stress (τ_{yp}). The plate shear yield stress may be determined by considering the von Mises yield criterion as

$$(\sigma_{xx}-\sigma_{yy})^2+\sigma_{yy}^2+\sigma_{xx}^2+6\tau_{xy}^2=2\sigma_{yp}^2 \tag{4.5}$$

in which, σ_{xx}, σ_{yy}, and τ_{xy} are the in-plane normal and shear stresses, and also σ_{yp} is the plate yield stress. In order to obtain a general expression for the shear yield stress of a plate subjected to shear and uniaxial compressive loads representing the effects of lateral as well as vertical ground motion and/or gravity loads while used as a lateral force-resisting element in SPSW systems and as shown in Fig. 4.1(c), it is assumed that $\sigma_{xx} = 0$ and $\sigma_{yy} = \sigma_c$, and also $\tau_{xy} = \tau_{yp}$, where σ_c denotes the vertical uniformly-distributed compressive stress. By substituting the corresponding stress components into Eq. (4.5), τ_{yp} can be generally expressed as

$$\tau_{yp} = \sqrt{\frac{\sigma_{yp}^2 - \sigma_c^2}{3}} \,. \tag{4.6}$$

In this study, two cases are considered as follows. First, plates are assumed to be subjected to pure shear, i.e. $\sigma_c = 0$, which results in

$$\tau_{yp} = \frac{\sigma_{yp}}{\sqrt{3}} \,. \tag{4.7}$$

Second, plates are also assumed to be subjected to combined shear and compressive loads, where compressive load is considered to be proportional and literally 50% of the shear load, i.e. $\sigma_c = 0.5\tau_{yp}$, which in turn results in

$$\tau_{yp} = \frac{\sigma_{yp}}{\sqrt{3.25}} \,. \tag{4.8}$$

Ultimately, in order to obtain the limiting thickness of a plate under pure shear, Eq. (4.1) is set equal to Eq. (4.7), while for a plate subjected to combined shear and compressive loads τ in Eq. (4.3) is substituted by the τ_{yp} expression in Eq. (4.8). Properties of the LYP steel plates

considered in this study are summarized in Table 4.1. E, ν, and σ_{yp} are taken as 200000 MPa, 0.3, and 100 MPa, respectively, in theoretical calculations. Highlighted rows in Table 4.1 are indicative of the moderate plates.

Table 4.1 Specifications of plate models

Model	$l \times h \times t_p$ (mm)	Load	Support	Type	h/t_p
P1	2000×3000×13.4	Pure Shear	Simple	Moderate	224
P2	3000×3000×11.7	Pure Shear	Simple	Slender	256
P3	3000×3000×17.5	Pure Shear	Simple	Moderate	171
P4	3000×3000×23.3	Pure Shear	Simple	Stocky	129
P5	4500×3000×20.1	Pure Shear	Simple	Moderate	149
P6	2000×3000×10.6	Pure Shear	Clamped	Moderate	283
P7	3000×3000×9.3	Pure Shear	Clamped	Slender	323
P8	3000×3000×14.0	Pure Shear	Clamped	Moderate	214
P9	3000×3000×18.7	Pure Shear	Clamped	Stocky	160
P10	4500×3000×15.8	Pure Shear	Clamped	Moderate	190
P11	2000×3000×15.8	Shear & Compression	Simple	Moderate	190
P12	3000×3000×15.1	Shear & Compression	Simple	Slender	199
P13	3000×3000×22.7	Shear & Compression	Simple	Moderate	132
P14	3000×3000×30.3	Shear & Compression	Simple	Stocky	99
P15	4500×3000×28.4	Shear & Compression	Simple	Moderate	106
P16	2000×3000×12.2	Shear & Compression	Clamped	Moderate	246
P17	3000×3000×10.9	Shear & Compression	Clamped	Slender	275
P18	3000×3000×16.4	Shear & Compression	Clamped	Moderate	183
P19	3000×3000×21.9	Shear & Compression	Clamped	Stocky	137
P20	4500×3000×19.5	Shear & Compression	Clamped	Moderate	154

As it is seen in Table 4.1, consideration of the compressive load in addition to the shear load increases the limiting thicknesses of both simply supported and clamped plates. This is because compression basically lowers the buckling load and in order to impose the concurrent geometrical-material bifurcation condition, the corresponding plate thickness has to be increased to compensate for the loss of buckling strength.

4.3 Finite Element Analysis and Discussion of Results

4.3.1 Elastic Buckling Analysis and Convergence Studies

Linear eigen buckling analysis option of the finite element software, ANSYS 11.0 (2007), is incorporated to determine the elastic critical load of plates. Shell63 element is used for the linear/elastic buckling analysis. This four-node elastic element with six degrees of freedom at each node has both bending and membrane capabilities. Uniformly distributed shear and compressive loads are applied along the middle plane of the edge nodes, and the corner nodes are given half the value of the middle ones. Details of the boundary conditions applied in modeling and analysis of simply supported and clamped plates are illustrated in Fig. 4.3.

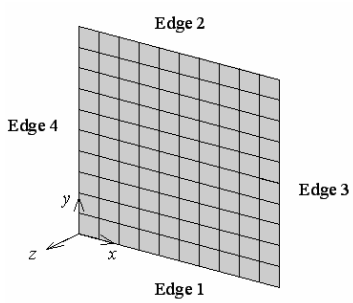

Simply Supported

Edge	Ux	Uy	Uz	ROTx	ROTy	ROTz
1	●	●	●		●	
2			●		●	
3			●	●		
4			●	●		

Clamped

Edge	Ux	Uy	Uz	ROTx	ROTy	ROTz
1	●	●	●	●	●	
2			●	●	●	
3			●	●	●	
4			●	●	●	

Note: ● Constrained

Fig. 4.3 Plate support conditions

In order to ensure high accuracy in modeling and analysis, convergence and mesh refinement studies are initially performed. Plate models P3 and P8 are selected as two typical cases for convergence and sensitivity analysis. Fig. 4.4 shows the variation of percentage discrepancy between the numerical and theoretical values for different numbers of incorporated elements.

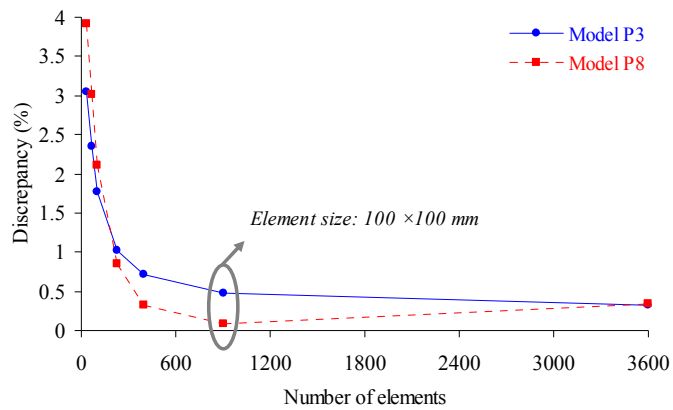

Fig. 4.4 Convergence study and validity of results

As seen in the figure, both models with mesh refinement of 100×100 mm elements produce results which are well-correlated with the theory. This is therefore taken as the minimum requirement in the analyses. The theoretical as well as numerical predictions of elastic buckling loads of the plate models are also tabulated in Table 4.2.

Table 4.2 Theoretical and numerical elastic buckling loads of plates

Model	$P_{cr-Theoretical} = \tau_{cr} \times lt_p$ (kN)	$P_{cr-Numerical}$ (kN)	Discrepancy (%)
P1	1550.05	1532.98	1.1
P2	902.31	898.05	0.5
P3	3019.34	3005.10	0.5
P4	7126.32	7092.60	0.5
P5	5231.42	5182.20	0.9
P6	1234.57	1227.02	0.6
P7	706.63	707.19	0.1
P8	2410.61	2412.54	0.1
P9	5744.71	5749.20	0.1
P10	4088.55	4075.11	0.3
P11	1753.19	1718.84	2.0
P12	1112.12	1097.58	1.3
P13	3779.55	3729.00	1.3
P14	8990.01	8868.30	1.4
P15	7076.59	6772.95	4.3
P16	1354.91	1337.30	1.3
P17	799.52	768.24	3.9
P18	2723.22	2616.72	3.9
P19	6484.59	6231.00	3.9
P20	4855.01	4681.80	3.6

From the table, it is evident that agreement between theoretical and numerical predictions is quite satisfactory. Also, it is noted that predictions of Eq. (4.3), which was originally developed for simply supported plates, are pretty close to the numerical results in cases of both simple and clamped support conditions and the discrepancy is below 5% in all cases. Lastly, the typical first buckling mode shapes of simply supported (P3) and clamped (P8) plate models under pure shear are shown in Fig. 4.5.

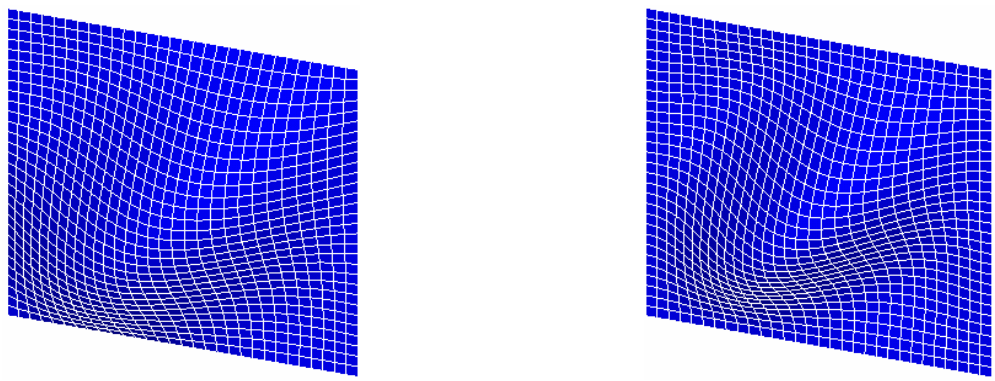

(a) Model P3 **(b)** Model P8

Fig. 4.5 Typical first buckling mode shapes

4.3.2 Nonlinear Buckling Analysis

The nonlinear large deflection static analysis of ANSYS 11.0 (2007) is used for nonlinear buckling analysis of plates. Shell181 element is used for nonlinear analysis. This four-node element with six degrees of freedom at each node is suitable for analyzing thin to moderately-thick shell structures and is also well-suited for linear, large rotation, and/or large strain nonlinear applications.

LYP100 steel material with a bilinear stress-strain relation is adopted for nonlinear buckling analyses. Material properties are consistent with those applied in theoretical calculations as noted in Section 4.2, and the tangent modulus (E_t) is taken as 3333.3 MPa. Moreover, the von Mises

yield criterion is used for material yielding, and the isotropic hardening rule is also incorporated in the nonlinear pushover analyses.

In order to initiate buckling and consider the effect of initial imperfections, a very small out-of-plane force of about 0.01% of plate elastic buckling capacity is applied at the center of the plate, which is consistent with the first buckling mode shape of the plate.

Geometrical and material nonlinearities of plates are included in the analyses, and the arc-length method is implemented to achieve a fast convergence and capture the unloading behavior of the plate. The load versus out-of-plane displacement curves of the slender, moderate, and stocky plates with various support and loading conditions, obtained from the nonlinear buckling analyses are shown in Fig. 4.6.

From the figures, it is evident that regardless of support and loading conditions, the slender plates experience elastic buckling and continue to absorb more load beyond their buckling capacity up to the ultimate load which is in turn followed by softening. Moderate plates with the theoretically-predicted limiting thicknesses, on the other hand, undergo simultaneous buckling and yielding which is followed by sudden stiffness loss, while the stocky plates yield first and then undergo post-yield plastic buckling which is considerably below their elastic critical loads. These results demonstrate that the limiting plate thickness is accurately determined theoretically in all considered cases.

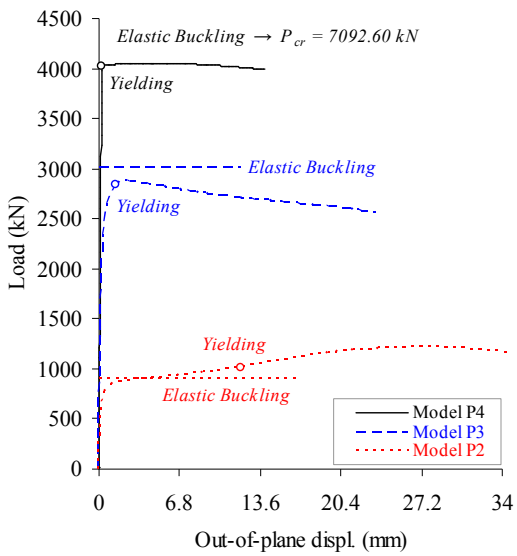

(a) Pure shear and simply supported

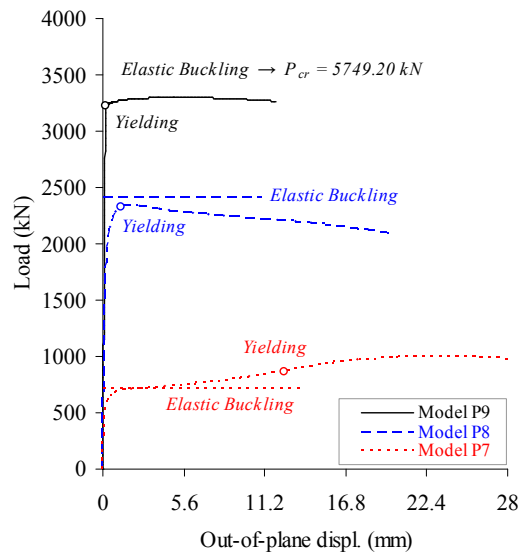

(b) Pure shear and clamped

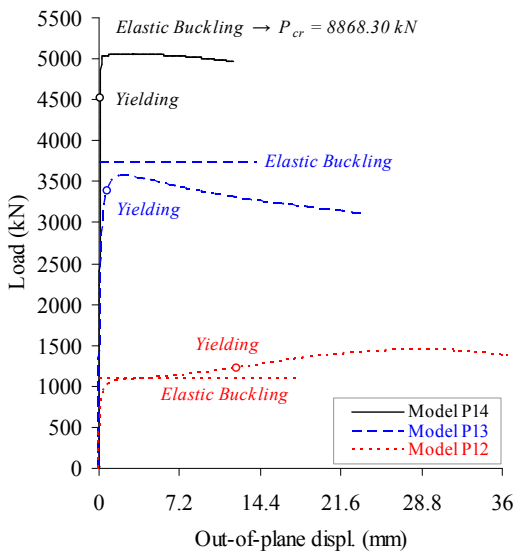

(c) Combined S&C and simply supported

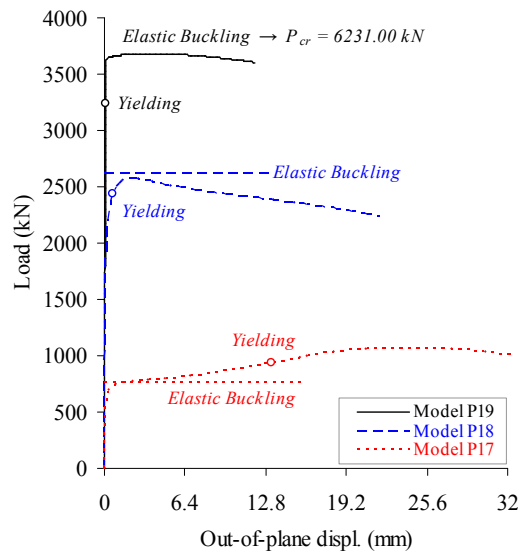

(d) Combined S&C and clamped

Fig. 4.6 Load vs. out-of-plane displacement curves of plates

The load versus in-plane lateral displacement curves of the clamped plates under pure shear as well as combined shear and compression are also shown in Fig. 4.7.

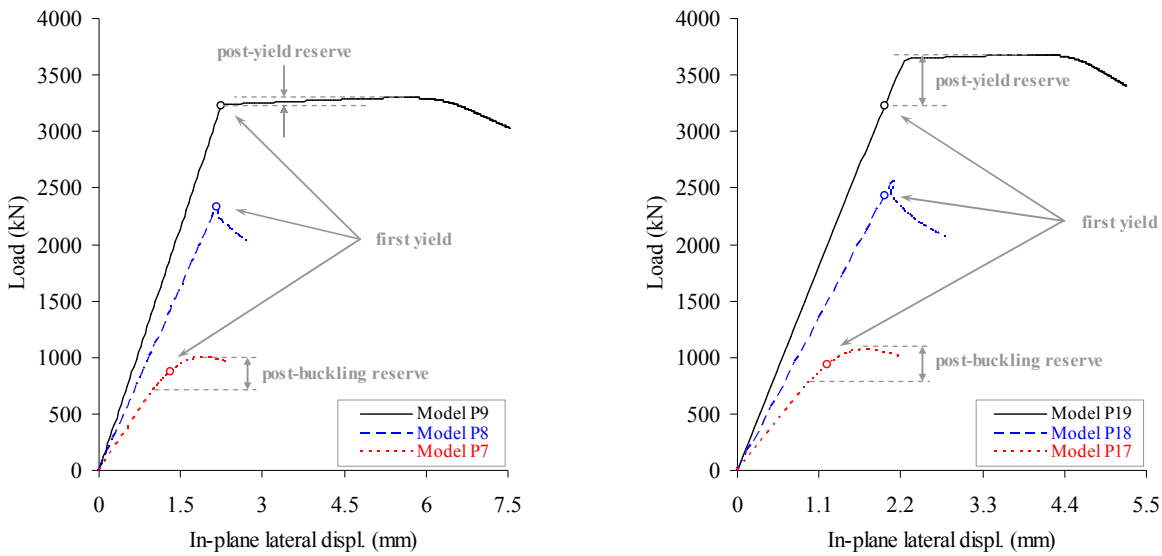

(a) Pure shear and clamped **(b)** Combined S&C and clamped

Fig. 4.7 Load vs. in-plane lateral displacement curves of plates

From Figs. 4.6 and 4.7, it is evident that slender plates possess post-buckling reserve, and stocky plates exhibit some post-yield strength, whereas moderate plates exhibit neither post-buckling nor post-yield reserves. Slender plate models P2, P7, P12, and P17 (refer to Table 4.1) possess 26%, 29%, 24%, and 28% post-buckling reserve, respectively, which indicates that consideration of compressive load slightly reduces the post-buckling reserve. On the other hand, stocky plate models P4, P9, P14, and P19 (refer to Table 4.1) possess 1%, 2%, 10%, and 12% post-yield reserve, respectively, which demonstrates that consideration of compressive load results in considerable increase in post-yield reserve.

Theoretical and numerical predictions of the in-plane lateral displacement and shear load corresponding to the first yield point of moderate and stocky plates, i.e. δ_y and P_y, are tabulated and compared in Table 4.3.

Table 4.3 Comparison of theoretical and numerical results of first yield point properties

Plate	Theoretical		Numerical		Num. / Theo. Ratio	
	$\delta_y = (\tau_{yp}/G)\times h$	$P_y = \tau_{yp}\times lt_p$	δ_y	P_y		
	(mm)	(kN)	(mm)	(kN)	Displ.	Load
P1	2.252	1547.30	2.138	1468.68	0.95	0.95
P3	2.252	3031.09	2.111	2841.32	0.94	0.94
P4	2.252	4035.68	2.242	4018.83	1.00	1.00
P5	2.252	5222.13	2.098	4864.85	0.93	0.93
P6	2.252	1223.98	2.197	1193.73	0.98	0.98
P8	2.252	2424.87	2.162	2327.41	0.96	0.96
P9	2.252	3238.94	2.242	3224.92	1.00	1.00
P10	2.252	4104.96	2.148	3915.11	0.95	0.95
P11	2.163	1752.85	1.998	1586.93	0.92	0.91
P13	2.163	3777.51	1.993	3378.36	0.92	0.89
P14	2.163	5042.22	2.002	4528.75	0.93	0.90
P15	2.163	7089.07	1.960	6133.29	0.91	0.87
P16	2.163	1353.47	2.023	1240.77	0.94	0.92
P18	2.163	2729.12	1.987	2433.54	0.92	0.89
P19	2.163	3644.38	1.939	3171.30	0.90	0.87
P20	2.163	4867.49	1.980	4254.03	0.92	0.87

Despite the presence of the nonlinearities in finite element analyses and also the approximations in theoretical calculations, theoretical and numerical predictions of the plate first yield point characteristics match fairly closely in almost all cases, as shown in Table 4.3. It is noted that the accentuated discrepancy between the theoretical and numerical results in case of plates under combined shear and compression is because of presence of the compressive load which results in higher geometrical nonlinearities by augmenting the out-of-plane deformations.

Ultimately, the von Mises stress contour plots of the clamped plates under pure shear at their respective ultimate strengths are shown in Fig. 4.8. In the figure, the plate side facing the positive *z*-direction (refer to Fig. 4.3) is called as the "external" face, and the other side is alternatively called as the "internal" face.

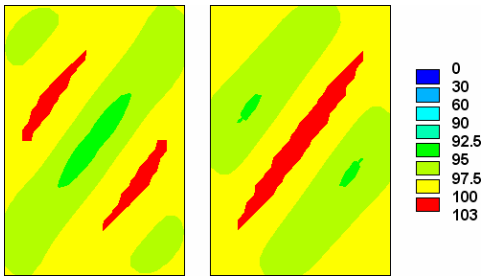

(a) Model P6 (2000×3000×10.6, Moderate)

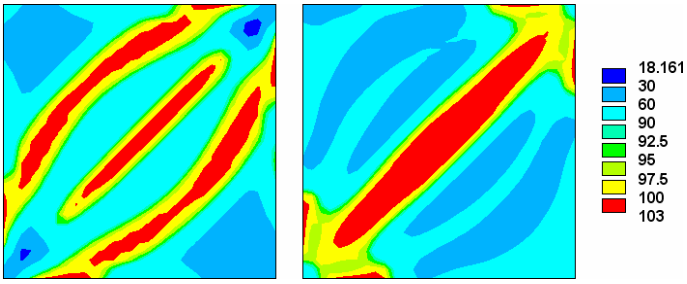

(b) Model P7 (3000×3000×9.3, Slender)

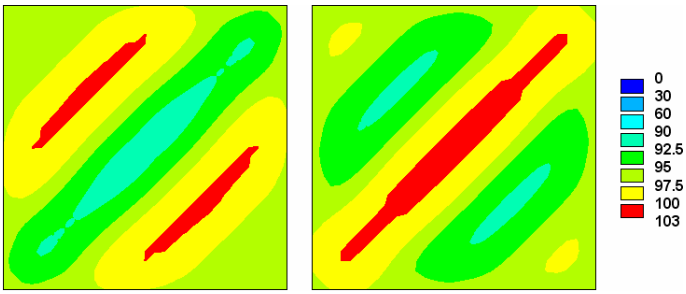

(c) Model P8 (3000×3000×14.0, Moderate)

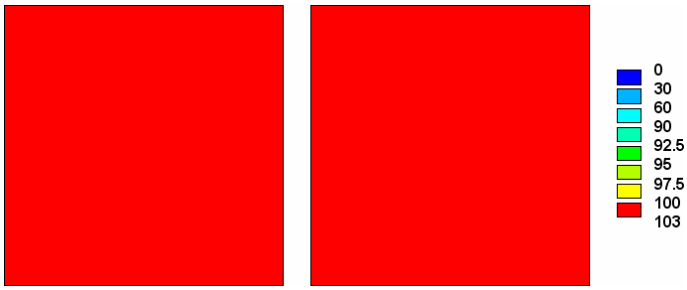

(d) Model P9 (3000×3000×18.7, Stocky)

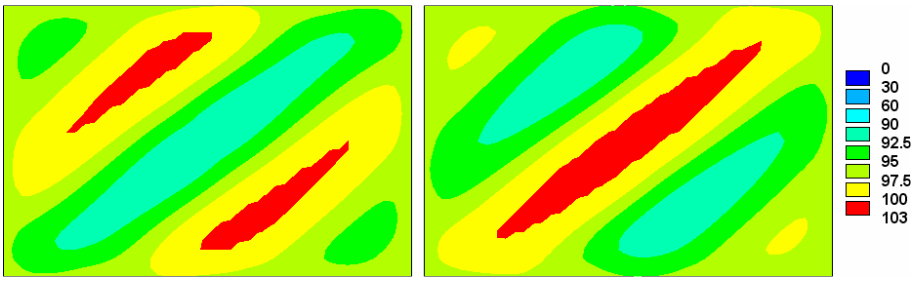

(e) Model P10 (4500×3000×15.8, Moderate)

Fig. 4.8 von Mises stress contour plots at ultimate strengths of various plates: external face (left) and internal face (right)

Formation of diagonal tension field and consequently diagonal yielding is clearly observed in the figures. Moderate plate models P6, P8, and P10 with various aspect ratios by and large possess similar stress contours and yielding patterns. Respective slender, moderate, and stocky plate models P7, P8, and P9, on the other hand, exhibit utterly distinct stress contours, stress levels, and yielding patterns. It is clearly observed that all points on both faces of the stocky plate model P9 (Fig. 4.8(d)) reach the yield stress at the ultimate strength, while only some points on either faces of the slender plate model P7 (Fig. 4.8(b)) reach the yield stress at its ultimate strength. In fact, this is of great importance in efficient design of lateral force-resisting and energy dissipating shear panels in the light of use of LYP steel, since first, this results in early yielding of panel and dissipating most of seismic energy through plastic deformation which consequently decreases the amount of the absorbed energy by the other structural components, e.g. frame members, and second, larger amount of yielded points is indicative of effective and optimal use of LYP steel panels as damping elements in SPSW systems.

4.3.3 Cyclic Analysis of Plates with Two and Four Restrained Edges

Hysteresis behavior of 3000×3000×9.3, 3000×3000×14.0, and 3000×3000×18.7 mm plates with four clamped as well as two clamped-two free edges under shear loading is studied via nonlinear finite element analysis using ANSYS 11.0 (2007) software. Kinematic hardening rule is used in the analysis of the plates under cyclic loading. Moreover, both geometrical and material nonlinearities are included in the analyses.

The finite element analysis, in this study, is performed in a displacement-controlled manner. The in-plane shear load is transferred into the plate by applying displacements to the nodes located on the upper edge of the plate, i.e. edge 2 in Fig. 4.3. Furthermore, clamped support

conditions are applied on either all four edges or just two upper and lower edges, i.e. edges 1 and 2 in Fig. 4.3, while the other two edges are left unrestrained.

The time history of displacement applied to the models as well as the hysteresis shear load-displacement curves of the three plates with the two different support conditions are shown in Fig. 4.9.

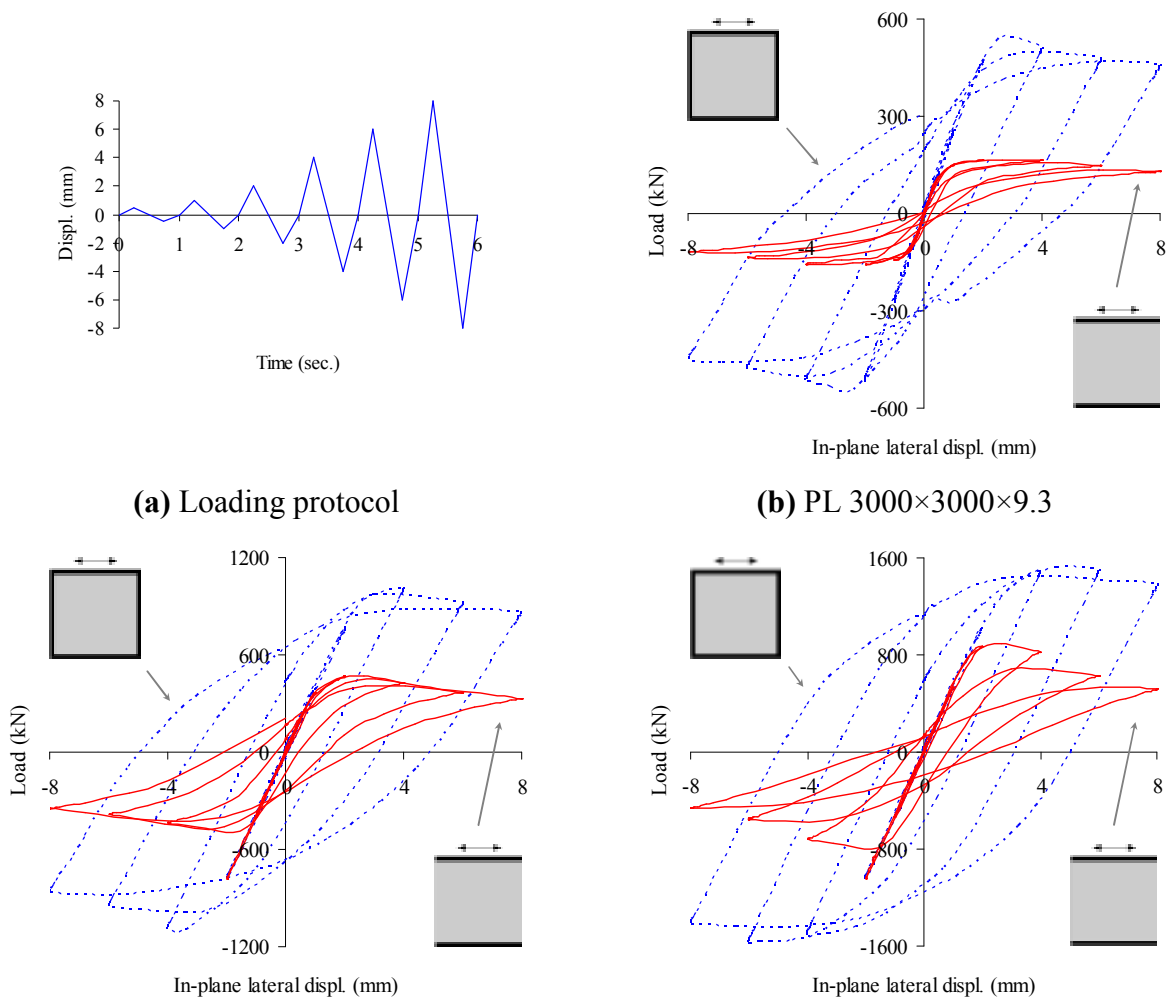

(a) Loading protocol

(b) PL 3000×3000×9.3

(c) PL 3000×3000×14.0

(d) PL 3000×3000×18.7

Fig. 4.9 Cyclic loading and hysteresis behaviors of plates with two and four clamped edges

As seen in Fig. 4.9, despite the identical initial stiffnesses of plates with equal thicknesses and different support conditions, stiffness and strength of plates with two clamped edges tend to

diminish considerably at higher levels of loading. Furthermore, compared to plates with all four clamped edges, plates with two clamped edges exhibit relatively weak cyclic behavior accompanied by pinching of the hysteresis loops, which is of course remarkably pronounced as the slenderness of the plate increases. Cumulative dissipated energy (CDE) curves of the plate models are also given in Fig. 4.10.

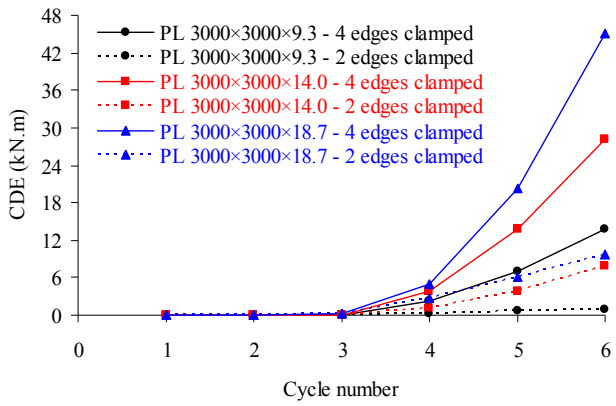

Fig. 4.10 Cumulative dissipated energy

From the figure, it is quite evident that dissipated energy increases as the plate thickness increases and results in better inelastic performance with less pinching effect. However, it is observed that plates with two clamped edges possess relatively lower energy absorption capacity in comparison with those clamped at all four edges.

Weak stiffness and strength performance, and reduced energy dissipation capacity of plates with two clamped edges is directly related to the large out-of-plane deformations which occur from early stages of loading and increase considerably at higher levels of loading due to the presence of the two unrestrained edges. This is clearly illustrated in Fig. 4.11, where out-of-plane displacement contour plots of 3000×3000×14.0 mm plate with the two support conditions are compared at 8.00 mm in-plane lateral displacement.

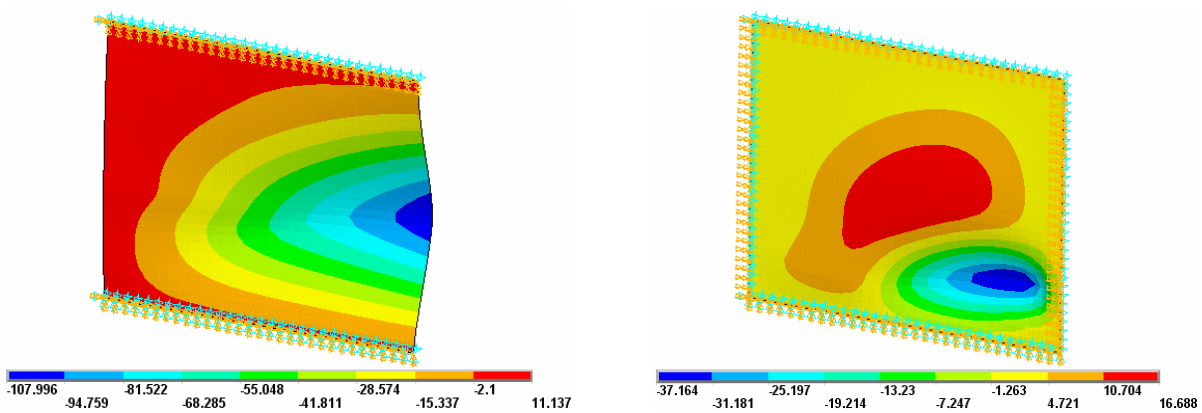

(a) Two edges clamped **(b)** Four edges clamped

Fig. 4.11 Out-of-plane displacement contour plots of PL 3000×3000×14.0 at 8.00 mm in-plane lateral displacement

From Fig. 4.11, it is evident that out-of-plane deformations at the given in-plane lateral displacement in plate with two clamped edges are much larger than those in plate with all four clamped edges. These deformations may be effectively controlled and/or limited by local stiffening in lieu of complete restraining of the two vertical edges. This issue is of great significance in design and application of beam-attached infill panels in SPSW systems, which requires further research and detailed investigation.

4.4 Effects of Use of LYP Steel and Aspect Ratio on Limiting Plate Thickness

The limiting thickness of a plate is a function of its material and geometrical properties. Hence, the amounts of effectiveness of the steel material type and plate aspect ratio on the required limiting plate thickness are evaluated in this section.

ASTM A36 steel with σ_y = 250 MPa is generally the preferred material standard for plates. ASTM A572 Gr. 50 steel with σ_y = 345 MPa, on the other hand, is quite common for structural components with plates thicker than ¾ in or 19.05 mm (Zoruba and Liddy, 2007). In addition,

LYP100 steel with $\sigma_y \approx 100$ MPa is developed for seismic control structures with high energy absorption capacity. The advantages of use of LYP100 steel compared to the two aforementioned conventional steel types are demonstrated in Fig. 4.12. As shown in the figure, $b/t_{p-limit}$ slenderness ratios of simply supported and clamped plates are calculated for broad range of a/b aspect ratios for the three steel material types, where $t_{p-limit}$ is the limiting plate thickness.

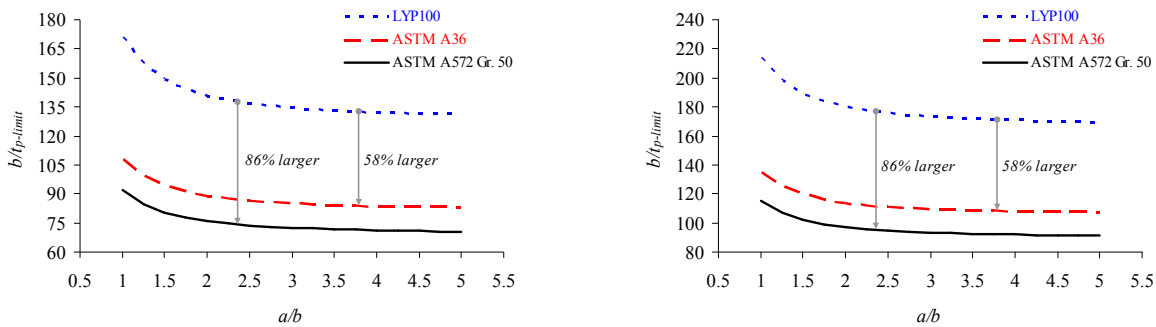

(a) Simply supported **(b)** Clamped

Fig. 4.12 Effect of use of LYP steel on the required limiting plate thickness

As seen, application of LYP100 steel in both support conditions results in 58% and 86% larger $b/t_{p-limit}$ slenderness ratios relative to the application of ASTM A36 and A572 Gr. 50 steel material, respectively. Larger $b/t_{p-limit}$ slenderness ratio implies smaller limiting plate thickness required to impose the concurrent geometrical-material bifurcation condition. Thus, it may be concluded that use of LYP100 steel substantially reduces the required limiting plate thickness compared to the conventional steel material.

The effect of aspect ratio on the required limiting thickness of simply supported as well as clamped plates is also demonstrated in Fig. 4.13, in which $h/t_{p-limit}$ slenderness ratios determined by considering LYP100 steel material are plotted against the length-to-height (l/h)

aspect ratios. As illustrated in the figure, this case study covers practical ranges of plate dimensions as well as aspect ratios.

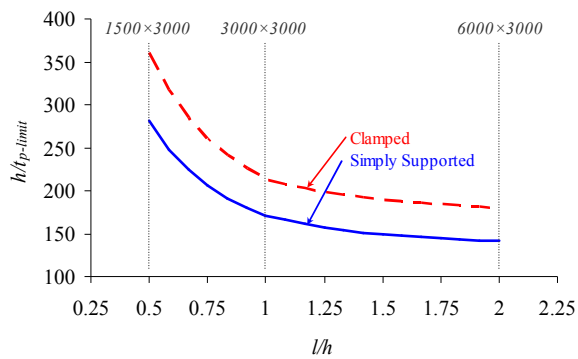

Fig. 4.13 Effect of aspect ratio on the required limiting plate thickness

From the figure, it is evident that $h/t_{p-limit}$ ratio generally decreases in both support condition cases as the l/h ratio increases. However, it is observed that rate of change of $h/t_{p-limit}$ ratios in both cases is high for l/h ratios between 0.5 and 1.0. In other words, the required limiting plate thickness reduces as the plate length-to-height ratio decreases and this reduction is further pronounced as the aforementioned aspect ratio becomes smaller than 1.0. This issue is of practical importance in design of SPSW systems with high energy absorption capacity, since wider infilled spans in buildings will require thicker plates to provide high seismic performance, which may be uneconomical. Lastly, it is noted that consideration of clamped support condition results in relatively smaller limiting plate thicknesses compared to simple support condition.

4.5 Buckling of Plates and Application of Extrapolation Techniques

Extrapolation techniques are some plotting methods developed for experimental determination of buckling loads of structures, without having to test them to failure. By plotting the results of a structure test in a certain manner, it would be possible to determine the structure's

buckling load (Zirakian, 2010). These methods have been mostly used to determine the lateral buckling loads of beams, columns, and frames. This study aims at evaluating the applicability of these methods in case of buckling of plates.

Southwell, Massey, and Modified Plots developed by Southwell (1932), Massey (1963), and Trahair (1969), respectively, are utilized in here to predict the critical loads of moderate plates. These plotting methods are applied on the initial portions of the load versus out-of-plane displacement curves in all cases, as illustrated in Fig. 4.14, and the unloading portions of the curves are ignored. In fact, the considered initial portions of the curves have a parabolic shape and contain all data points up to the ultimate strength.

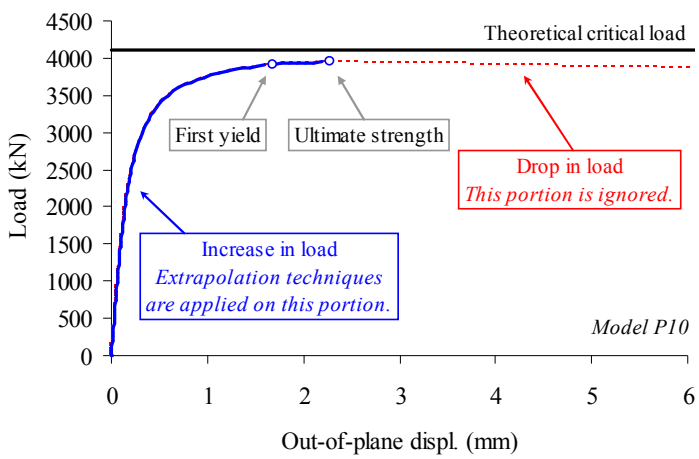

Fig. 4.14 Data points and application of the extrapolation techniques

As discussed before, failure of a moderate plate becomes evident when the plate undergoes simultaneous buckling and yielding, and once the plate reaches its ultimate strength, unloading takes place. The load at the ultimate strength is considered to be an inaccurate measure of the critical load, and the extrapolation techniques are used to obtain the buckling load corresponding to the theoretical critical load.

Southwell Plot graphs δ / P against δ, where δ is the out-of-plane displacement. Massey Plot, on the other hand, graphs δ / P^2 against δ, while Modified Plot graphs $\delta \times P$ against δ. The critical load may be obtained from relevant straight lines of best fit from these. For the Southwell Plot, the slope of the linear relationship between δ / P and δ is the reciprocal of the critical load. For the Massey Plot, the slope of the straight line is the square of the reciprocal of the critical load, while for the Modified Plot, this load is given by the slope of the $\delta \times P$ against δ plot. As an example, Fig. 4.15 provides the Southwell, Massey, and Modified plots obtained for plate model P20 (refer to Table 4.1). From the figure it is evident that Southwell and Modified Plots are in general superior to Massey Plot because of their relatively extended range of linearity. Nevertheless, Modified Plot exhibits the most extended range of linearity. The extrapolated as well as theoretical critical load predictions of the moderate plate models are also tabulated in Table 4.4.

As seen in the table, the three plotting techniques have quite successfully predicted the critical loads in all cases as compared to the theoretical predictions, and the smallest discrepancy between the extrapolated and theoretical estimates is found in case of the Modified Plot.

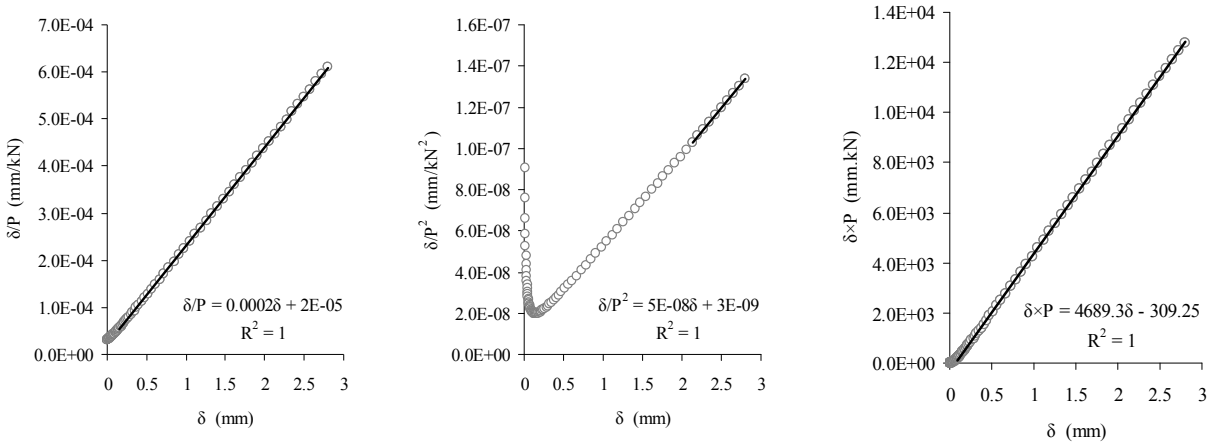

(a) Southwell Plot **(b)** Massey Plot **(c)** Modified Plot

Fig. 4.15 Typical Southwell, Massey, and Modified Plots (Model P20)

Table 4.4 Theoretical and extrapolated buckling loads of moderate plates

Model	$P_{cr-Theoretical}$ (kN)	$P_{cr-Southwell}$ (kN)	$P_{cr-Massey}$ (kN)	$P_{cr-Modified}$ (kN)
P1	1550.05	1516.53	1498.73	1542.58
P3	3019.34	2932.55	2913.58	2993.27
P5	5231.42	5042.86	4995.01	5163.76
P6	1234.57	1215.95	1216.08	1255.76
P8	2410.61	2383.22	2362.28	2431.24
P10	4088.55	4029.01	3979.68	4104.96
P11	1753.19	1750.09	1687.9	1722.28
P13	3779.55	3644.31	3604.69	3682.53
P15	7076.59	6811.99	6627.02	6709.56
P16	1354.91	1352.81	1353.21	1397.28
P18	2723.22	2670.94	2597.62	2632.37
P20	4855.01	4757.37	4624.48	4689.29

These observations and results are consistent with those reported for the buckling of beams, e.g. Zirakian (2008 and 2010), and also verify the applicability of the extrapolation techniques in case of buckling of moderate plates. However, experimental studies may further substantiate these findings.

4.6 Determination of Limiting Shear Panel Thickness in SPSW Systems

This section focuses on determination of the limiting shear panel thickness in SPSWs, in which infill plates are surrounded and restrained on all four edges by the horizontal and vertical boundary frame members of certain stiffness and strength. It is noted that steel plates in this section are considered to be under pure shear loading.

As discussed before, behavior of the SPSW may be considered as analogous to that of a vertical plate girder. Numerous studies have been performed on the edge support conditions of web panels in plate girders, which were summarized by Alinia and Dastfan (2006). Various support conditions viz. simple, partially-restrained, and clamped, have been considered in the studies of different researchers. Nevertheless, it has been demonstrated (Berman and Bruneau,

2004) that SPSWs are similar to plate girders in a qualitative manner only, since the stiffnesses of the boundary elements in the two structural systems are different. On this basis and in order to learn about the real amount of fixity of the edge supports of infill panels in SPSW systems, five code-designed SPSWs are studied in here through detailed numerical simulations. Properties of the SPSW models are provided in Table 4.5. It is noted that infill plate dimensions are consistent with those of models P6 through P10 as tabulated in Table 4.1, and the frame boundary members have been designed based on AISC 341-10 (2010) code strength and stiffness requirements.

Table 4.5 Specifications of code-designed SPSW models

Model	Infill Plate $l \times h \times t_p$ (mm)	HBE (Beam)	VBE (Column)
SPSW1	2000×3000×10.6	W14×120	W14×311
SPSW2	3000×3000×9.3	W14×233	W14×257
SPSW3	3000×3000×14.0	W14×311	W14×342
SPSW4	3000×3000×18.7	W14×398	W14×426
SPSW5	4500×3000×15.8	W30×391	W14×370

Finite element models of the SPSWs with geometrical and material nonlinearities are developed and analyzed using ANSYS 11.0 (2007) software. Shell181 element, as introduced before, is used to model the infill plate and boundary frame members. The columns are fully fixed at their bases and the exterior nodes of the column flange and stiffener elements around the perimeter of the panel zones are restrained against out-of-plane displacement. In order to account for initial imperfections, very small initial out-of-plane deformations of about $\sqrt{l \times h}/1000$ and proportional to the lowest eigen-mode shape of elastic buckling are introduced to the plates. LYP100 steel is used for the infill plate and ASTM A572 Gr. 50 steel is used for the boundary frame members. The stress-strain relationships as well as mechanical properties of the steel material are shown in Fig. 4.16. Moreover, the von Mises yield criterion is used for material yielding, and the isotropic and kinematic hardening rules are incorporated in the respective

nonlinear pushover and cyclic analyses. Lastly, in-plane lateral load is applied to the beam-column connection in a displacement-controlled and incremental manner.

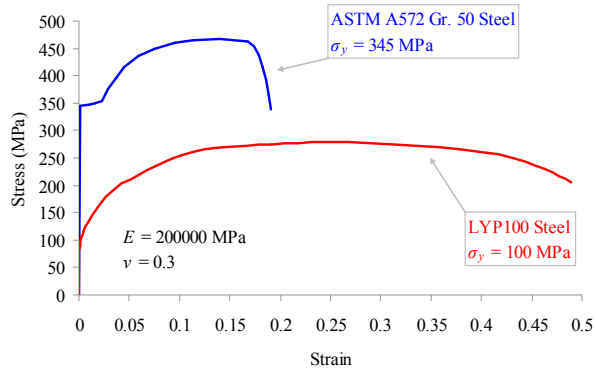

Fig. 4.16 Material properties of the steel used in SPSWs

Numerical modeling of SPSWs is validated by considering the experimental results of two specimens tested by Lubell (1997) and Chen and Jhang (2006) representing SPSWs with respective slender conventional steel and stocky LYP steel infill plates. The comparison details and results are illustrated in Figs 4.17 and 4.18.

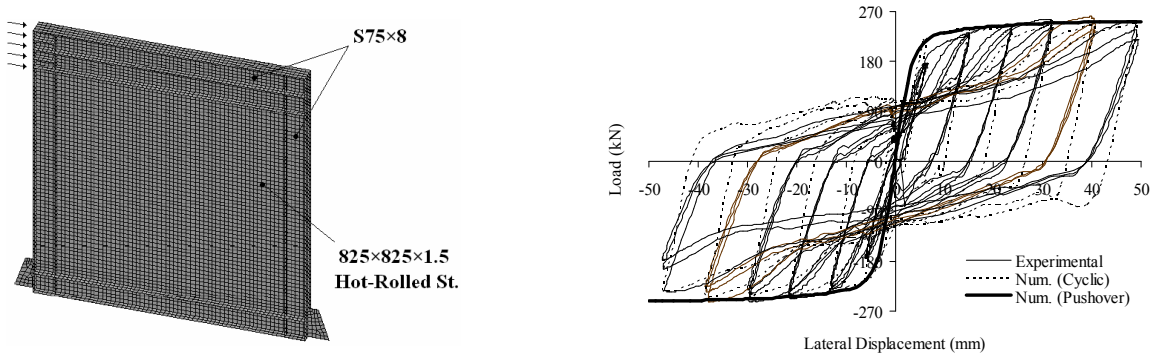

(a) SPSW2 specimen FE model **(b)** Experimental vs. numerical results

Fig. 4.17 SPSW finite element model validation by Lubell's (1997) test results

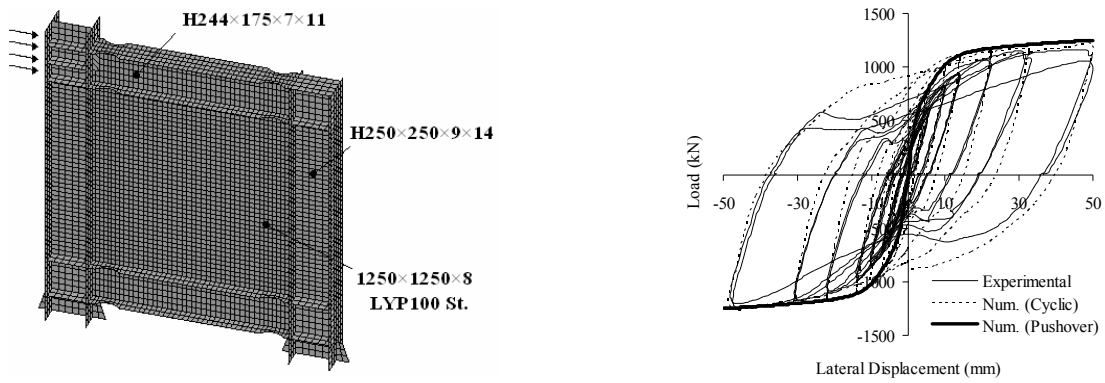

(a) Specimen no. 1 FE model **(b)** Experimental vs. numerical results

Fig. 4.18 SPSW finite element model validation by Chen and Jhang's (2006) test results

As it is observed in Figs. 4.17 and 4.18, the agreement between the numerical and experimental results is quite satisfactory in both cases.

The finite element models as well as first buckling mode shapes of SPSW1, SPSW3, and SPSW5 with different aspect ratios and geometrical properties, obtained from the linear eigen buckling analyses are shown in Fig. 4.19. Additionally, theoretical as well as numerical elastic buckling loads of the infill plates under simple and clamped support conditions, and also restrained by the boundary frame members in SPSW systems are determined and presented in Table 4.6.

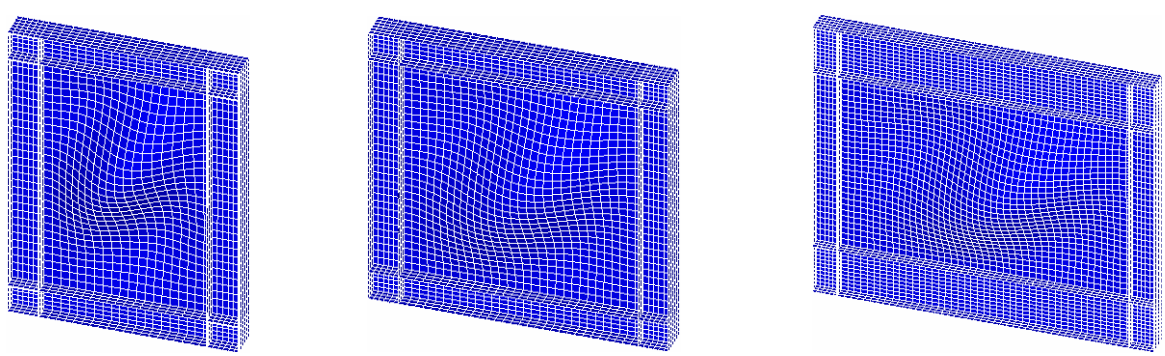

(a) SPSW1 **(b)** SPSW3 **(c)** SPSW5

Fig. 4.19 Finite element models and buckling mode shapes of SPSWs

Table 4.6 Elastic buckling loads of plates under different edge support conditions

Plate $l \times h \times t_p$ (mm)	$P_{cr-Theoretical}$ (kN)		Model	$P_{cr-Nunerical}$ (kN)
	Simply Supported	Clamped		
2000×3000×10.6	767.27	1234.57	SPSW1	1456.90
3000×3000×9.3	453.15	706.63	SPSW2	772.58
3000×3000×14.0	1545.90	2410.61	SPSW3	2598.10
3000×3000×18.7	3684.02	5744.71	SPSW4	6174.40
4500×3000×15.8	2540.99	4088.55	SPSW5	3801.70

As seen in the table, numerical buckling loads of the plates in SPSW1 through SPSW4 models are larger than the corresponding buckling loads for clamped support condition, while numerical buckling load of the infill plate in SPSW5 model lies between those calculated for simple and clamped support conditions and is pretty close to that of clamped support condition. It should be noted that by considering the edge deformation compatibility conditions between infill plates and boundary frame members in SPSW systems, infill plates in these structural systems are restrained against translations and rotations in all directions and the amount of effectiveness of these restraints in particular and fixity of plate edge supports in general is directly related to the relative stiffness of the boundary frame members. On this basis, it is observed that the buckling loads of infill plates in most of the code-designed SPSW models are beyond those predicted for clamped support condition. In any case, in spite of the scatter in results, these findings demonstrate that the support conditions of infill plates in SPSW systems are very close to the clamped support condition.

In this study, the limiting thicknesses of infill plates in the SPSW models are determined through two different approaches, whose results are compared with theoretical predictions for clamped support condition. The exact values of the limiting thicknesses of infill plates in SPSW models are obtained through an iterative process to reach a concurrent geometrical-material bifurcation condition where $P_y / P_{cr} = 1.0$. This approach is quite cumbersome and time-

consuming; however, exact values are found to evaluate the accuracy of other theoretical predictions. A linear interpolation equation, i.e. Eq. (4.9), is also developed for predicting the limiting thicknesses of infill plates (t_{p-SPSW}), which accounts for the real edge support conditions of infill plates in SPSW models by using the exact numerically-predicted buckling loads of SPSW models.

$$t_{p\text{-}SPSW}(=t_{p\text{-}limit}) = t_{p-SS} - \frac{(t_{p-SS} - t_{p-Cl}) \times (P_{cr-SPSW} - P_{cr-SS})}{P_{cr-Cl} - P_{cr-SS}} \tag{4.9}$$

In Eq. (4.9), t_{p-SS} and t_{p-Cl} are the respective limiting plate thicknesses determined for simple (Eq. (4.10)) and clamped (Eq. (4.11)) support conditions,

$$t_{p\text{-}SS} = b \times \sqrt{\frac{12 \times (1-\nu^2) \times \sigma_{yp}}{(5.34 + 4.0/(a/b)^2) \times \pi^2 \times E \times \sqrt{3}}} \tag{4.10}$$

and

$$t_{p\text{-}Cl} = b \times \sqrt{\frac{12 \times (1-\nu^2) \times \sigma_{yp}}{(8.98 + 5.6/(a/b)^2) \times \pi^2 \times E \times \sqrt{3}}}, \tag{4.11}$$

and also P_{cr-SS} and P_{cr-Cl} are the respective theoretically-determined critical buckling loads for simple and clamped support conditions. $P_{cr-SPSW}$ is the critical buckling load of SPSW model which is obtained through linear eigen buckling analysis. P_{cr-SS}, P_{cr-Cl}, and $P_{cr-SPSW}$ values are presented in Table 4.6. Also, included in Table 4.7 are the values of t_{p-SS}, t_{p-Cl}, and t_{p-SPSW}, which are determined through the aforementioned theoretical and numerical approaches.

Table 4.7 Limiting thicknesses of plates under pure shear with various edge conditions

$l \times h$ (mm)	$t_{p\text{-}limit}$ (mm)		Model	$t_{p\text{-}limit}$ (mm)	
	Simply Supported (Eq. (4.10))	Clamped (Eq. (4.11))		Eq. (4.9)	Exact
2000×3000	13.4	10.6	SPSW1	9.3	10.3
3000×3000	17.5	14.0	SPSW2	13.1	13.5
3000×3000	17.5	14.0	SPSW3	13.2	
3000×3000	17.5	14.0	SPSW4	13.3	
4500×3000	20.1	15.8	SPSW5	16.6	16.0

From the table, agreement between the theoretical estimates for clamped support condition (Eq. (4.11)), predictions of Eq. (4.9) as well as exact values of the limiting plate thicknesses is quite satisfactory. It is found that Eq. (4.9) yields reliable predictions for the limiting plate thickness; however, it should be noted that application of this equation requires the numerical determination of the SPSW elastic buckling load. Theoretical predictions by considering the clamped support condition (Eq. (4.11)), on the other hand, are found to be quite close to the exact values as well. The accuracy of these predictions is further verified by the results obtained from nonlinear finite element analyses and provided in Figs. 4.20 and 4.21. These figures show the buckling and yielding behaviors of the SPSW models with exact limiting plate thickness values (Fig. 4.20) as well as those determined considering clamped support condition (Fig. 4.21).

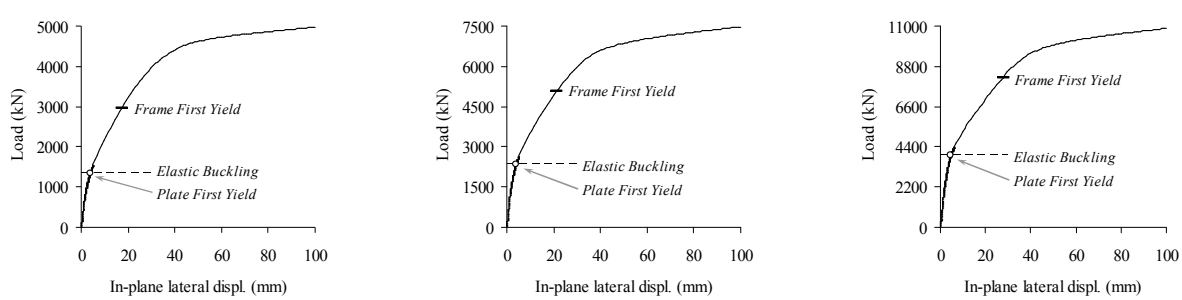

(a) SPSW1, $t_p = 10.3$ mm **(b)** SPSW3, $t_p = 13.5$ mm **(c)** SPSW5, $t_p = 16.0$ mm

Fig. 4.20 Simultaneous geometrical buckling and material yielding of SPSW models with exact limiting plate thicknesses

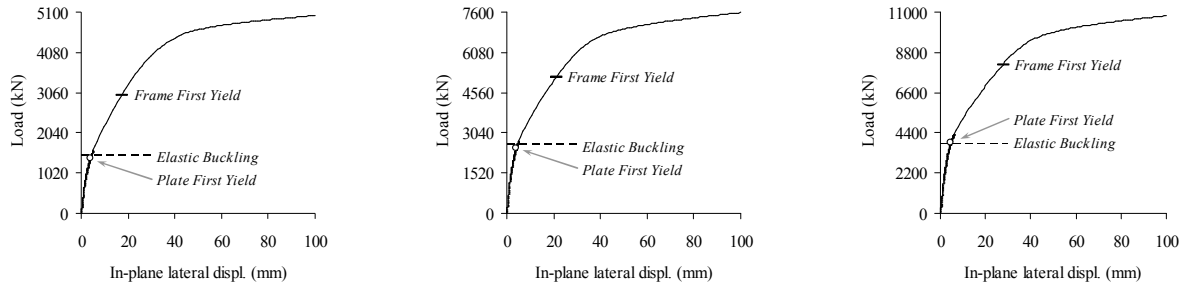

(a) SPSW1, $t_p = 10.6$ mm **(b)** SPSW3, $t_p = 14.0$ mm **(c)** SPSW5, $t_p = 15.8$ mm

Fig. 4.21 Geometrical buckling and material yielding of SPSW models with limiting plate thicknesses corresponding to clamped support condition

By comparing the results in Figs. 4.20 and 4.21, it is found that theoretical predictions of the limiting plate thickness considering clamped support condition result in simultaneous buckling and yielding of infill plates in all three cases. Considering the simplicity of this theoretical approach as discussed in Section 4.2, and also based on the findings of this study, it may be concluded that the limiting thicknesses of the infill shear panels in SPSW systems can be fairly accurately predicted by considering the clamped support condition and using Eq. (4.11).

4.7 Concluding Remarks

Buckling and yielding behavior of unstiffened LYP steel plates with various support and loading conditions was investigated in this chapter through finite element analysis. The limiting thicknesses of simply supported and clamped plates under pure shear as well as combined shear and compression, corresponding to concurrent geometrical-material bifurcation were determined through theoretical approaches, the accuracy of which was subsequently verified via linear and nonlinear finite element analyses.

The structural and hysteresis behaviors of plates with four clamped as well as two clamped-two free edges under cyclic loading were also evaluated. Plates with two clamped-two free edges

exhibited relatively weak performance as a result of excessive out-of-plane deformations due to the presence of two unrestrained edges. Optimal local stiffening of the unrestrained edges is believed to effectively control the deformations and increase the performance of such plates. This issue is of great importance in design and application of beam-attached infill panels in SPSW systems, which of course requires further investigation.

It was shown that use of LYP steel with low yield strength compared to the conventional steel, considerably reduces the required limiting plate thickness. Moreover, it was found that larger plate length-to-height (l/h) ratio unfavorably results in larger required limiting plate thickness. These issues may be of great importance in economical design of SPSW systems with high structural and energy absorption characteristics.

The critical buckling loads of moderate plates were predicted using the Southwell, Massey, and Modified plotting techniques, and the extrapolated loads were compared with theoretical predictions. Based on the findings of this study, the critical buckling loads of moderate plates were accurately predicted by the extrapolation techniques.

Finally, the limiting thicknesses of infill shear panels in five code-designed SPSW models with various aspect ratios were successfully determined through theoretical and numerical approaches. Accordingly, it was concluded that the limiting thicknesses of infill plates in SPSW systems can be easily and fairly accurately determined in practice by considering the clamped support condition. Determination of the limiting plate thickness corresponding to simultaneous geometrical buckling and material yielding will enable the efficient design of SPSW systems with high structural, energy dissipation, and serviceability characteristics, which is of course made economically possible in the light of use of LYP steel.

5. STUDY OF MONOTONIC AND CYCLIC BEHAVIORS OF SPSWS WITH LYP STEEL INFILL PLATES

5.1 Introduction

As it was mentioned before, SPSWs have been used with two different design strategies. The common practice in Japan has been to employ stiffened and/or stocky-web SPSWs to ensure that the wall panel achieves its full plastic strength prior to out-of-plane buckling. The current North American practice, on the other hand, is to use unstiffened and slender-web SPSWs which exhibit nonlinear behavior at relatively small story drifts as they buckle out of plane, and lateral forces are consequently resisted through development of tension-field action in the post-buckling stage. It is notable that the labor/fabrication costs in North America indicate that unstiffened panels are preferable (Kulak et al., 2001).

By considering the previously-discussed advantages and disadvantages of the two configurations, efficient and practical adjustment of stiffening and damping characteristics of SPSW systems requires proper addressing of both structural and economical considerations. Application of LYP steel with desirable material properties is believed to provide the possibility to design relatively cost-effective SPSW systems with high structural and seismic performance.

In this chapter, the behavior of some code-designed and unstiffened LYP steel shear wall systems under monotonic and cyclic loadings is studied via finite element analysis. The advantages of use of LYP steel material in SPSW systems as compared to the conventional steel material are demonstrated through detailed case studies. Additionally, the performance of SPSW models with slender, moderate, and stocky LYP steel infill plates is investigated as well. Lastly, the effectiveness of a modified PFI model in predicting the response of SPSW systems with

moderate and stocky infill plates is evaluated through comparison with some experimental as well as experimentally-verified numerical results.

5.2 Design and Properties of SPSW Models

Six single-story, single-bay, and full-scale steel shear walls with 2000×3000, 3000×3000, and 4500×3000 mm infill plates of various slenderness ratios and steel material are designed in accordance with the AISC 341-10 (2010) seismic provisions for the purpose of this study. Properties of the SPSW models are provided in Table 5.1. As it is seen in the table, ASTM A572 Gr. 50 steel with 345 MPa yield stress is selected for the boundary frame, and LYP100 and ASTM A36 steel with respective 100 and 250 MPa yield stresses are selected for the infill plates.

Table 5.1 Properties of the code-designed SPSW models

Model	Infill Plate		HBE (Beam)	VBE (Column)	Design Steel Type	
	$l \times h \times t_p$ (mm)	Type			Frame	Plate
SPSW1	2000×3000×10.6	Moderate	W14×120	W14×311	ASTM A572 Gr. 50	LYP100
SPSW2	3000×3000×4.7	Slender	W14×120	W14×132	ASTM A572 Gr. 50	ASTM A36, LYP100
SPSW3	3000×3000×9.3	Slender	W14×233	W14×257	ASTM A572 Gr. 50	LYP100
SPSW4	3000×3000×14.0	Moderate	W14×311	W14×342	ASTM A572 Gr. 50	LYP100
SPSW5	3000×3000×18.7	Stocky	W14×398	W14×426	ASTM A572 Gr. 50	LYP100
SPSW6	4500×3000×15.8	Moderate	W30×391	W14×370	ASTM A572 Gr. 50	LYP100

In order to design the boundary frame members in SPSWs, respective infill plate thicknesses are initially determined. The limiting thicknesses corresponding to simultaneous buckling and yielding of infill plates in SPSW1, SPSW4, and SPSW6 models are determined by considering clamped edge condition and using Eq. (4.11). In theoretical calculations, Young's modulus (E) and Poisson's ratio (ν) are taken as 200000 MPa and 0.3, respectively.

Following the determination of the infill plate thickness of SPSW4 model, infill plate thicknesses of SPSW2-3 and SPSW5 models are selected in a manner to represent the behaviors of slender-web and stocky-web steel shear wall systems, respectively.

As it is seen in Table 5.1, design of SPSW2 model for both LYP100 and ASTM A36 steel material results in identical sections for the boundary frame members. This is because the HBE and VBE design is dominated by the specified "stiffness" criterion rather than the "strength" criterion, which is independent of the material type. From Eqs. (3.7) and (3.8), it is quite evident that the specified stiffness criterion is only a function of the infill plate thickness and geometrical dimensions of the panel.

5.3 Finite Element Modeling and Analysis

The finite element analysis software, ANSYS 11.0 (2007), is utilized to develop and analyze the SPSW numerical models under monotonic and cyclic loadings. Boundary frame members as well as infill plates of the SPSWs are modeled by Shell181 element, which was introduced before. SPSW1, SPSW4, and SPSW6 finite element models are illustrated in Fig. 5.1.

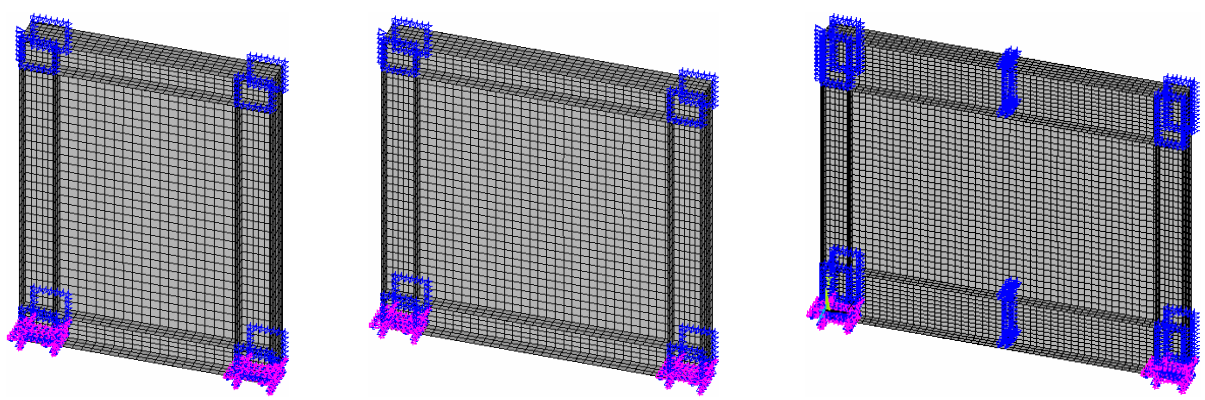

(a) SPSW1 **(b)** SPSW4 **(c)** SPSW6

Fig. 5.1 Finite element models

As shown in Fig. 5.1, both columns are fully fixed at their bases, and the HBE-to-VBE connections around the perimeter of the panel zones are restrained against out-of-plane displacement. It is notable that HBEs in SPSW6 model with the largest span length are braced at

their midspan against lateral (out-of-plane) displacement. Furthermore, shown in the figures is also the in-plane lateral load, which is applied to the beam-column connection in a displacement-controlled and incremental manner.

The respective steel material selected for the boundary frame members and infill plates of SPSW models were given in Table 5.1. Shown in Fig. 5.2 are the stress-strain relationships as well as mechanical properties of the steel material applied in finite element modeling. Moreover, von Mises yield criterion is used for material yielding, and isotropic and kinematic hardening rules are incorporated in the respective nonlinear monotonic (pushover) and cyclic analyses.

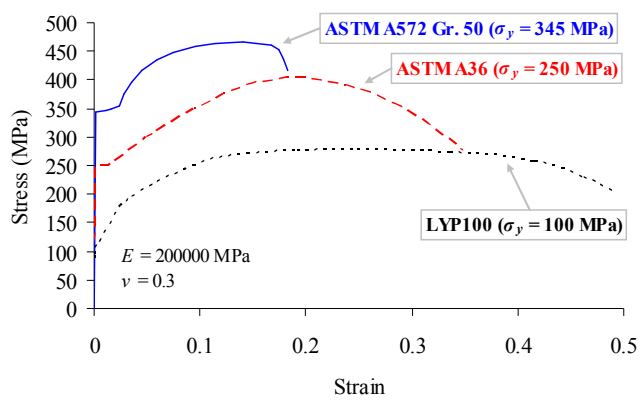

Fig. 5.2 Material properties of the steel used in SPSWs

In order to account for initial imperfections, very small out-of-plane deformations of about $\sqrt{l \times h}/1000$ and proportional to the lowest eigen-mode shape of elastic buckling are introduced to the SPSW models. To achieve this, an eigen buckling analysis is performed to determine the first buckling mode prior to the nonlinear analysis of each SPSW model. The applied imperfection magnitudes are smaller than 1% of $\sqrt{l \times h}$ limit proposed by Behbahanifard et al. (2003), and therefore their effects on the stiffness and capacity of the SPSW models are negligible.

Both geometrical and material nonlinearities are considered in the finite element analyses. Finally, as it was discussed in Chapter 4 and Section 4.6, finite element modeling of the SPSWs is validated by considering two sets of experimental results, and the comparison details were given in Figs. 4.17 and 4.18.

5.4 Advantages of Use of LYP Steel Infill Plates in SPSW Systems

One of the significant advantages of LYP steel is its low yield stress of about 90-120 MPa, which is approximately 1/3 of that of ASTM A36 steel. Use of such a low-yield steel in lieu of the conventional mild steels as the material for lateral force-resisting and energy dissipating elements in buildings ensures early yielding of such structural elements, and consequently reduces forces imposed on frame members. In fact, by employing LYP steel infill plates, it is easier to design the system in such a manner to let the infill plate yield prior to that of the surrounding frame and to ensure that the frame would not collapse before the infill plate reaches its ultimate strength (Chen and Jhang, 2006). LYP steel shear walls, in addition, may be utilized to retrofit the existing frame buildings requiring additional strength and stiffness. Moreover, buckled and/or damaged infill plates of existing SPSW systems after an earthquake may be properly replaced by LYP steel plates. Such retrofits and/or replacements not only may increase the seismic performance, but also may enhance the structural characteristics of the existing buildings in the light of use of LYP steel.

In this section, it is attempted to scrutinize the effects and advantages of use of LYP steel infill plates by addressing the above-mentioned issues. In order to achieve the objectives of this study, infill plate thickness in SPSW2 model is increased from 4.7 mm to 18.7 mm and the structural behavior and performance of the SPSW system and its components are investigated

through finite element analyses. It is noted that the boundary frame members in SPSW2 model were originally designed for 4.7 mm LYP and conventional steel slender web-plates as shown in Table 5.1, which are not changed in these case studies. The lateral load versus out-of-plane displacement and drift ratio curves of SPSW2 model with respective 4.7, 9.3, 14.0, and 18.7 mm infill plates are shown in Figs. 5.3(a) through 5.3(d), where out-of-plane displacement-lateral load curves exhibit the buckling behavior, and drift ratio-lateral load curves demonstrate the in-plane stiffness and strength performance of the SPSW system. Plate and frame first yield points are denoted by P.Y. and F.Y., respectively, and E.B. stands for elastic buckling.

As it is shown in Table 5.1, the limiting thickness corresponding to simultaneous buckling and yielding of a 3000×3000 mm LYP steel infill plate is estimated to be 14.0 mm, so consideration of thicknesses below and above this limit will result in disparate buckling and yielding behaviors. On this basis and as seen in Fig. 5.3, infill plates in SPSW2-4.7 and SPSW2-9.3 models yield in the post-buckling stage. Infill plate in SPSW2-14.0 model, on the other hand, undergoes simultaneous buckling and yielding as expected, while that of SPSW2-18.7 model yields prior to buckling.

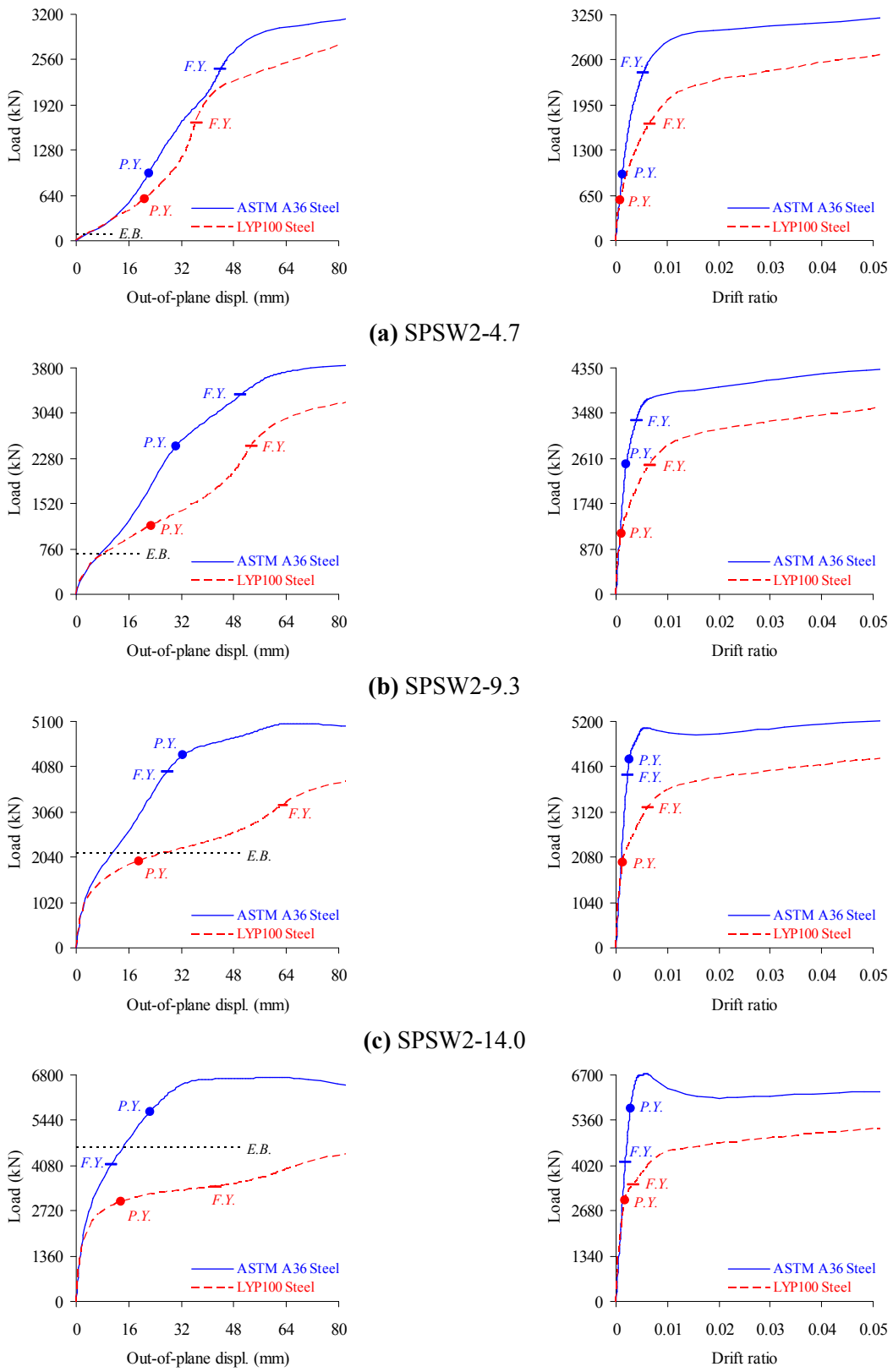

(a) SPSW2-4.7

(b) SPSW2-9.3

(c) SPSW2-14.0

(d) SPSW2-18.7

Fig. 5.3 Behavior of SPSW2 model with various infill plate thicknesses and steel types

It is clearly observed that increase of the infill plate thickness reduces the interval between plate and frame first yield points. However, yielding of the LYP steel infill plates in all cases occurs in advance of frame yielding due to low yield stress of this steel material, while yielding of the conventional steel infill plates in SPSW2-14.0 (Fig. 5.3(c)) and SPSW2-18.7 (Fig. 5.3(d)) models occurs unfavorably after frame yielding. As seen in Figs. 5.3(c) and 5.3(d), early yielding of the frame members, especially columns, results in significant stiffness and strength degradation and relatively weak performance of the structural system. In addition, it is evident that LYP steel shear walls undergo early yielding and consequently large inelastic deformations compared to conventional steel shear walls with identical infill plate thicknesses. This can be of great importance in seismic design of SPSW systems since the earthquake input energy can be absorbed through plastic deformations of LYP steel infill plates, which will consequently result in the limitation of the plastic deformation demand to the frame structure.

Replaceability of conventional steel infill plates and employment of LYP steel plates with improved structural and seismic characteristics are investigated in further detail by taking a closer look at behaviors and performances of SPSW-4.7 and SPSW-9.3 models. SPSW2 model with 4.7 mm infill plate made of ASTM A36 steel denoted by SPSW2-4.7-ASTM A36, is considered as a typical slender-web SPSW system, infill plate of which is required to be replaced after an earthquake. This infill plate may be replaced by either 9.3 mm ASTM A36 or LYP100 steel plates. The structural behavior as well as stiffness performance of the SPSW system with the original and two alternative infill plates are shown in Figs. 5.4 and 5.5, respectively.

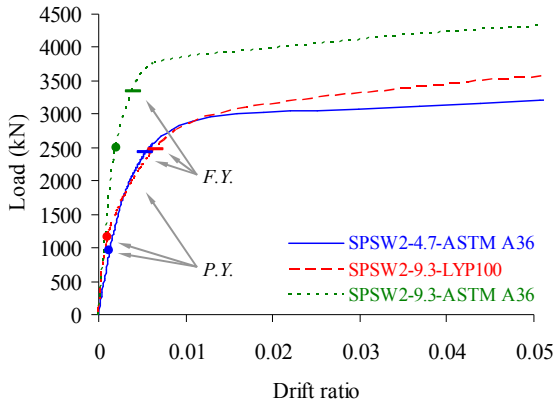

Fig. 5.4 Structural strength and behavior

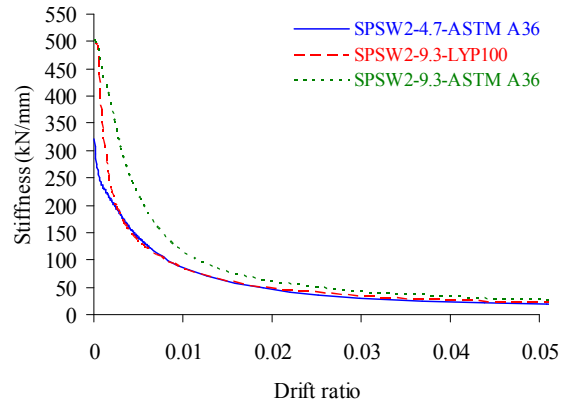

Fig. 5.5 Stiffness performance

From Figs. 5.4 and 5.5, it is quite evident that the overall performance of SPSW2-4.7-ASTM A36 and SPSW2-9.3-LYP100 models is pretty similar. However, as seen in Fig. 5.5, due to larger plate thickness, SPSW2-9.3-LYP100 model possesses higher initial stiffness relative to SPSW2-4.7-ASTM A36 model, which is of course declined due to early yielding of LYP100 steel material and the stiffnesses of both models tend to get closer. The von Mises stress contour plots of SPSW2-4.7-ASTM A36, SPSW2-9.3-LYP100, and SPSW2-9.3-ASTM A36 models at 0.01 and 0.02 drift ratios are also shown in Fig. 5.6 in which, according to the stress contour legend, yielded zones in boundary frame members are in red color.

As it is seen in Fig. 5.6, stress level, in general, and yielded points, in particular, are increased in the boundary frame members at 0.02 drift ratio compared to 0.01 drift ratio due to higher deformations and forces imposed on these components. As well, due to the effect of diagonal tension-field action, yielding zones are confined to the HBE and VBE ends near the HBE-to-VBE connection areas where plastic hinges are expected to be formed. However, it is shown that the stress contours as well as yielding patterns in boundary frame members of SPSW2-4.7-ASTM A36 and SPSW2-9.3-LYP100 models are pretty similar at both levels of drift ratio, while HBEs and VBEs in SPSW2-9.3-ASTM A36 model possess comparatively different

stress contours and of course expanded yielding zones. In addition, comparison of stress contours of SPSW2-9.3-LYP100 (Figs. 5.6(c) and (d)) and SPSW2-9.3-ASTM A36 (Figs. 5.6(e) and (f)) models indicates that application of LYP steel infill plate ensures a larger energy dissipation capacity since it allows the yielding of the material to be spread over the entire plate component.

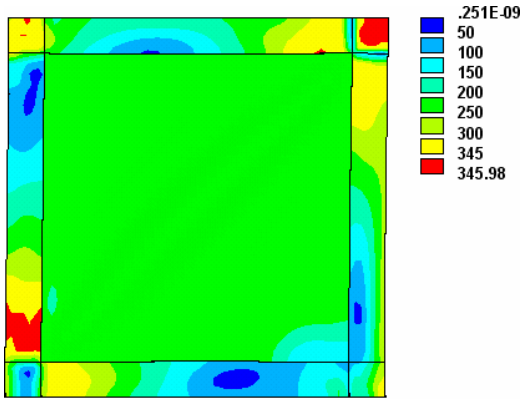

(a) SPSW2-4.7-ASTM A36 (Drift ratio = 0.01)

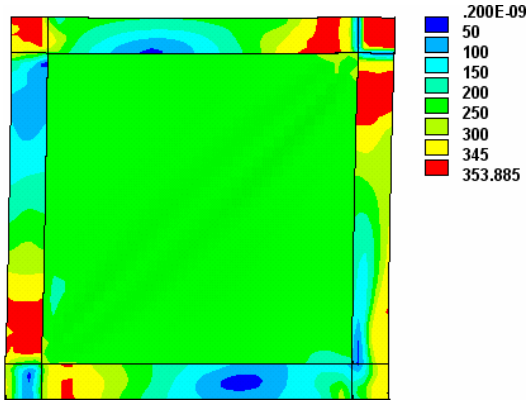

(b) SPSW2-4.7-ASTM A36 (Drift ratio = 0.02)

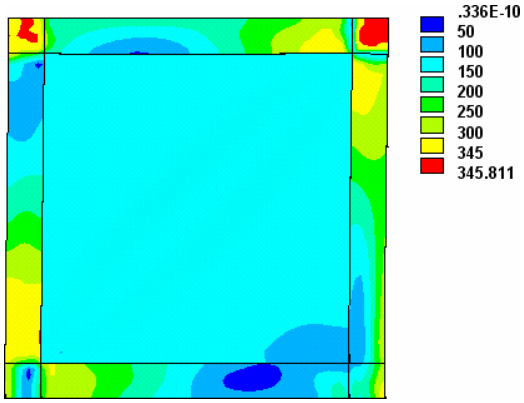

(c) SPSW2-9.3-LYP100 (Drift ratio = 0.01)

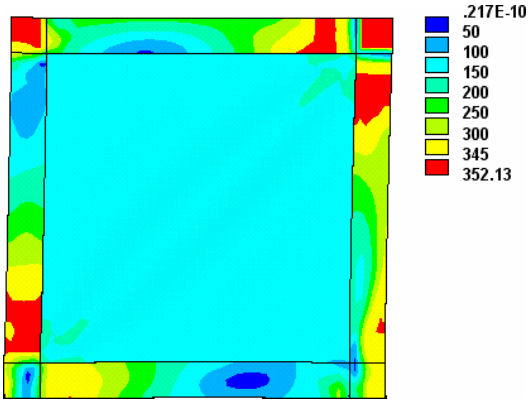

(d) SPSW2-9.3-LYP100 (Drift ratio = 0.02)

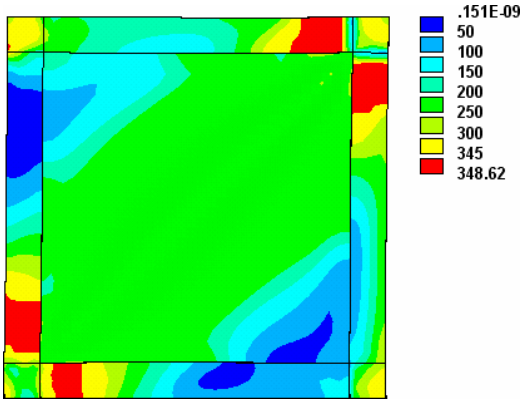

(e) SPSW2-9.3-ASTM A36 (Drift ratio = 0.01)

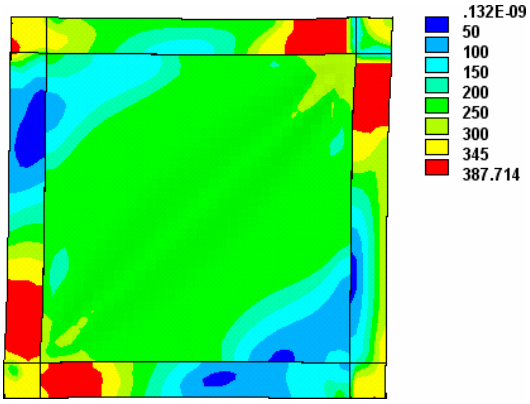

(f) SPSW2-9.3-ASTM A36 (Drift ratio = 0.02)

Fig. 5.6 von Mises stress contour plots of SPSW2 model with various infill plate thicknesses and steel types at 0.01 and 0.02 drift ratios

Evaluation of magnitudes of the axial loads developed in columns of SPSW2-4.7-ASTM A36 and SPSW2-9.3-LYP100 models, shown in Fig. 5.7, confirms the similarity in overall performance of both systems. Lastly, the hysteretic behaviors of SPSW2-4.7-ASTM A36 and SPSW2-9.3-LYP100 models with similar structural characteristics are evaluated by performing nonlinear cyclic analyses. Cyclic loading protocol is provided in Table 5.2, and also the hysteresis curves of both SPSW models are shown in Fig. 5.8.

Table 5.2 Loading protocol

Cycle No.	1	2	3	4	5	6	7	8	9
Drift ratio	0.001	0.0025	0.005	0.01	0.015	0.02	0.03	0.04	0.05

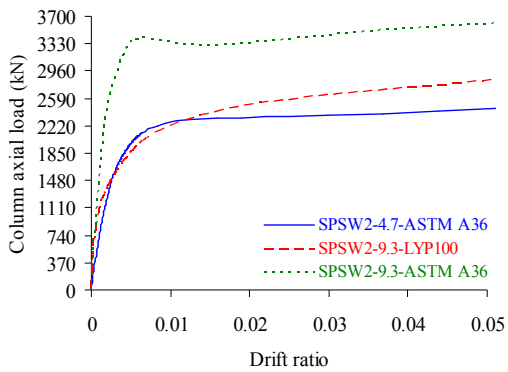

Fig. 5.7 Comparison of the developed column axial loads

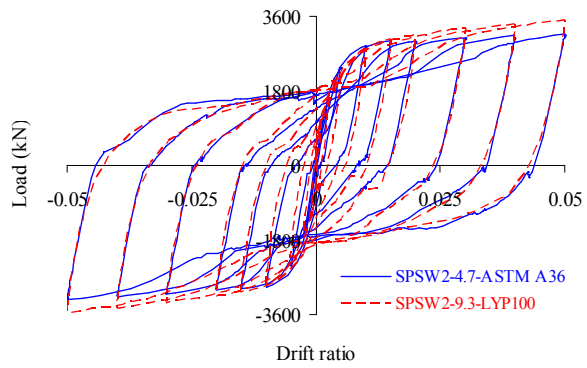

Fig. 5.8 Comparison of the hysteretic behaviors

From Fig. 5.8, it is clear that both SPSW models have similar hysteretic behaviors. The total cumulative energies dissipated by SPSW2-4.7-ASTM A36 and SPSW2-9.3-LYP100 models are 3284.2 and 3671.3 kN.m, respectively, which indicates that SPSW2-9.3-LYP100 model possesses 11.8% more energy absorption capacity.

These findings indicate that the 4.7 mm ASTM A36 steel infill plate can be properly replaced by a 9.3 mm LYP100 steel plate with improved initial stiffness, buckling and energy dissipation capacities, and serviceability. Also, it is notable that application of the LYP steel plate with

lower slenderness ratio does not increase the overall system demand on the boundary frame members and shows promise towards alleviating stiffness and over-strength concerns using the alternative conventional steel plate.

Overall, it can be concluded that application of LYP steel not only facilitates the design of SPSW systems, but also may enable upgrading the structural performance through seismic retrofit of existing buildings.

5.5 Performance of SPSWs with Slender, Moderate, and Stocky LYP Steel Infill Plates

Behaviors of slender-web (SPSW2 and SPSW3), moderate-web (SPSW4), and stocky-web (SPSW5) steel shear wall models under monotonic and cyclic loadings are studied in this section. Use of LYP steel may result in employment of infill plates with various slenderness ratios and geometrical-material bifurcation characteristics. Hence, this study aims at addressing the specifications of such SPSW systems on the basis of the aforementioned infill plate slenderness classification.

Buckling stability of the SPSW models is illustrated in Fig. 5.9, where out-of-plane displacements are plotted against the applied lateral load. Lateral load versus drift ratio curves of the SPSW models are also presented in Fig. 5.10.

Fig. 5.9 shows the buckling and yielding sequence in SPSW models with slender, moderate, and stocky infill plates, in which occurrence of simultaneous buckling and yielding of the infill plate in SPSW4 model is verified. This indicates that Eq. (4.11) provides reliable predictions for the limiting thickness, given that the plate is under shear loading. From the figure, it is clear that increasing of plate thickness results in a considerable increase in buckling strength and decrease in out-of-plane deformation which is, in turn, indicative of improved serviceability. Fig. 5.10,

also, shows that the strength and stiffness of the SPSW system under in-plane lateral load are remarkably enhanced due to the increase in infill plate thickness. The key factor herein is the use of LYP steel which results in relatively lower plate thicknesses, more or less within practical limits, required to ensure high performance.

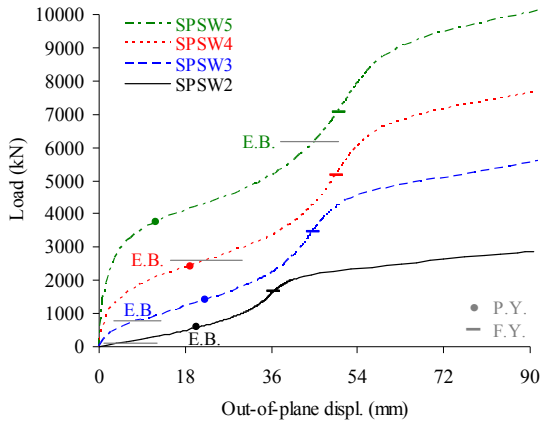

Fig. 5.9 Buckling stability of SPSWs with various infill plate slenderness ratios

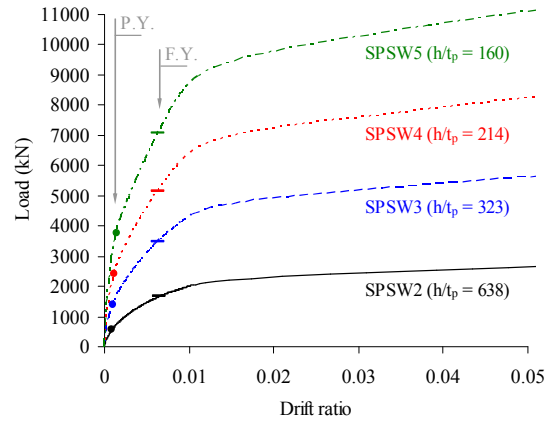

Fig. 5.10 Load-drift ratio curves of SPSWs with various infill plate slenderness ratios

Stiffness performance of the SPSW models is further illustrated in Fig. 5.11. The von Mises stress contour plot of SPSW4 model with moderate LYP steel infill plate at 3% drift ratio is also shown in Fig. 5.12.

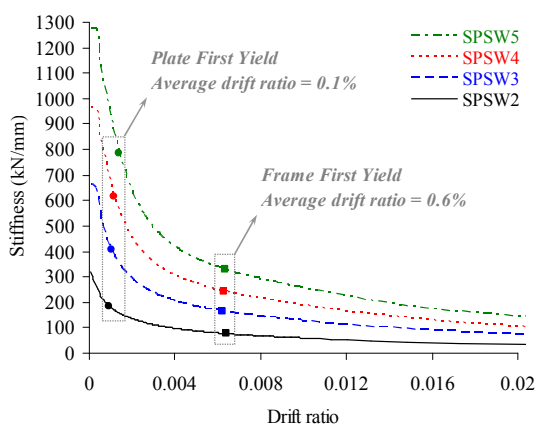

Fig. 5.11 Stiffness-drift ratio curves of SPSWs with various infill plate thicknesses

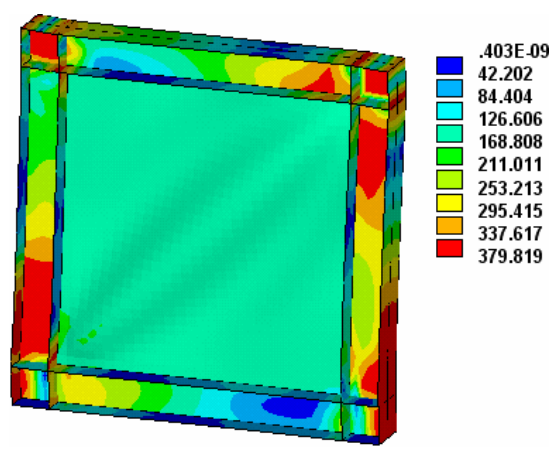

Fig. 5.12 von Mises stress contour plot of SPSW4 model at 0.03 drift ratio

As seen in Fig. 5.11, all four LYP steel shear wall models have similar and stable stiffness performance in the elastic and inelastic ranges of structural response. The stiffness of the SPSW models gradually diminishes as the drift ratio increases. However, most of the stiffness reduction occurs at lower drift ratios due to yielding and buckling of the LYP steel infill plate. Also, as shown in Figs. 5.10 and 5.11, the plate and frame first yields in the SPSW models occur at 0.1% and 0.6% average drift ratios, respectively. It is believed that the stable stiffness performance and the desirable plate-frame yielding sequence in all four SPSW models are mainly contributed by the LYP steel material properties and also proper design of the boundary frame members. These findings are consistent with those reported by Habashi and Alinia (2010). In addition, as seen in Fig. 5.12, the infill plate of SPSW4 model is fully yielded at 3% drift ratio which is accompanied by partial yielding of the boundary frame members due to the effect of diagonal tension-field action within the web-plate.

Hysteresis plots of the SPSW lateral load versus drift ratio are shown in Fig. 5.13. SPSW models are loaded cyclically according to the history given in Table 5.2. From the figure, it is found that the code-designed LYP steel shear wall models in general exhibit reliable cyclic performance by dissipating the energy with stable hysteresis loops. Increasing of infill plate thickness betters the hysteretic behavior of the SPSW system by improving the buckling stability and decreasing the severity of pinching effect in the hysteresis loops resulting in the change of shape of the hysteresis loops from “S” shape to “spindle” shape, as seen in Fig. 5.13. Fig. 5.14, also, shows the variations of cumulative dissipated energy of the SPSW models.

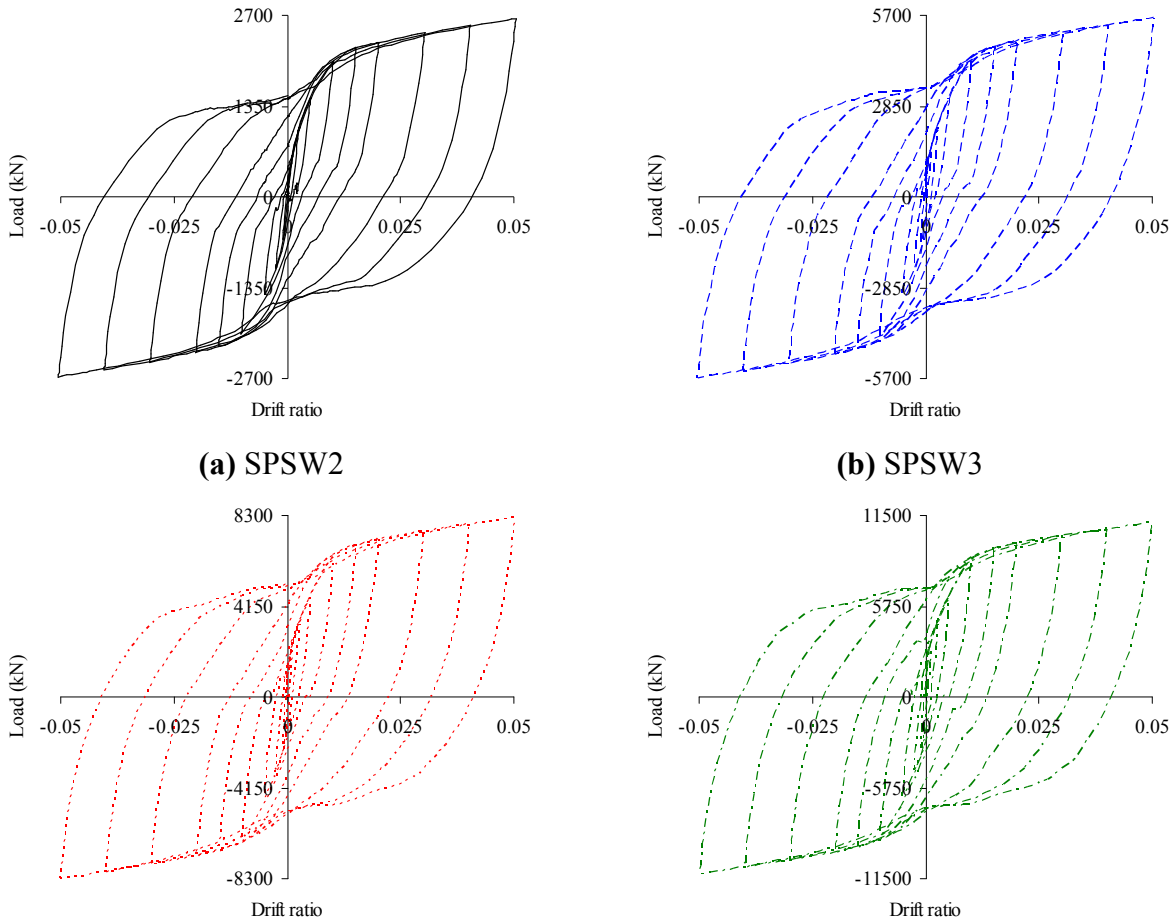

(a) SPSW2 **(b)** SPSW3

(c) SPSW4 **(d)** SPSW5

Fig. 5.13 Hysteresis curves of the LYP steel shear wall models with various infill plate slenderness ratios

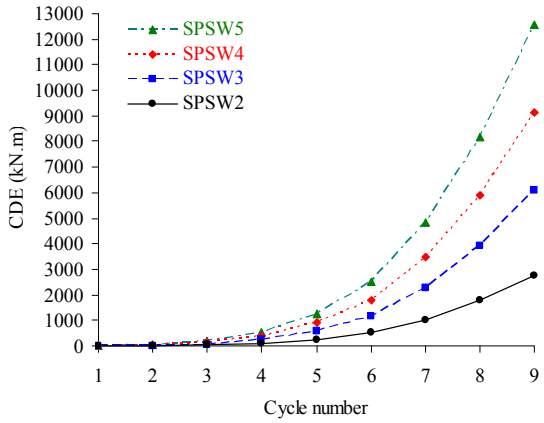

Fig. 5.14 Cumulative dissipated energy at various cycles

From this figure, it is apparent that energy dissipation capacity of the SPSW system increases substantially as the infill plate slenderness decreases. Also, it is clearly observed that application of LYP steel infill plates results in early yielding and energy dissipation of the SPSW system from the initial stages of loading process.

Stiffness, strength, and energy dissipation capacity are three important characteristics of a SPSW system which affect its structural and seismic performance. On this basis and in order to provide an overall quantitative assessment of the current findings, the infill plate thickness (t_p), initial stiffness (K_i), strength at 0.05 drift ratio ($P_{DR=0.05}$), and total cumulative dissipated energy ($(CDE)_t$) values of the LYP steel shear wall models are captured and summarized in Table 5.3. These quantities are also presented in a normalized manner by dividing each by the corresponding quantities of SPSW2 model.

Table 5.3 Stiffness, strength, and energy dissipation characteristics of SPSW models

Model	t_p (mm)	$t_p / t_{p\text{-}SPSW2}$	K_i (kN/mm)	$K_i / K_{i\text{-}SPSW2}$	$P_{DR=0.05}$ (kN)	P / P_{SPSW2}	$(CDE)_t$ (kN.m)	$(CDE)_t / (CDE)_{t\text{-}SPSW2}$
SPSW2	4.7	1.00	322.5	1.00	2653.2	1.00	2756.2	1.00
SPSW3	9.3	1.98	664.7	2.06	5606.4	2.11	6074.6	2.20
SPSW4	14.0	2.98	967.7	3.00	8198.9	3.09	9111.5	3.31
SPSW5	18.7	3.98	1275.2	3.95	11042.1	4.16	12563.0	4.56

From the tabulated results, it is found that stiffness, strength, and energy dissipation capacity values increase almost proportionally with the increase in infill plate thickness. It is also noted that CDE ratios possess the highest rate of increase compared to stiffness and strength ratios. These findings demonstrate the stiffening and damping characteristics and capabilities of LYP steel shear wall systems.

5.6 Modified Plate-Frame Interaction Model for SPSWs with Moderate and Stocky Infill Plates

Sabouri-Ghomi et al. (2005) introduced the PFI model and demonstrated that this modeling technique is able to predict the behavior of different SPSW configurations with thin or thick infill plates, and with or without stiffeners and openings. This analytical method provides the designers with a powerful tool to efficiently design SPSW systems by evaluating the individual properties of the plate and frame components and their interaction as well as contribution to the overall performance of the system. The purpose of this section is to present a slightly-modified PFI model for predicting the response of SPSW systems with moderate and stocky infill plates, and also to evaluate its effectiveness through detailed comparison with some experimental and numerical results.

This method considers the behavior of the infill plate and surrounding frame separately, and accounts for the interaction of these two structural components. A schematic representation of the PFI method was provided in Fig. 2.6(b). As illustrated in the figure, the shear load-displacement diagrams for the infill plate and for the surrounding frame are obtained separately, and by superimposing these two diagrams, that of the steel shear wall panel is obtained consequently.

It was demonstrated that moderate plates reach their ultimate strength immediately after geometrical-material bifurcation and neither possess post-buckling nor post-yield reserves, while stocky plates exhibit some post-yield capacity prior to failure due to plastic buckling. This indicates that stability and resistance of such plates are highly influenced by material bifurcation. Accordingly, it is assumed that the limit state of moderate and stocky infill plates under shear loading is reached when the shear stress acting on the plate attains the shear yield stress, i.e. $\tau_{yp} = \sigma_{yp} / \sqrt{3}$, and hence the effects of geometrical buckling are neglected. Point A in Fig.

2.6(b) corresponds to the plate material bifurcation limit. The shear yield strength (P_p) and the corresponding lateral displacement (U_p) of the plate may be obtained from

$$P_p = \tau_{yp} \times lt_p \tag{5.1}$$

and

$$U_p = \left(\frac{\tau_{yp}}{G}\right) \times h + \frac{P_p \times h^3}{3EI_p} \tag{5.2}$$

in which, G is the elastic shear modulus of the plate steel material and I_p is the moment of inertia of the infill plate. It is noted that U_p in Eq. (5.2) is determined by considering the deflection due to both shear and bending, since the deformation of a SPSW system is a combination of shear and bending deformations.

The shear load-displacement diagram of a frame may also be reasonably defined by assuming that the beam-column connections are fixed and the beams behave as rigid elements (Fig. 2.6(a)). Accordingly, the ultimate shear strength (P_f) and the corresponding lateral displacement (U_f) of the frame, defining point B in Fig. 2.6(b), may be determined by

$$P_f = \frac{4 \times M_{pc}}{h_s} \tag{5.3}$$

and

$$U_f = \frac{M_{pc} \times h_s^2}{6EI_c} \tag{5.4}$$

where, M_{pc} and I_c are respective plastic moment and moment of inertia of the column.

It is evident that the behavior of steel infill plate and frame are assumed to be elastic-perfectly plastic in this method. Once the idealized shear load-displacement diagrams of the infill plate and surrounding frame are defined using the above equations, the shear load-displacement diagram of the SPSW system can be obtained by superposition of the two diagrams. It should be noted that in accordance with Sabouri-Ghomi et al.'s (2005) recommendation, $U_f > U_p$ requirement has to be satisfied, since this will ensure that the plate dissipates more energy than the frame. Moreover, boundary frame members have to be strong and stiff enough to ensure full development of tension field in the web plate.

The effectiveness of the modified PFI model is demonstrated by comparing the predicted response with experimental and numerical results. The analytical results are initially compared with the experimental results obtained from tests performed by Chen and Jhang (2006) as well as Tsai and Lin (2005), as shown in Figs. 5.15 and 5.16, respectively. The first test specimen, i.e. specimen no. 2 in Chen and Jhang (2006), is an unstiffened steel shear wall with stocky LYP steel infill plate and an extension of 15 cm steel plate added to the bottom of the boundary beam, whose details are illustrated in Fig. 5.15(a). The second specimen, i.e. specimen 3T in Tsai and Lin (2005), is a stiffened LYP steel shear wall with 3.0 mm thick and stocky sub-panels as shown in Fig. 5.16(a).

As shown in Fig. 5.15(b), the ultimate strength of the first test specimen is closely predicted by the modified PFI model; however, the initial stiffness is overestimated by this model. Fig. 5.16(b), on the other hand, shows that the analytical model closely predicts both initial stiffness and ultimate strength from the envelope of the cyclic response of the second test specimen. Regardless of theoretical considerations, the stiffness performance of the test specimens is believed to be largely influenced by the LYP and conventional steel material nonlinearities

present in both elastic and inelastic ranges which are not captured by the analytical model. In any case, the agreement between the analytical and experimental results is found to be by and large satisfactory in both cases.

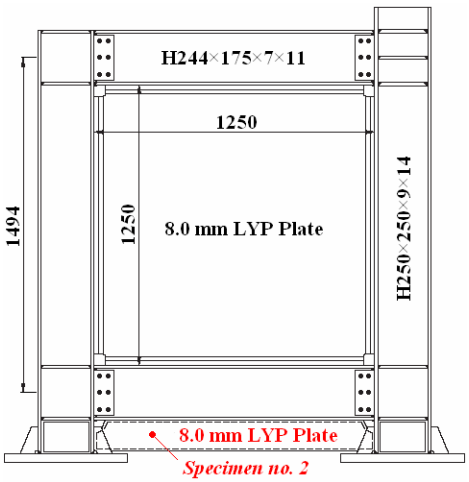

(a) Specimen no. 2

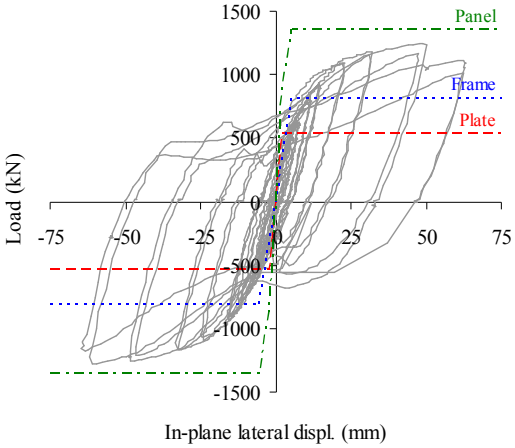

(b) Analytical vs. experimental results

Fig. 5.15 Comparison with Chen and Jhang's (2006) experimental results

(a) Specimen 3T

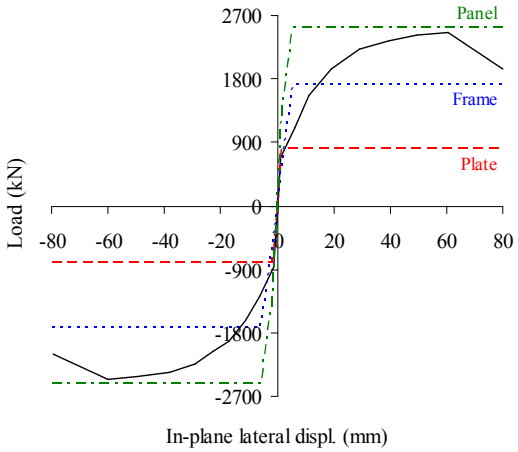

(b) Analytical vs. experimental results

Fig. 5.16 Comparison with Tsai and Lin's (2005) experimental results

The accuracy and performance of the modified PFI model are also evaluated by considering the numerical results from finite element analysis of SPSW specimens tested by Lubell (1997) and Chen and Jhang (2006), as shown in Figs. 4.17(a) and 4.18(a), respectively, with various infill plate thicknesses. It is reiterated that SPSW2 specimen tested by Lubell (1997) and specimen no. 1 tested by Chen and Jhang (2006) originally employed slender conventional steel and stocky LYP steel infill plates, respectively, which are replaced by moderate and stocky LYP steel infill plates in the finite element models. The limiting plate thicknesses of these small-scale test specimens are determined by using Eq. (4.9). Table 5.4 summarizes the results of calculations regarding determination of the limiting plate thicknesses.

Table 5.4 Results of calculations for determining the limiting plate thicknesses of the experimental SPSW specimens

Test	Infill Plate $l \times h \times t_p$ (mm)	Steel Type	$t_{p\text{-}SS}$ (mm)	$t_{p\text{-}Cl}$ (mm)	$P_{cr\text{-}SS}$ (kN)	$P_{cr\text{-}Cl}$ (kN)	$P_{cr\text{-}SPSW}$ (kN)	$t_{p\text{-}SPSW}$ (mm)
Lubell (1997)	825×825×1.5	Hot-Rolled	8.6	6.9	6.91	10.78	10.96	6.8
	825×825×1.5	LYP100	4.6	3.7	6.91	10.78	10.96	3.7
Chen and Jhang (2006)	1250×1250×8.0	LYP100	7.0	5.6	692.28	1079.50	949.13	6.1

As seen in the table, the limiting plate thickness in case of Lubell's test specimen is determined by considering both conventional and LYP steel material, and it is evident that use of LYP steel results in a considerably reduced limiting thickness value. Based on these results, four SPSW models have been considered for the purpose of this study, whose properties are provided in Table 5.5. Included in Table 5.6, also, are the material properties of the SPSWs considered in theoretical calculations as well as numerical modeling.

Table 5.5 Considered numerical models of tested SPSW specimens

Test	Model	Steel Type	t_p (mm)	Plate Type
Lubell (1997)	Lubell-3.7-Moderate	LYP100	3.7	Moderate
	Lubell-6.8-Stocky	LYP100	6.8	Stocky
Chen and Jhang (2006)	C&J-6.1-Moderate	LYP100	6.1	Moderate
	C&J-8.0-Stocky	LYP100	8.0	Stocky

Table 5.6 Material properties of the modeled experimental SPSW specimens

Test	Material Properties		
	Plate		Frame
Lubell (1997)	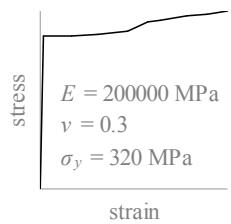	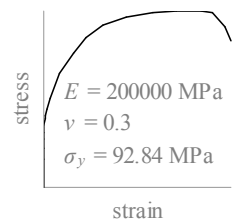	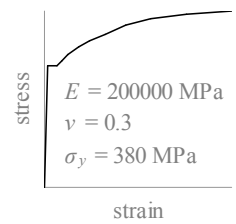
Chen and Jhang (2006)	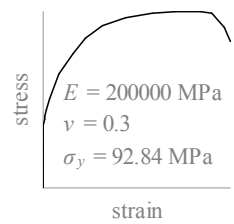		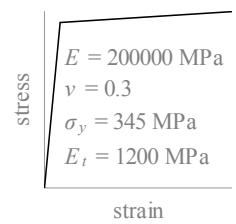

In order to verify the accuracy of predictions of Eq. (4.9) in here, linear and nonlinear finite element analyses are performed to evaluate the buckling and yielding behaviors of the four SPSW models listed in Table 5.5, the results of which are shown in Fig. 5.17. From the figure, it is quite evident that in both Lubell-3.7-Moderate and C&J-6.1-Moderate models buckling and yielding occur almost simultaneously, and Lubell-6.8-Stocky and C&J-8.0-Stocky models undergo early yielding prior to buckling as expected. This, time and again, demonstrates that Eq. (4.9) is able to predict the limiting thickness of infill plates fairly accurately.

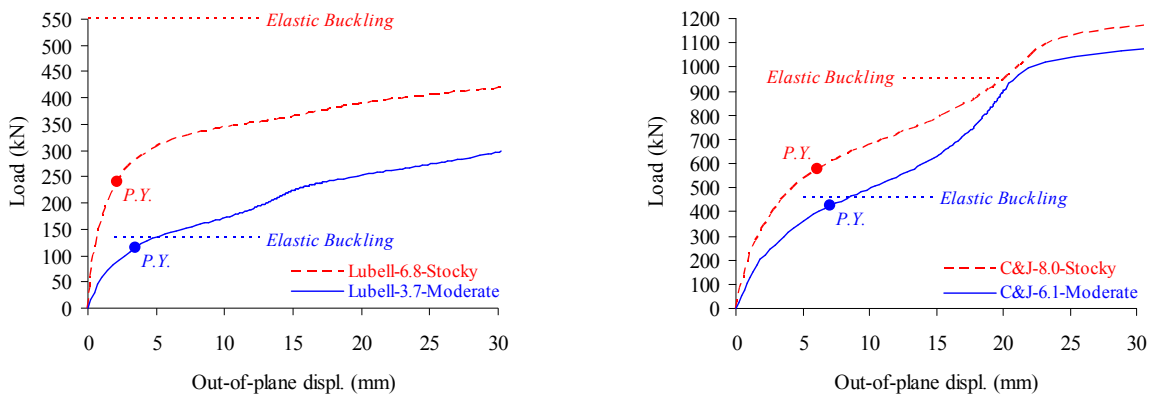

(a) Lubell (1997) **(b)** Chen and Jhang (2006)

Fig. 5.17 Buckling and yielding behavior of the modeled experimental SPSW specimens

The numerical results from finite element analysis of Lubell-3.7-Moderate & Lubell-6.8-Stocky as well as C&J-6.1-Moderate & C&J-8.0-Stocky SPSW models are compared with the predictions of the modified PFI model as shown in Figs. 5.18 and 5.19, respectively.

From the figures, it is found that the modified PFI model is able to effectively predict the overall behavior of the SPSW models. Consistent with all four cases, predictions of the initial stiffness, plate first yield displacement, and ultimate strength of the panel are satisfactory. However, as seen in Fig. 5.18, the modified PFI model underestimates the ultimate strength in cases of Lubell-3.7-Moderate and Lubell-6.8-Stocky models compared to those shown in Fig. 5.19. It is noted that the analytical model also shows the contributions from the infill plate and surrounding frame to the shear resistance of the panel. From Fig. 5.18, it is apparent that in this case infill plate contributes significantly to the shear resistance of the panel compared to the frame, while in the second case as shown in Fig. 5.19, frame contribution is relatively high. This capability of the PFI method, in fact, properly reflects the fact that the surrounding frame members in Lubell's specimen were originally designed for the slender infill plate rather than moderate and stocky infill plates with relatively larger thicknesses, while the frame members in

Chen and Jhang's specimen were properly designed for the stocky infill plate and hence exhibit higher contribution and performance.

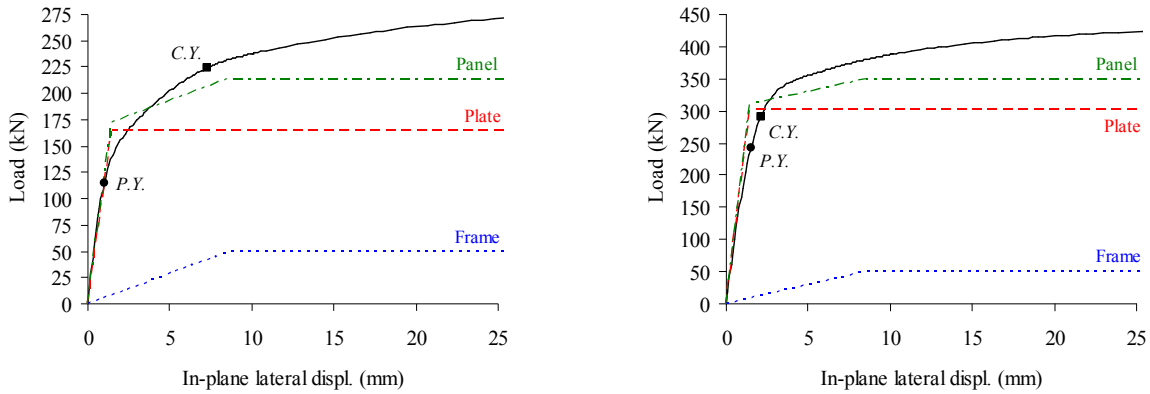

(a) Lubell-3.7-Moderate **(b)** Lubell-6.8-Stocky

Fig. 5.18 Comparison of the modified PFI model predictions with numerical results of Lubell's (1997) SPSW2 specimen model

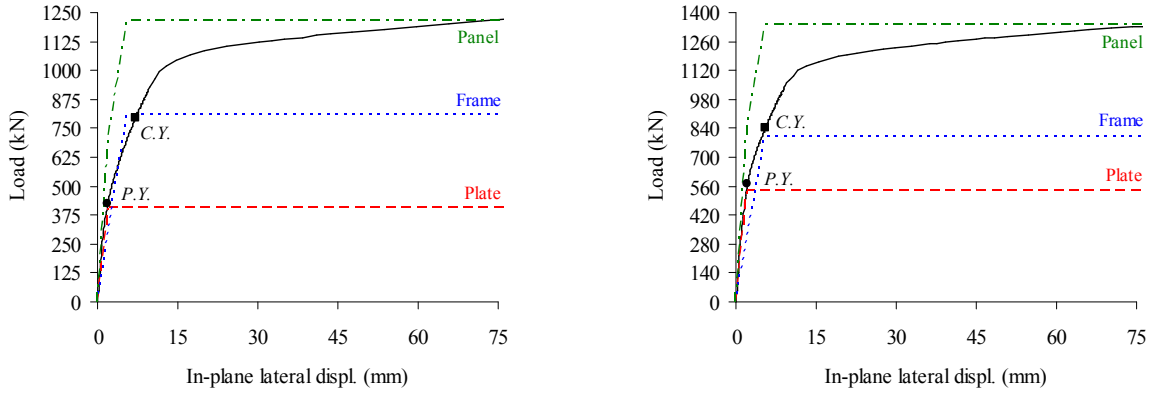

(a) C&J-6.1-Moderate **(b)** C&J-8.0-Stocky

Fig. 5.19 Comparison of the modified PFI model predictions with numerical results of Chen and Jhang's (2006) specimen no. 1 model

Finally, finite element results of SPSW1, SPSW4, SPSW5, and SPSW6 models with various aspect ratios are compared with the predicted response by the modified PFI model. Comparison results are given in Fig. 5.20.

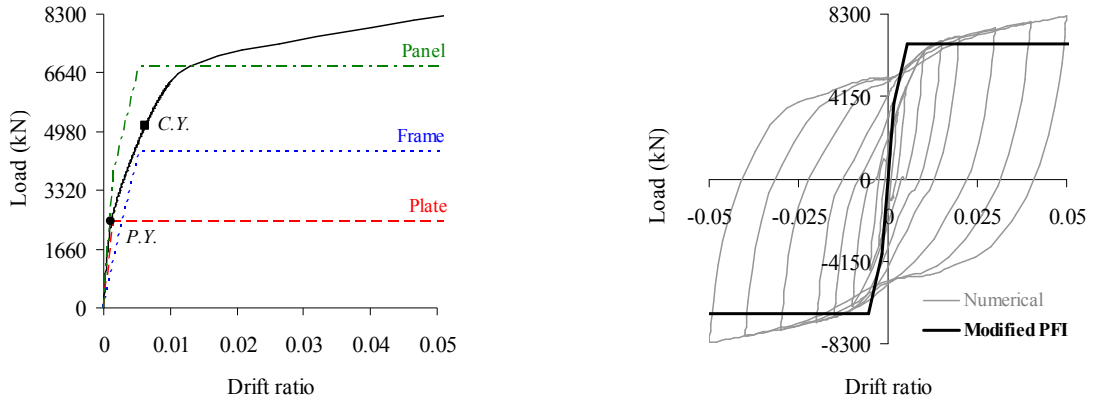

(a) SPSW4

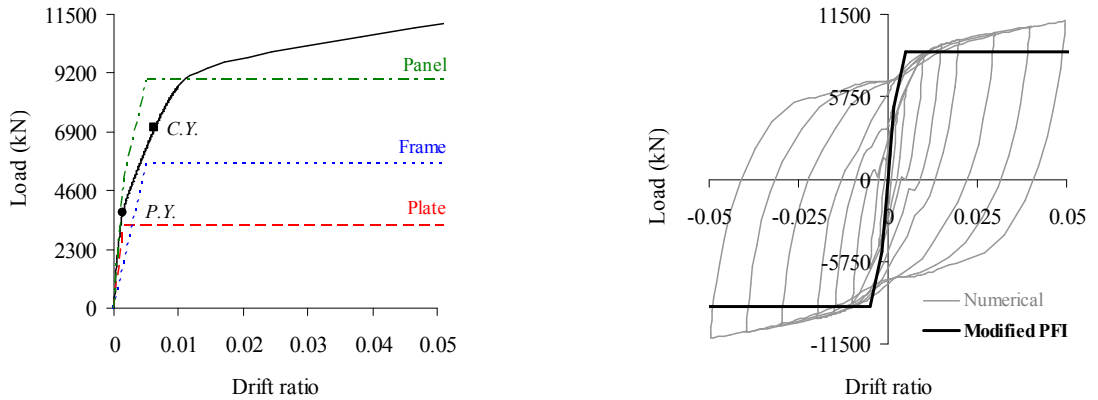

(b) SPSW5

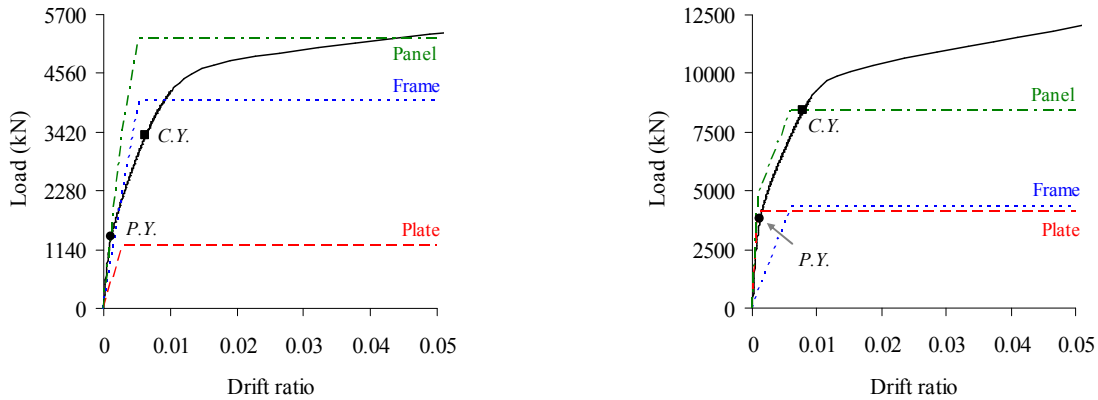

(c) SPSW1 **(d)** SPSW6

Fig. 5.20 Comparison of the modified PFI model predictions with numerical results of full-scale and code-designed SPSW models with various aspect ratios and under lateral load

As it is seen in Figs. 5.20(a) and (b), the modified PFI model has successfully captured the overall performance of SPSW4 and SPSW5 models with $l/h = 1.00$. Initial stiffness and plate first yield displacement of these models have been closely predicted by the analytical model, while the ultimate capacity is underestimated in both cases. On the other hand, analytical predictions for SPSW1 and SPSW6 models with respective l/h ratios of 0.67 and 1.50, exhibit various degrees of accuracy as shown in Figs. 5.20(c) and (d). Good agreement is observed between the finite element results and analytical predictions of the initial stiffness in both cases. However, the modified PFI model overestimates the plate first yield displacement of SPSW1 model as shown in Fig. 5.20(c), while provides acceptable predictions in case of SPSW6 model as shown in Fig. 5.20(d). This implies that the modified parameter, U_p, may require further refinement by considering the panel aspect ratio and also amount of contribution of each deformation, i.e. bending and shear, to the ultimate deformation of the panel, which of course needs more investigation. Additionally, analytical predictions of the ultimate strength seem to be overly conservative in case of SPSW6 model (Fig. 5.20(d)), while these are reasonably consistent with the finite element results of SPSW1 model (Fig. 5.20(c)), which may be attributed to the relative lower (SPSW6) and higher (SPSW1) contribution of the frame to the ultimate strength of the system.

All in all, it is concluded that the PFI model is in general a powerful tool which can be effectively used to predict the overall behavior of a SPSW system and also characterize the performance and interaction of the plate and frame components. The findings of this study also demonstrate that the modified PFI model is capable of predicting the behaviors of LYP steel shear walls with moderate and stocky infill plates. However, further experimental and parametric studies are still needed for improving this model which will eventually result in accurate

prediction of the behavioral properties of such efficient lateral force-resisting and damping structural elements.

5.7 Concluding Remarks

Application of LYP steel shear walls has been shown in a number of studies to be highly promising towards improving the stiffening as well as damping characteristics of SPSW systems. However, for efficient design and prevalent use of such systems, further research work is still required to balance between structural demands and economical considerations. On this basis, the advantages as well as structural behavior and performance of some code-designed LYP steel shear wall systems with unstiffened slender, moderate, and stocky infill plates were identified and investigated in this chapter via finite element and analytical methods.

It was demonstrated that application of LYP steel infill plates results in reduced forces imposed on the boundary frame members as compared to the conventional steel infill plates, and also offers the possibility of repair and retrofit of existing structures.

Application of unstiffened steel shear wall systems with relatively high buckling and low yielding capacities, enhanced serviceability as well as energy dissipation capacity is made possible in the light of use of LYP steel material. This was addressed by evaluating the monotonic and cyclic behaviors of LYP steel shear wall models with slender, moderate, and stocky infill plates. The limiting thicknesses corresponding to concurrent geometrical-material bifurcation of moderate infill plates were successfully predicted through two approaches, i.e. Eqs. (4.9) and (4.11). This limiting thickness is believed to serve as an effective criterion in seismic design of SPSW systems with high stiffening and damping performance.

Ultimately, the well-known PFI method was modified to account for bending and shear deformations, which was subsequently used to predict the behaviors of SPSW systems with moderate and stocky infill plates. The effectiveness of this modified analytical model was verified through detailed comparison with various experimental and numerical results. In spite of the overall acceptable performance of the model, further experimental results and parametric studies are required in order to improve the accuracy of the predicted response.

6. STUDY ON SEISMIC DESIGN AND STRUCTURAL PERFORMANCE OF SPSWS WITH LYP STEEL INFILL PLATES

6.1 Introduction

In general, SPSWs have been demonstrated to be promising and efficient lateral force-resisting systems and accordingly increasingly used in the construction of buildings. However, the priorities of high structural performance in Japan and economical considerations in North America have resulted in design and use of stiffened and/or stocky-web as well as unstiffened and slender-web systems, respectively, in these countries.

SPSWs were introduced into the U.S. codes as "special plate shear walls" in 2005 edition of the AISC Seismic Provisions for Structural Steel Buildings (AISC 341-05, 2005). Continuous research has led to specifying refined design requirements in 2010 edition of the AISC code (AISC 341-10, 2010). The AISC 341 seismic design provisions require capacity design of SPSWs, which implies that HBEs must be designed to resist demands resulting from tension field yielding of the infill plates and VBEs must be designed to resist the tension field yielding of the infill plates and flexural yielding of the HBEs (Berman, 2011). It is noted that the AISC 341 seismic design provisions typically address SPSWs with unstiffened and slender infill plates which buckle first and subsequently undergo material yielding in the post-buckling stage. However, SPSWs with LYP steel infill plates may possess relatively low yielding and high buckling capacities, and consequently undergo material yielding prior to buckling due to early yielding of the steel material.

The objective of the research presented in this chapter is to investigate the structural behavior and performance of SPSWs with unstiffened LYP steel infill plates under the action of combined shear and compressive forces, designed for high-seismic loading. Specifically, nonlinear pushover and cyclic analyses of SPSWs are performed to investigate: i) the strength, stiffness, and cyclic performances of the code-designed LYP steel shear walls with different aspect ratios, ii) the effectiveness of some AISC 341 code-specified design requirements and considerations, and iii) the performance of the modified PFI model in predicting and characterizing the behaviors of SPSWs with low yielding and high buckling capacities and different aspect ratios.

6.2 Design of SPSW Models

Three single-story, single-bay, and full-scale SPSWs with 2100×3100, 3100×3100, and 4600×3100 mm unstiffened LYP steel infill plates under gravity and in-plane lateral loads are designed based on AISC 341-10 (2010) seismic provisions and recommendations provided in AISC Steel Design Guide 20 (Sabelli and Bruneau, 2006) for high-seismic loading.

Buildings are generally subjected to gravity and lateral loads. As the primary lateral force-resisting components, infill plates in SPSW systems resist the lateral loads, and hence are typically subjected to shear forces. On the other hand, the building frames, including the SPSW boundary elements, should be designed to carry gravity loads while neglecting the contribution of the SPSW panels (Seilie and Hooper, 2005). Per AISC 341-10 (2010) provisions, the webs of SPSW shall not be considered as resisting gravity forces. However, due to the effects of vertical ground motion, construction sequence, etc., infill plates in SPSWs may be subjected to some levels of compressive forces in addition to the shear forces. In this study, in order to account for the effects of combined shear and compressive forces, as illustrated in Fig. 6.1, the sum of the

two column axial forces is divided by the sum of areas of the two columns and the infill plate, and the resulting vertical uniformly-distributed compressive stress (σ_c) is used in design of SPSWs.

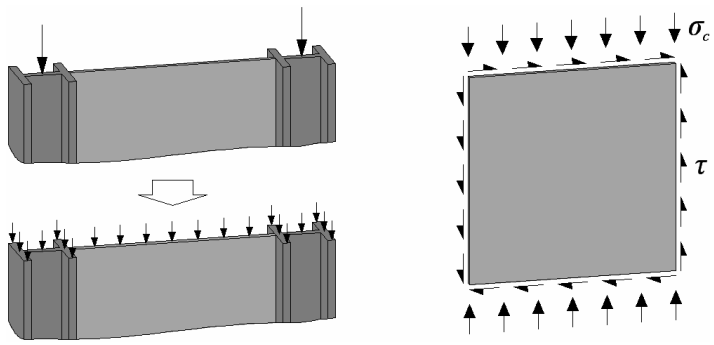

Fig. 6.1 Consideration of compressive load

The compressive stress (σ_c) is obtained using

$$\sigma_c = \frac{2 \times 0.10 \times \sigma_{yc} \times A_c}{2A_c + lt_p} \tag{6.1}$$

in which, σ_{yc} and A_c are the yield stress and cross-section area of the column, and l and t_p are the length and thickness of the infill plate, respectively. As it is seen in Eq. (6.1), the column axial force is taken as 10% of the column yield capacity.

For comparison purposes, the infill plate thicknesses are determined in a manner to ensure that SPSWs with different aspect ratios undergo simultaneous geometrical buckling and material yielding. To achieve this, the limiting thicknesses ($t_{p\text{-}limit}$) corresponding to concurrent geometrical buckling and material yielding of plates with simple and clamped support conditions are primarily estimated by using Eqs. (4.3) and (4.6), as discussed in Chapter 4. In theoretical calculations, Young's modulus (E), Poisson's ratio (ν), and plate yield stress (σ_{yp}) are taken as 200000 MPa, 0.3, and 100 MPa, respectively.

The theoretical predictions for the limiting thicknesses of plates with simple and clamped support conditions are summarized in Table 6.1. Included in the table are also the accurate values for the limiting thicknesses of infill plates in SPSWs, which are obtained through an iterative process by performing nonlinear pushover analyses to reach a condition at which plate yielding and buckling occur simultaneously.

Table 6.1 Comparison of theoretically-predicted and exact limiting plate thicknesses

$l \times h$ (mm)	$t_{p\text{-}limit}$ (mm)		Model	$t_{p\text{-}limit}$ (mm)
	Simply Supported	Clamped		Exact
2100×3100	16.6	12.9	SPSW1	12.6
3100×3100	23.2	17.0	SPSW2	16.5
4600×3100	28.0	19.8	SPSW3	20.0

From Table 6.1, agreement between the theoretical estimates for clamped support condition and the exact values of the limiting plate thicknesses is quite satisfactory. This indicates that the limiting thicknesses of infill plates in SPSWs under combined shear and compressive loads can be fairly accurately determined by simply considering the clamped support condition. In this study, the exact values of the limiting plate thicknesses are considered in design of SPSWs. Boundary frame members are subsequently designed based on the geometrical properties of the infill plates, and also by selecting ASTM A572 Gr. 50 steel with 345 MPa yield stress for the boundary frame, and LYP100 steel with 100 MPa yield stress for the infill plates. Specifications of the code-designed SPSWs are provided in Table 6.2.

Table 6.2 HBE, VBE, and infill plate cross-sectional and geometrical properties of SPSWs

Model	Infill Plate	HBE	VBE	l/h	l/t_p	h/t_p
	$l \times h \times t_p$ (mm)					
SPSW1	2100×3100×12.6	W14×132	W14×398	0.68	166	246
SPSW2	3100×3100×16.5	W14×426	W14×605	1.00	188	188
SPSW3	4600×3100×20.0	W36×529	W36×800	1.48	230	155

The tabulated results in Tables 6.1 and 6.2 demonstrate that as the plate length-to-height (l/h) aspect ratio increases, the required limiting plate thickness corresponding to concurrent buckling and yielding increases as well which, in turn, results in larger HBE and VBE sections required to satisfy the code-specified seismic design requirements. Thus, proficient selection of the aspect ratio parameter in practice can result in design of relatively cost-effective LYP steel shear wall systems with high stiffening and damping capabilities. Also, it should be noted that employment of stiffeners in LYP steel shear walls can result in significantly reduced limiting plate thicknesses and consequently highly-efficient lateral force-resisting and energy dissipating systems but at the cost of some extra fabrication expenses.

It is also noted that per AISC 341-10 (2010) design requirements, boundary columns shall have moments of inertia (I_c) not less than $0.0031 t_p h_s^4 / l_s$ (Eq. (3.7)), and boundary beams shall have moments of inertia (I_b) not less than $0.0031 l_s^4 / h_s$ times the difference in web plate thicknesses above and below (Eq. (3.8)). Findings of this study indicate that these stiffness criteria seem to be fairly stringent in controlling the design. Hence, further research is required to evaluate the effectiveness of the specified stiffness criteria.

6.3 Finite Element Modeling and Verification

Finite element models of the SPSWs are developed and analyzed using ANSYS 11.0 (2007) software. Consistent with previously-discussed analyses, Shell181 element is used to model the infill plate and boundary frame members in this study as well. The SPSW finite element models are shown in Fig. 6.2.

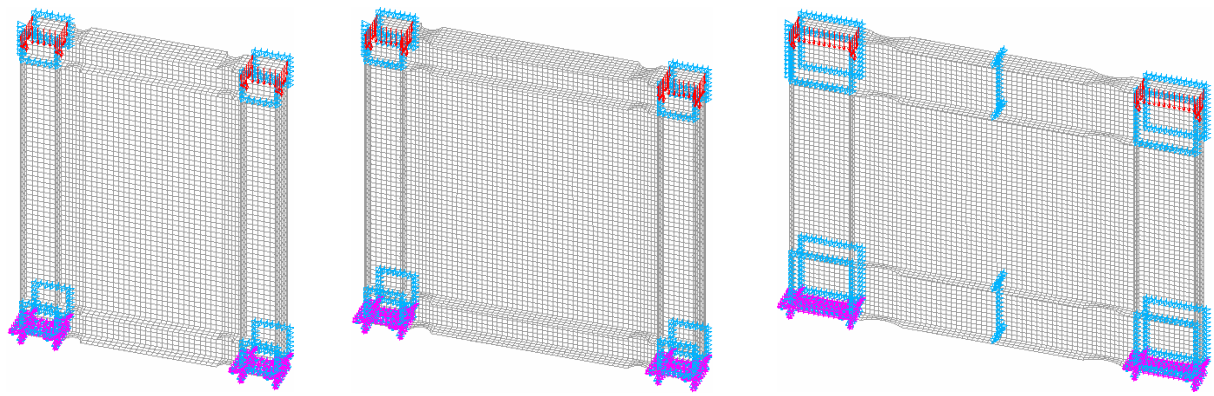

(a) SPSW1 **(b)** SPSW2 **(c)** SPSW3

Fig. 6.2 Finite element models

As seen in Fig. 6.2, columns are fully fixed at their bases and the exterior nodes of the column flange and stiffener elements around the perimeter of the panel zones are restrained against out-of-plane displacement. Also, as shown in Fig. 6.2(c), beams in SPSW3 model are laterally braced against out-of-plane displacement at midspan.

The stress-strain curves of the LYP100 and ASTM A572 Gr. 50 steel material considered in modeling of the infill plate and boundary frame members, respectively, are shown in Fig. 4.16. In addition, von Mises yield criterion is used for material yielding, and isotropic and kinematic hardening rules are incorporated in the respective nonlinear pushover and cyclic analyses.

Initial imperfections of about $\sqrt{l \cdot h}/1000$ mm based on the first buckling mode of the plate are incorporated in the finite element models. This is achieved by primarily conducting an eigen buckling analysis to determine the first buckling mode prior to the nonlinear analysis of each SPSW model. It is noted that the applied imperfection magnitudes are smaller than 1% of $\sqrt{l \cdot h}$ limit proposed by Behbahanifard et al. (2003), and therefore their effects on the stiffness and capacity of the SPSW models are negligible.

In pushover and cyclic analyses with geometrical and material nonlinearities, gravity load up to 10% of the column's axial yield load is initially applied to the top of each column which is uniformly distributed across the column's cross-section, as shown in Fig. 6.2. Subsequently, the gravity load is kept constant and in-plane lateral load is applied to the beam-column connection in a displacement-controlled and incremental manner. The loading protocol applied in the cyclic analyses is given in Table 6.3, where δ is the in-plane lateral displacement.

Table 6.3 Cyclic loading protocol

Cycle No.	1	2	3	4	5	6
δ/h	± 0.001	± 0.005	± 0.013	± 0.024	± 0.048	± 0.073

As discussed in Chapter 4, the accuracy of the finite element modeling of the SPSWs is verified through comparison with two sets of experimental results, as shown in Figs. 4.17 and 4.18.

6.4 Strength, Stiffness, and Cyclic Performances of Code-Designed SPSW Models

The structural performances of the code-designed LYP steel shear wall models under monotonic and cyclic loadings are evaluated in this section. Fig. 6.3 shows the strength and stiffness performances of the SPSW models, in which the first yield points of the infill plate, HBE, and VBE components are displayed as well. Drift ratio is calculated by δ/h_s .

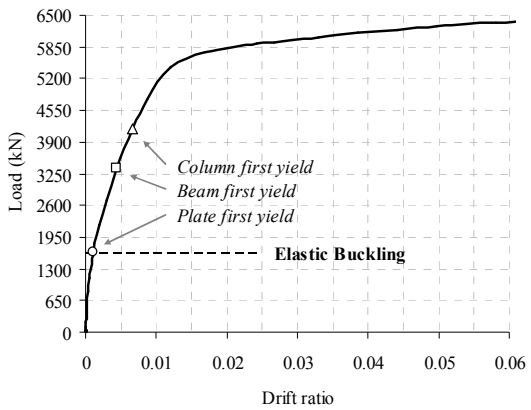

(a) Load vs. drift ratio (SPSW1)

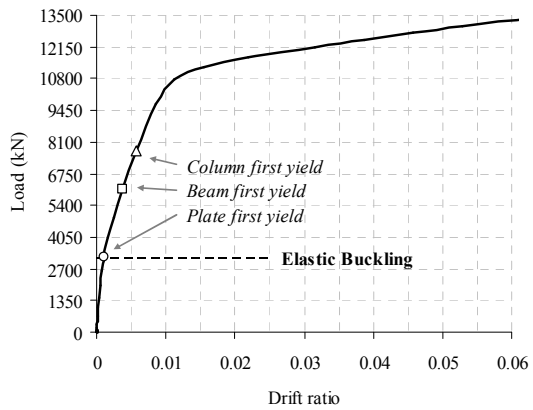

(b) Load vs. drift ratio (SPSW2)

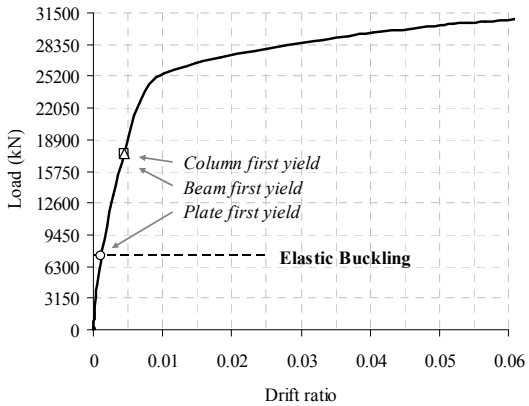

(c) Load vs. drift ratio (SPSW3)

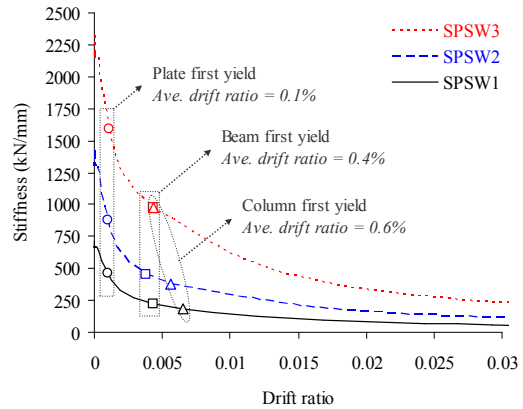

(d) Stiffness vs. drift ratio

Fig. 6.3 Monotonic behaviors of SPSW models

These results indicate that strength and stiffness of SPSWs are augmented remarkably by increasing of the l/h ratio. As it is seen in Figs. 6.3(a), 6.3(b), and 6.3(c), yielding and buckling of the LYP steel infill plates with the limiting thicknesses in respective SPSW1, SPSW2, and SPSW3 models occur simultaneously, as expected. Also, as it is shown in Figs. 6.3(a) through 6.3(d), plate first yield occurs at 0.1% average drift ratio prior to frame yielding, which is followed by the HBE and VBE yielding at respective 0.4% and 0.6% average drift ratios. Moreover, the stiffness performance of the SPSW models is shown in Fig. 6.3(d), from which it is evident that the SPSW models with different aspect ratios desirably possess large initial stiffness which gradually decays due to primarily buckling and yielding of the LYP steel infill

plate, and subsequently yielding of the boundary frame members at higher drift ratios. In fact, such desirable yielding sequence, stable stiffness performance, and ductile behavior are achieved as a result of proper design of the frame members in SPSW models, and especially application of LYP steel infill plates with extremely low yielding strength and high elongation capacity which facilitates the design of SPSW systems as well.

The hysteretic performances of the LYP steel shear wall models loaded cyclically according to the history given in Table 6.3, are shown in Fig. 6.4. The hysteresis lateral load-drift ratio curves of SPSW1, SPSW2, and SPSW3 models are shown in Figs. 6.4(a), 6.4(b), and 6.4(c), respectively, and the cumulative dissipated energy (CDE)-drift ratio curves of the three models are shown in Fig. 6.4(d).

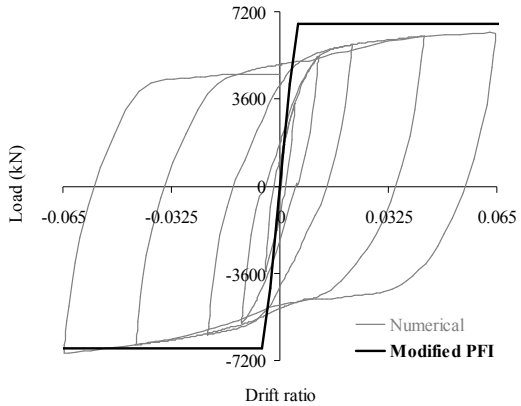

(a) Load vs. drift ratio (SPSW1)

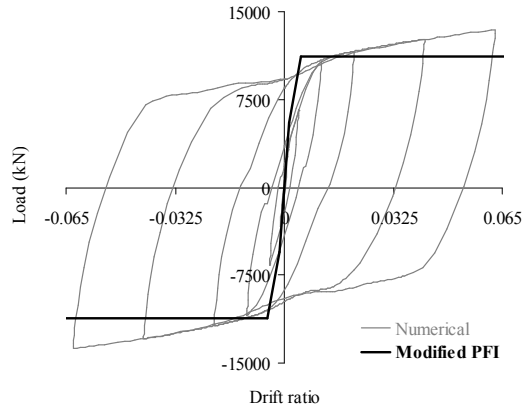

(b) Load vs. drift ratio (SPSW2)

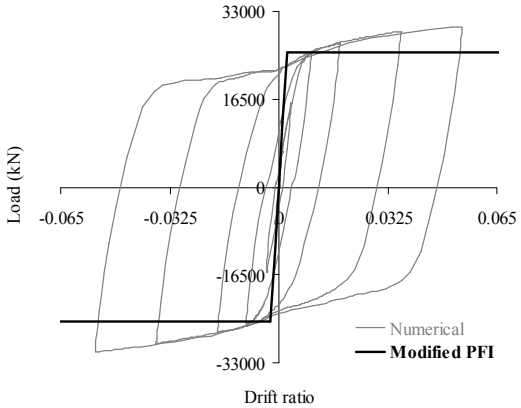

(c) Load vs. drift ratio (SPSW3)

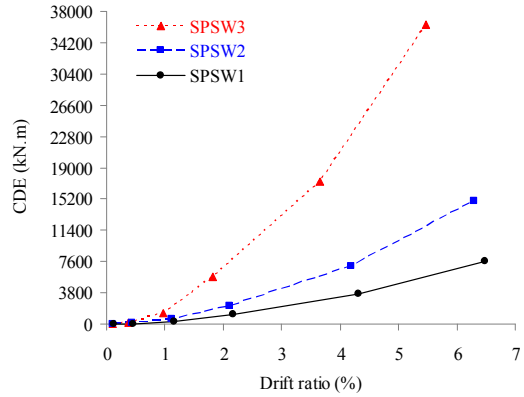

(d) CDE vs. drift ratio

Fig. 6.4 Cyclic behaviors of SPSW models

Results presented in Figs. 6.4(a) through 6.4(c) demonstrate that the code-designed SPSW models dissipate the energy through stable hysteresis loops with relatively small pinching effect due to improved buckling stability of the LYP steel infill plate with the limiting thickness. From Fig. 6.4(d), it is apparent that larger l/h ratio results in increased energy dissipation capacity, and also application of LYP steel infill plates results in early yielding and energy dissipation of the SPSW systems from the initial stages of the loading process.

Stiffness, strength, and energy dissipation capacity are three important characteristics of a lateral force-resisting system which are directly related to the aspect ratio of a SPSW system. The responses of the SPSW models with different aspect ratios are evaluated by considering non-dimensional stiffness (K^*), strength (P^*), and energy dissipation capacity (E^*) parameters, as given in Eq. (6.2). Non-dimensional stiffness is defined as the ratio of SPSW initial stiffness (K_i) to shear stiffness of infill plate. Non-dimensional strength, on the other hand, is defined as the ratio of SPSW strength at 0.05 drift ratio ($P_{DR=0.05}$) to shear yield (buckling) capacity of infill plate, while non-dimensional energy dissipation capacity is defined as the ratio of SPSW total cumulative dissipated energy ($(CDE)_t$) to energy dissipation capacity of infill plate up to shear yielding (buckling) limit.

$$K^* = \frac{K_i \cdot 2(1+\nu)}{E \cdot (l/h) \cdot t_p}, \qquad P^* = \frac{P_{DR=0.05}}{\tau_{yp} \cdot l t_p}, \qquad E^* = \frac{(CDE)_t \cdot E}{\tau_{yp}^2 \cdot V_p \cdot (1+\nu)} \tag{6.2}$$

In Eq. (6.2), V_p is the volume of the infill plate. Fig. 6.5 shows the normalized responses of the three SPSW models with different aspect ratios. From Fig. 6.5(a), it is found that in spite of minor increasing/decreasing trends, variations of the non-dimensional stiffness are not significant, and the normalized stiffness parameter possesses a relatively constant performance

for different aspect ratios. Fig. 6.5(b), on the other hand, indicates that the non-dimensional strength increases by increasing of aspect ratio; however, this increase is considerable in case of SPSW3 model with aspect ratio more than 1.00. Variations of the non-dimensional energy dissipation capacity shown in Fig. 6.5(c), also, demonstrate that the normalized dissipated energy parameter has a comparatively similar performance in cases of SPSW1 and SPSW2 models with respective 0.68 and 1.00 l/h ratios, whereas this parameter exhibits a noticeable increase in case of SPSW3 model with $l/h = 1.48$.

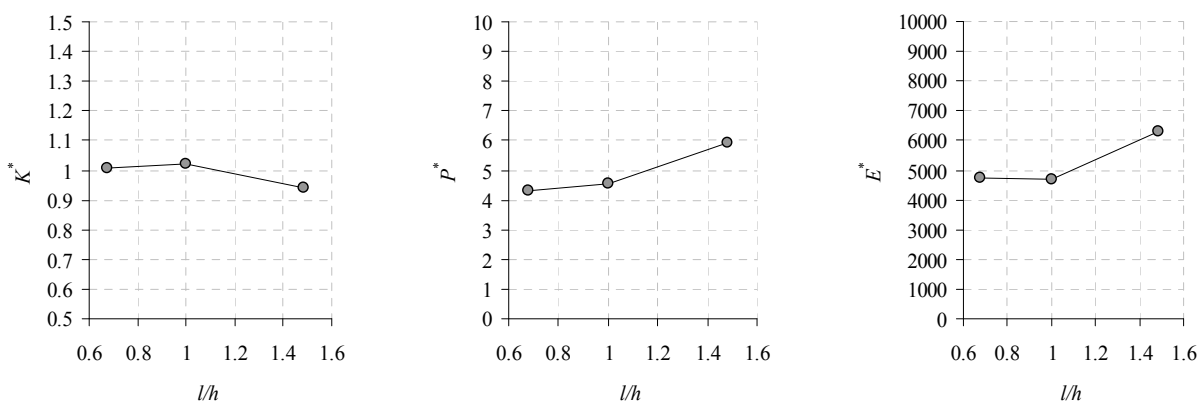

(a) Stiffness **(b)** Strength **(c)** Energy dissipation capacity

Fig. 6.5 Normalized responses of SPSW models for different aspect ratios

The considerable increase in non-dimensional strength and energy dissipation capacity of SPSW3 model may be attributed to the contribution of the boundary frame with relatively heavier HBE and VBE sections. Such improved capabilities, however, may be accompanied by increased construction costs in practice which should be taken into consideration. Overall, these findings are indicative of lateral force-resisting as well as energy dissipating capabilities of SPSW systems, which are economically attainable in the light of use of LYP steel.

6.5 Design Considerations and Structural Performance

6.5.1 Diagonal Tension Field and Angle of Inclination

In SPSWs, lateral shears are carried by tension fields that develop in the infill plates stressing in the direction α, defined as the inclination angle of the tension field and measured by the angle between the direction of the tension field and the vertical direction.

As mentioned before, Thorburn et al. (1983) developed an analytical model, known as the strip model, in which the infill plates were represented by a series of pin-ended, tension-only strips oriented at angle α, and proposed an equation for estimating α. The inclination angle of the tension field was obtained using the principle of least work and considering only the energy of the tension field and axial energy in the beams and columns. Based on experimental investigations, Timler and Kulak (1983) modified the angle of inclination of the tension field proposed by Thorburn et al. (1983), and added the bending strain energy of the columns to the energy calculation, and consequently came up with a revised equation for α, i.e. Eq. (3.6), which was shown to yield reasonable predictions compared to the test results (Behbahanifard et al., 2003). It is noted that this equation is based on the assumption that the infill plate has no compression strength. Per AISC 341-10 (2010) provisions, the angle of inclination, α, is permitted to be calculated using Eq. (3.6), or to be taken as 40°.

The inclination angles of the tension fields developed in LYP steel infill plates of the SPSW models with relatively low yielding and high buckling capacities are determined in this study and compared with predictions of Eq. (3.6). To achieve this, as shown in Fig. 6.6, the angles of inclination of the principal tensile stresses in the infill plates are measured at 0.01, 0.03, and 0.05 drift ratios and the average values are provided in Table 6.4. Included in the table are also the analytical predictions of Eq. (3.6). It should be noted that the angle of principal stresses is

representative of the formation of tension-field action, and principal stresses act at the angle of inclination.

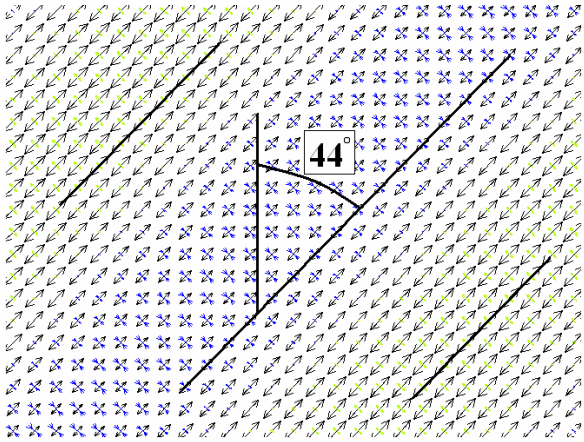

Fig. 6.6 Angle of inclination of the principal tensile stresses developed in the infill plate of SPSW2 model at 0.03 drift ratio

Table 6.4 Numerically- and analytically-obtained values for the angle of inclination

Model	Angle of Inclination (α)	
	Finite Element Analysis	Prediction of Eq. (3.6)
SPSW1	45°	37.4°
SPSW2	44°	41.1°
SPSW3	46°	42.6°

Despite the simplifying assumptions in the derivation of Eq. (3.6), e.g. elastic behavior of the infill plate and the boundary members as well as simple beam-to-column connections, from Table 6.4 the agreement between the finite element and analytical estimates of the orientation of the tension field is fairly satisfactory. These results indicate that using a single value of 40° for the angle of inclination, per AISC 341-10 (2010) provisions, throughout the design of LYP steel shear walls with relatively low yielding and high buckling capacities will usually suffice. In addition, the orientation of the principal tensile stresses developed in the LYP steel infill plates as summarized in Table 6.4, confirms that for the purposes of analysis using the strip model,

these components with low yielding strength can be modeled as a series of pin-ended inclined strips oriented at 45° relative to the vertical.

6.5.2 Performance of Reduced Beam Section (RBS) Connections

SPSWs designed in accordance with the AISC 341-10 (2010) provisions are expected to provide significant inelastic deformation capacity primarily through infill plate yielding and as plastic-hinge formation at the ends of HBEs. Hence, plastic hinging at the beam ends is needed to develop the plastic collapse mechanism of the SPSW system.

RBS beam-to-column connections have been suggested to be used in SPSWs in order to ensure that frame plastic hinging occurs at beam ends, and not within beam span or in columns. The use of RBSs at the ends of the horizontal boundary members has been investigated by Vian and Bruneau (2004) and Vian et al. (2009) as a means of reducing the overall system demand on the vertical boundary members, and also has been recommended to control boundary frame yielding during a significant earthquake.

On the other hand, one major problem with the RBS type of connection is the deterioration of the load-carrying capacity owing to lateral and local buckling in beams. Reduction of the beam flange section degrades the restraints against out-of-plane deformations (Moslehi Tabar and Deylami, 2005). RBS connection web and flange local buckling as well as HBE out-of-plane distortions were observed in the experiments conducted by Vian and Bruneau (2004) and Vian et al. (2009).

In this study, the buckling stability as well as performance of RBS connections in developing the plastic collapse mechanism of the SPSW models with LYP steel infill plates are evaluated. It is noticeable that the frame members in SPSW models are designed to meet the AISC 341-10

(2010) seismic compactness requirements. Fig. 6.7 provides the von Mises contour plots of the SPSW models at 0.05 drift ratio.

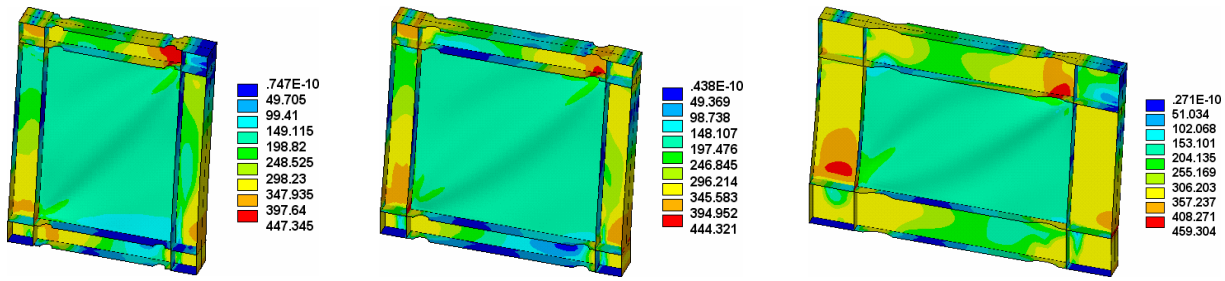

(a) SPSW1 **(b)** SPSW2 **(c)** SPSW3

Fig. 6.7 von Mises stress (MPa) contour plots at 0.05 drift ratio

In Fig. 6.7, the stress concentration at the RBS connections of the SPSW models demonstrates that inelastic action (plastic hinging) in the beams is forced to these specific regions and undesirable midspan hinges are prevented. Additionally, the out-of-plane displacement contour plots of the boundary frames in the three SPSW models at 0.05 drift ratio are also provided in Fig. 6.8.

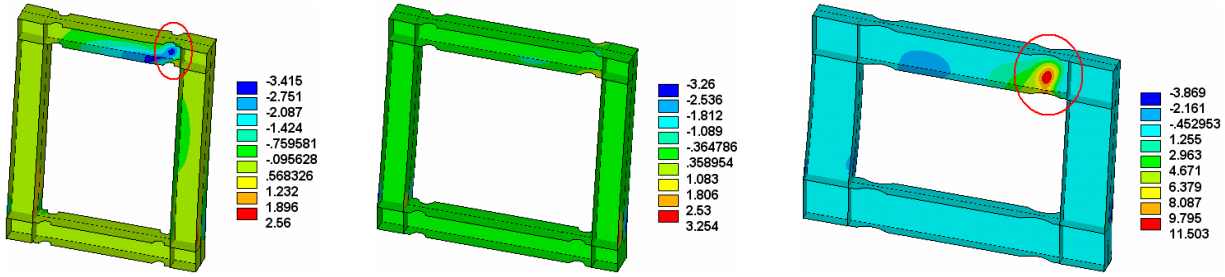

(a) SPSW1 **(b)** SPSW2 **(c)** SPSW3

Fig. 6.8 Frame out-of-plane displacement (mm) contour plots at 0.05 drift ratio

As seen in Fig. 6.8(b), the contour plot does not exhibit any global and/or local out-of-plane instabilities in boundary frame of SPSW2 model, while the occurrence of web local buckling at the RBS connections of the upper beams in SPSW1 and SPSW3 models is evident from Figs.

6.8(a) and 6.8(c), respectively. The growth of these local out-of-plane deformations is shown in Fig. 6.9, where out-of-plane displacements at mid-length and mid-height of the RBS connections in all three LYP steel shear wall models are plotted against drift ratio.

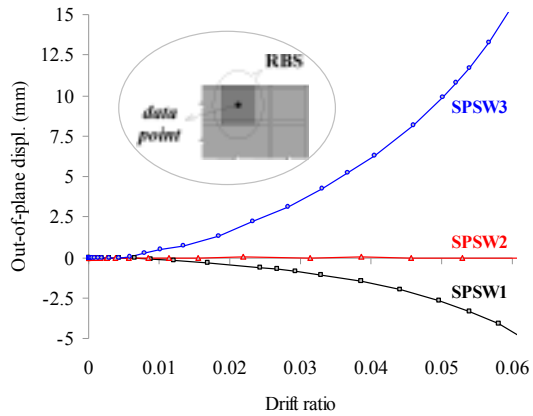

Fig. 6.9 Web local instability at the RBS portion of the upper beam

From Fig. 6.9, it is evident that the RBS connection in SPSW2 model with l/h = 1.00 does not undergo web local buckling. The RBS connection in SPSW1 model with l/h = 0.68, on the other hand, experiences minor out-of-plane deformations occurring initially at about 0.01 drift ratio, while out-of-plane deformations at the RBS connection in SPSW3 model with l/h = 1.48 are found to be the largest which develop from small drift ratios. It is noted that despite the web local instabilities in SPSW1 and SPSW3 models, the global behaviors of these models were not adversely affected.

Overall, evaluation of the finite element results demonstrates that the RBS connections performed as expected, by forming a controlled beam plastic hinge region within the horizontal boundary frame member. As well, the findings of this study indicate that the stability behavior of the RBS connections may be influenced by the system aspect ratio, which albeit requires further investigation. In any case, it should be noted that design of SPSW systems with large length-to-

height aspect ratios will require the application of heavier HBE and VBE sections with relatively large web and flange component slenderness ratios, which will consequently make these frame components more vulnerable to buckling, particularly at RBS regions with reduced lateral restraint and plastic deformations.

6.5.3 Performance of Panel Zones

In addition to the roles of the infill plates and RBS connections as the respective primary and secondary fuses in SPSW systems, the input seismic energy can also be partially dissipated through yielding of the panel zones in shear. It has been demonstrated that well-detailed panel zones usually possess stable energy dissipation characteristics and can sustain large cyclic inelastic deformations. On the other hand, excessive panel zone deformations may influence the overall behavior of the system (Chen et al., 1996). In addition, panel zone ductility is one of the parameters which can considerably influence the failure mode of the beams with RBS moment connections, and it has been shown that moderately strong (neither weak nor overly strong) panel zones show appropriate performance (Moslehi Tabar and Deylami, 2005).

According to AISC 341-10 (2010) Section F5.6b(2) provisions, panel zones of HBE-to-VBE connections at the top and bottom of the SPSW must comply with the Special Moment Frame (SMF) requirements. In order to minimize shear buckling of the panel zone during inelastic deformations, the minimum panel zone thickness is set by Eq. (E3-7) in AISC 341-10 (2010) Section E3.6e(2), at one-ninetieth of the sum of its depth (d_z) and width (w_z), i.e. $t_{pz} \geq (d_z + w_z)/90$, where t_{pz} is the panel zone thickness. In design of the SPSW models in the current research, the code-specified panel zone requirements are met.

The performances of the panel zones in LYP steel shear wall models with relatively low yielding and high buckling capacities are investigated in this study for possible stresses (σ_{pz}) and out-of-plane deformations developed at these regions. The finite element analysis results for the panel zones in SPSW1, SPSW2, and SPSW3 models are presented in Figs. 6.10, 6.11, and 6.12, respectively.

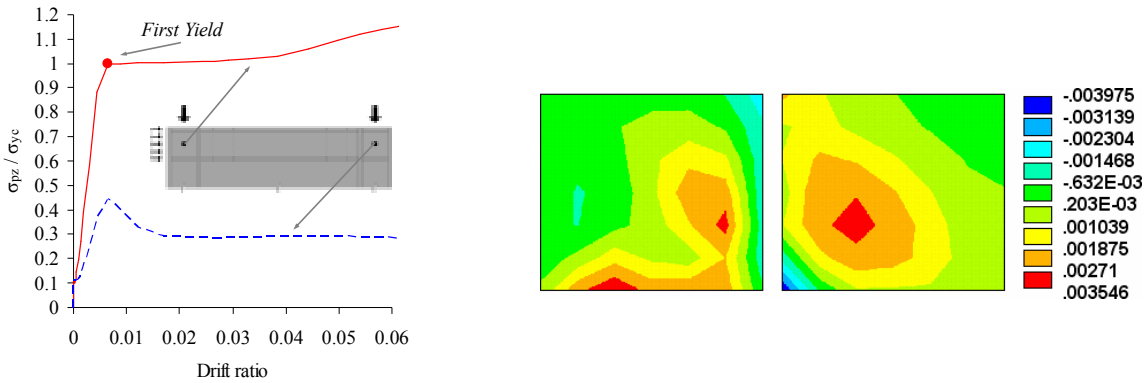

(a) Variation of developed stresses **(b)** Out-of-plane displ. (mm) contour plots at 0.05 drift ratio

Fig. 6.10 Performance of upper left and right panel zones in SPSW1 model

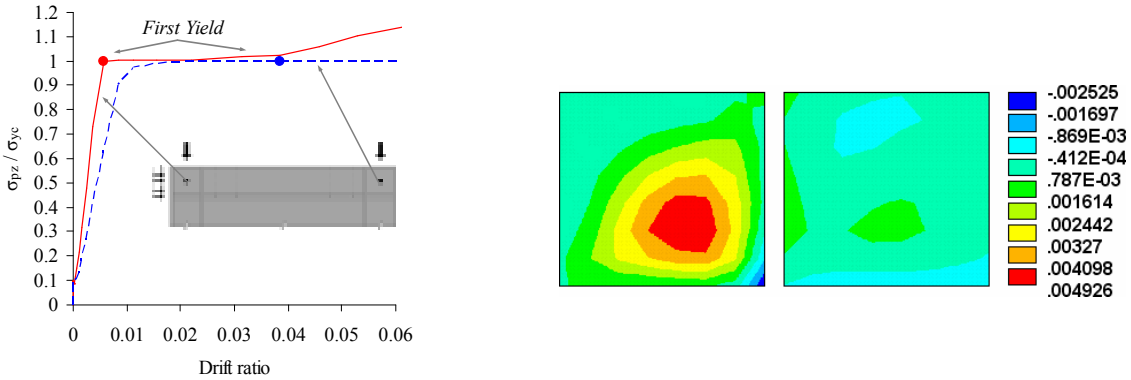

(a) Variation of developed stresses **(b)** Out-of-plane displ. (mm) contour plots at 0.05 drift ratio

Fig. 6.11 Performance of upper left and right panel zones in SPSW2 model

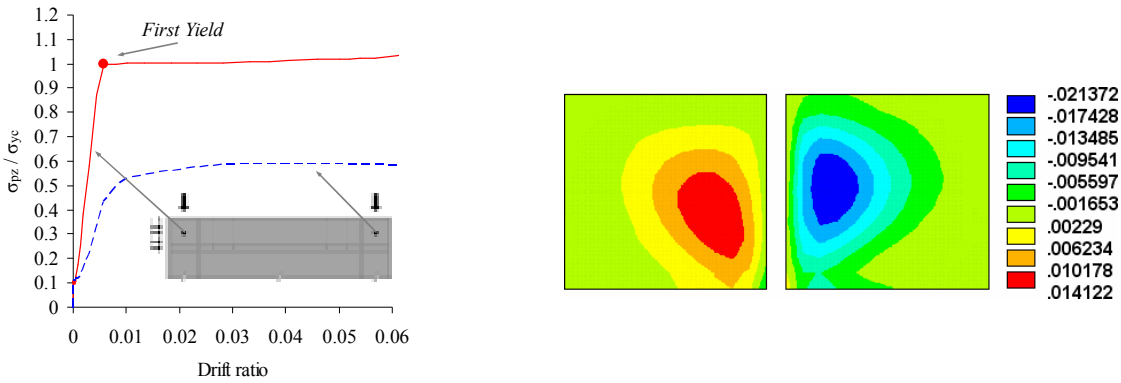

(a) Variation of developed stresses **(b)** Out-of-plane displ. (mm) contour plots at 0.05 drift ratio

Fig. 6.12 Performance of upper left and right panel zones in SPSW3 model

The pushover analysis results shown in Figs. 6.10(a), 6.11(a), and 6.12(a) indicate that aspect ratio parameter affects on the stressing of the panel zones. As seen in these figures, the upper left and right panel zones in SPSW2 model with l/h = 1.00 are almost similarly stressed, while these regions get subjected to different levels of stresses as the l/h ratio differs from unity. Also, it is found that the panel zones first yielding occurs at 0.4% drift ratio on average; however, the amount of participation of these frame components in energy dissipation process differs by the aspect ratio of the system.

Evaluation of the out-of-plane displacement contour plots of the upper left and right panel zones in SPSW1, SPSW2, and SPSW3 models at 0.05 drift ratio, as shown in Figs. 6.10(b), 6.11(b), and 6.12(b), respectively, reveals that the out-of-plane deformations and buckling instability are effectively controlled at these locations. Nonetheless, it is found that by increasing of the panel l/h ratio, out-of-plane deformations of panel zones exhibit an increasing trend. In any case, these findings indicate that the panel zones remained as effectively rigid areas throughout the duration of lateral loading.

Based on the findings of this study, it may be concluded that the panel zones fully compliant with the AISC 341-10 (2010) design requirements perform stably and desirably by yielding and participating in the energy dissipation process of the LYP steel shear wall models. However, aspect ratio parameter seems to be somewhat effective on the performance of these frame components.

6.5.4 Lateral Bracing of Frame Members

Providing stability of SPSW boundary elements is necessary for proper performance and ductile behavior of the system. Hence, stability bracing shall be provided in order to restrain lateral buckling of structural steel beams subject to flexure with specified levels of ductility demand. Per AISC 341-10 (2010) Section F5.4c, HBE shall be braced to satisfy the requirements for *moderately ductile members* in Section D1.2a. It is noted that in AISC 341-10 (2010), members of the seismic force resisting system that are anticipated to undergo inelastic deformation have been classified as either moderately ductile or highly ductile members. During the design earthquake, moderately ductile members are anticipated to undergo moderate plastic rotation of 0.02 rad. or less, whereas highly ductile members are anticipated to undergo significant plastic rotation of more than 0.02 rad..

According to AISC 341-05 (2005) provisions, HBEs were required to be laterally braced at a spacing not to exceed $0.086 r_y E / \sigma_y$ in which r_y is the radius of gyration about *y*-axis and σ_y is the specified minimum yield stress of the steel material, while per AISC 341-10 (2010) bracing requirements of moderately ductile members, beam bracing shall have a maximum spacing of $0.17 r_y E / \sigma_y$. It is noted that in AISC 341-10 (2010), maximum spacing of $0.086 r_y E / \sigma_y$ is only specified for highly ductile beam members.

In this study, HBEs in the three SPSW models are checked for the AISC 341-10 (2010) code-specified unbraced length limitation, and accordingly no intermediate lateral bracing is required in any case. Even, HBEs in SPSW3 model with the largest unbraced length do not require any additional lateral bracing; nevertheless, as seen in Fig. 6.2(c) these are laterally braced at midspan, since in this specific case the HBE unbraced length (L_b) exceeds the limiting laterally unbraced length for the limit state of yielding (L_p), i.e. $L_b > L_p$, and per AISC 360-10 (2010) specifications the limit state of lateral-torsional buckling would control the design. It should be noted that the ductility of structural members with plastic hinges could be significantly reduced by the possibility of lateral buckling.

The effectiveness of the midspan lateral bracing in SPSW3 model is evaluated in this section via investigating the overall response of the system and also monitoring the HBE out-of-plane deformations in this model with no midspan lateral bracing. Fig. 6.13 shows the responses of SPSW3 models with and without HBE midspan lateral bracing. The out-of-plane displacements in the top and bottom flange levels of the upper and lower HBEs at the mid-length of the SPSW3 model with no intermediate lateral bracing are also shown in Fig. 6.14.

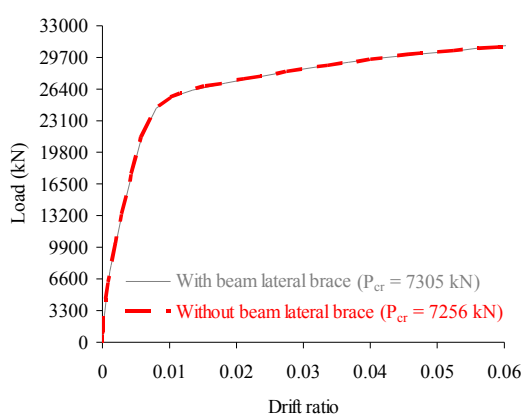

Fig. 6.13 Performance of SPSW3 model with and without beam midspan lateral brace

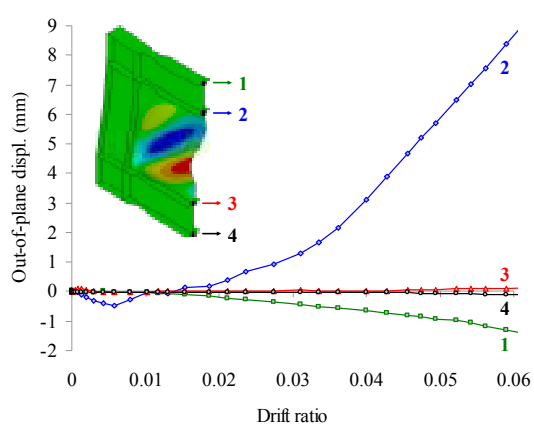

Fig. 6.14 Out-of-plane displacements at mid-length of SPSW3 model without beam lateral brace

As it is observed in Fig. 6.13, HBE midspan lateral bracing has little effect on the elastic buckling capacity of the system and consideration of the restraint increases the buckling load by only 0.7%. Moreover, Fig. 6.13 shows that the overall responses of the two systems with and without HBE midspan lateral bracing are quite similar. On the other hand, Fig. 6.14 demonstrates the partial effectiveness of the midspan lateral braces in controlling the HBE out-of-plane deformations. Developed displacements at points 1 and 2 in Fig. 6.14 are indicative of out-of-plane deformation of the upper HBE in SPSW3 model with no intermediate lateral bracing, while the out-of-plane displacements at points 3 and 4 located on the lower beam are pretty small. Specifically, the rate of increase of the out-of-plane displacement at point 2 located in the bottom flange level of the upper HBE rises at about 0.03 drift ratio, and this frame member undergoes larger out-of-plane deformations.

In all, the findings of this study demonstrate the effectiveness of the intermediate lateral bracing in controlling the out-of-plane deformations of the upper horizontal boundary frame member in SPSW3 model. It is important to note that various and inevitable construction defects and imperfections in practice can result in accentuated out-of-plane deformations of the frame members, which may consequently result in undesirable and weak performance of SPSW systems. Hence, more research is required to evaluate the effectiveness of the respective codified requirements and also address the potential challenges in design of SPSW systems.

6.6 Prediction of SPSW Behavior Using Modified PFI Method

In this section, the structural responses of the code-designed and real-size LYP steel shear wall models under gravity and lateral loads with different aspect ratios and concurrent

geometrical-material bifurcation characteristics are predicted using the modified PFI model proposed in Chapter 5.

In reality, deformation of the SPSW system is a combination of both shear (Fig. 6.15(a)) and bending (Fig. 6.15(b)) deformations; therefore, in a comprehensive analysis it is necessary to consider both shear and bending deformations. This issue has been considered in some studies reported by other researchers, e.g. Sabouri-Ghomi and Roberts (1992) and Topkaya and Atasoy (2009). The modified PFI model applied in this study also accounts for both shear and bending deformations. It is noted that in narrow and tall shear walls with small (l/h) aspect ratio bending is the governing factor, while in wide and short shear walls with large (l/h) aspect ratio shear deformations govern the behavior of the system (Behbahanifard et al., 2003). Thus, as a function of the aspect ratio parameter, shear and bending behaviors may have various contributions to the overall response of the SPSW system. This issue is further investigated in this section.

(a) Shear deformation **(b)** Bending deformation

Fig. 6.15 Deformation modes in SPSWs with fixed joints

In addition, it should be noted that the modified PFI model in this study also accounts for the effects of the compressive forces acting on the infill plate as shown in Fig. 6.1. This is achieved by calculating the shear yield stress (τ_{yp}) in Eqs. (5.1) and (5.2) using Eq. (4.6), which accounts for the effects of shear and compressive forces.

The performance of the modified PFI model was evaluated in Chapter 5, Section 5.6, by comparing the predicted response with various experimental and numerical results. However, the

SPSWs considered in the previous study were only subjected to lateral load and the effects of compressive (gravity and/or vertical) forces were not taken into account. In this study, the behaviors of further sophisticated and code-designed LYP steel shear wall models under the action of lateral (horizontal) and gravity (vertical) loads are predicted by the modified PFI model, and the comparison results are shown in Figs. 6.4 and 6.16.

As it is shown in Figs. 6.4(a) through 6.4(c), the analytical model has successfully captured the overall responses of the three SPSW models with different aspect ratios and accordingly disparate shear and bending behaviors. Detailed comparisons are made based on the analytical and numerical results provided in Fig. 6.16.

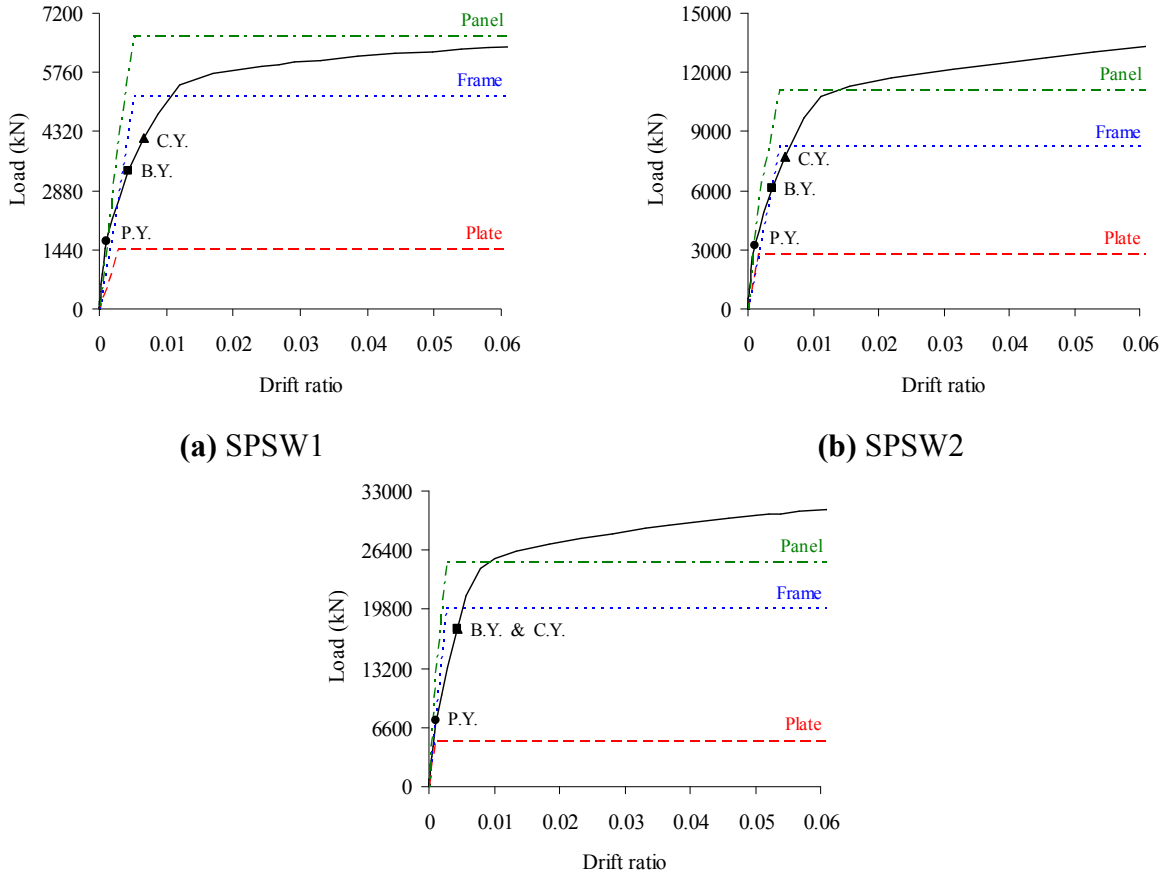

(a) SPSW1

(b) SPSW2

(c) SPSW3

Fig. 6.16 Comparison of the modified PFI model predictions with numerical results of full-scale and code-designed SPSW models with various aspect ratios and under gravity and lateral loads

Comparison results indicate that the initial stiffness of the SPSW model is satisfactorily predicted by the analytical method in all cases. Predictions of the infill plate first yield point, on the other hand, show various degrees of accuracy as the aspect ratio parameter changes and results in various shear and bending behaviors and contributions to the overall response of the system. The column yielding point is fairly satisfactorily predicted in case of SPSW2 model with l/h = 1.0, while change of aspect ratio results in some discrepancy between the analytical and numerical predictions. It is noted that geometrical and material nonlinearities as well as strain hardening are not considered in the analytical model. However, despite some scatter in results, agreement between the analytical predictions of the ultimate strength and numerical results up to 0.06 drift ratio is by and large satisfactory.

A significant advantage of the PFI method is that many design parameters, such as SPSW initial stiffness, performance and interaction of the plate and frame components and their contribution to the overall system capacity can be evaluated. This can consequently provide the designer with great flexibility for the efficient design of the SPSW systems. The results of this study demonstrate that the behaviors and responses of the LYP steel shear walls with desirable lateral force-resisting and energy dissipating capabilities can be effectively predicted and characterized using the modified PFI model. Lastly, consideration of further results from experimental and numerical studies addressing the effects of the system aspect ratio and interaction of the shear and bending behaviors can improve the performance and accuracy of this method.

6.7 Concluding Remarks

In this chapter, the seismic design and behaviors of SPSWs with unstiffened LYP steel infill plates under the action of gravity and lateral loads were evaluated through detailed numerical

simulations. Three real-size LYP steel shear walls with different aspect ratios and concurrent geometrical-material bifurcation characteristics were designed per AISC 341 seismic provisions for high-seismic applications, and their behaviors were studied through nonlinear pushover and cyclic analyses and predicted using the modified PFI method. Effects of both shear and compressive forces acting on the web plate were taken into consideration in design of SPSWs, and the effectiveness of some code-specified design requirements was also evaluated in this study.

It was shown that use of LYP steel facilitates the design of SPSWs and results in a desirable plate and frame yielding sequence by ensuring the early yielding of the infill plate compared to those of HBE and VBE components. The variations in the initial stiffness, strength, and energy absorption capacity of SPSWs due to the changes in the panel aspect ratio were also investigated. The results of this study showed that as the aspect ratio gets larger than unity, relatively heavier HBE and VBE sections are needed to meet the design requirements, which in turn contribute to the considerable increase in strength and energy dissipation capacity of the system.

It was found that consideration of 40° inclination angle in design and 45° orientation in strip modeling of LYP steel plate shear walls with different aspect ratios will usually suffice in analysis and design of such systems. Application of RBS beam-to-column connections resulted in development of a desirable plastic collapse mechanism in LYP steel plate shear walls; however, findings of this study indicate that buckling stability of RBS connections may be influenced by the system aspect ratio, which requires further investigation. Panel zones of HBE-to-VBE connections fully compliant with the AISC 341 seismic design requirements were also found to perform stably in all three SPSWs; nonetheless, aspect ratio parameter seems to be effective on the behavior of these regions. Evaluation of influence of the HBE intermediate

lateral bracing in SPSW3 model with the largest length-to-height ratio revealed that application of lateral bracing resulted in effective controlling of the out-of-plane deformations of the upper HBE component in this model, while such additional lateral bracing was not required in accordance with the AISC 341-10 (2010) seismic provisions.

The modified PFI model which accounted for the effects of both shear and compressive forces as well as shear and bending deformations, was also demonstrated to satisfactorily predict and characterize the behaviors of the LYP steel plate shear walls with different aspect ratios. This simplified analytical model can be effectively used in analysis and design of SPSWs with relatively low yielding and high buckling capacities. Nevertheless, further experimental and numerical studies can improve the performance and accuracy of this method.

Desirable behavior and performance of SPSWs are primarily provided by proper design of such structures and also use of LYP steel infill plates as the primary lateral force-resisting and energy dissipating components in such systems. The AISC 341 seismic provisions based on a capacity-based design methodology ensure that these systems have adequate ductility and seismic performance. However, more research is still required to address some potential design challenges and aspects such as the effectiveness of the code-specified frame stiffness criteria, effects of panel aspect ratio, and lateral bracing of the boundary frame members, which may eventually lead to the refinement of some codified design requirements.

7. STUDY ON SEISMIC RETROFIT OF STRUCTURES USING SPSW SYSTEMS AND LYP STEEL MATERIAL

7.1 Introduction

There are many seismically vulnerable existing buildings which are not designed in accordance with the modern seismic codes, and hence are susceptible to exhibit weak performance and undergo failure when subjected to earthquake excitations. The lateral force-resisting systems of such buildings are typically retrofitted using steel braces, steel plates, and reinforced concrete shear walls for improved structural and seismic performance.

Some retrofitting systems are becoming more favorable based on their performance, construction and implementation costs, ease of implementation, availability of material, and minimum disruption to the function as well as occupants of the building. On this basis, the use of bulky retrofitting systems, e.g. reinforced concrete shear walls, becomes more limited due to the complications in erection and high costs for foundation, while the application of lighter retrofitting systems such as steel braces and shear walls has become relatively more favorable (Dung, 2011).

In addition to new construction, SPSW systems have been increasingly used in the seismic retrofit of existing building structures due to the various advantages they offer compared to other lateral force-resisting systems. Mahtab and Zahedi (2008) have demonstrated the relative superiority of steel shear walls to steel cross braces in retrofitting of a 10-story structure. Moreover, Park et al.'s (2007) test results have shown that unlike conventional reinforced concrete walls and braced frames, well-designed steel plate walls exhibit high strength and large ductility as well as energy dissipation capacity. In addition, due to the exceptional hysteretic

behavior and the capability to early undergo plastic deformations, low yield metal shear panels have also been conceived as hysteretic dampers which could be profitably used as new methodology for the seismic retrofitting of existing steel and concrete structures (Mistakidis et al., 2007).

In addition to the reported studies on the subject of seismic retrofit of structures using SPSW systems especially with LYP steel infill plates, nonlinear and inelastic dynamic response of SPSW systems has also been investigated by some researchers. For instance, Rezai (1999) reported experimental and analytical studies on the behavior of SPSWs under cyclic and dynamic loadings. In addition, Bhowmick et al. (2009a and 2009b), Kurban and Topkaya (2009a and 2009b), and Berman (2011) studied the dynamic response and characteristics of SPSW systems through nonlinear time-history analyses and provided interesting and effective results. However, a search of the literature reveals that apart from the aforementioned studies and also some additional scattered investigations, the dynamic response and seismic retrofit of structures using SPSW systems and LYP steel material have not been studied systematically and adequately, and most of the reported studies have emerged in the recent years.

Considering the importance of assessment of dynamic response as well as seismic retrofit of structures using SPSW systems and LYP steel material, system-level investigations are made via nonlinear time-history analysis of multi-story structures subjected to earthquake ground motions and the results and findings of this study are presented and discussed in this chapter.

7.2 Design and Properties of Structural Systems

In order to investigate the seismic retrofit and behavior of structures employing SPSW systems and LYP steel material, a modified version of the 9-story SAC building (FEMA 355C,

2000) designed for seismic and wind conditions in Los Angeles is considered in this study. The floor plan and elevation for the considered and modified Los Angeles 9-story SAC building model are shown in Fig. 7.1. This building consists of perimeter moment-resisting frames shown by solid lines as the lateral force-resisting system and also interior gravity frames shown by dashed lines. As shown in the figure, in contrast to the original 9-story SAC building, fixed column bases and constant story height are considered in the modified version of this building. In addition, no basement is considered in the building under study.

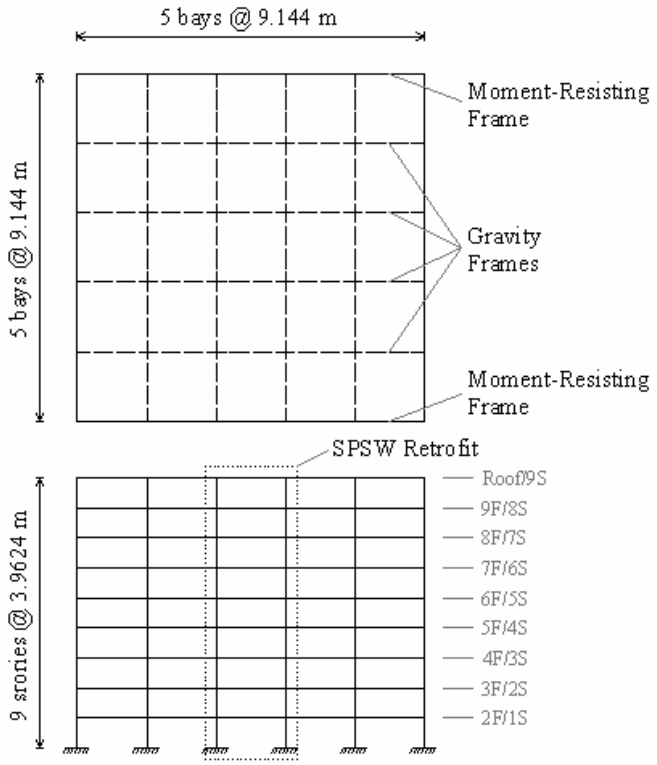

Fig. 7.1 Floor plan and elevation for the modified Los Angeles 9-story SAC building model

In order to achieve the objectives of this study and also evaluate the seismic performance of moment-resisting and SPSW lateral force-resisting systems, two-dimensional numerical models of moment-resisting and gravity-SPSW frames are developed and studied, which represent only the lateral force-resisting system of the building. Furthermore, the *P*-delta effects caused by

gravity loads tributary to the interior simple gravity frames are also taken into account. Hence, in addition to consideration of the designed moment-resisting frame, an existing interior gravity frame is retrofitted with steel infill plates applied in the middle bay, as shown in Fig. 7.1.

The design of the considered 9-story SAC building was based on design practices prevalent before the Northridge earthquake with the standard beam-to-column welded connection details (FEMA 355C, 2000). The sections used in the moment-resisting and gravity frames (pre-Northridge design) are summarized in Table 7.1. Included in the table are also the designed SPSW boundary element sections and web-plate thicknesses.

Table 7.1 Properties of the moment-resisting and gravity frames (pre-Northridge design) from the Los Angeles 9-story SAC building model and SPSW structure

Story/Floor	Moment-Resisting Frame			Gravity Frame		SPSW		
	Girders	Columns		Beams	Columns	HBEs	VBEs	t_p (mm)
		Exterior	Interior					
9/Roof	W24×68	W14×233	W14×257	W16×26	W14×48	W30×391	W14×605	1.59
8/9	W27×84	W14×233, W14×257	W14×257, W14×283	W18×35	W14×48, W14×82	W30×391	W14×605	3.18
7/8	W30×99	W14×257	W14×283	W18×35	W14×82	W30×391	W14×665	4.76
6/7	W36×135	W14×257, W14×283	W14×283, W14×370	W18×35	W14×82, W14×109	W30×391	W14×665	6.35
5/6	W36×135	W14×283	W14×370	W18×35	W14×109	W30×391	W14×730	7.94
4/5	W36×135	W14×283, W14×370	W14×370, W14×455	W18×35	W14×109, W14×145	W27×146	W14×730	7.94
3/4	W36×135	W14×370	W14×455	W18×35	W14×145	W30×391	W14×730	9.53
2/3	W36×160	W14×370, W14×370	W14×455, W14×500	W18×35	W14×145, W14×193	W27×146	W14×730	9.53
1/2	W36×160	W14×370	W14×500	W18×35	W14×193	W27×146	W14×730	9.53

The SPSWs have been designed for a site class D (stiff) soil and the adjusted maximum considered earthquake spectral response parameters at 0.2 and 1.0 sec periods, S_{MS} and S_{M1}, are 2.415g and 1.269g, respectively, where g is the acceleration of gravity. Resulting design spectral acceleration parameters at 0.2 and 1.0 sec, S_{DS} and S_{D1}, are 1.610g and 0.846g, respectively. The equivalent lateral force procedure, per ASCE 7-10 (2010), is used to determine the design seismic loads for the web plates. In design of the SPSW, the web plates are assumed to resist the entire story shear demand and the horizontal as well as vertical boundary elements are designed using capacity design principles per AISC 341-10 (2010) seismic provisions. ASTM A36 and

ASTM A572 Gr. 50 steel material are considered in design of the infill plates and boundary frame elements, respectively. Some SPSW design parameters and the resulting values are summarized in Table 7.2.

Table 7.2 Design parameters for SPSWs

Story/Floor	Vertical distribution factor, C_{vx}	Story shear, V_x (kN)	Demand/Capacity ratio, $V_u/\phi V_n$	Calculated angle of inclination, α (deg.)
9/Roof	0.222	1662.26	1.29	44.7
8/9	0.181	3016.96	1.17	44.4
7/8	0.156	4185.75	1.08	44.1
6/7	0.132	5171.41	1.00	43.9
5/6	0.108	5977.14	0.93	43.6
4/5	0.084	6606.73	1.04	40.9
3/4	0.061	7064.80	0.92	43.5
2/3	0.039	7357.40	0.97	40.5
1/2	0.018	7493.38	0.98	40.5

As it is seen in the table, the demand/capacity ratio in some floors is unconservatively larger than unity, especially at the top floors. In fact, the selected web-plate thicknesses at these floors are slightly smaller than the required values in order to apply practical thicknesses and also avoid overly conservative designs. It is noted that the capacity design procedure is somewhat conservative and simultaneous yielding of all web plates and HBEs is unlikely (Berman, 2011). Moreover, the story shear is distributed between the infill plate and VBEs, and only a portion of the shear is resisted by the infill plate. Therefore, selection of practical and larger thicknesses will increase the necessary sizes of boundary frame members and foundation demands, since these members are generally designed for the strength of the plate. As well, it is notable that the calculated average value for the angle of web yielding/inclination (α) is 42.9°, while the single value of 40° is used in design. This indicates that the agreement between the calculated and applied values for α is by and large satisfactory.

Eight structural models including moment-resisting frame and retrofitted gravity frame using conventional and LYP steel infill plates are considered in this study, which are listed in Table 7.3. The SPSW frame is originally designed by considering conventional steel infill plates, i.e. GF-CSPSW model, as explained before. These infill plates are replaced by LYP steel infill pates with increasing thickness, i.e. GF-LYPSPSW model series, as shown in Table 7.3. LYP steel shear walls with increasing web-plate thicknesses are considered in this research in order to address the retrofit of new and existing structures using LYP steel shear wall systems with relatively thicker plates compared to those with conventional steel plates. It should be noted that consideration of LYP steel with considerably lower yield stress will result in relatively thicker plates in design of SPSW systems compared to the application of conventional steel material.

Table 7.3 Considered structural models

Model	Description	Infill plate thickness
MRF	Moment-resisting frame	-
GF	Gravity frame	-
GF-CSPSW	Gravity frame with conventional steel plate shear wall	t_p
GF-LYPSPSW1	Gravity frame with replaced LYP steel plate shear wall	t_p
GF-LYPSPSW1.5	Gravity frame with replaced LYP steel plate shear wall	$1.5\times t_p$
GF-LYPSPSW2	Gravity frame with replaced LYP steel plate shear wall	$2.0\times t_p$
GF-LYPSPSW2.5	Gravity frame with replaced LYP steel plate shear wall	$2.5\times t_p$
GF-LYPSPSW3	Gravity frame with replaced LYP steel plate shear wall	$3.0\times t_p$

In addition, results and findings of the studies reported in Chapter 5 showed that a 4.7 mm ASTM A36 steel infill plate can be properly replaced by a 9.3 mm LYP100 steel plate with improved buckling stability and structural performance, while the increase in plate thickness desirably does not increase the overall system demand on the boundary frame members. In fact, one of the objectives of this chapter is to evaluate the effectiveness of such retrofitting strategy

via nonlinear time-history analysis of multi-story SPSW frames subjected to earthquake ground motions.

As discussed before, use of LYP steel enables the design of SPSW systems with moderate and stocky infill plates with relatively lower yielding and higher buckling capacities. On this basis, the limiting plate thicknesses for the ASTM A36 and LYP100 steel material are estimated by considering clamped support condition in order for evaluating the buckling and yielding behavior of web plates in the SPSW frames. The web-plate slenderness ratios of all stories for the structural models are plotted in Fig. 7.2. As well, the limiting plate slenderness ratios for respective conventional and LYP steel material are depicted by solid and dashed lines.

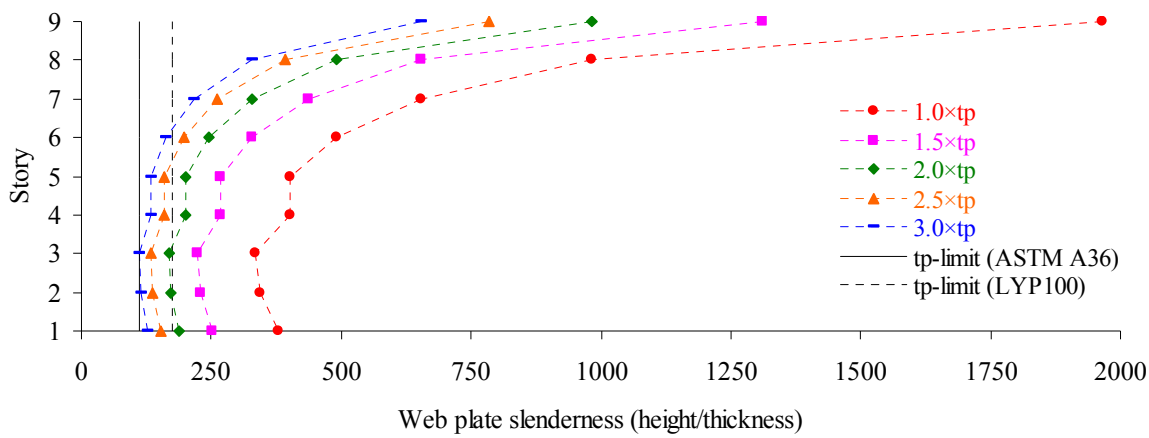

Fig. 7.2 Evaluation of buckling and yielding behavior of web plates in the structural models

From Fig. 7.2, it is apparent that consideration of LYP steel results in relatively lower limiting plate thickness and consequently higher slenderness ratio. This results in inclusion of infill plates of more structural models and stories in moderate and stocky categories. As seen in the figure, due to larger thickness and lower slenderness of plates at lower stories, these plates can exhibit improved buckling and desirable yielding behaviors. In particular, plates in lower

stories of GF-LYPSPSW3, GF-LYPSPSW2.5, and GF-LYPSPSW2 models are expected to undergo early yielding and inelastic buckling.

7.3 Finite Element Modeling and Verification

Finite element models of the considered structures are developed and analyzed using ANSYS 14.0 (2011) software. The typical bare frame and wall-frame structural models along with the considered finite element mesh scheme are shown in Fig. 7.3. As discussed before, columns are fully fixed at their bases and the frame beam and column components are assumed to be laterally braced against out-of-plane deformations. Also, constraints are used at story level column nodes in order to simulate the effect of a rigid diaphragm.

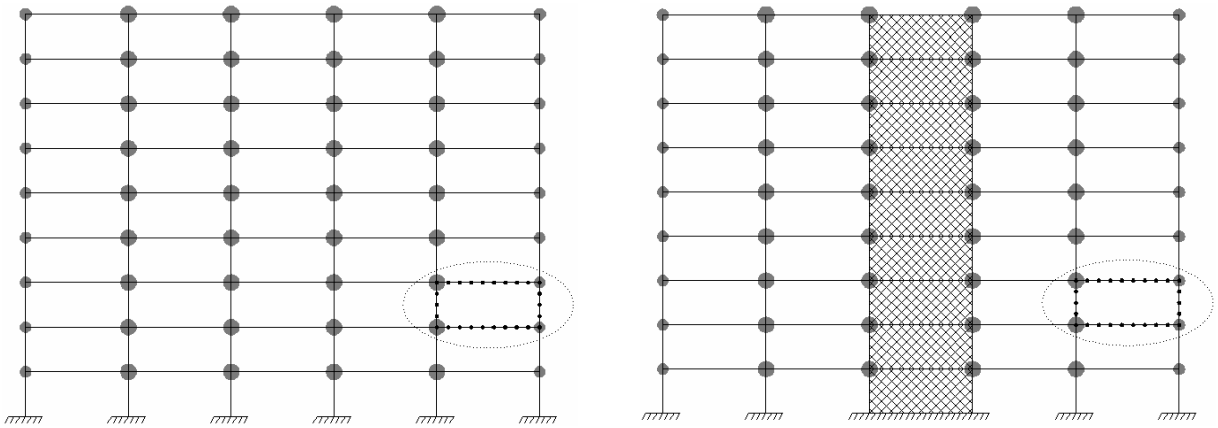

(a) Bare frame model **(b)** Wall-frame model

Fig. 7.3 Bare frame and wall-frame structural models

BEAM188 element is used to model the beam and column components of the frame. This three-dimensional two-node line element with six or seven (warping magnitude) degrees of freedom at each node is suitable for analyzing slender to moderately stubby/thick beam structures and is also well-suited for linear, large rotation, and/or large strain nonlinear applications. In addition, the element is based on Timoshenko beam theory which includes shear-

deformation effects, and provides options for unrestrained and restrained warping of cross-sections.

As shown in Fig. 7.3(b), the strip model approach is used to represent SPSW behavior, and accordingly the web plates are represented by 15 equally-spaced discrete pin-ended and tension-only strips. The strip model is computationally expedient and adequately captures the global SPSW behavior (Berman, 2011). The angle of inclination of the tension field (α) is considered as the strip angle, which is taken as 45° in the finite element modeling. The strips are modeled using LINK180 three-dimensional truss element. This element is a uniaxial tension-compression element with three degrees of freedom at each node, which can be used to simulate the tension- and compression-only options, and has plasticity, creep, rotation, large deflection, and large strain capabilities. Strip elements are used in both tension field directions in order for representing the dynamic behavior of the SPSW frames.

Seismic and lumped masses consistent with the FEMA 355C (2000) reported values are placed at each story level on the beam-column intersection nodes, as illustrated in Fig. 7.3. The exterior and interior applied story lumped masses are also tabulated in Table 7.4. Lumped masses are modeled using MASS21 point element with up to six degrees of freedom.

Table 7.4 Story seismic and lumped masses

Level	Total story seismic mass		Story lumped masses (ton)	
	kips-sec^2/ft	ton	Exterior	Interior
Roof	73.10	1066.81	53.34	106.68
2F to 9F	67.86	990.34	49.52	99.03

ASTM A36 and LYP100 steel material are considered for the infill plates, and ASTM A572 Gr. 50 steel is employed in modeling of the frame beam and column components. The stress-strain curves and mechanical properties of the aforementioned steel material are shown in Fig.

5.2. The von Mises yield criterion is adopted for material yielding, and kinematic hardening rule is incorporated in the nonlinear time-history analyses.

Rayleigh proportional damping with a damping ratio of 2% is selected and applied in all seismic analyses, which is consistent with the level of damping used in studies on the performance of moment-resisting and SPSW frames by Gupta and Krawinkler (1999) and Berman (2011), respectively.

Modal and nonlinear time-history analyses with geometrical and material nonlinearities have been conducted in this study, which are discussed in the subsequent sections.

In order to verify the adequacy of the finite element strip modeling approach in capturing the dynamic behaviors of the structures with various material and geometrical properties, finite element results are validated through comparison with published experimental as well as additional experimentally-verified numerical results. To achieve this, single- and multi-story reference SPSWs with slender and stocky infill plates employing conventional and LYP steel material have been considered.

First, the one-story one-bay SPSW2 specimen employing slender and conventional steel infill plate tested by Lubell (1997) has been modeled using the strip modeling approach. The infill plate is represented by 12 equally-spaced pin-ended and tension-only strips. The geometrical and modeling details along with the experimental and numerical results are presented in Fig. 7.4. Figs. 7.4(b) and (c) show that the finite element strip model provides good results in both pushover and cyclic cases by predicting the response of the tested specimen in a quite satisfactory manner.

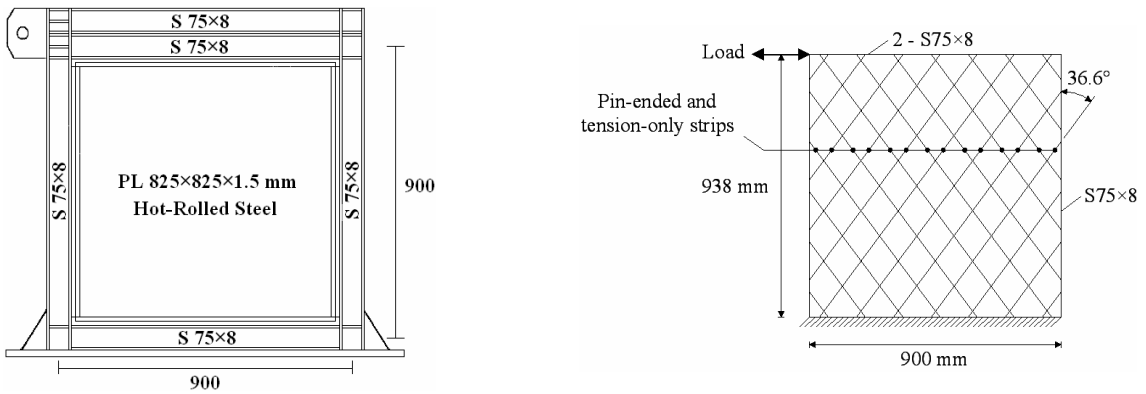

(a) Test specimen and strip model

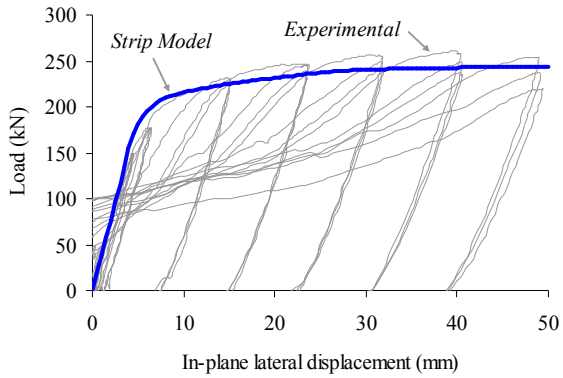

(b) Pushover analysis results

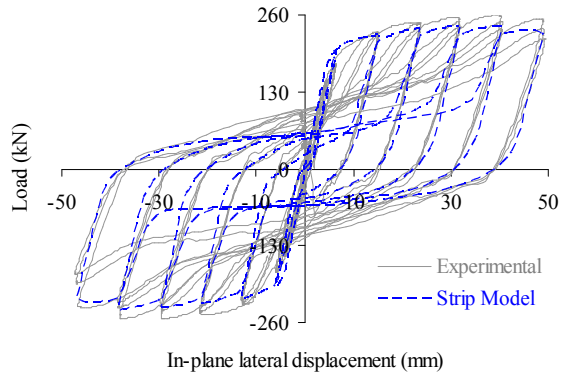

(c) Cyclic analysis results

Fig. 7.4 Modeling details and results for Lubell's (1997) SPSW2 specimen

Chen and Jhang's (2006) specimen no. 1 with stocky and LYP100 steel infill plate has subsequently been modeled through strip modeling approach. The infill plate is modeled by 12 equally-spaced pin-ended and tension-only strips. As illustrated in Fig. 7.5(a), the strips are inclined at 45° with the vertical in accordance with Chen and Jhang's (2006) proposed model, and the RBS connections are properly considered in finite element modeling. The comparison results presented in Figs. 7.5(b) and (c) indicate that the agreement between the numerical and experimental results is very good in both pushover and cyclic cases.

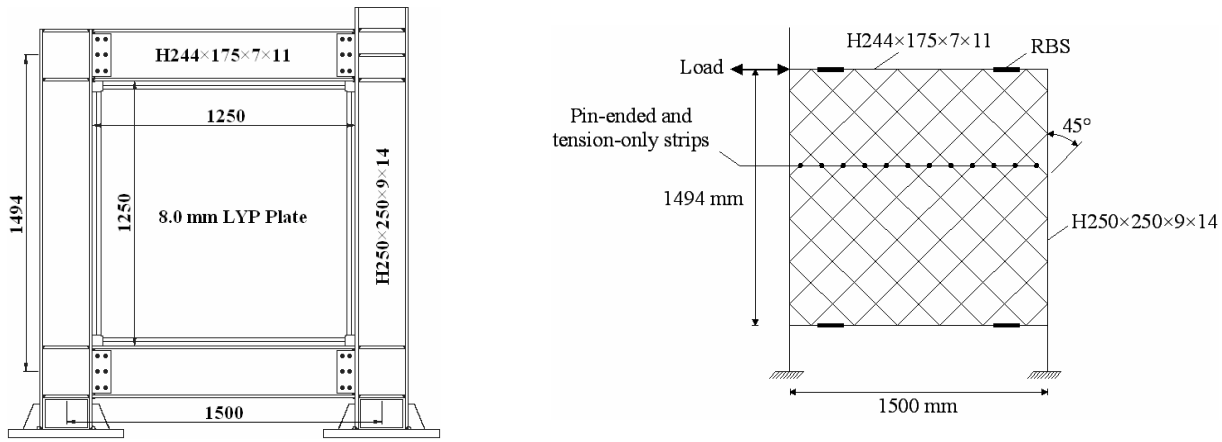

(a) Test specimen and strip model

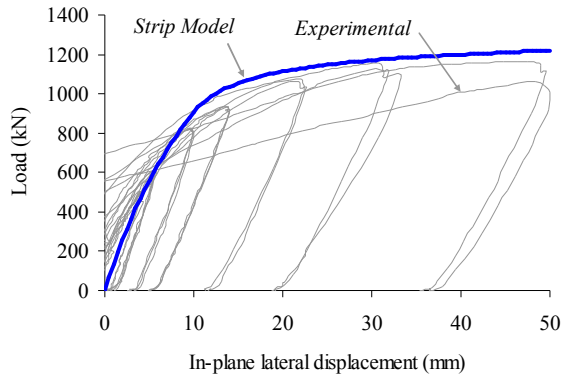

(b) Pushover analysis results

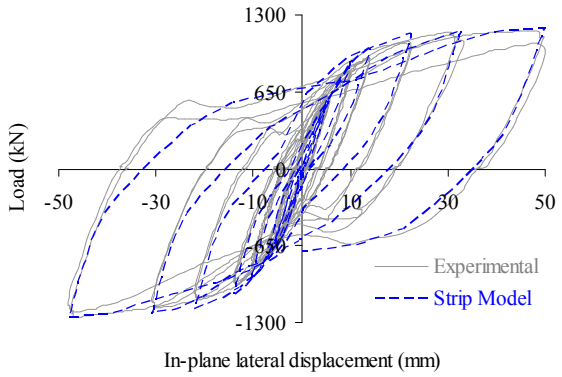

(c) Cyclic analysis results

Fig. 7.5 Modeling details and results for Chen and Jhang's (2006) specimen no. 1

In addition to the two single-story SPSW test specimens, the three-story SC2T specimen with thin infill plates and strong columns tested by Park et al. (2007) has also been modeled for verification purposes. The infill plates and frame members of this specimen were made of SS400 and SM490 steel material (Korean Standard) with 240 and 330 MPa yield stresses, respectively. The geometrical and modeling details of the test specimen and developed finite element model are provided in Fig. 7.6(a). As seen, each infill plate is represented by 12 equally-spaced pin-ended and tension-only strips inclined at 45° with the vertical. The numerical predictions and test results are compared in Figs. 7.6(b) through 7.6(e). From the figures, it is quite evident that the predictions of the strip model agree well with the test results. This indicates the adequacy and

efficiency of the applied strip model in predicting the response of the multi-story SPSW specimen.

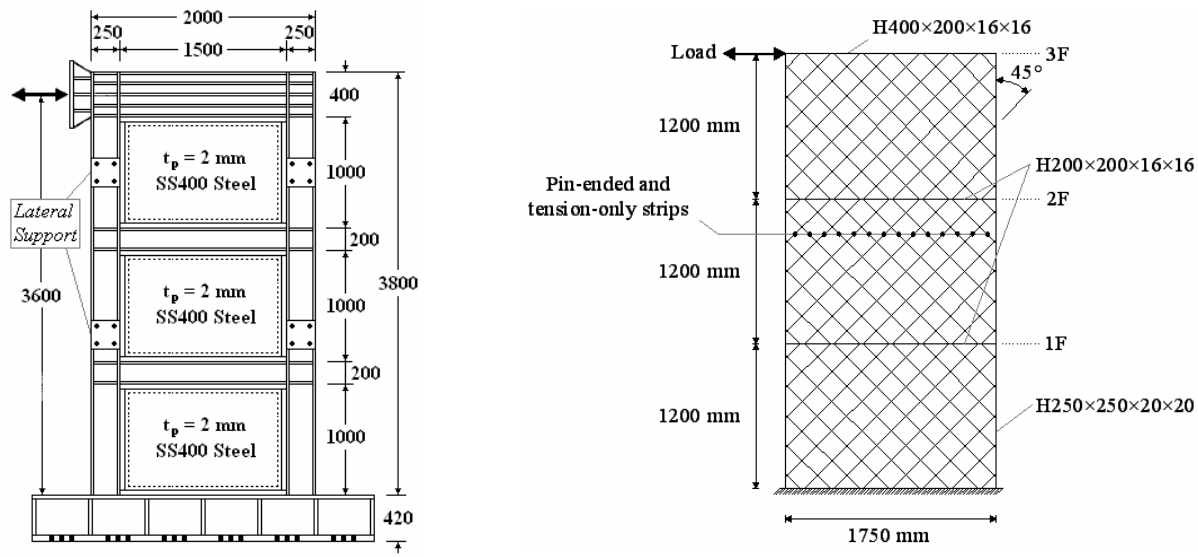

(a) Test specimen and strip model

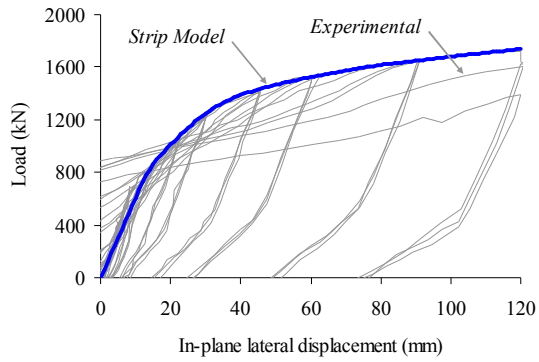

(b) Pushover analysis results (3F)

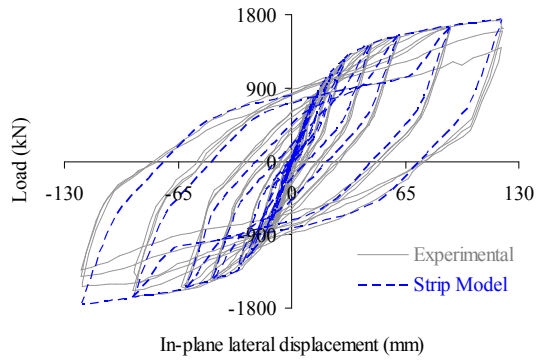

(c) Cyclic analysis results (3F)

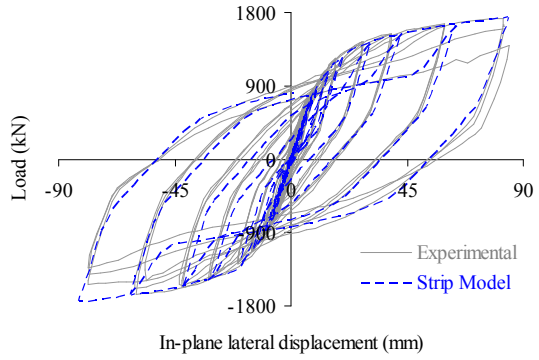

(d) Cyclic analysis results (2F)

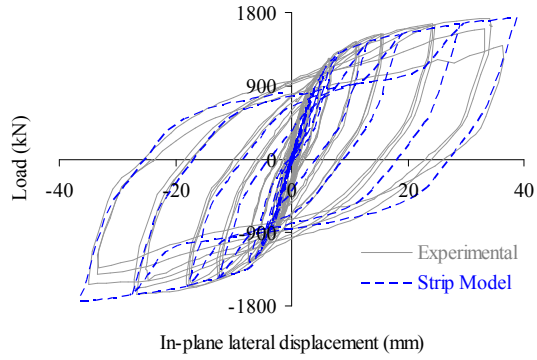

(e) Cyclic analysis results (1F)

Fig. 7.6 Modeling details and results for Park et al.'s (2007) SC2T specimen

Two single-story, single-bay, and full-scale steel shear walls, i.e. SPSW2 and SPSW5 models studied in Chapter 5 and defined in Table 5.1, are also modeled in this study, and the strip modeling results have been compared with those from the analysis of three-dimensional finite element models. It is noted that SPSW2 and SPSW5 models employ slender and stocky LYP steel infill plates, respectively. In the strip model, the web plates are represented by 12 equally-spaced pin-ended and tension-only strips inclined at 40.5° with the vertical. The modeling details as well as comparison results for SPSW2 and SPSW5 models are presented in Figs. 7.7 and 7.8, respectively.

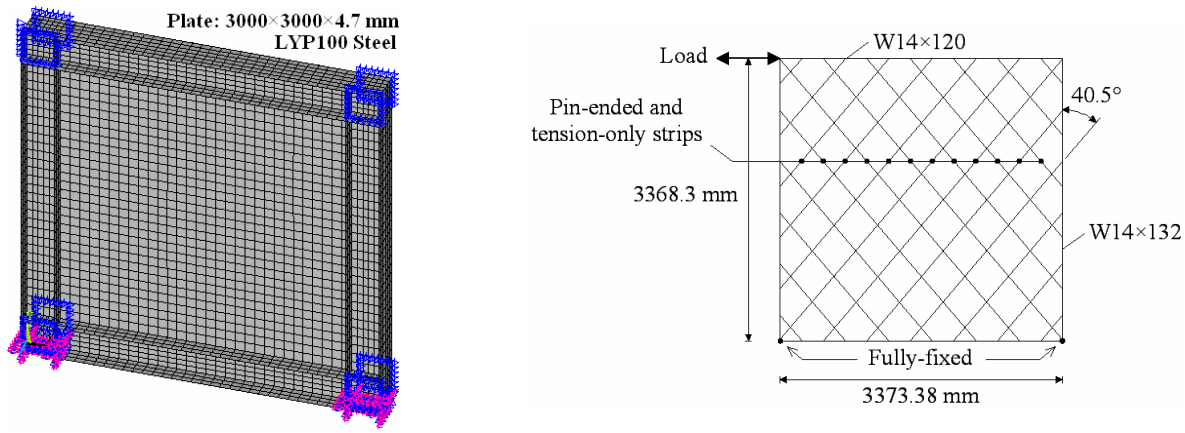

(a) 3D finite element and strip models

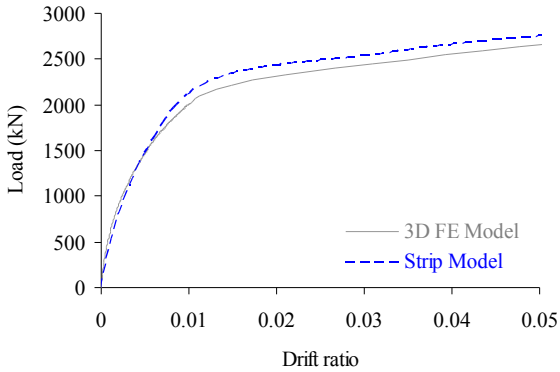

(b) Pushover analysis results

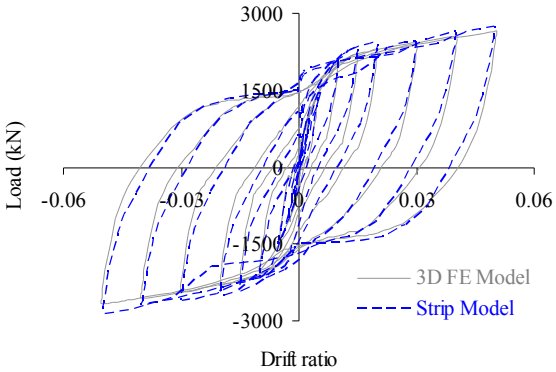

(c) Cyclic analysis results

Fig. 7.7 Modeling details and results for a 3D finite element slender-web SPSW model

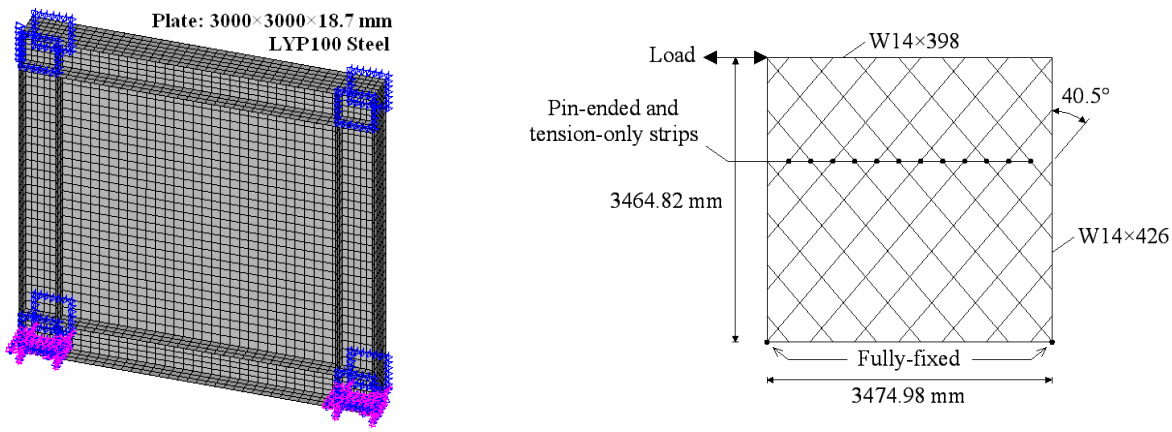

(a) 3D finite element and strip models

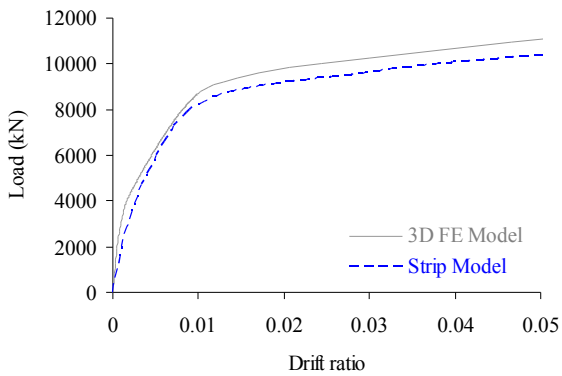

(b) Pushover analysis results

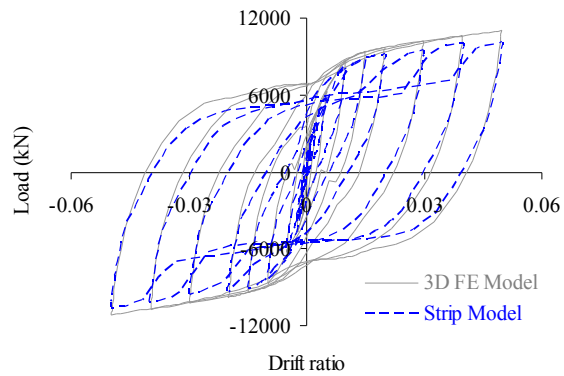

(c) Cyclic analysis results

Fig. 7.8 Modeling details and results for a 3D finite element stocky-web SPSW model

As it is observed in Figs. 7.7 and 7.8, the agreement between the numerical results from three-dimensional and strip modeling of the two SPSWs is satisfactory. However, it is found that the two sets of numerical results are better correlated in case of SPSW2 model with slender infill plate (Fig. 7.7), while due to the early yielding and inelastic buckling of the stocky infill plate in SPSW5 model with improved buckling stability (Fig. 7.8) strip model slightly underpredicts the response. In the final analysis, it may be concluded that predictions of the strip model are reliable in both cases.

Overall, the findings of these case studies demonstrate that the applied strip model, using ANSYS 14.0 (2011) software, is quite capable of predicting the response of single- and multi-story SPSWs with various geometrical and material properties.

7.4 Modal Analysis and Elastic Behavior

Modal analyses are performed first to determine the vibration characteristics including natural frequencies as well as mode shapes, and initial stiffnesses of structures. Modal analysis considers the linear behavior only and any nonlinearities, such as plasticity, are not considered in such an analysis. Figs. 7.9 and 7.10 show the first three mode shapes of vibration obtained from modal analyses of MRF and GF-CSPSW models, respectively.

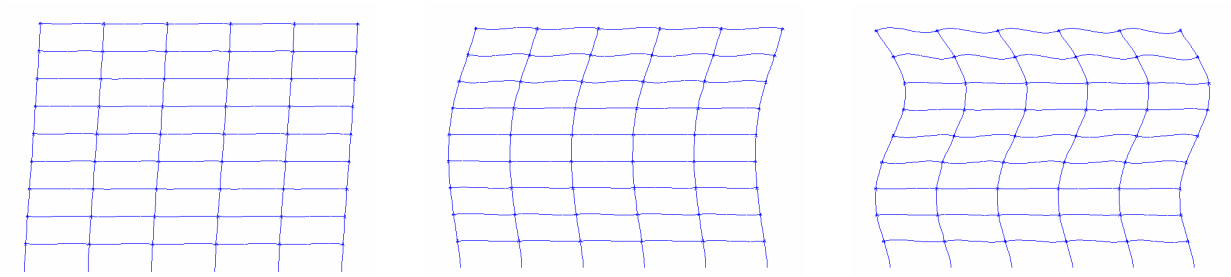

(a) 1st mode shape **(b)** 2nd mode shape **(c)** 3rd mode shape

Fig. 7.9 Mode shapes of MRF model

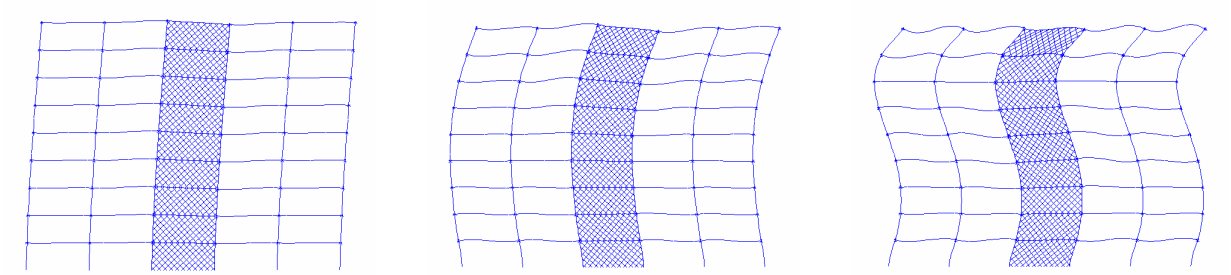

(a) 1st mode shape **(b)** 2nd mode shape **(c)** 3rd mode shape

Fig. 7.10 Mode shapes of GF-CSPSW model

Accurate determination of vibration characteristics, in particular, the fundamental period of vibration is of great importance in calculating the lateral forces and seismic design of a structure. Most building codes propose simple empirical expressions to evaluate the fundamental period of vibration. According to ASCE 7-10 (2010), the approximate fundamental period (T_a), in seconds, can be determined from the following equation:

$$T_a = C_t h_n^x \tag{7.1}$$

in which h_n is the height of the structure above the base, $C_t = 0.0724$ and $x = 0.8$ for steel moment-resisting frames, and $C_t = 0.0488$ and $x = 0.75$ for other structural systems including SPSWs. The accuracy of the code predictions for the fundamental periods of SPSW systems has been evaluated through numerical analyses by Topkaya and Kurban (2009), Berman (2011), and Bhowmick et al. (2011). These studies have demonstrated that, in general, the code-specified formulae fail in providing accurate estimates for the fundamental periods of SPSWs, and accordingly simple and relatively accurate methods and formulae have been proposed by Topkaya and Kurban (2009) and Bhowmick et al. (2011) for predicting the fundamental period of SPSW systems. In this study, the periods of first five modes of vibration for the considered structural models are determined from the modal analyses and tabulated in Table 7.5. These numerical estimates are compared with the period values reported in FEMA 355C (2000) and predicted by the ASCE 7-10 (2010) specified equation, i.e. Eq. (7.1), in Table 7.5, as appropriate.

Table 7.5 Periods of the considered structural models

Model	$T_{Analysis}$ (sec)	T_{SAC} (sec)	T_{ASCE} (sec)	$T_{Analysis}/T_{ASCE}$
MRF	$T_1 = 2.097$ $T_2 = 0.789$ $T_3 = 0.456$ $T_4 = 0.309$ $T_5 = 0.231$	$T_1 = 2.34$ $T_2 = 0.88$ $T_3 = 0.50$	1.264	1.66
GF	$T_1 = 6.286$ $T_2 = 2.071$ $T_3 = 1.162$ $T_4 = 0.760$ $T_5 = 0.549$	-	1.264	4.97
GF-CSPSW	$T_1 = 1.036$ $T_2 = 0.300$ $T_3 = 0.169$ $T_4 = 0.121$ $T_5 = 0.096$	-	0.711	1.46
GF-LYPSPSW1	$T_1 = 1.036$ $T_2 = 0.300$ $T_3 = 0.169$ $T_4 = 0.121$ $T_5 = 0.096$	-	0.711	1.46
GF-LYPSPSW1.5	$T_1 = 0.976$ $T_2 = 0.263$ $T_3 = 0.146$ $T_4 = 0.105$ $T_5 = 0.083$	-	0.711	1.37
GF-LYPSPSW2	$T_1 = 0.944$ $T_2 = 0.241$ $T_3 = 0.131$ $T_4 = 0.094$ $T_5 = 0.075$	-	0.711	1.33
GF-LYPSPSW2.5	$T_1 = 0.923$ $T_2 = 0.226$ $T_3 = 0.121$ $T_4 = 0.087$ $T_5 = 0.070$	-	0.711	1.30
GF-LYPSPSW3	$T_1 = 0.909$ $T_2 = 0.215$ $T_3 = 0.114$ $T_4 = 0.081$ $T_5 = 0.066$	-	0.711	1.28

As seen in the table, in spite of the modifications made in the original 9-story SAC building, the first three periods of the considered MRF model obtained from the modal analysis are found to be in good agreement with the values reported in FEMA 355C (2000). Nevertheless, the two values of the fundamental period for this structural system, i.e. $T_{1,Analysis}$ and $T_{1,SAC}$, are considerably larger than that predicted by Eq. (7.1). Also, it is evident that the GF model, which is not considered as a lateral force-resisting system, possesses overly large period values due to its flexibility.

Table 7.5, also, shows that Eq. (7.1) specified by the ASCE 7-10 (2010) code provides a constant value for the fundamental periods of SPSWs with increasing infill plate thicknesses, while the fundamental periods obtained from modal analyses exhibit a decreasing trend, as expected, due to the increase in stiffness. In addition, consistent with the results of the aforementioned studies on the periods of SPSW systems, ASCE 7-10 (2010) code-specified equation, i.e. Eq. (7.1), is found to yield lower estimates for the fundamental periods of SPSW systems compared to numerical predictions. This discrepancy diminishes slightly as the infill plate thickness increases and the system gains more stiffness.

The values of initial stiffness of the considered structural models determined from the modal analyses are shown in Fig. 7.11. As seen in the figure, the GF model possesses a very low initial stiffness, and also the GF-SPSW models in general exhibit a considerably higher initial stiffness compared to the MRF model. It is also evident that the initial stiffness of a GF-LYPSPSW model increases due to the increase in the infill plate thickness. Table 7.6, also, shows the percentage variations in initial stiffness and fundamental period due to the retrofit of structures in this study.

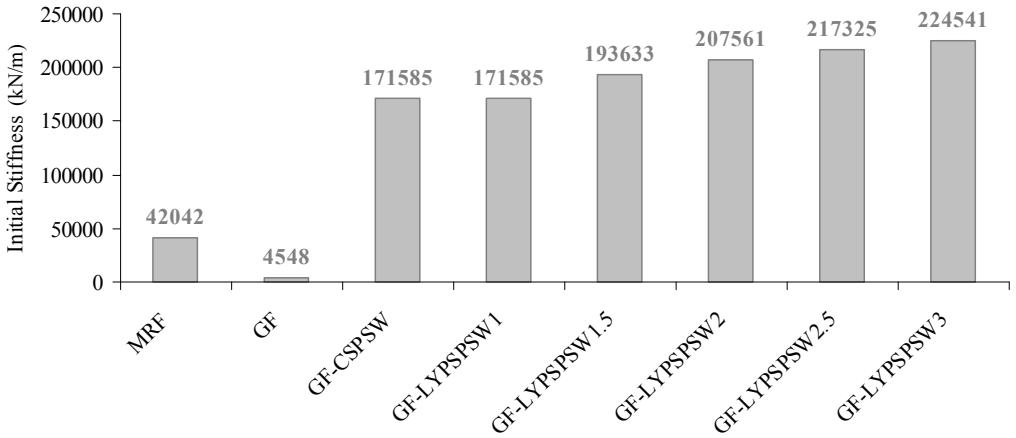

Fig. 7.11 Initial stiffnesses of the considered structural models

Table 7.6 Percentage variations in initial stiffness and period

Structural models (Retrofit)	Increase in initial stiffness	Decrease in period
MRF → GF-CSPSW	308 %	51 %
GF-CSPSW → GF-LYPSPSW1	0 %	0 %
GF-CSPSW → GF-LYPSPSW1.5	13 %	6 %
GF-CSPSW → GF-LYPSPSW2	21 %	9 %
GF-CSPSW → GF-LYPSPSW2.5	27 %	11 %
GF-CSPSW → GF-LYPSPSW3	31 %	12 %

These results indicate that GF-CSPSW model possesses much higher initial stiffness and lower fundamental period compared to the MRF model. Furthermore, retrofit of the GF-CSPSW model with thicker and LYP steel infill plates results in increasing of the initial stiffness by maximum 30% and decreasing of the fundamental period by maximum 10% approximately in the extreme considered case, i.e. GF-LYPSPSW3 model. In spite of the fact that higher initial stiffness can effectively control the drift and damages to the structural system and drift-sensitive nonstructural components, it may make the structure shake at higher acceleration levels and more damage may be expected to acceleration-sensitive nonstructural components and contents (HAZUS-MH MR5, 2010). Therefore, evaluation of seismic performance and level of induced

floor accelerations due to ground motion excitations is essential in efficient seismic design and retrofit of structures.

Lastly, modal analysis results have been utilized to determine the Rayleigh damping coefficients, i.e. the mass and stiffness matrix multipliers, by considering the 1st and 5th modal frequencies in order to set the damping ratio at 2%. The obtained values of the Rayleigh damping coefficients for the considered structural models are provided in Table 7.7. These tabulated values have been applied in the nonlinear time-history dynamic analyses.

Table 7.7 Rayleigh damping coefficients determined using the 1st and 5th modal frequencies and 2% damping ratio

Model	Mass matrix multiplier	Stiffness matrix multiplier
MRF	0.10795	0.00133
GF	0.03677	0.00321
GF-CSPSW	0.22208	0.00056
GF-LYPSPSW1	0.22208	0.00056
GF-LYPSPSW1.5	0.23728	0.00049
GF-LYPSPSW2	0.24670	0.00044
GF-LYPSPSW2.5	0.25318	0.00041
GF-LYPSPSW3	0.25794	0.00039

7.5 Nonlinear Time-History Analysis and Selection of Ground Motions

In order to evaluate the seismic drifts, accelerations, and other behavioral characteristics, nonlinear time-history dynamic analyses are performed for the structural models considered in this study. In order to account for the *P*-delta effects on the seismic response, gravity loads are initially applied on the two-dimensional structural models prior to the time-history dynamic analysis, and then these loads are kept constant while ground accelerations are applied to the base of the structure. *P*-delta effects are usually critical in either flexible or tall structures which may be subjected to relatively large lateral displacements. The results of the studies reported by Bhowmick et al. (2009b) have shown that *P*-delta effects for low- and mid-rise structures are not

important for SPSWs that are stiff enough to meet certain code-specified interstory drift limit. In any case, considering the potential importance of *P*-delta effects on the seismic response of structures, these effects have been considered in this study. As mentioned before, damping ratio of 2% is also applied in the dynamic analysis of the structural models.

A total of eleven earthquake acceleration time histories are selected from the Los Angeles ground motions developed for the SAC steel research project (FEMA 355C, 2000) for the time-history response analysis. Details of the selected earthquake records including the magnitude, distance, scale factor, peak ground velocity (PGV), peak ground acceleration (PGA), and hazard level are given in Table 7.8.

Table 7.8 Details of selected Los Angeles ground motions for seismic performance evaluation

SAC name	Record	Earthquake magnitude	Distance (km)	Scale factor	PGV (mm/s)	PGA (mm/s^2)	Probability of exceedance
LA02	Imperial Valley, El Centro, 1940	6.9	10	2.01	599.0	6628.8	10% in 50 years
LA06	Imperial Valley, Array #06, 1979	6.5	1.2	0.84	474.4	2300.8	10% in 50 years
LA11	Loma Prieta, Gilroy, 1989	7	12	1.79	791.4	6524.9	10% in 50 years
LA16	Northridge, Rinaldi RS, 1994	6.7	7.5	0.79	1007.6	5685.8	10% in 50 years
LA18	Northridge, Sylmar, 1994	6.7	6.4	0.99	1189.3	8014.4	10% in 50 years
LA19	North Palm Springs, 1986	6	6.7	2.97	682.7	9994.3	10% in 50 years
LA21	Kobe, 1995	6.9	3.4	1.15	1427.0	12580.0	2% in 50 years
LA23	Loma Prieta, 1989	7	3.5	0.82	737.6	4099.5	2% in 50 years
LA25	Northridge, Rinaldi, 1994	6.7	7.5	1.29	1603.1	8516.2	2% in 50 years
LA28	Northridge, Sylmar, 1994	6.7	6.4	1.61	1935.3	13041.0	2% in 50 years
LA29	Tabas, 1974	7.4	1.2	1.08	710.5	7934.5	2% in 50 years

Time-history acceleration records are selected in a manner to cover earthquakes with minimum, average, and maximum PGV and PGA values within both 10/50 (10% probability of exceedance in 50 years) and 2/50 (2% probability of exceedance in 50 years) hazard levels. Hence, the selected ground motions will enable the seismic behavior to be studied at 10/50 and 2/50 seismic hazard levels that represent design and maximum earthquakes. Time histories of the selected Los Angeles ground motions are shown in Fig. 7.12. The selected earthquake records have PGA values ranging between 0.23*g* and 1.33*g*.

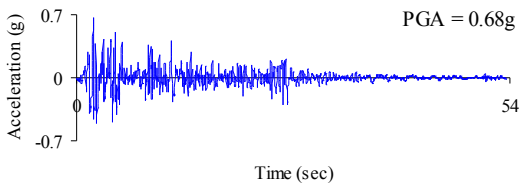

(a) LA02

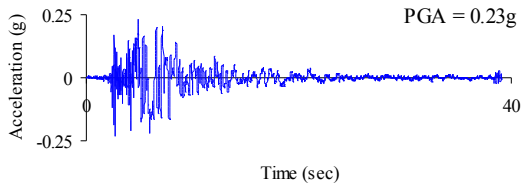

(b) LA06

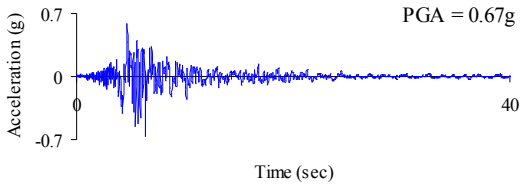

(c) LA11

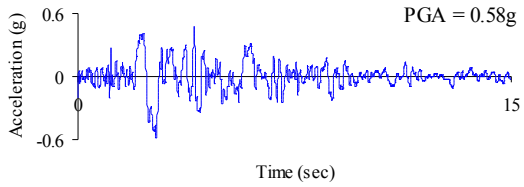

(d) LA16

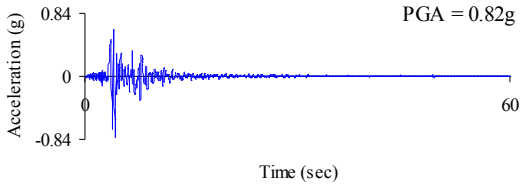

(e) LA18

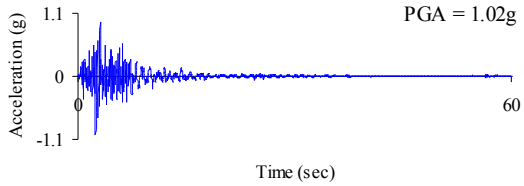

(f) LA19

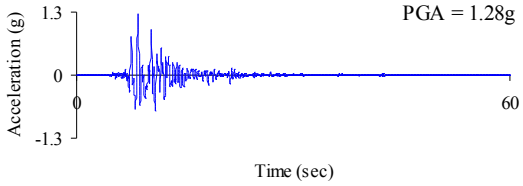

(g) LA21

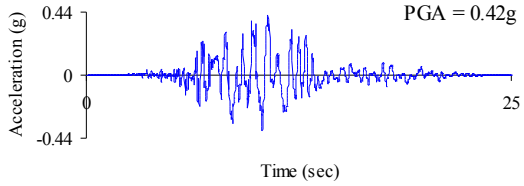

(h) LA23

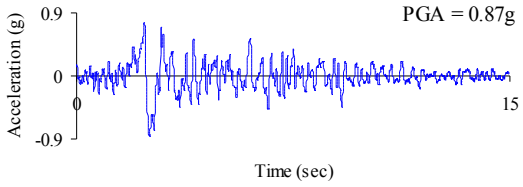

(i) LA25

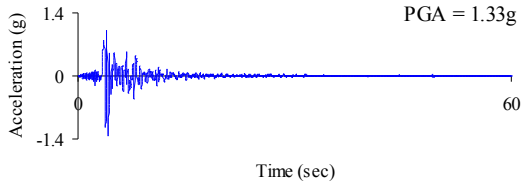

(j) LA28

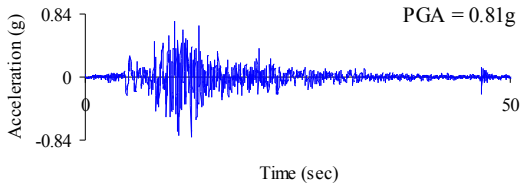

(k) LA29

Fig. 7.12 Time histories of selected Los Angeles ground motions for seismic performance evaluation

The results of the nonlinear time-history dynamic analyses are discussed in the subsequent sections.

7.6 Nonlinear Time-History Analysis Results

7.6.1 Story and Interstory Drift Ratios

Lateral displacement or drift is one of the important parameters in design of structures, and structures should be designed to accommodate the displacements imposed by lateral forces since excessive drift may constitute unacceptable performance. Hence, design codes, e.g. ASCE 7-10 (2010), specify certain limitations on displacements of structures which should be appropriately met especially when drift is the governing criterion in design.

Among the lateral force-resisting systems, SPSWs are deemed to be highly-efficient systems which can be considered for many retrofit applications and are very effective in controlling the drift as one of the important seismic design criteria. According to Seilie and Hooper (2005), SPSW systems are capable of surviving up to 4% drift ratio. Similar conclusion may be drawn from the study reported by Baldvins et al. (2012). LYP steel shear walls, in particular, have been shown to reach even larger drift ratios up to 5-6% through stable deformation. Despite these findings, widespread use of SPSW systems particularly with LYP steel infill plates requires further investigation of various design and performance aspects.

As part of the dynamic response assessment, “story” and “interstory” drift ratios of the considered structural models induced by seismic excitations are evaluated in this section. It is noted that *story* drift ratio is the horizontal deflection at the top of the story relative to the base of the structure divided by the height above the base to the same level, while *interstory* drift ratio is the horizontal deflection at the top of the story relative to the bottom of the story divided by the

story height. The maximum story and interstory drift ratios induced by three sample ground motions with small, average, and large PGV and PGA values are shown in Fig. 7.13.

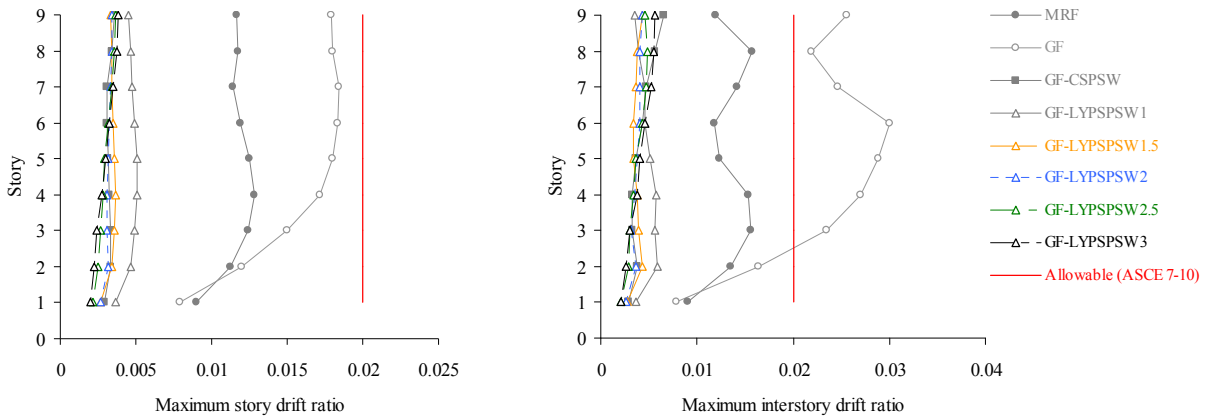

(a) LA06 *(small PGV and PGA)*

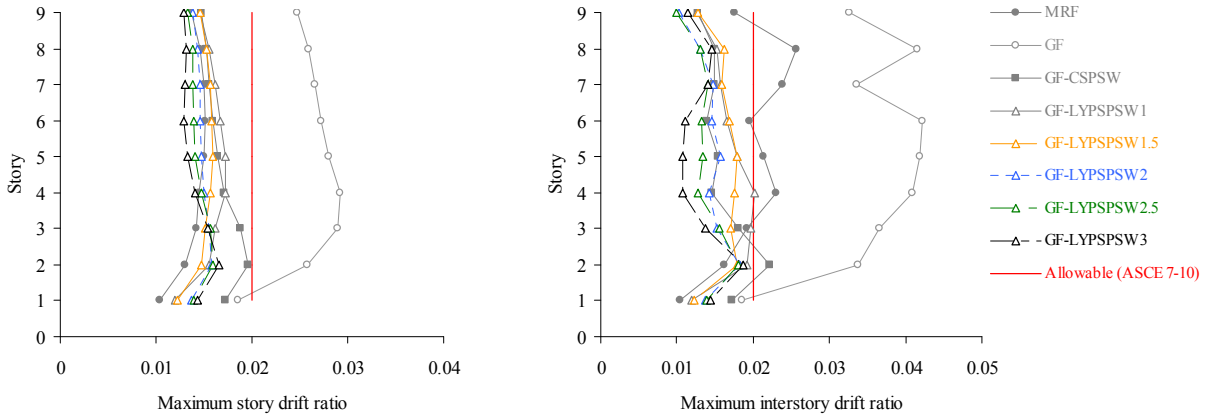

(b) LA18 *(average PGV and PGA)*

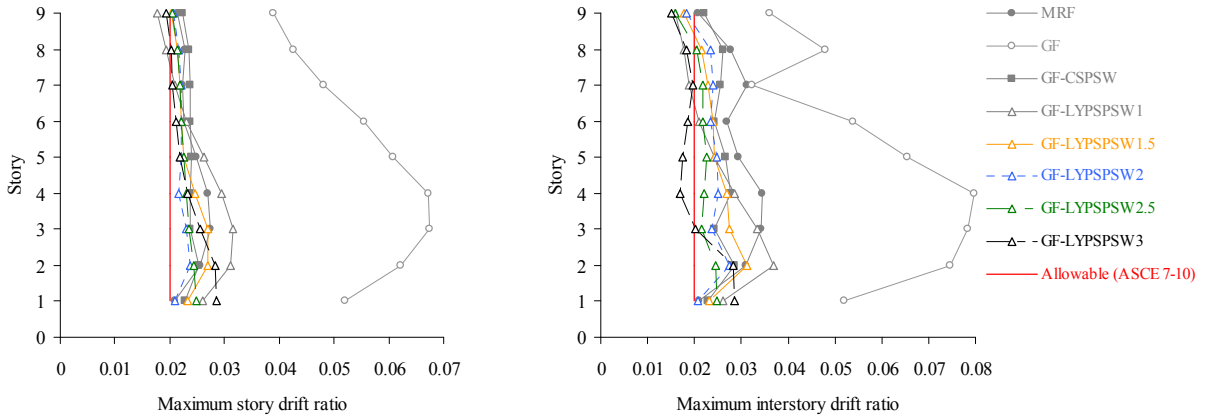

(c) LA28 *(large PGV and PGA)*

Fig. 7.13 Maximum story and interstory drift ratios induced by three sample ground motions

As seen in Fig. 7.13(a), all maximum story and interstory drift ratios are less than the maximum 2.0% allowed for Risk Category I or II structures per ASCE 7-10 (2010), with the exception of the GF model which is not essentially designed to accommodate the seismic drift requirements. On the other hand, the drift ratios for most lateral force-resisting systems are less than 2.0% under the ground motion with average PGV and PGA values, as shown in Fig. 7.13(b), while Fig. 7.13(c) shows that the story and interstory drift ratios are mostly more than the allowable limit under the earthquake with large intensity quantities. The average story and interstory drift ratios of the lateral force-resisting systems obtained by considering the maximum story responses for all ground motions are shown in Fig. 7.14.

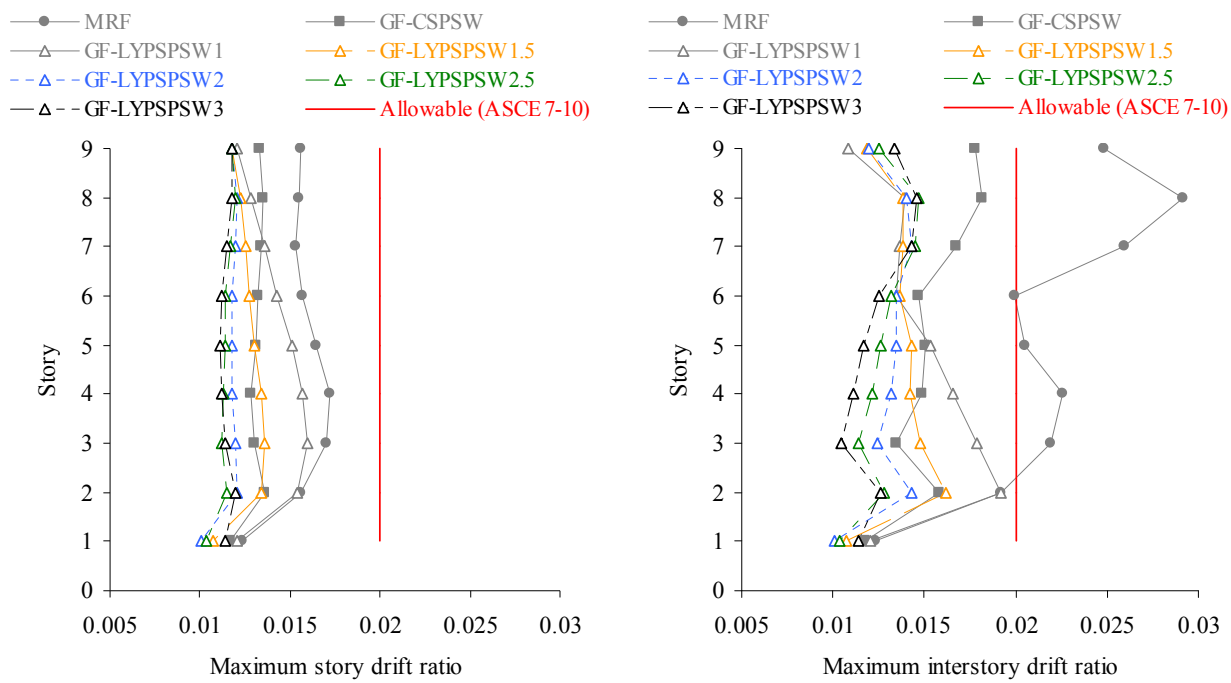

(a) Story **(b)** Interstory

Fig. 7.14 Maximum story and interstory drift ratios induced by the considered ground motions

From Figs. 7.14(a) and (b), it is apparent that the values of the interstory drift ratio are relatively larger than those of the story drift ratio. These results indicate that the interstory drift

ratio parameter is more critical and controlling than the story drift ratio parameter in seismic design of structures. Moreover, as seen in the figures, the story and interstory drift ratios of all structures are less than the prescribed 2.0% limit, except for the interstory drift ratios of the MRF model which exceed the 2.0% limit at some stories. It is also found that the code-designed GF-CSPSW model has been quite effective in reducing the drifts compared the MRF model. In addition, retrofitting of the GF-CSPSW model with LYP steel infill plates of the same thickness has unfavorably resulted in larger drift ratios, while consideration of thicker LYP steel infill plates for retrofit purposes has yielded desirable results in limiting the drift ratios.

The peak story and interstory drift ratio values of the structural models induced by the ground motions are tabulated in Tables 7.9 and 7.10, respectively.

Table 7.9 Peak story drift ratios (%) of the structural models induced by ground motions

Model	Ground motion										
	LA02	LA06	LA11	LA16	LA18	LA19	LA21	LA23	LA25	LA28	LA29
MRF	1.73	1.29	1.97	1.90	1.52	0.78	2.01	1.56	2.39	2.73	1.82
GF	1.58	1.84	3.66	4.86	2.92	1.29	4.02	2.16	> 10	6.76	3.75
GF-CSPSW	0.87	0.36	1.83	1.52	1.96	1.04	2.20	1.32	1.71	2.53	1.05
GF-LYPSPSW1	0.96	0.51	1.96	1.54	1.72	0.83	2.24	1.13	2.47	3.16	1.36
GF-LYPSPSW1.5	0.72	0.36	1.80	1.40	1.59	0.80	2.24	0.90	2.06	2.70	1.28
GF-LYPSPSW2	0.64	0.34	1.54	1.39	1.58	0.71	2.17	0.92	1.76	2.38	1.13
GF-LYPSPSW2.5	0.72	0.37	1.21	1.38	1.60	0.71	2.20	0.82	1.70	2.48	0.96
GF-LYPSPSW3	0.74	0.38	1.02	1.37	1.65	0.74	2.32	0.75	1.75	2.85	0.82

Table 7.10 Peak interstory drift ratios (%) of the structural models induced by ground motions

Model	Ground motion										
	LA02	LA06	LA11	LA16	LA18	LA19	LA21	LA23	LA25	LA28	LA29
MRF	2.68	1.57	2.87	4.28	2.56	2.21	4.81	2.37	3.98	3.46	2.46
GF	4.09	3.01	4.61	5.94	4.22	2.32	5.64	4.15	> 10	7.97	4.98
GF-CSPSW	1.58	0.65	2.10	2.19	2.22	1.62	3.64	1.99	2.27	2.87	1.82
GF-LYPSPSW1	1.17	0.59	2.32	1.85	2.01	1.06	2.87	1.41	2.96	3.68	1.68
GF-LYPSPSW1.5	1.08	0.43	2.14	1.66	1.79	1.04	2.77	1.13	2.46	3.13	1.53
GF-LYPSPSW2	1.05	0.43	1.82	1.67	1.81	1.21	2.90	1.08	2.05	2.74	1.31
GF-LYPSPSW2.5	1.14	0.49	1.32	1.61	1.80	1.56	3.07	0.95	2.20	2.48	1.10
GF-LYPSPSW3	1.21	0.57	1.32	1.62	1.87	1.85	2.80	0.99	2.20	2.85	1.10

From the tabulated results, it is found that the GF model has comparatively large peak story and interstory drift ratios in almost all considered cases, and even in some cases, e.g. ground motion LA25, the peak drift ratios are dramatically large which is indicative of failure of the structure. Variations of the seismic-induced peak story and interstory drift ratios as a result of retrofit of structures using SPSW systems and LYP steel material are shown in Fig. 7.15. These average values for the peak drift ratios are obtained by considering the peak drift responses for all ground motions as summarized in Tables 7.9 and 7.10.

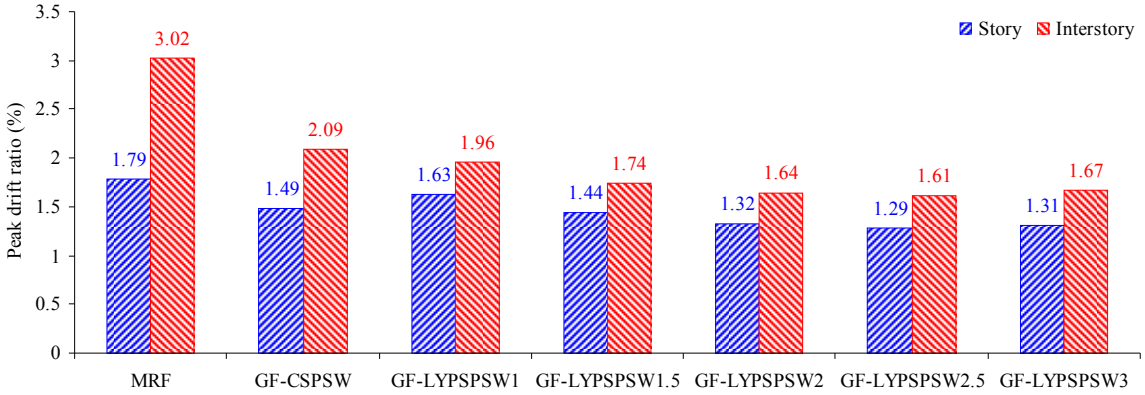

Fig. 7.15 Variations of seismic-induced peak story and interstory drift ratios due to retrofit of structures using SPSW systems and LYP steel material

These results demonstrate that the peak interstory drift ratios are larger than the peak story drift ratios in all cases which is, in turn, indicative of importance of the interstory drift ratio as an effective design criterion. Discrepancy between the two peak drift ratio parameters is the largest in case of the MRF model, while this discrepancy is decreased in cases of the GF-SPSW models especially those with LYP steel infill plates. From the figure, it is evident that the peak interstory drift ratio for the MRF model is close to 3.0% and for the GF-CSPSW model is slightly larger than 2.0%, while SPSW systems retrofitted with LYP steel infill plates have been effective at limiting the peak drift ratios to less that 2.0%. Even, it is interesting to note that retrofitting of the

GF-CSPSW model with LYP steel infill plates of the same thickness, i.e. GF-LYPSPSW1 model, has resulted in a slight decrease in the peak interstory drift ratio from 2.09% to 1.96%. What is indeed important here is not the slight decrease in the peak interstory drift ratio, but no increase in the peak interstory drift ratio due to the use of LYP steel infill plates with the same thickness and considerably lower yield stress relative to the conventional ASTM A36 steel. One important finding which requires attention is the slight increase in the peak story and interstory drift ratios in case of the GF-LYPSPSW3 model in spite of the decreasing trend in the peak drift ratios due to the increase in thicknesses of the LYP steel infill plates. Based on the results of the studies reported by Caccese et al. (1993) and Habashi and Alinia (2010), the increase in peak drift ratios in this case may be attributed to the fact that large plate thicknesses increase the overall system demand on the adjacent frame particularly vertical boundary members and the performance and failure of the structure may be governed by the column instability.

The assessment of the drift response of the 9-story GF-CSPSW and GF-LYPSPSW2 models under seismic loading, also, shows that retrofit of a conventional steel shear wall system with LYP steel infill plates having twice the existing plate thickness, as addressed in Chapter 5, results in a desirable drift performance as the story and interstory drifts are effectively decreased due to such a retrofitting strategy. The 9th story drift ratio time histories of the MRF, GF-CSPSW, and GF-LYPSPSW2 models for three sample ground motions are shown in Fig. 7.16.

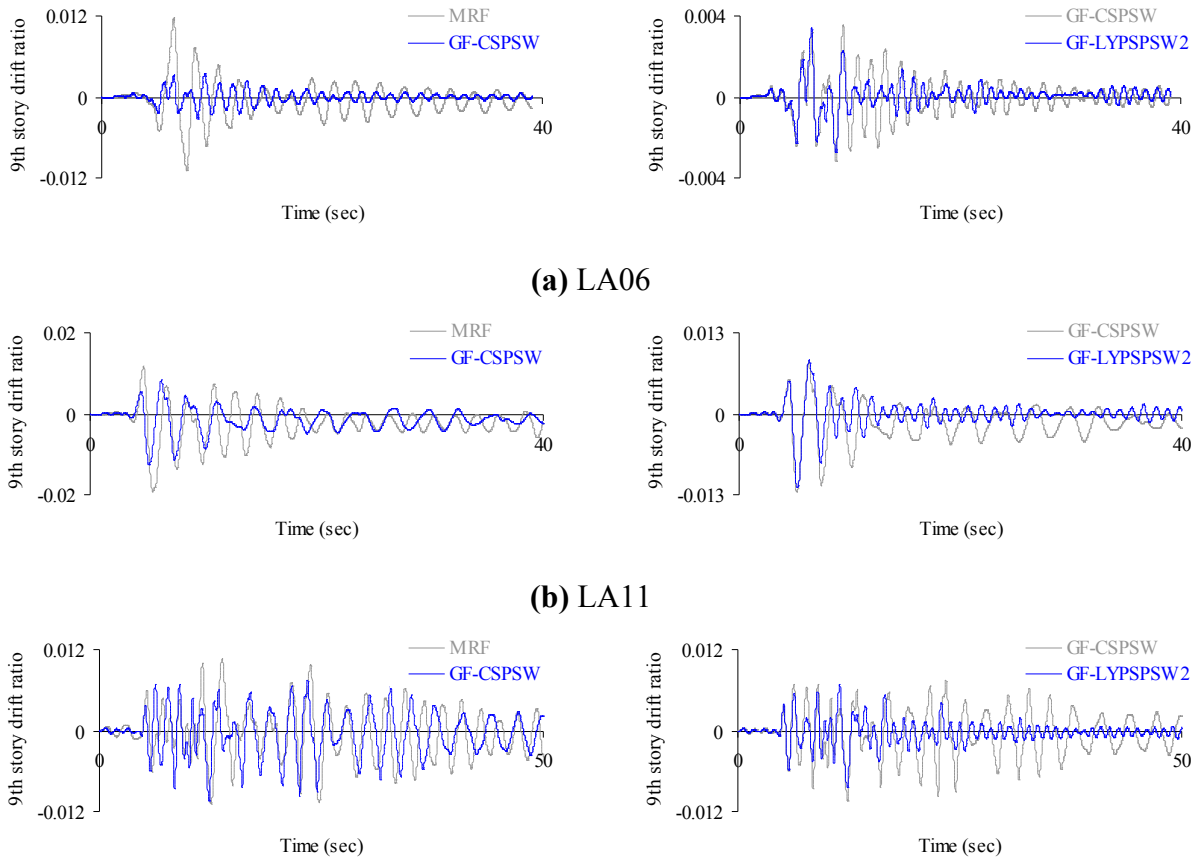

(a) LA06

(b) LA11

(c) LA29

Fig. 7.16 Comparison of 9th story drift ratio time histories of MRF, GF-CSPSW, and GF-LYPSPSW2 models

The drift time-history results, in particular, and findings of the case study reported in this section, in general, indicate that retrofit of the considered structure with a conventional steel shear wall system and also retrofit of the existing SPSW system with LYP steel infill plates limit the seismic-induced drifts and improve the drift performance of the structure in an effective manner.

7.6.2 Story Acceleration

Acceleration is another important criterion in seismic design and retrofit of structures which may cause damages to the structural and especially nonstructural systems as well as contents and consequently result in considerable economic loss. While damage to the structural system is the most important measure of building damage affecting casualties and catastrophic loss of function, damage to nonstructural systems and contents tends to dominate economic loss (HAZUS-MH MR5, 2010).

Considering the relatively high stiffness of SPSW systems and its effectiveness in controlling the lateral displacements, the seismic-induced accelerations also have to be taken into consideration in efficient seismic design and retrofit of buildings using such lateral force-resisting systems. In fact, high stiffness may result in elastic behavior of SPSW systems and amplify the acceleration response of the structures. If the SPSW infill plate thicknesses, boundary frame members, and configuration are properly designed to meet the seismic provisions without significant design over-strength, then nonlinearities in the seismic response will reduce expected accelerations (Eatherton, 2006).

A well-known example of the acceleration-related damages is the Olive View Medical Center building in Sylmar, California, which employed stiffened SPSWs as part of its lateral force-resisting system. During the Northridge earthquake, this building experienced peak acceleration of 2.31*g* at the roof level due to the high stiffness while its peak ground floor acceleration was 0.82*g*. This building suffered minor structural damage but considerable nonstructural damage during the earthquake (Çelebi, 1997).

On this basis, the acceleration responses of the designed and retrofitted structural systems are evaluated in this study. The average story accelerations of the structural models obtained by considering the maximum story responses for all ground motions are shown in Fig. 7.17.

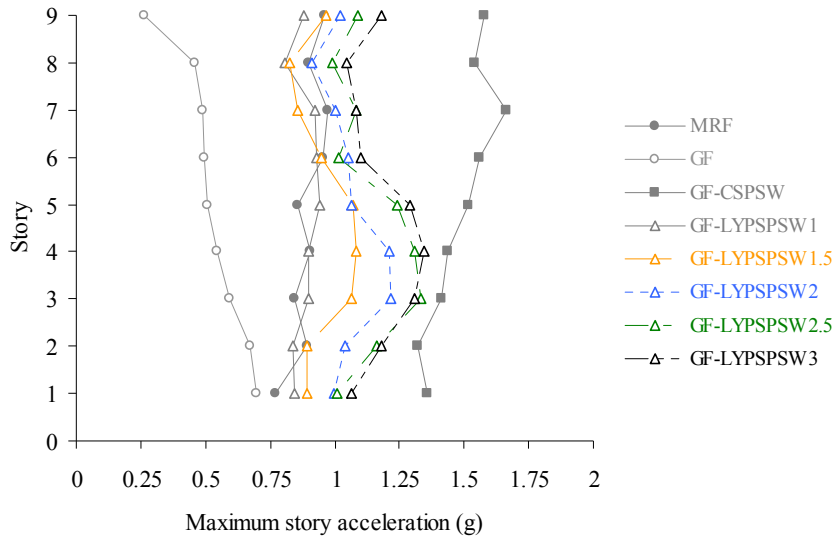

Fig. 7.17 Maximum story accelerations induced by the considered ground motions

As seen in the figure, the GF model experienced story accelerations of less than 0.70g due to its relative flexibility, while the GF-CSPSW model exhibits the largest story acceleration response ranging between 1.32*g* and 1.66*g*. In addition, as shown, increasing of the infill plate thickness in the GF-LYPSPSW models increases the story accelerations. However, it is notable that retrofit of the GF-CSPSW model with LYP steel infill plates of even larger thicknesses still results in relatively smaller seismic-induced story accelerations. This is indeed due to the exclusive material properties of the LYP steel material which results in early plate yielding and desirable nonlinear seismic response of the structure.

The peak floor accelerations of the structural models induced by the ground motions are summarized in Table 7.11. Also, variations of the seismic-induced peak floor accelerations as a result of retrofit of structures using SPSW systems and LYP steel material are illustrated in Fig.

7.18. The average values for the peak floor acceleration shown in Fig. 7.18 are obtained by considering the peak acceleration responses for all ground motions as provided in Table 7.11.

Table 7.11 Peak floor accelerations (g) of the structural models induced by ground motions

Model	Ground motion										
	LA02	LA06	LA11	LA16	LA18	LA19	LA21	LA23	LA25	LA28	LA29
MRF	1.158	0.586	0.887	0.775	1.185	1.205	1.388	0.872	1.173	1.549	1.273
GF	0.586	0.287	0.546	0.546	0.661	0.871	1.042	0.872	0.785	1.281	0.809
GF-CSPSW	1.847	0.762	1.562	2.066	1.659	1.764	2.664	2.087	1.965	2.208	2.169
GF-LYPSPSW1	0.807	0.463	1.061	1.349	1.266	1.040	1.355	1.046	1.052	1.625	0.919
GF-LYPSPSW1.5	0.863	0.475	1.366	1.323	1.352	1.043	1.650	0.758	1.365	1.880	0.868
GF-LYPSPSW2	1.181	0.574	1.296	1.399	1.202	1.419	2.215	0.820	1.442	2.110	1.029
GF-LYPSPSW2.5	1.109	0.555	1.243	1.459	1.695	1.603	2.533	1.030	1.487	2.351	1.125
GF-LYPSPSW3	1.067	0.745	1.017	1.397	1.509	1.765	2.695	0.977	1.731	2.571	1.195

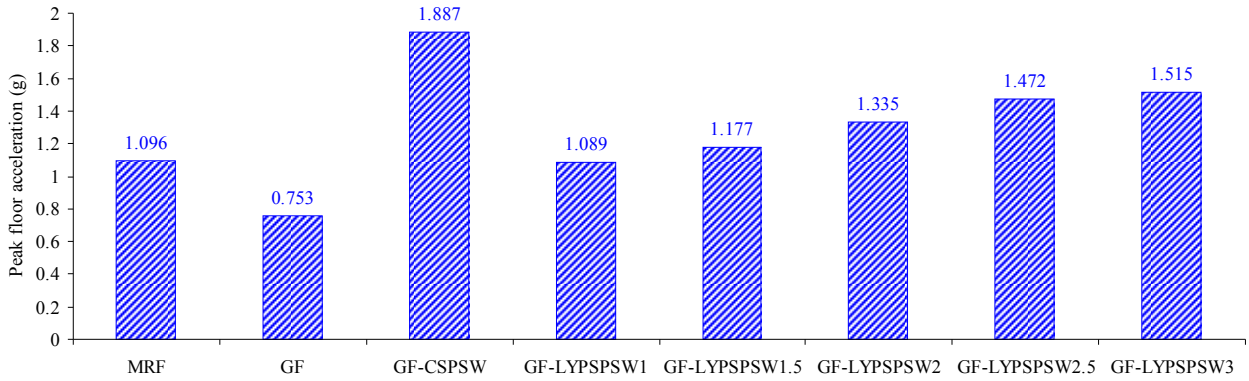

Fig. 7.18 Variations of seismic-induced peak floor accelerations due to retrofit of structures using SPSW systems and LYP steel material

These results indicate that employment of LYP steel material in design and retrofit of structures in areas with high seismicity would result in desirable seismic performance with limited earthquake-induced peak floor accelerations. From the figure, it is evident that employment of conventional steel infill plates significantly amplifies the peak floor acceleration of the GF-CSPSW model relative to that of the MRF model, whereas retrofitting of the GF-CSPSW model with LYP steel infill plates effectively controls the seismic-induced peak floor acceleration. Even in the extreme case, i.e. GF-LYPSPSW3 model with the largest infill plate thickness, the peak floor acceleration is still below that of the GF-CSPSW model.

Additionally, it is found that the peak floor acceleration of the GF-LYPSPSW2 model (1.335*g*) is remarkably smaller than that of the GF-CSPSW model (1.887*g*). This demonstrates the effectiveness of the retrofitting strategy discussed in Chapter 5 and implies that a conventional steel shear wall system can be effectively retrofitted with LYP steel infill plates having twice the existing plate thickness. Although increasing of the infill plate thickness results in increased stiffness of the SPSW system, as illustrated in Fig. 7.11 and Table 7.6, employment of LYP steel material effectively controls the acceleration response of the structure. The 9th story acceleration time histories of the MRF, GF-CSPSW, and GF-LYPSPSW2 models for three sample ground motions are shown in Fig. 7.19.

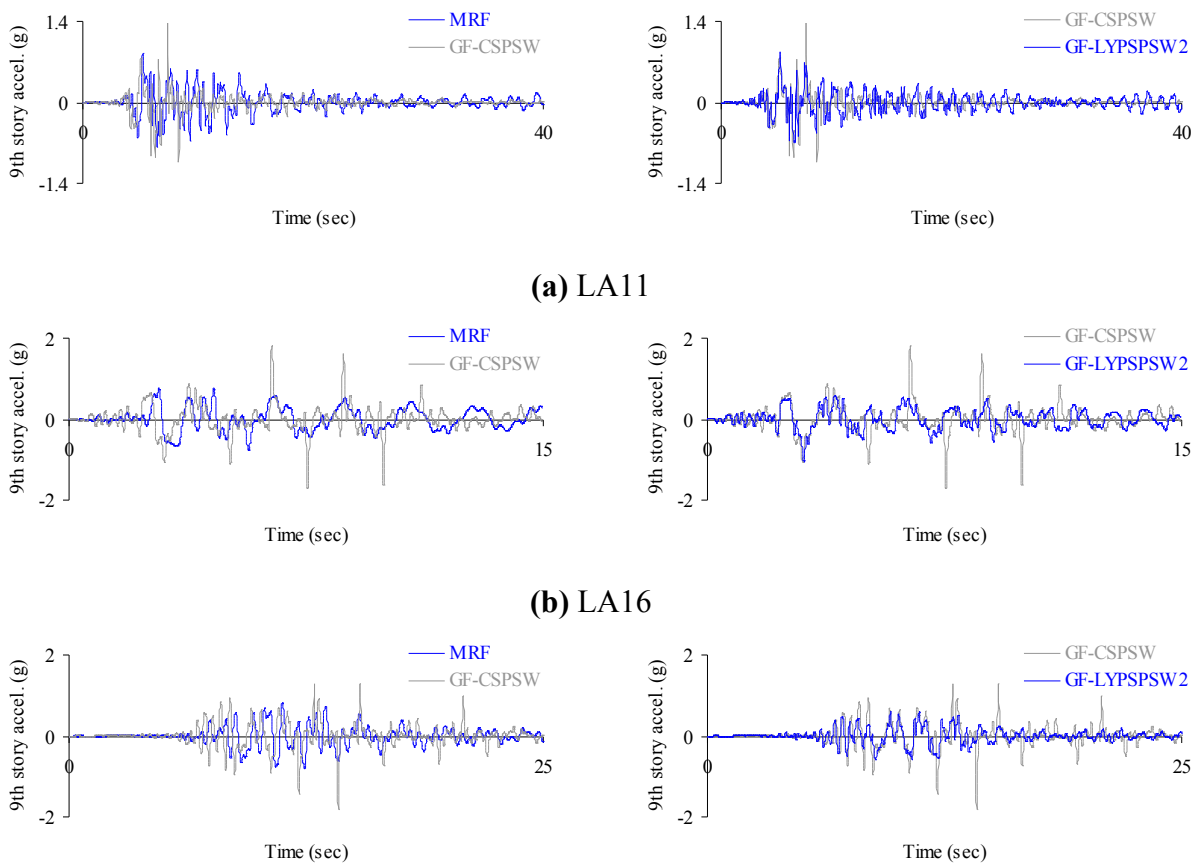

(a) LA11

(b) LA16

(c) LA23

Fig. 7.19 Comparison of 9th story acceleration time histories of MRF, GF-CSPSW, and GF-LYPSPSW2 models

The time-history analysis results depicted in Fig. 7.19, confirm the findings of this study discussed above. Overall, it may be concluded that use of LYP steel infill plates in design and retrofit of SPSWs will improve the seismic behavior of such structural systems by limiting the acceleration response of the structure in a quite desirable and efficient manner.

7.6.3 Base Shear

In order to further assess the seismic performance and effectiveness of retrofitting of structures using SPSW systems and LYP steel material, the seismic-induced base shear demands of the structural models are evaluated in this section. The base shear demands (V_b) are obtained from the nonlinear time-history dynamic analyses and normalized with the seismic weight (W_s) of the structure. The normalized maximum base shear demands (V_b/W_s) of the structural models for all ground motions are listed in Table 7.12.

Table 7.12 Normalized maximum base shear demands (V_b/W_s) of the structural models induced by ground motions

Model	Ground motion										
	LA02	LA06	LA11	LA16	LA18	LA19	LA21	LA23	LA25	LA28	LA29
MRF	0.280	0.257	0.294	0.289	0.291	0.221	0.341	0.285	0.308	0.320	0.259
GF	0.071	0.040	0.077	0.081	0.090	0.071	0.125	0.065	0.112	0.103	0.082
GF-CSPSW	0.388	0.270	0.404	0.360	0.358	0.373	0.374	0.379	0.377	0.389	0.386
GF-LYPSPSW1	0.213	0.159	0.231	0.220	0.235	0.181	0.263	0.204	0.270	0.278	0.227
GF-LYPSPSW1.5	0.238	0.181	0.305	0.288	0.289	0.252	0.311	0.247	0.316	0.333	0.283
GF-LYPSPSW2	0.247	0.224	0.342	0.322	0.342	0.302	0.333	0.285	0.388	0.378	0.324
GF-LYPSPSW2.5	0.274	0.225	0.385	0.371	0.422	0.351	0.372	0.326	0.425	0.421	0.362
GF-LYPSPSW3	0.323	0.232	0.383	0.397	0.487	0.405	0.425	0.375	0.452	0.522	0.407

From the table, it is evident that the maximum base shear demands of the GF model are remarkably smaller than those of the other structural models in all cases. In fact, due to the low stiffness and high flexibility of the GF model (see Fig. 7.11), less base shear is absorbed by this

frame. Fig. 7.20 shows the variations of the seismic-induced normalized maximum base shear demands due to the retrofit of structures using SPSW systems and LYP steel material. The average V_b/W_s values shown in the figure are obtained by considering the V_b/W_s values for all ground motions as listed in Table 7.12.

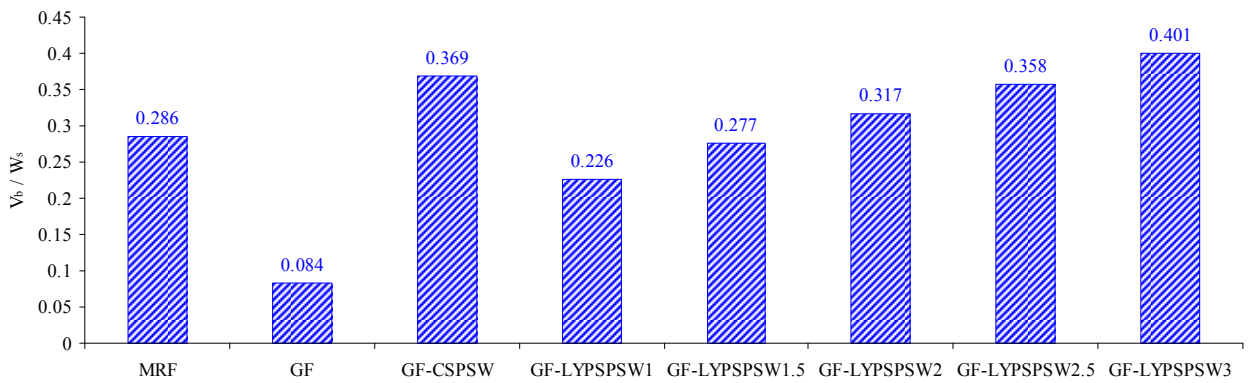

Fig. 7.20 Variations of seismic-induced normalized maximum base shear demands due to retrofit of structures using SPSW systems and LYP steel material

As shown in Fig. 7.20, the base shear demand of the GF-CSPSW model is larger than that of the MRF model. Retrofit of the GF-CSPSW model with LYP steel infill plates of the same or slightly larger thicknesses, on the other hand, significantly reduces the base shear demand of the SPSW system. However, use of thicker plates, particularly in GF-LYPSPSW2.5 and GF-LYPSPSW3 models, increases the base shear absorbed by the SPSW system and unfavorably results in relatively large base shear demands.

From the figure, it is also evident that the base shear demand for the GF-LYPSPSW2 model with double plate thickness is lower than that for the GF-CSPSW model. This demonstrates another aspect of effectiveness of the retrofitting strategy discussed in Chapter 5. The base shear time-history plots of MRF, GF-CSPSW, and GF-LYPSPSW2 models for three sample ground motions are provided in Fig. 7.21.

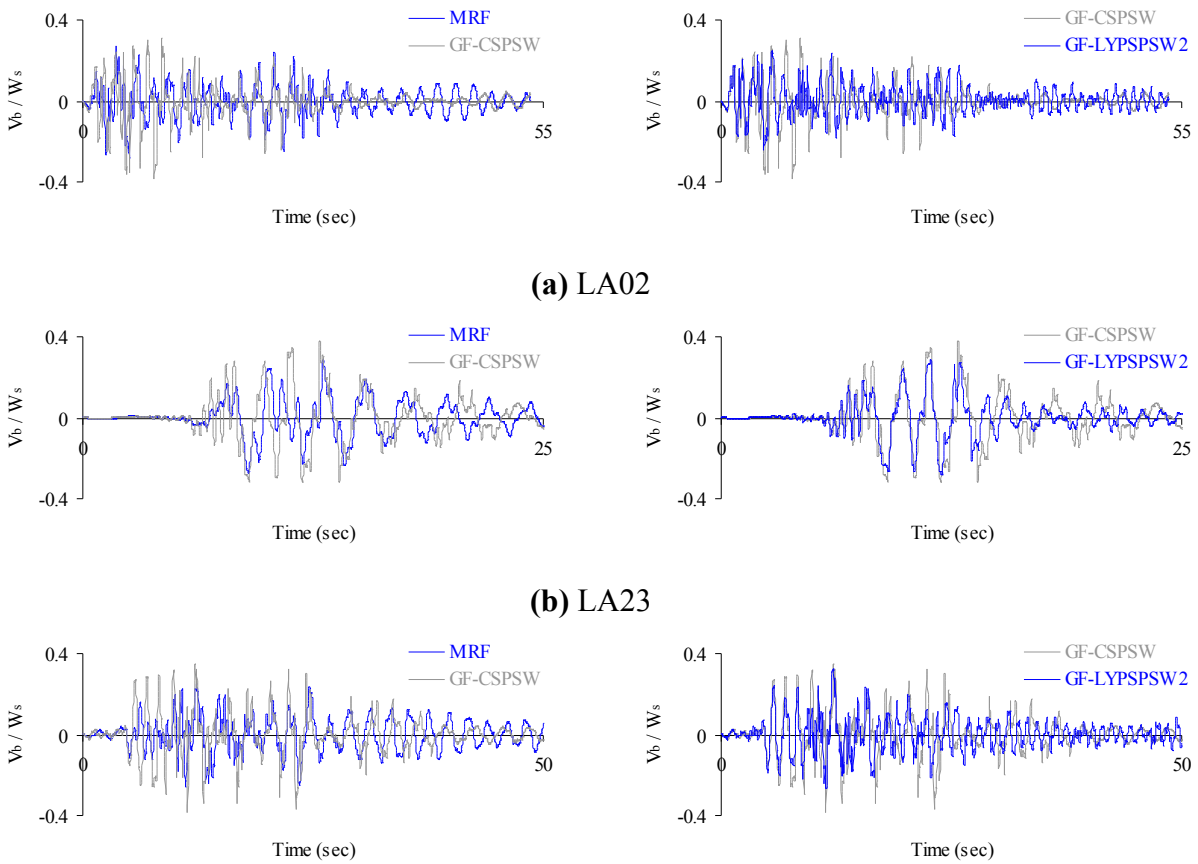

(a) LA02

(b) LA23

(c) LA29

Fig. 7.21 Comparison of base shear time histories of MRF, GF-CSPSW, and GF-LYPSPSW2 models

These results together with the other findings of the case study addressed in this section indicate that conventional steel shear wall systems may possess higher base shear demands compared to the MRF systems due to higher stiffness. Use of LYP steel infill plates with relatively larger thicknesses in retrofit of the conventional steel shear wall systems can desirably improve the stiffness and in the meanwhile decrease the seismic-induced base shear demands of SPSW systems.

7.6.4 Base Moment

The base moment demands of the structural models are assessed in this section, which are estimated by adding the moments developed at column bases due to seismic loading. Base moments (M_b) have been normalized by the product of the seismic weight (W_s) and total height of the structure (H_t). The normalized maximum base moment demands (in percentage), i.e. $M_b/(W_s \times H_t) \times 100$ values, for all ground motions are given in Table 7.13. Also, shown in Fig. 7.22 are the variations of the seismic-induced normalized maximum base moment demands due to the retrofit of structures using SPSW systems and LYP steel material. The illustrated average $M_b/(W_s \times H_t) \times 100$ values are obtained by considering the tabulated values in Table 7.13 for all ground motions.

Table 7.13 Normalized maximum base moment demands ($M_b/(W_s \times H_t) \times 100$) of the structural models induced by ground motions

Model	Ground motion										
	LA02	LA06	LA11	LA16	LA18	LA19	LA21	LA23	LA25	LA28	LA29
MRF	2.22	1.90	2.14	2.06	2.15	1.57	2.48	2.21	2.36	2.43	1.95
GF	0.64	0.43	0.84	0.85	0.86	0.51	0.90	0.63	1.22	0.90	0.84
GF-CSPSW	1.14	0.53	1.42	1.30	1.58	1.23	1.37	1.34	1.47	1.74	1.28
GF-LYPSPSW1	1.07	0.58	1.35	1.20	1.29	0.86	1.58	0.98	1.49	1.54	1.23
GF-LYPSPSW1.5	0.81	0.44	1.28	1.19	1.23	0.91	1.37	0.94	1.34	1.42	1.17
GF-LYPSPSW2	0.59	0.46	1.32	1.07	1.12	0.89	1.15	0.82	1.29	1.42	1.04
GF-LYPSPSW2.5	0.61	0.39	1.06	0.92	1.22	1.00	1.37	0.89	1.16	1.51	0.89
GF-LYPSPSW3	0.60	0.40	0.89	1.21	1.17	0.93	1.55	0.79	1.14	1.63	0.85

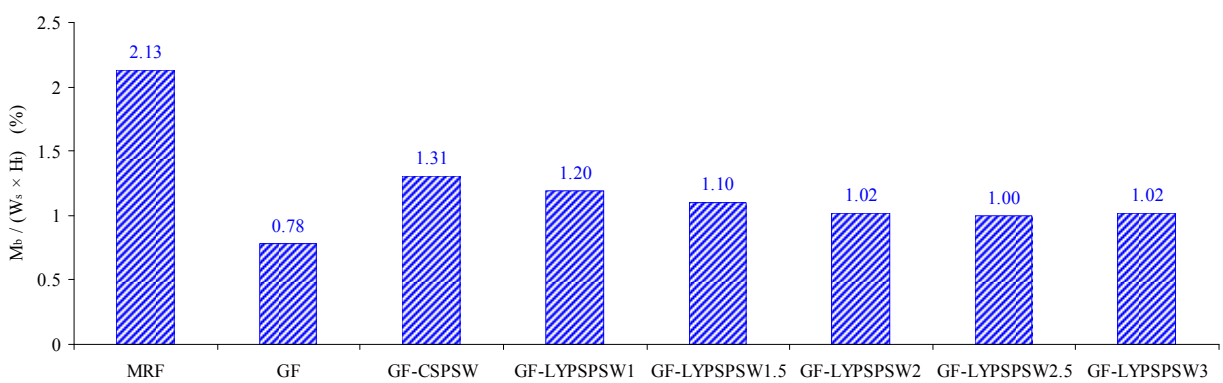

Fig. 7.22 Variations of seismic-induced normalized maximum base moment demands due to retrofit of structures using SPSW systems and LYP steel material

As it is seen in the figure, the base moment demand of the GF model is smaller than those of the other models for the lateral force-resisting systems with considerably higher stiffness. More importantly, it is found that the GF-CSPSW model possesses remarkably lower base moment demand compared to the MRF model, and use of LYP steel infill plates with increasing thickness further reduces the base moment demand. However, from the figure it is apparent that the base moment demand increases slightly in case of the GF-LYPSPSW3 model with the thickest infill plates. It is also evident that GF-LYPSPSW2 model with double plate thickness possesses lower base moment demand relative to the GF-CSPSW model. The base moment time-history plots of MRF, GF-CSPSW, and GF-LYPSPSW2 models for three sample ground motions are shown in Fig. 7.23.

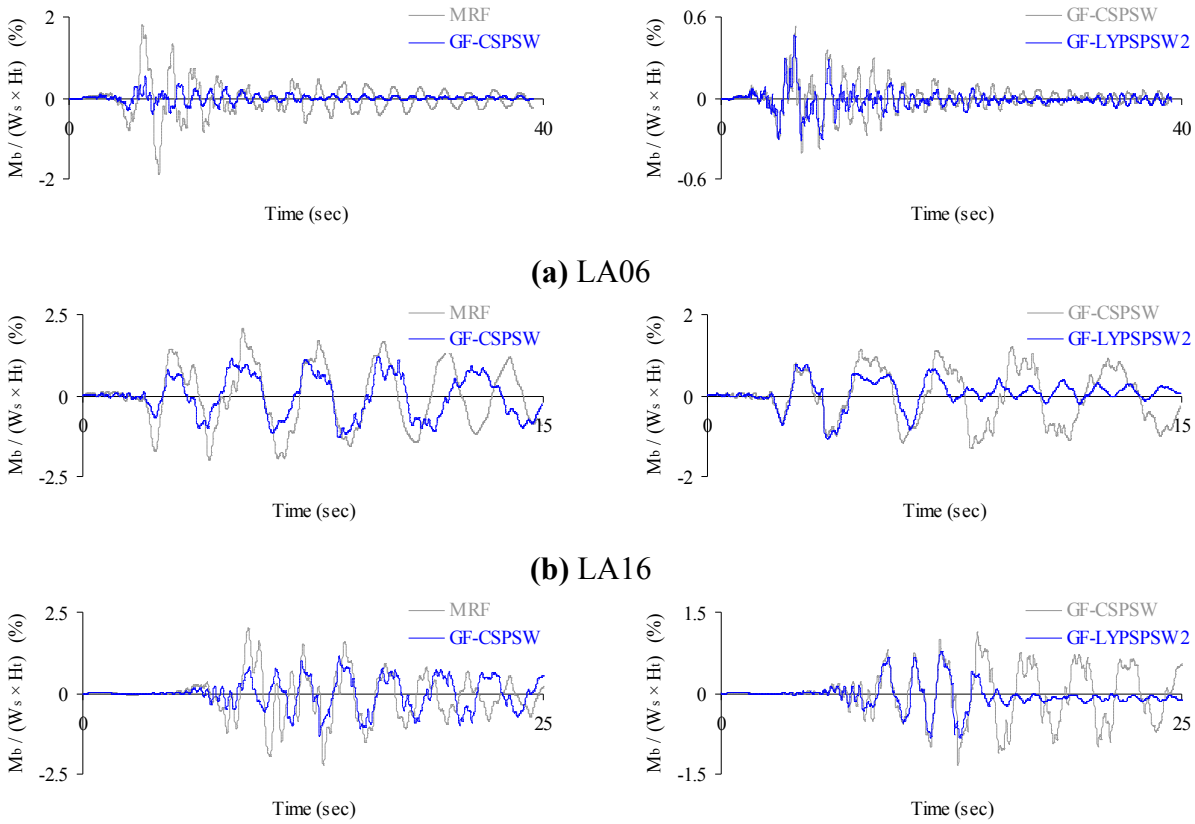

(a) LA06

(b) LA16

(c) LA23

Fig. 7.23 Comparison of base moment time histories of MRF, GF-CSPSW, and GF-LYPSPSW2 models

Consistent with the other findings of this case study, the time-history plots clearly show that the base moment demands of the GF-CSPSW model are lower than those of the MRF model. Also, employment of LYP steel infill plates with double thickness in the GF-LYPSPSW2 model effectively reduces the base moment demands in comparison with the response of the GF-CSPSW model.

On the whole, these results indicate the relative effectiveness of SPSW systems in limiting the base moment demands compared to the moment-resisting frames, and also retrofit of SPSW systems with LYP steel infill plates results in reduced base moment demands due to early yielding and energy absorption capacity of the LYP steel material as the plate thicknesses increase up to a certain limit.

7.6.5 VBE Axial Loads at Column Bases

According to the fundamental mechanics of SPSWs, VBEs are subjected to combined axial force and transverse force developed by the tension-field action of the infill plates. Therefore, changes in web-plate thickness as well as material properties can have a significant impact on the design and performance of the surrounding column members in such systems. On this basis, in order to evaluate the effects of retrofitting of SPSW systems with LYP steel infill plates having relatively larger thicknesses on the VBE axial load demands, the maximum VBE axial load demands at the column bases of the SPSW models are evaluated in this section. The maximum VBE axial loads at the column bases ($P_{VBE-base}$) have been normalized by the axial yield strength (P_y) of the first story VBE, i.e. W14×730 as shown in Table 7.1. The normalized maximum VBE axial load demands at column bases, i.e. $P_{VBE-base}/P_y$ values, from nonlinear time-history

analyses for all ground motions are provided in Table 7.14. The average $P_{VBE-base}/P_y$ values are also shown in Fig. 7.24.

Table 7.14 Normalized maximum VBE axial load demands ($P_{VBE-base}/P_y$) at column bases of the SPSW models induced by ground motions

Model	Ground motion										
	LA02	LA06	LA11	LA16	LA18	LA19	LA21	LA23	LA25	LA28	LA29
GF-CSPSW	0.71	0.49	0.87	0.89	0.81	0.59	0.86	0.81	0.87	0.90	0.75
GF-LYPSPSW1	0.41	0.35	0.53	0.55	0.55	0.32	0.58	0.46	0.49	0.58	0.48
GF-LYPSPSW1.5	0.51	0.41	0.69	0.71	0.69	0.40	0.75	0.58	0.62	0.76	0.61
GF-LYPSPSW2	0.63	0.50	0.82	0.84	0.80	0.52	0.88	0.73	0.79	0.92	0.69
GF-LYPSPSW2.5	0.75	0.55	0.91	0.95	0.87	0.56	0.98	0.84	0.97	0.97	0.76
GF-LYPSPSW3	0.87	0.62	0.98	0.98	0.94	0.62	1.00	0.91	0.99	0.97	0.85

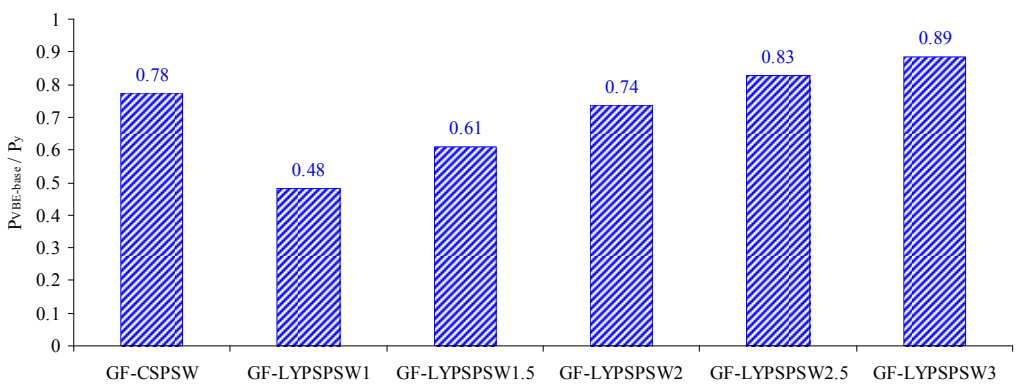

Fig. 7.24 Variations of seismic-induced normalized maximum VBE axial load demands at column bases due to retrofit of SPSWs using LYP steel material

From the analysis results in Table 7.14, it is found that all $P_{VBE-base}/P_y$ values are below 1.00. This indicates that the seismic-induced axial loads at the column bases of the SPSW frames did not exceed the axial yield strength of the first story VBE designed in accordance with the AISC 341-10 (2010) seismic provisions. Additionally, Fig. 7.24 shows that increasing of the infill plate thickness increases the VBE axial load demand. Also, retrofit of the GF-CSPSW model using LYP steel infill plates with 1.0, 1.5, and 2.0 times (larger) thicknesses results in relatively

smaller VBE axial load demands, while the GF-LYPSPSW2.5 and GF-LYPSPSW3 models possess larger VBE axial load demands compared to the GF-CSPSW model. This interesting finding clearly shows that the GF-LYPSPSW2 model can be a desirable retrofit option for the GF-CSPSW model. It is important to note that such a favorable seismic response is provided as a result of impact of the beneficial LYP steel material properties.

7.6.6 Web Plate Ductility Ratio and Energy Dissipation Mechanism

Structural systems designed for high-seismic loading are expected to undergo multiple cycles of loading into the inelastic range with controlled damage accepted as a means of dissipating the energy of the earthquake. The ability of a system to withstand such loading is termed "system ductility". In the case of SPSW systems, the web plates are the locations where inelastic strain demands are primarily expected to occur, and hence ductility of steel web plates in such lateral force-resisting systems will result in good performance under severe seismic loading. On this basis, the high-seismic design of SPSW systems is based on confining ductility demands primarily to the web plates and also to plastic hinges in the HBE at the VBE face (Sabelli and Bruneau, 2006).

Based on various reported experimental and analytical studies on SPSWs, as partly listed by Sabelli and Bruneau (2006), properly-designed systems have by and large exhibited significant ductility. For instance, some conventional and LYP steel shear walls tested by Berman and Bruneau (2005) and Chen and Jhang (2006 and 2011), respectively, reached a web plate ductility ratio of 12 prior to failure. Also, recent analytical studies reported by Berman (2011) on seismic behavior of code-designed SPSWs using nonlinear response history analysis for ground motions representing different hazard levels have demonstrated that web plate ductility demands are

significantly larger for low rise walls than for high rise walls where higher modes of vibrations impact the response.

In this section, the web plate ductility demands for all stories of the GF-CSPSW and GF-LYPSPSW2 models are determined from nonlinear time-history analyses and evaluated comparatively in order to further verify the effectiveness of the conventional steel shear wall retrofit strategy using LYP steel infill plates with double thicknesses. The maximum web plate ductility ratios for all stories of the GF-CSPSW and GF-LYPSPSW2 models and for all selected ground motions are given in Table 7.15. The maximum ductility ratio for each story is determined from the maximum plastic strain of a strip element with the largest maximum plastic strain value divided by the yield strain.

Table 7.15 Maximum web plate ductility ratios of GF-CSPSW and GF-LYPSPSW2 models

Story	Model	Ground motion										
		LA02	LA06	LA11	LA16	LA18	LA19	LA21	LA23	LA25	LA28	LA29
9	GF-CSPSW	5.7	1.0	3.3	6.7	2.8	5.7	11.3	6.3	6.0	6.8	6.2
	GF-LYPSPSW2	2.9	1.3	2.9	3.9	3.2	4.7	11.1	1.9	5.4	7.3	3.1
8	GF-CSPSW	4.7	0.7	3.2	6.6	3.8	4.6	13.1	5.2	5.7	8.0	5.1
	GF-LYPSPSW2	3.8	0.8	4.2	5.3	4.8	4.6	11.8	3.3	8.2	9.2	3.8
7	GF-CSPSW	4.3	0.0	2.9	5.2	3.8	3.6	10.7	4.0	6.3	8.1	3.9
	GF-LYPSPSW2	3.5	0.7	4.1	6.0	6.0	3.7	12.5	3.8	8.6	9.4	2.6
6	GF-CSPSW	2.0	0.0	3.1	5.2	3.6	1.2	8.9	3.6	6.4	7.8	2.3
	GF-LYPSPSW2	2.8	0.6	3.8	6.3	6.0	2.0	11.4	3.9	7.7	9.7	2.4
5	GF-CSPSW	1.2	0.0	3.2	6.3	4.4	1.2	7.4	4.9	7.0	8.6	2.1
	GF-LYPSPSW2	1.9	0.4	4.5	6.6	6.2	1.0	10.9	4.3	7.9	10.1	3.0
4	GF-CSPSW	2.7	0.0	4.4	7.2	5.3	1.5	7.5	6.4	7.5	10.6	3.0
	GF-LYPSPSW2	2.2	0.6	6.1	7.0	6.2	1.4	10.6	4.6	8.7	11.8	4.5
3	GF-CSPSW	2.3	0.0	5.2	4.5	6.2	2.3	5.0	4.1	4.6	8.4	3.1
	GF-LYPSPSW2	1.8	0.5	6.5	5.9	6.7	2.8	8.2	3.9	7.1	10.7	4.8
2	GF-CSPSW	3.8	0.1	8.1	5.5	8.5	5.1	5.4	4.8	7.6	10.8	5.0
	GF-LYPSPSW2	2.6	0.8	8.1	6.1	7.8	4.4	7.8	4.1	9.0	13.1	6.0
1	GF-CSPSW	2.3	0.0	5.5	3.3	5.8	2.8	3.6	3.2	4.9	9.6	3.4
	GF-LYPSPSW2	1.9	0.6	6.3	4.2	6.4	3.5	5.6	2.2	7.5	10.7	4.7

As it is seen in the table, infill plates in the GF-CSPSW model do not exhibit any ductility in some limited cases. In contrast, the maximum web plate ductility ratios for both models reach

13.1 in a couple of cases. These smallest and largest ductility ratios are found in cases of 10/50 and 2/50 ground motions, respectively. The average values of the maximum web plate ductility ratio for all stories of the two considered models are also shown in Fig. 7.25.

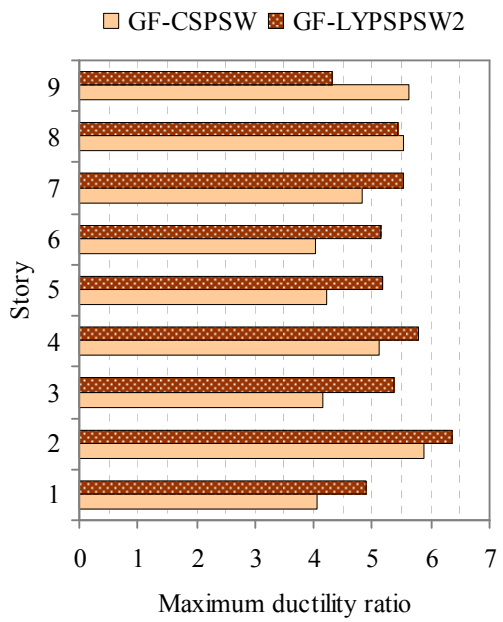

Fig. 7.25 Average web plate ductility ratios of GF-CSPSW and GF-LYPSPSW2 models

From the figure, it is found that the web plate ductility ratios for all stories of the two models lie between 4 and 6.5. Also, it is evident that the story ductility ratios of the GF-LYPSPSW2 model are in general larger than those of the GF-CSPSW model except for the upper stories, in particular the 9th story, where GF-CSPSW web plates exhibit relatively larger ductility ratio. These results demonstrate that ductility performance of the GF-CSPSW and GF-LYPSPSW2 models is by and large similar and even application of LYP steel in GF-LYPSPSW2 model with thicker infill plates results in relatively larger ductility and desirable energy dissipation mechanism of the system in which most of the earthquake energy is dissipated through inelastic deformations developed in the web-plate components.

Fig. 7.26 shows the strain energy contour plots for MRF, GF-CSPSW (frame only), and GF-LYPSPSW2 (frame only) models at the end of application of LA28 ground motion. This figure intends to show the plastification zones in frame members through which the earthquake energy is partly dissipated in addition to the inelastic deformations in web-plate components in SPSW systems.

Fig. 7.26(a) shows that in the MRF model the seismic energy is fully dissipated through development of plastic hinges at the ends of beam members and all 1st story column bases. Fig. 7.26(b), on the other hand, shows that in the GF-CSPSW model plastic hinges are formed at the ends of HBEs and all 1st story VBE and column bases, while from Fig. 7.26(c) it is found that the plastic hinges are desirably confined to HBE ends and 1st story VBE bases. These findings indicate that the code-designed GF-CSPSW model has provided inelastic deformation capacity primarily through web plate yielding and also plastic-hinge formation in the ends of HBEs, as expected. However, the GF-LYPSPSW2 model has apparently exhibited a more favorable behavior by even confining the column-base plastic hinges to the 1st story VBE bases and reducing the overall system demand on the frame column members outside the SPSW.

Fig. 7.27, also, shows the deformed shapes of the MRF, GF-CSPSW, and GF-LYPSPSW2 models at the end of application of LA28 ground motion. From the figure, it is clear that residual deformations are developed due to inelastic behaviors and responses of the structural models.

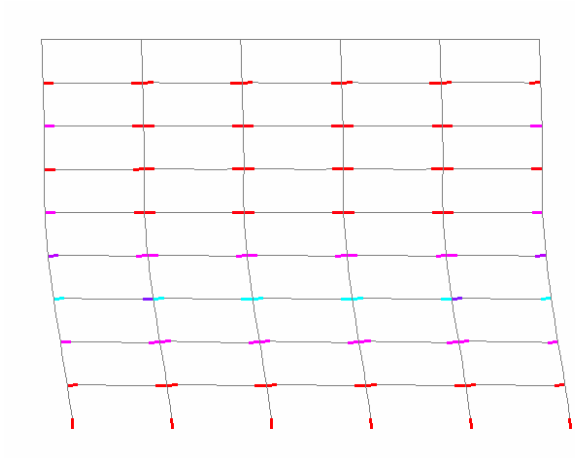

(a) MRF

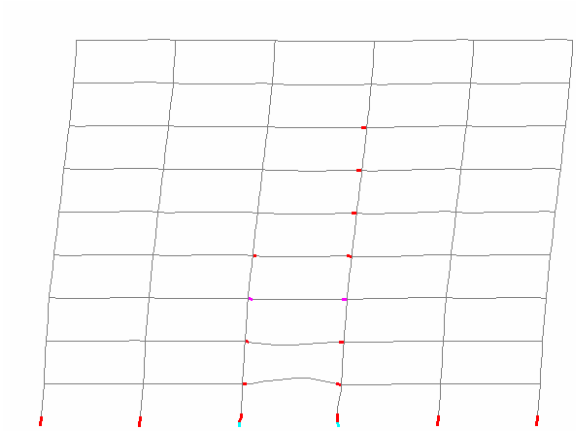

(b) GF-CSPSW *(frame only)*

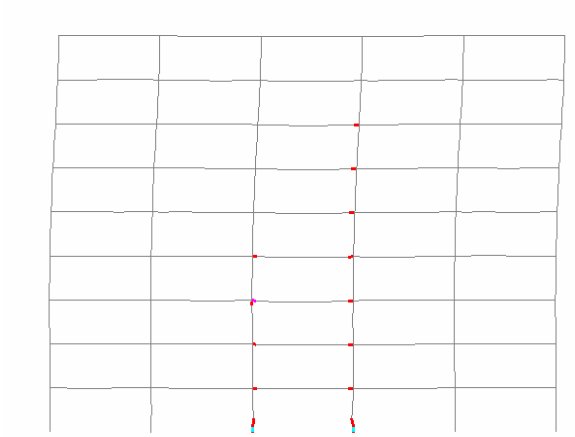

(c) GF-LYPSPSW2 *(frame only)*

Fig. 7.26 Strain energy contour plots for MRF, GF-CSPSW (frame only), and GF-LYPSPSW2 (frame only) models at the end of application of LA28 ground motion showing the plastification zones in beam/HBE and column/VBE frame members

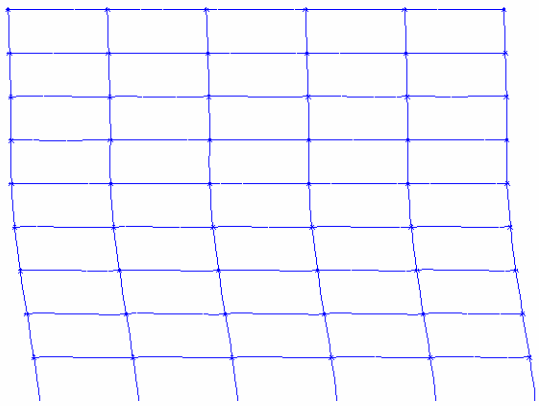

(a) MRF

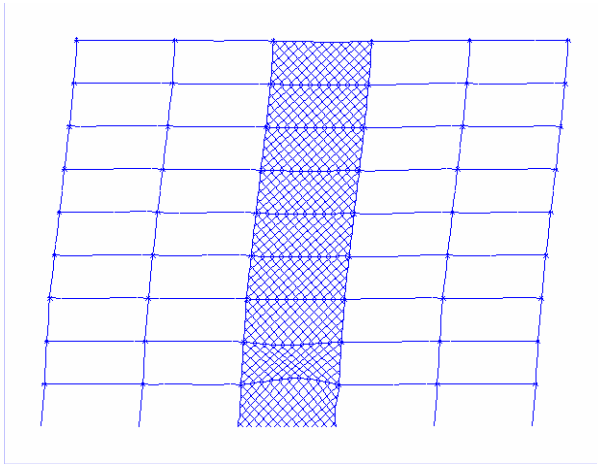

(b) GF-CSPSW

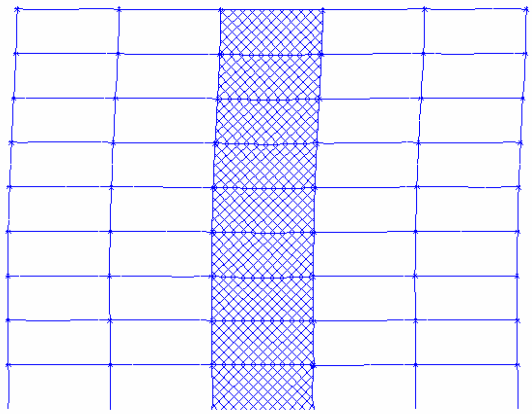

(c) GF-LYPSPSW2

Fig. 7.27 Deformed shapes (×15) of MRF, GF-CSPSW, and GF-LYPSPSW2 models at the end of application of LA28 ground motion

As a result, it may be concluded that both the GF-CSPSW and GF-LYPSPSW2 models have provided a desirable energy dissipation mechanism. Nevertheless, the GF-LYPSPSW2 model seems to provide a superior energy dissipation mechanism as a result of employment of LYP steel material with relatively higher energy absorption capacity.

7.7 Concluding Remarks

In this chapter, the seismic behavior of code-designed and retrofitted lateral force-resisting systems including 9-story moment-resisting and SPSW frames has been investigated using nonlinear time-history analysis of a suite of structural models originally designed for seismic conditions in Los Angeles, California. The conventional and LYP steel shear walls were modeled using the strip model which was shown to adequately represent the behavior of single- and multi-story SPSWs with different geometrical-material bifurcation characteristics. Modal analyses were initially performed to determine the vibration characteristics of the structural models. These models were then analyzed under eleven earthquake acceleration time histories selected to represent Los Angeles ground motions with minimum, average, and maximum PGV and PGA values within 10/50 and 2/50 hazard levels.

Fundamental periods obtained from the ASCE 7-10 (2010) code-specified formula were found to be lower than those obtained from modal analysis of the moment-resisting and SPSW frames. Such lower estimates of the fundamental period may lead to conservative estimates of the design seismic forces. Based on the modal analysis results, the considered SPSW-frame models possessed remarkably higher initial stiffness and lower period values compared to the MRF model. Moreover, retrofitting of the GF-CSPSW model in the extreme case, i.e. with LYP steel infill plates of triple thickness, resulted in maximum 30% increase in initial stiffness and

10% decrease in the fundamental period values approximately. In addition to the assessment of the elastic behavior through modal analyses, different seismic response parameters were considered and investigated through nonlinear time-history analyses in order to evaluate the seismic performance of the structural models and also the effectiveness of retrofit of structures using LYP steel infill plates with relatively larger thicknesses.

Results of the nonlinear time-history analyses showed that "interstory" drift ratio parameter is more controlling and of further significance relative to "story" drift ratio parameter in seismic design of structures. The SPSW systems were found to be quite effective in limiting the drifts of the structural models, and LYP steel shear walls, in particular, exhibited good performance in improving the drift response of the structures. Acceleration response assessment of the designed and retrofitted structural models revealed that employment of LYP steel infill plates with even larger thicknesses in retrofitting of the GF-CSPSW model results in relatively smaller floor accelerations. The LYP steel shear wall frames, also, showed a good performance in reducing the base shear and moment demands compared to the GF-CSPSW model. Furthermore, retrofit of the conventional steel SPSW using LYP steel infill plates was found to be effective in lowering the VBE axial load demands at column bases as the web-plate thicknesses increased up to a certain limit. Consistent with all case studies, it was found that employment of overly thick LYP steel infill plates in retrofit of the GF-CSPSW model may adversely affect the seismic response and result in weak or undesirable performance of the SPSW system.

In a comparative case study, it was also shown that the GF-LYPSPSW2 model possesses relatively larger ductility and energy dissipation capability compared to the GF-CSPSW model. All in all, evaluation of different seismic response parameters demonstrates that the GF-LYPSPSW2 model with LYP steel web-plates of double thickness seems to be a desirable

retrofit option for the code-designed and conventional steel GF-CSPSW model. These findings verify the effectiveness of the conventional steel shear wall retrofit strategy using LYP steel infill plates of double thickness discussed in Chapter 5. More experimental and analytical investigations are required to further substantiate the integrity of the considered retrofit strategy. To this end, Chapter 8 will further address the subject of retrofit of structures and evaluate the effectiveness of the considered retrofit strategy using the fragility function method.

Ultimately, the effectiveness of use of LYP steel with superior material properties compared to conventional steel in improving the seismic performance through either design of new or retrofit of existing structures is demonstrated through system-level investigations presented in this chapter. The results and findings of the present and previous chapters are all indicative of various advantages of use of LYP steel material in efficient seismic design and retrofit of structures. It is believed that application of such steel material will result in creation of more reliable, high-performing, and sustainable structures.

8. PROBABILISTIC ASSESSMENT OF SEISMIC RETROFIT OF STRUCTURES USING FRAGILITY FUNCTION METHOD

8.1 Introduction

Based on the lessons learned from the past and recent catastrophic seismic events with considerable casualties, structural damages, and economic losses along with the major advancements in the fields of structural and earthquake engineering, design methodology for structures is gradually moving from prescriptive design approaches based on code-specified minimum requirements to performance-based seismic design which explicitly evaluates how a building is likely to perform, given the potential hazard it is likely to experience, considering uncertainties inherent in the quantification of potential hazard and uncertainties in assessment of the actual building response (FEMA 445, 2006).

Performance-based seismic design is a seismic design methodology that permits design of new buildings or upgrade of existing buildings with a realistic understanding of the risk of casualties, occupancy interruption, and economic loss that may occur as a result of future earthquakes (FEMA 445, 2006). Also, according to Gould's (2003) definition, such seismic design methodology can provide a cost-effective means to i) reduce earthquake financial loss due to structural and nonstructural damage, ii) design a structure for a range of performance levels when subjected to different levels of ground motion, iii) obtain minimum structural and nonstructural damage in a moderate seismic event, and iv) allow for continued operations in a structure following a design level seismic event.

Fragility curves/functions are the basis for performance-based earthquake engineering and development of such functions for structural systems is a key component of the performance-based seismic design. Fragility functions are performance-prediction models that relate the probability of reaching, or exceeding, structural and nonstructural damage/repair states with a intensity measure of the earthquake input motions. They can be generated either empirically using experimental data or analytically through seismic response assessment using numerical simulations.

Development of such statistical models, i.e. fragility functions, for SPSWs is essential to enable the performance-based seismic design of such lateral force-resisting systems. In order to meet this need, damage and repair states based on the observations from experiments and an understanding of the SPSW system's behavior have been developed and proposed in studies reported by Berman et al. (2010) and Baldvins et al. (2012), and consequently fragility functions have been developed for the considered repair states (Baldvins et al., 2012). To the author's knowledge, apart from the aforementioned studies as well as a couple of studies reported by Ghosh et al. (2009) and Bayat (2010), the performance-based seismic design and probabilistic assessment of seismic response and retrofit of SPSW systems have not been addressed adequately, and in fact only initial steps have been taken towards the performance-based seismic design of SPSW systems through these studies.

In this chapter, the seismic performance of the 9-story moment-resisting and code-designed as well as retrofitted SPSW frames employing conventional and LYP steel infill plates will be primarily investigated through nonlinear time-history analyses. Drift and acceleration responses as two effective seismic demand parameters of structures will be considered for the seismic performance assessment. Proper and effective analytical fragility functions will be developed

using the numerical simulation results by considering various damage and repair states specified for the structural and nonstructural systems and components, and ultimately the seismic retrofit of new and existing structures using SPSW systems as well as LYP steel material will be addressed using the fragility function method.

8.2 Fragility Function Methodology

A major step in performance-based earthquake engineering assessments is to estimate the probabilistic structural response as a function of ground motion intensity. The objective of this step is to estimate the probability distribution of a structural response parameter, herein termed as the Engineering Demand Parameter (*EDP*), as a function of earthquake ground motion intensity, herein termed as the Intensity Measure (*IM*). There are several methods available for obtaining such an estimate, which have been discussed by Baker and Cornell (2006).

The ground motions are characterized by the intensity measure which can be selected from the peak ground velocity (PGV), peak ground acceleration (PGA), and other characteristics of the earthquake recordings. The structural responses of buildings, on the other hand, may be represented by various parameters such as interstory drift and/or floor acceleration. In any case, the choice of the intensity measure (*IM*) and the structural response parameter (*EDP*) plays an important and effective role in running the fragility analysis and also evaluating the seismic performance of the structures.

In this study, the Probabilistic Seismic Demand Model (PSDM) has been employed to derive analytical fragility functions using nonlinear time-history responses of the structural models. The PSDM is developed using a "cloud" approach for relating *EDPs* to *IMs*, which uses a set of un-scaled ground motions (Baker and Cornell, 2006) and is termed as the Probabilistic Seismic Demand Analysis (PSDA) in here. It is noted that the PSDM can be also developed using a

"scaling" approach, termed as the Incremental Dynamic Analysis (IDA), in which all motions are scaled to selective intensity levels corresponding to a prescribed seismic hazard level and incremental dynamic analysis is performed at different hazard levels (Zhang and Huo, 2009). The PSDA method uses regression analysis in order to estimate the conditional mean and standard deviation of *EDP* given *IM*. Accordingly, the mean *EDP* can be related to the *IM* using

$$EDP = a(IM)^b \quad \text{or} \quad \ln(EDP) = b\ln(IM) + \ln(a) \tag{8.1}$$

where a and b are constant coefficients to be estimated from linear regression of the response data of nonlinear time-history analyses, which are referred to as the regression coefficients. If the remaining variability in ln(*EDP*) for a given *IM* is assumed to have a constant variance for all *IM*, then its standard deviation can be estimated using (Baker and Cornell, 2006)

$$\zeta_{EDP|IM} = \sqrt{\frac{\sum_{i=1}^{N}[\ln(EDP_i) - \ln(a(IM_i)^b)]^2}{N-2}}, \tag{8.2}$$

in which N is the number of *EDP-IM* data pairs, and EDP_i and IM_i are the values of the i-th data pair. Ultimately, by assuming a lognormal distribution of *EDP* for a given *IM*, the fragility functions defining the probability of *EDP* reaching or exceeding a specified limit state (*LS*) for a given *IM* can be represented using

$$P(EDP \geq LS \mid \mathrm{IM}) = 1 - \int_0^{LS} \frac{1}{\sqrt{2\pi} \cdot \zeta_{EDP|\mathrm{IM}} \cdot EDP} \cdot e^{\left[-\frac{1}{2}\left(\frac{\ln(EDP) - \ln(a(IM)^b)}{\zeta_{EDP|\mathrm{IM}}}\right)^2\right]} \cdot d(EDP). \tag{8.3}$$

When it is assumed that the *EDP* variable has a lognormal distribution, then ln(*EDP*) can be considered to be normally distributed. Accordingly, the probability that *EDP* attains or exceeds *LS* for a given *IM* can be alternatively calculated using the standard normal cumulative distribution function, denoted by $\Phi(\bullet)$, as

$$P(EDP \geq LS \mid IM) = 1 - \Phi\left(\frac{\ln(LS) - \ln(a(IM)^b)}{\zeta_{EDP|IM}}\right). \tag{8.4}$$

8.3 Specifications and Modeling of Structural Systems

8.3.1 Selected Structural Systems

By considering the main objective of this research, i.e. probabilistic assessment of seismic response and vulnerability of code-designed and retrofitted SPSW systems employing conventional and LYP steel infill plates, the modified Los Angeles 9-story pre-Northridge moment-resisting frame (MRF model), code-designed and conventional steel SPSW frame (GF-CSPSW model), and retrofitted SPSW frame using LYP steel infill plates of double thickness (GF-LYPSPSW2 model) are selected in here. According to the findings from the studies discussed in previous chapters, the GF-LYPSPSW2 model is considered to be a proper and desirable retrofit option for the GF-CSPSW model; therefore, this particular retrofitted SPSW model, i.e. the GF-LYPSPSW2 model, is selected for the purpose of the current study.

The specifications of the MRF, GF-CSPSW, and GF-LYPSPSW2 structural models are shown in Tables 7.1 through 7.3 in Chapter 7, and their seismic performance was studied by evaluating different seismic response parameters from nonlinear time-history analyses. It is noted that the fragility methodology adopted in this chapter makes it possible to probabilistically deal with the uncertainties in ground motions as well as variability of structural properties and offer a system-level evaluation of the damage and/or repair potential for the considered lateral force-resisting systems under earthquakes.

8.3.2 Finite Element Modeling and Analysis

The finite element modeling and analysis details for the three considered lateral force-resisting systems, i.e. the MRF, GF-CSPSW, and GF-LYPSPSW2 models, were provided in Chapter 7. The bare frame and wall-frame structural models are shown in Fig. 7.3. These models were developed and analyzed in ANSYS 14.0 (2011), and analysis results were verified through comparison with experimental results. The strip model approach was utilized to represent SPSW behavior. The frame beam and column and also the SPSW web-plate components were represented using beam and discrete tension-only strip elements, respectively, and lumped masses were modeled using point mass elements. ASTM A572 Gr. 50 steel was employed in modeling of the frame components, and ASTM A36 and LYP100 steel material were considered for the infill plates in the respective GF-CSPSW and GF-LYPSPSW2 models. The vibration characteristics and initial stiffnesses of the structural models were primarily determined through modal analyses. A series of nonlinear time-history analyses with geometrical as well as material nonlinearities and consideration of a 2% damping ratio were subsequently performed for the moment-resisting and SPSW frames, which included *P*-delta effects as well.

8.3.3 Ground Motion Suite

In the PSDA method, it is important to select a sufficient number of earthquake records and accordingly perform nonlinear time-history analyses in order to generate reliable fragility functions and obtain a conceptually and statistically acceptable and good prediction of the seismic response. On this basis, a suite of thirty Los Angeles ground motion records considered in the SAC steel research project (FEMA 355C, 2000) having probabilities of exceedance of 50% in 50 years, 10% in 50 years, 2% in 50 years are used in this study in order for developing

fragility functions and probabilistically evaluating the seismic response and vulnerability of the code-designed and retrofitted structural models. The suite consists of ground motions with three different probability levels and includes uncertainty in the seismic characteristics. Details of the selected earthquake records are provided in Table 8.1.

Table 8.1 Details of selected Los Angeles ground motions for probabilistic seismic demand analysis

SAC name	Record	Earthquake magnitude	Distance (km)	Scale factor	PGV (mm/s)	PGA (mm/s^2)	Probability of exceedance
LA02	Imperial Valley, El Centro, 1940	6.9	10	2.01	599.0	6628.8	10% in 50 years
LA04	Imperial Valley, Array #05, 1979	6.5	4.1	1.01	771.0	4786.5	10% in 50 years
LA06	Imperial Valley, Array #06, 1979	6.5	1.2	0.84	474.4	2300.8	10% in 50 years
LA08	Landers, Barstow, 1992	7.3	36	3.2	656.8	4174.9	10% in 50 years
LA10	Landers, Yermo, 1992	7.3	25	2.17	603.5	3533.5	10% in 50 years
LA11	Loma Prieta, Gilroy, 1989	7	12	1.79	791.4	6524.9	10% in 50 years
LA13	Northridge, Newhall, 1994	6.7	6.7	1.03	955.5	6649.3	10% in 50 years
LA16	Northridge, Rinaldi RS, 1994	6.7	7.5	0.79	1007.6	5685.8	10% in 50 years
LA18	Northridge, Sylmar, 1994	6.7	6.4	0.99	1189.3	8014.4	10% in 50 years
LA19	North Palm Springs, 1986	6	6.7	2.97	682.7	9994.3	10% in 50 years
LA21	Kobe, 1995	6.9	3.4	1.15	1427.0	12580.0	2% in 50 years
LA22	Kobe, 1995	6.9	3.4	1.15	1231.6	9027.5	2% in 50 years
LA23	Loma Prieta, 1989	7	3.5	0.82	737.6	4099.5	2% in 50 years
LA24	Loma Prieta, 1989	7	3.5	0.82	1369.1	4637.6	2% in 50 years
LA25	Northridge, Rinaldi, 1994	6.7	7.5	1.29	1603.1	8516.2	2% in 50 years
LA26	Northridge, Rinaldi, 1994	6.7	7.5	1.29	1639.8	9252.9	2% in 50 years
LA27	Northridge, Sylmar, 1994	6.7	6.4	1.61	1304.9	9087.0	2% in 50 years
LA28	Northridge, Sylmar, 1994	6.7	6.4	1.61	1935.3	13041.0	2% in 50 years
LA29	Tabas, 1974	7.4	1.2	1.08	710.5	7934.5	2% in 50 years
LA30	Tabas, 1974	7.4	1.2	1.08	1388.3	9725.8	2% in 50 years
LA41	Coyote Lake, 1979	5.7	8.8	2.28	1390.4	5783.4	50% in 50 years
LA43	Imperial Valley, 1979	6.5	1.2	0.4	848.6	1406.7	50% in 50 years
LA44	Imperial Valley, 1979	6.5	1.2	0.4	451.3	1094.5	50% in 50 years
LA45	Kern, 1952	7.7	107	2.92	247.0	1414.9	50% in 50 years
LA46	Kern, 1952	7.7	107	2.92	243.0	1560.2	50% in 50 years
LA49	Morgan Hill, 1984	6.2	15	2.35	269.4	3124.1	50% in 50 years
LA54	Parkfield, Cholame 8W, 1966	6.1	8	2.92	320.8	7750.5	50% in 50 years
LA56	North Palm Springs, 1986	6	9.6	2.75	254.2	3716.6	50% in 50 years
LA57	San Fernando, 1971	6.5	1	1.3	216.7	2481.4	50% in 50 years
LA58	San Fernando, 1971	6.5	1	1.3	270.8	2265.4	50% in 50 years

Fig. 8.1 shows the distributions of the peak ground velocity and acceleration of the selected ground motion records. From Table 8.1 and Figs. 8.1(a) and (b), the selected earthquake records have PGV values ranging between 0.22 and 1.94 m/s and PGA values ranging between 0.11*g*

and 1.33*g*. The ground motions are indeed selected in a manner in order to cover wide ranges of PGV and PGA intensity measures as much as possible.

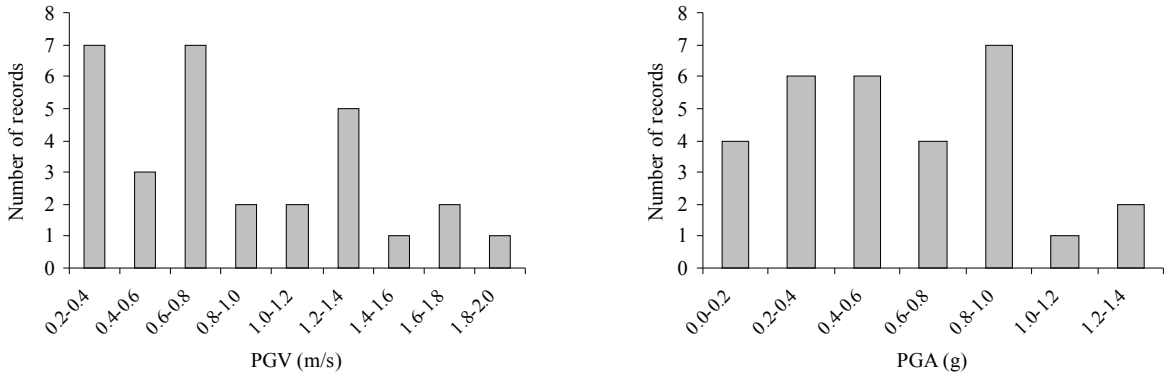

(a) PGV **(b)** PGA

Fig. 8.1 Characteristics of selected earthquake records for probabilistic seismic demand analysis

8.3.4 Seismic Response of Structural Models

The nonlinear dynamic analysis of a structural model produces a wealth of information. The process of selecting effective and appropriate demand measures in order to characterize the seismic performance and probabilistically assess the seismic vulnerability of the system is a challenging task. In general, the choice of an appropriate seismic demand parameter is a function of both the structural system and the desired performance objectives (Chen and Lui, 2006). A search of the literature on probabilistic seismic demand analysis of structures reveals that in spite of various demand parameters proposed and applied for the purpose of the aforementioned probabilistic methodology, interstory drift and floor acceleration have been deemed significant demand measures in this regard. HAZUS methods, for instance, estimate building damage based on interstory drift and floor acceleration (HAZUS-MH MR5, 2010). On this basis, the peak interstory drift ratio (PIDR) and peak floor acceleration (PFA) seismic response parameters are considered as the potential *EDPs* in this study.

On the other hand, various ground motion intensity parameters have been considered by different researchers and their relative reliability and superiority in investigating the seismic response and performance of structures have been examined through comparative studies. Among various ground motion intensity measures, PGV and PGA can be considered as fairly robust and easy to compute (Akkar et al., 2005), which have been employed by many researchers in the development of fragility curves (Yakut and Yilmaz, 2008). Accordingly, PGV and PGA are taken as the potential *IMs* for the probabilistic seismic demand analysis of the considered structural systems.

PIDR and PFA demand parameters are obtained from the nonlinear dynamic analyses of the structural models under the considered suite of Los Angeles earthquake records. The values of the seismic response and ground motion intensity parameters, i.e. respective *EDP* and *IM* values, for all earthquake records and the three structural models are summarized in Table 8.2.

In order to evaluate the peak drift and acceleration responses of the moment-resisting and code-designed as well as retrofitted SPSW frames under seismic loading, the average PIDR (%) and PFA (g) values are computed from the corresponding values tabulated in Table 8.2 and shown in Fig. 8.2.

Table 8.2 Summary of ground motion intensity measure and seismic response parameter values

Ground motion	Intensity Measure - IM		Engineering Demand Parameter - EDP					
	PGV (m/s)	PGA (g)	Peak Interstory Drift Ratio - PIDR			Peak Floor Acceleration - PFA (g)		
			MRF	GF-CSPSW	GF-LYPSPSW2	MRF	GF-CSPSW	GF-LYPSPSW2
LA02	0.599	0.676	0.027	0.016	0.010	1.158	1.847	1.181
LA04	0.771	0.488	0.022	0.010	0.006	0.807	1.052	0.894
LA06	0.474	0.235	0.016	0.007	0.004	0.586	0.762	0.574
LA08	0.657	0.426	0.020	0.013	0.011	0.747	1.198	0.813
LA10	0.603	0.360	0.020	0.018	0.014	0.685	1.557	0.826
LA11	0.791	0.665	0.029	0.021	0.018	0.887	1.562	1.296
LA13	0.956	0.678	0.022	0.022	0.011	1.143	2.278	1.051
LA16	1.008	0.580	0.043	0.022	0.017	0.775	2.066	1.399
LA18	1.189	0.817	0.026	0.022	0.018	1.185	1.659	1.202
LA19	0.683	1.019	0.022	0.016	0.012	1.205	1.764	1.419
LA21	1.427	1.283	0.048	0.036	0.029	1.388	2.664	2.215
LA22	1.232	0.921	0.067	0.033	0.019	1.588	2.469	1.895
LA23	0.738	0.418	0.024	0.020	0.011	0.872	2.087	0.820
LA24	1.369	0.473	0.065	0.036	0.028	0.900	2.141	1.230
LA25	1.603	0.868	0.040	0.023	0.020	1.173	1.965	1.442
LA26	1.640	0.944	0.046	0.034	0.027	1.159	1.959	1.780
LA27	1.305	0.927	0.053	0.034	0.023	1.035	2.489	1.423
LA28	1.935	1.330	0.035	0.029	0.027	1.549	2.208	2.110
LA29	0.711	0.809	0.025	0.018	0.013	1.273	2.169	1.029
LA30	1.388	0.992	0.041	0.024	0.021	1.336	2.861	1.399
LA41	1.390	0.590	0.025	0.015	0.011	0.965	1.860	1.350
LA43	0.849	0.143	0.010	0.005	0.004	0.379	0.533	0.376
LA44	0.451	0.112	0.008	0.003	0.003	0.386	0.390	0.335
LA45	0.247	0.144	0.011	0.007	0.006	0.448	0.666	0.643
LA46	0.243	0.159	0.012	0.006	0.004	0.553	0.686	0.448
LA49	0.269	0.319	0.019	0.008	0.005	0.636	0.811	0.593
LA54	0.321	0.790	0.014	0.013	0.008	0.951	1.502	1.008
LA56	0.254	0.379	0.014	0.012	0.006	0.654	1.442	0.603
LA57	0.217	0.253	0.008	0.005	0.005	0.349	0.630	0.440
LA58	0.271	0.231	0.009	0.012	0.007	0.450	1.219	0.788

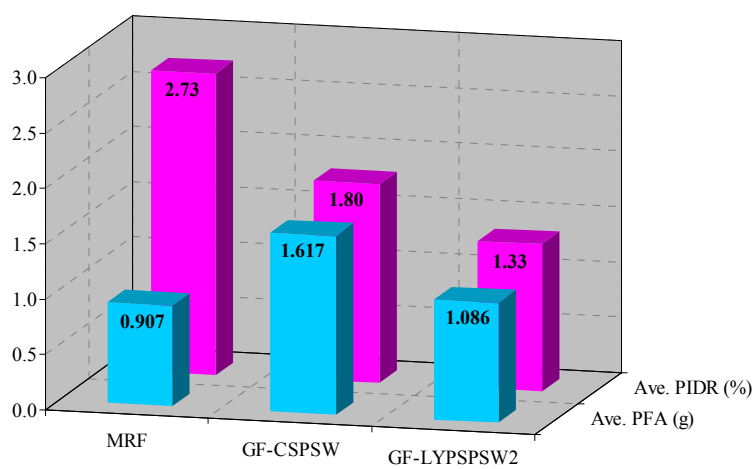

Fig. 8.2 Average PIDR (%) and PFA (g) values for MRF, GF-CSPSW, and GF-LYPSPSW2 models

As it is seen in the figure, the GF-LYPSPSW2 model by and large exhibits relatively desirable drift and acceleration performances. In case of the peak drift response, the GF-LYPSPSW2 model with the lowest average PIDR (%) value shows the best performance compared to the MRF and GF-CSPSW models in reducing the seismic-induced interstory drift. In case of the peak acceleration response, it is found that the GF-CSPSW model possesses a larger average PFA (g) value compared to the MRF model due to its considerably higher stiffness, while retrofitting the GF-CSPSW model with LYP steel infill plates of double thickness favorably results in a relatively lower average PFA (g) value. These findings are quite consistent with the results of the studies discussed in the previous chapter, and time and again demonstrate the superior seismic performance of the GF-LYPSPSW2 model with LYP steel infill plates of double thickness which is considered as a desirable retrofit option for the code-designed and conventional steel GF-CSPSW model. It is notable that in the current study a large number of earthquake records are considered compared to those applied in Chapter 7.

8.4 Fragility Analysis of Structural Systems

8.4.1 Selection of Appropriate EDP-IM Data Pairs

A PSDM relates *IMs* to *EDPs*, and hence the choice of *EDP-IM* pairs in the demand model is critical for a successful PSDA. An optimal PSDM is required to be practical, effective, sufficient, and efficient, and selection of an appropriate *EDP-IM* pair for such a PSDM is not easy (Mackie and Stojadinović, 2001).

An *EDP-IM* pair in a demand model is practical if it makes engineering sense and also can be easily derived from available ground motion measurements and nonlinear analysis response quantities. Effectiveness of a PSDM is a measure of how readily it yields itself to use in a

deaggregated performance-based design framework. For example, assuming lognormally-distributed ground motion *IMs*, an effective demand model should have an exponential form as shown in Eq. (8.1) (Mackie and Stojadinović, 2001). As well, PSDM is considered to be sufficient when *EDP* is conditionally independent, given *IM*, of earthquake magnitude and the source-to-site distance, and lastly efficiency implies a smaller dispersion of *EDP* results for a given *IM*, making fewer nonlinear dynamic analyses necessary to evaluate a PSDM with the same confidence (Janković and Stojadinović, 2004).

In this section, it is tried to search for appropriate *EDP-IM* pairs from the four potential *PIDR-PGV*, *PIDR-PGA*, *PFA-PGV*, and *PFA-PGA* data pairs for optimal PSDMs with lower degrees of scatter. To achieve this objective, ln[*EDP*] and ln[*IM*] are plotted against each other for the three considered structural models, with ln[*IM*] on the abscissa and ln[*EDP*] on the ordinate as shown in Figs. 8.3 through 8.6. As seen in the figures, a linear regression analysis of the ln[*EDP*] and ln[*IM*] data in each case has produced a line through the cloud of the *EDP-IM* data points, and the corresponding linear equation and R^2 value are provided in each individual case.

The coefficient of determination, i.e. R^2 value, is a statistic which is considered as a measure of variation in this study. This statistic is an estimate of the goodness-of-fit of the line that describes how well a regression line fits the set of data. An R^2 value near 1.0 indicates that a regression line fits the data well, while an R^2 value closer to 0.0 indicates a regression line does not fit the data very well. The R^2 values obtained from the linear regression analyses of the data pairs are given in Table 8.3.

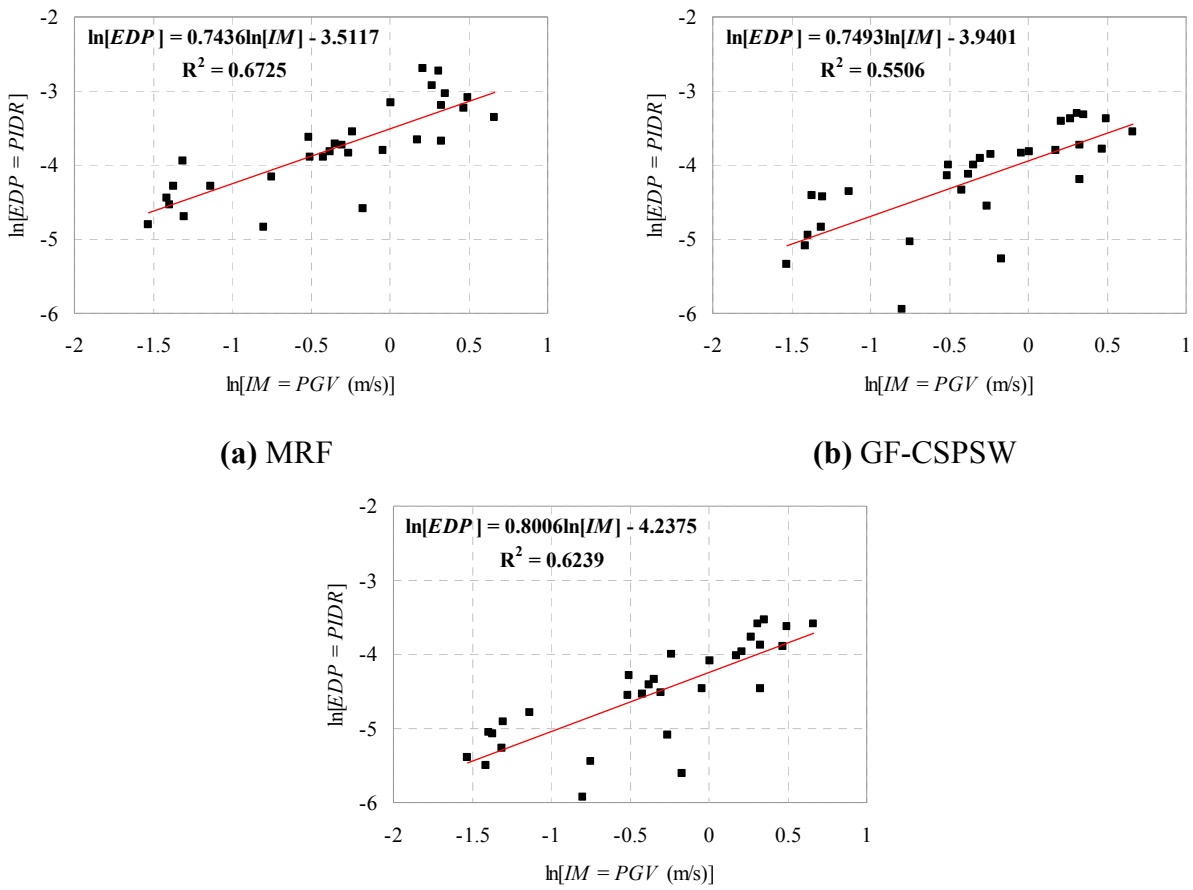

(a) MRF

(b) GF-CSPSW

(c) GF-LYPSPSW2

Fig. 8.3 Relationship between ln[*EDP* = *PIDR*] and ln[*IM* = *PGV* (m/s)]

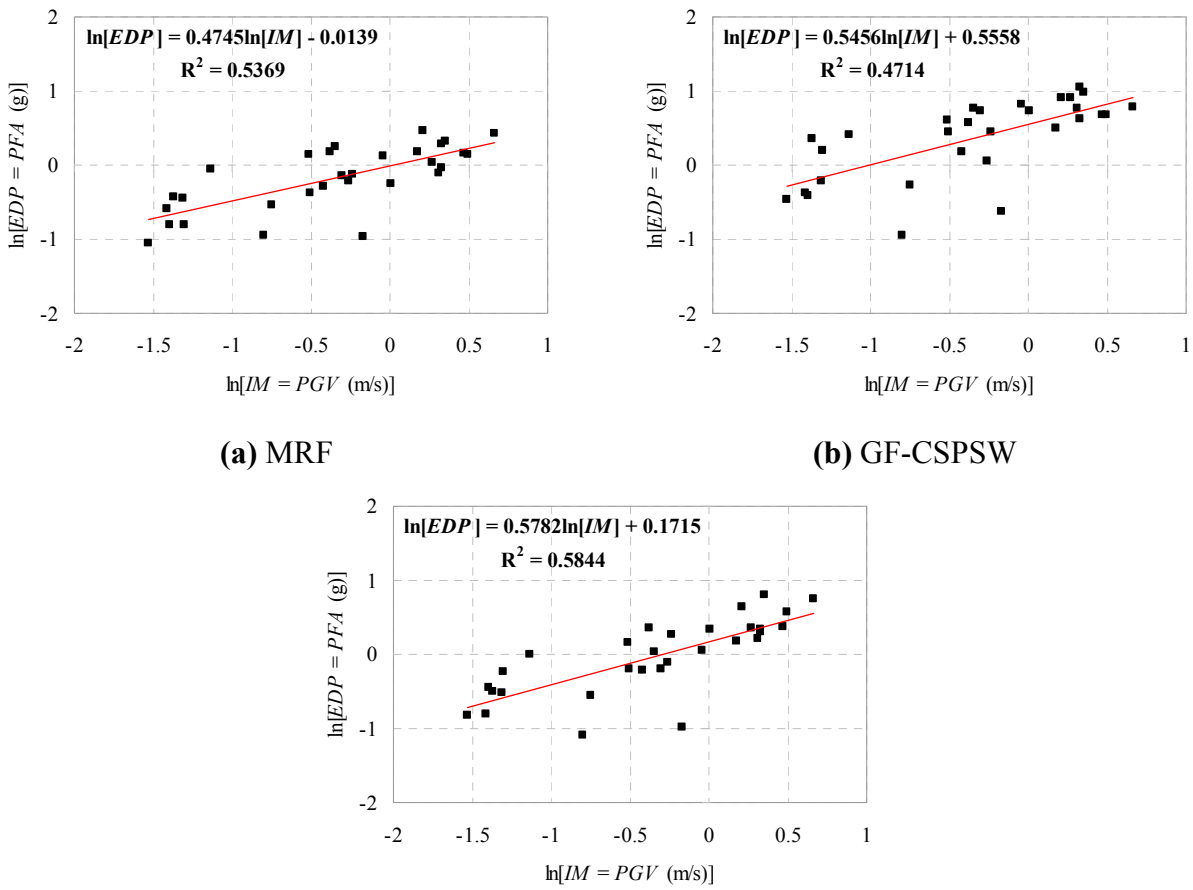

(a) MRF

(b) GF-CSPSW

(c) GF-LYPSPSW2

Fig. 8.4 Relationship between ln[*EDP* = *PFA* (g)] and ln[*IM* = *PGV* (m/s)]

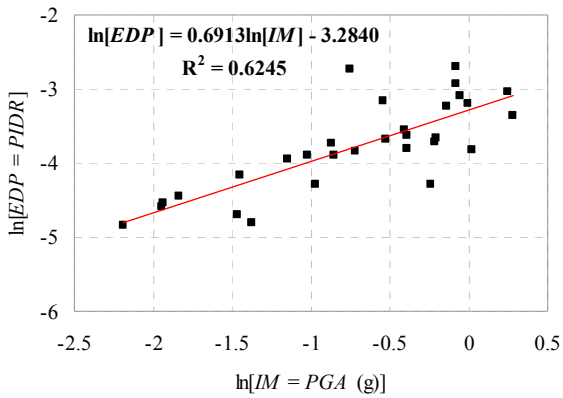

(a) MRF

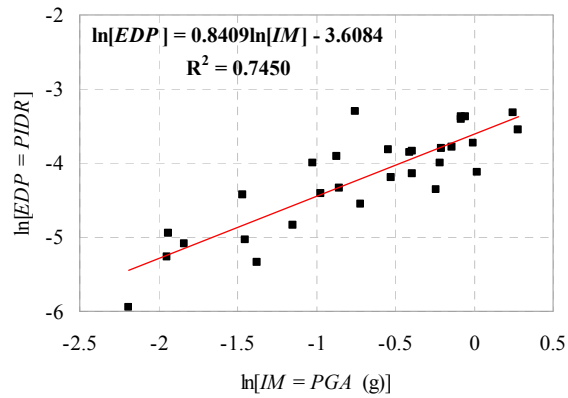

(b) GF-CSPSW

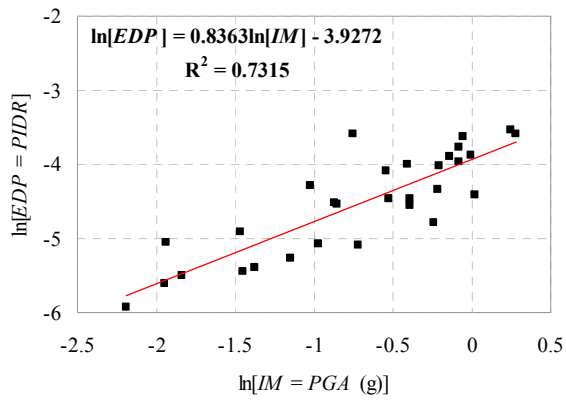

(c) GF-LYPSPSW2

Fig. 8.5 Relationship between ln[*EDP* = *PIDR*] and ln[*IM* = *PGA* (g)]

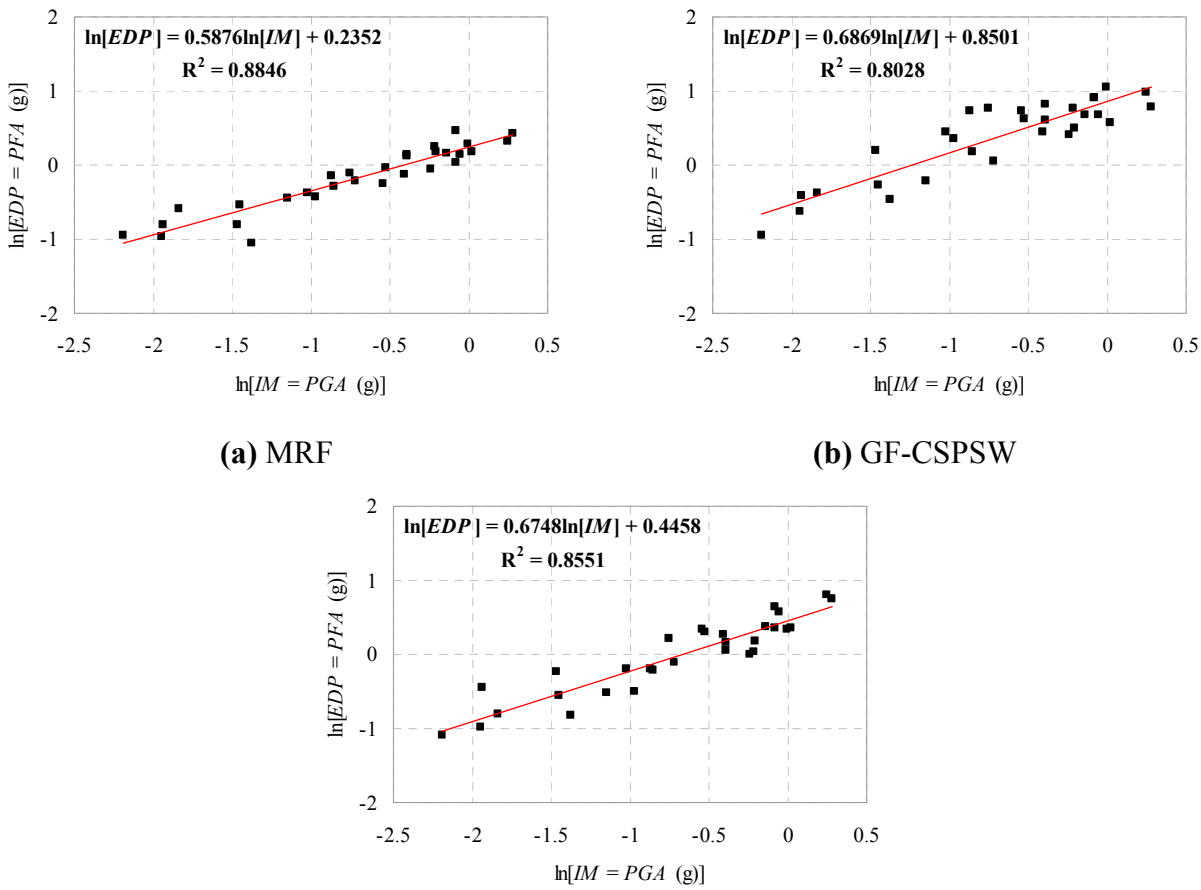

(a) MRF

(b) GF-CSPSW

(c) GF-LYPSPSW2

Fig. 8.6 Relationship between ln[*EDP* = *PFA* (g)] and ln[*IM* = *PGA* (g)]

Table 8.3 R^2 values obtained from linear regression of ln[*EDP*] and ln[*IM*] variables

ln[*EDP*]	Model	ln[*IM*]	
		ln[*PGV* (m/s)]	ln[*PGA* (g)]
ln[*PIDR*]	MRF	0.6725	0.6245
	GF-CSPSW	0.5506	0.7450
	GF-LYPSPSW2	0.6239	0.7315
ln[*PFA* (g)]	MRF	0.5369	0.8846
	GF-CSPSW	0.4714	0.8028
	GF-LYPSPSW2	0.5844	0.8551

From the tabulated results, *PGA* appears to have a stronger correlation with both considered *EDPs* relative to *PGV*. This *IM*, i.e. *PGA*, is found to be better correlated with *PFA* where R^2 values are in the range of 0.80-0.88, as compared to PIDR with R^2 values between 0.62 and 0.75. In comparison, R^2 values in cases of *PFA-PGV* and *PIDR-PGV* data pairs are in the ranges of 0.47 to 0.58 and 0.55 to 0.67, respectively. Based on these results, fragility curves developed based on *PFA-PGA* and *PIDR-PGA* data pairs are believed to be more reliable and provide a better representation of probability of the structural damage and/or repair.

8.4.2 Determination of Lognormal Distribution Parameters

Based on the satisfactory and relatively higher levels of linear correlation between *PFA-PGA* and *PIDR-PGA* data pairs, as discussed in the previous section, these *EDP* and *IM* parameters are selected for development of fragility curves and seismic vulnerability assessment of the structural models in this study. Accordingly, the values of the *a* and *b* constant coefficients determined from the linear regression analyses of the selected data pairs, and the standard deviations calculated using Eq. (8.2) for the selected *EDP-IM* pairs and the structural models, are given in Table 8.4. Included in the table are also the functional relations between the *EDP* and *IM* parameters, which have been determined using the regression coefficients and the power model in Eq. (8.1).

The tabulated PSDM parameters will be utilized in generating various fragility curves for the considered structural models. Different damage and repair states will also be considered in this regard, which will be addressed in the next section.

Table 8.4 Regression coefficients, standard deviation, and functional relation for selected *EDP-IM* data sets

Model	Selected		Regression coefficients		$\zeta_{EDP\|IM}$	Functional relation
	EDP	*IM*	*a*	*b*		
MRF	*PIDR*	*PGA* (g)	0.0375	0.6913	0.3792	$PIDR = 0.0375(PGA)^{0.6913}$
GF-CSPSW	*PIDR*	*PGA* (g)	0.0271	0.8409	0.3481	$PIDR = 0.0271(PGA)^{0.8409}$
GF-LYPSPSW2	*PIDR*	*PGA* (g)	0.0197	0.8363	0.3585	$PIDR = 0.0197(PGA)^{0.8363}$
MRF	*PFA* (g)	*PGA* (g)	1.2651	0.5876	0.1501	$PFA = 1.2651(PGA)^{0.5876}$
GF-CSPSW	*PFA* (g)	*PGA* (g)	2.3400	0.6869	0.2409	$PFA = 2.3400(PGA)^{0.6869}$
GF-LYPSPSW2	*PFA* (g)	*PGA* (g)	1.5618	0.6748	0.1965	$PFA = 1.5618(PGA)^{0.6748}$

The *EDP-IM* data plots along with the corresponding power trendlines for the selected data pairs as well as the structural models are illustrated in Figs. 8.7(a) through 8.7(f). The corresponding power function as well as the R^2 value are also shown in each figure, which are directly obtained from regression analysis in Microsoft Excel. It is noted that these results are quite consistent with those provided in Tables 8.3 and 8.4.

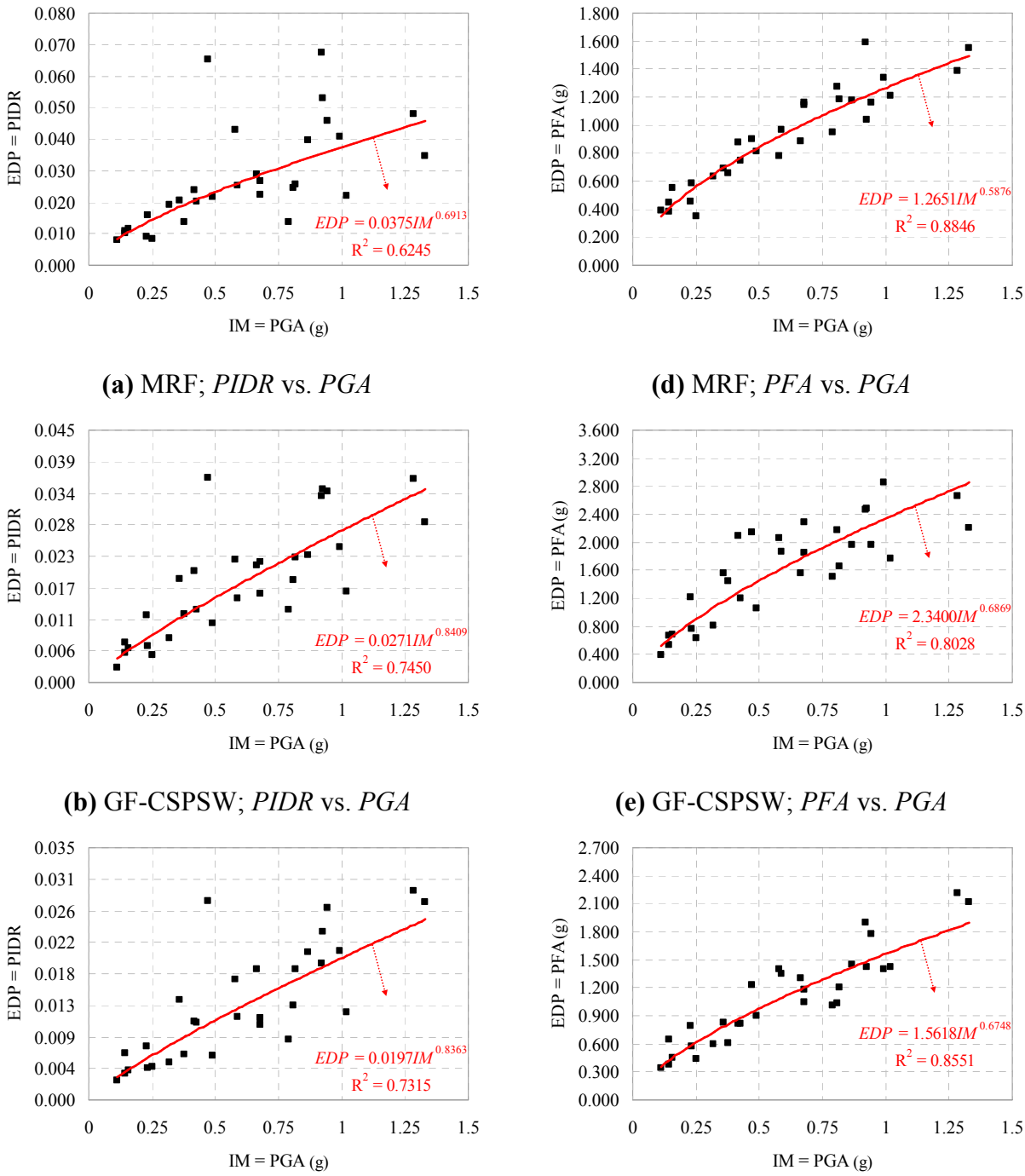

(a) MRF; *PIDR* vs. *PGA*

(d) MRF; *PFA* vs. *PGA*

(b) GF-CSPSW; *PIDR* vs. *PGA*

(e) GF-CSPSW; *PFA* vs. *PGA*

(c) GF-LYPSPSW2; *PIDR* vs. *PGA*

(f) GF-LYPSPSW2; *PFA* vs. *PGA*

Fig. 8.7 Selected *EDP-IM* data sets and the corresponding power trendlines for MRF, GF-CSPSW, and GF-LYPSPSW2 models

8.4.3 Considered Damage and Repair States

One of the important issues in performance-based earthquake engineering methodology is the definition of meaningful damage states in relation to repair actions. For economic loss estimation, understanding the type of damages is of great significance to establish if repair would be required and what the nature and cost of such repairs would be. Building damage is estimated based on threshold values of structural response parameters, e.g. interstory drift and floor acceleration, that initiate different states of damage, and discrete damage states provide the user with an understanding of the building's physical condition (HAZUS-MH MR5, 2010). These threshold values of damage (or associated repair) states are referred to as the "limit states", as denoted by *LS* in Eqs. (8.3) and (8.4). It is noted that damage and/or repair models are often developed based on experimental observations and engineering judgment.

According to the HAZUS-MH MR5 (2010) definition, fragility curves describe the probability of damage to the building's structural system, drift-sensitive nonstructural components, and acceleration-sensitive nonstructural components and contents. On this basis, damage states can be defined separately for structural and nonstructural systems of a building. By considering the importance of structural and nonstructural systems performance in performance-based seismic design and response assessment of buildings, separate fragility curves are developed in this study for the three aforementioned structural/nonstructural categories by adopting appropriate damage and repair states as provided in the following.

In HAZUS-MH MR5 (2010), damage is described by one of four discrete damage states: Slight, Moderate, Extensive or Complete, and Collapse as subset of Complete structural damage, and average interstory drift ratios of structural damage states for generic building types and different seismic design levels are provided. Table 8.5 lists the interstory drift ratios of structural

damage states for high-rise steel moment frames with high-code design level selected for the MRF model in this study.

Table 8.5 HAZUS-MH MR5 (2010) interstory drift ratios of structural damage states for high-rise steel moment frames with high-code design level

Structural model	Height range	Design level	Structural damage states			
			Slight	Moderate	Extensive	Complete
Steel moment frame	High-rise	High-code	0.003	0.006	0.015	0.040

In spite of consideration of various model building types in HAZUS-MH MR5 (2010), no data is provided in case of structural damage states for SPSW systems. To address this need, recourse is made to the results of the study reported by Baldvins et al. (2012), in which five repair states, as listed in Table 8.6, have been proposed based on collected experimental results and observations from previous studies, and appropriate story drift ratios of the structural repair states have been recommended for use in practice for predicting the performance of SPSWs. The recommended story drift ratios of structural repair states for SPSWs meeting certain seismic criteria have been adopted in this research, which are summarized in Table 8.6.

Table 8.6 Baldvins et al.'s (2012) recommended story drift ratios of structural repair states for SPSWs that meet certain seismic criteria

Structural model	Structural repair states				
	RS1	RS2	RS3	RS4	RS5
Steel plate shear wall	0.004	0.006	0.015	-	0.0275
Description	*Cosmetic repair*	*Replace web plate*	*VBE repair*	*HBE and connection repair*	*Replace boundary elements or frame*

It is noted that due to the lack of experimental data no story drift ratio has been recommended for RS4. Specification of a certain story drift ratio for this repair state is dependent upon availability and consideration of additional experimental data (Baldvins et al., 2012).

In addition to the damage and repair states of structural systems discussed above, the HAZUS-MH MR5 (2010) damage-state criteria for drift- and acceleration-sensitive nonstructural components and contents are adopted in the current study, which are provided in Tables 8.7 and 8.8, respectively. These tabulated limit states are applied in development of fragility curves for all three structural models.

Table 8.7 HAZUS-MH MR5 (2010) interstory drift ratios of nonstructural damage states for drift-sensitive components of all building types

Structural model	Design level	Nonstructural damage states			
		Slight	Moderate	Extensive	Complete
All	All	0.004	0.008	0.025	0.050

Table 8.8 HAZUS-MH MR5 (2010) peak floor accelerations of nonstructural damage states for acceleration-sensitive components/contents of all building types with high-code design level

Structural model	Design level	Nonstructural damage states			
		Slight	Moderate	Extensive	Complete
All	High-code	0.3g	0.6g	1.2g	2.4g

8.4.4 Fragility Curves of Structural Models

By selecting the effective *EDP-IM* data pairs, determining lognormal distribution parameters, and also considering the appropriate damage and repair states, fragility curves are developed for the MRF, GF-CSPSW, and GF-LYPSPSW2 models, which are presented in this section. Structural and nonstructural drift as well as acceleration fragility curves generated using the PSDA method are shown in Figs. 8.8 through 8.10, respectively.

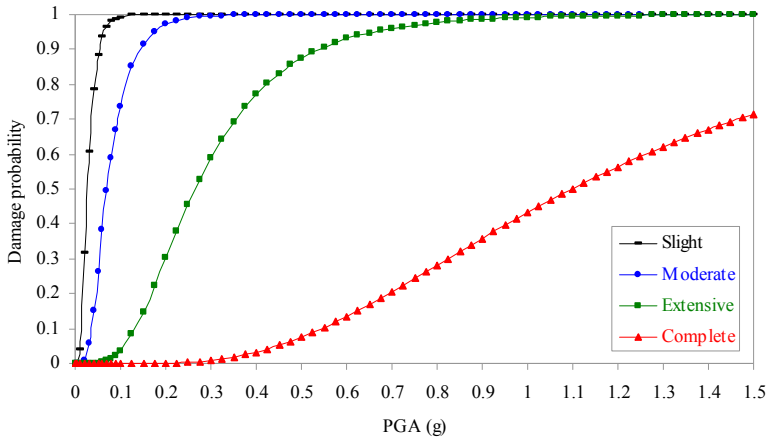

(a) MRF, damage states

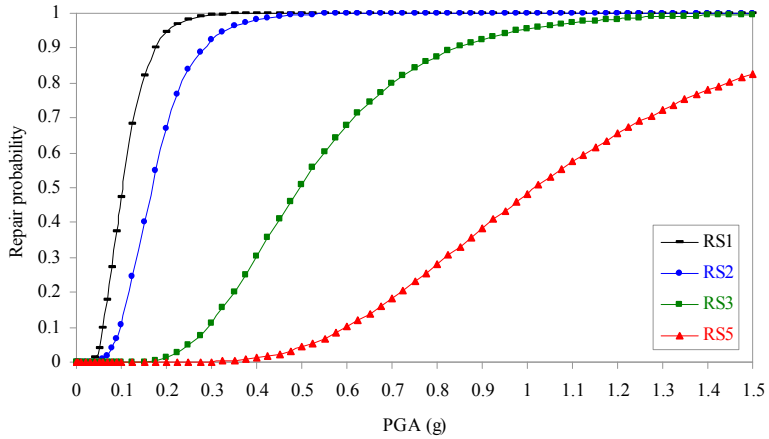

(b) GF-CSPSW, repair states

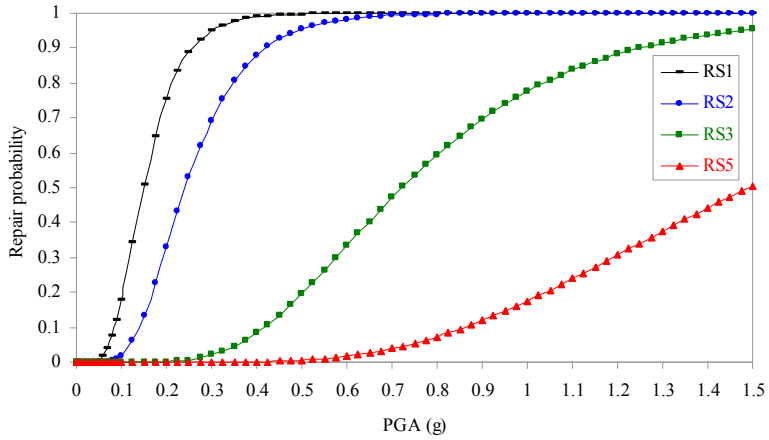

(c) GF-LYPSPSW2, repair states

Fig. 8.8 Fragility curves for predicting the probability of reaching or exceeding the damage states of MRF and repair states of GF-CSPSW and GF-LYPSPSW2 structural systems

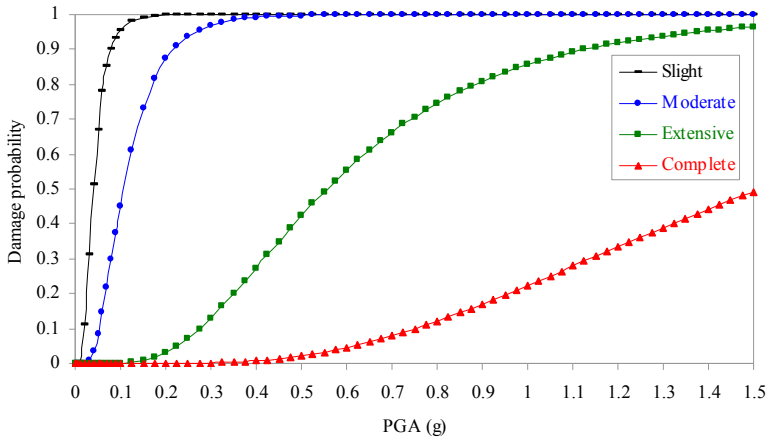

(a) MRF

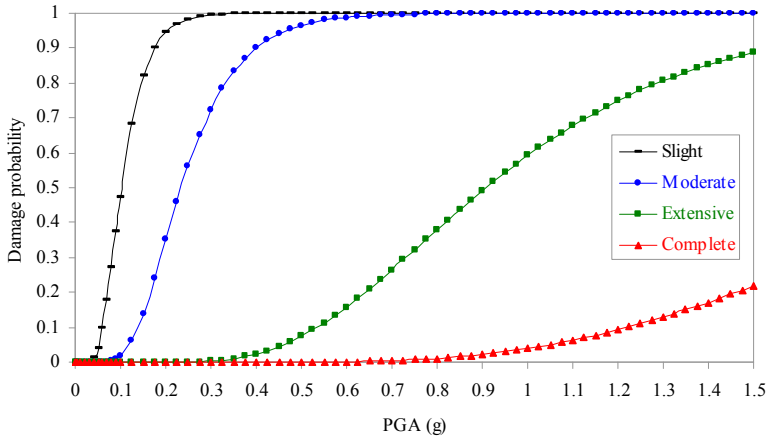

(b) GF-CSPSW

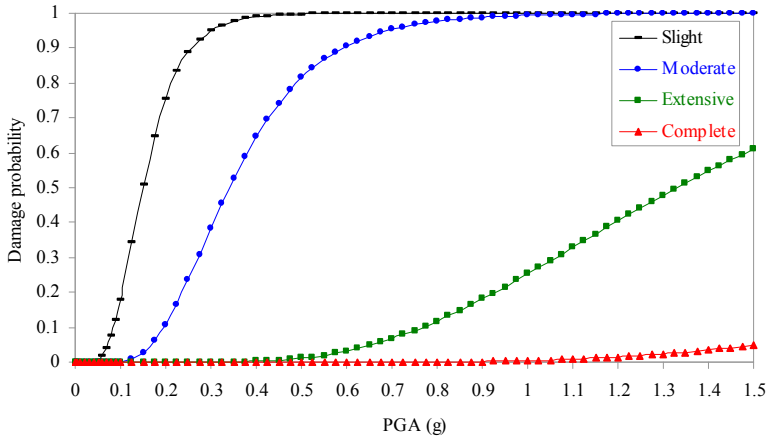

(c) GF-LYPSPSW2

Fig. 8.9 Fragility curves for predicting the probability of reaching or exceeding the nonstructural damage states for drift-sensitive components of buildings

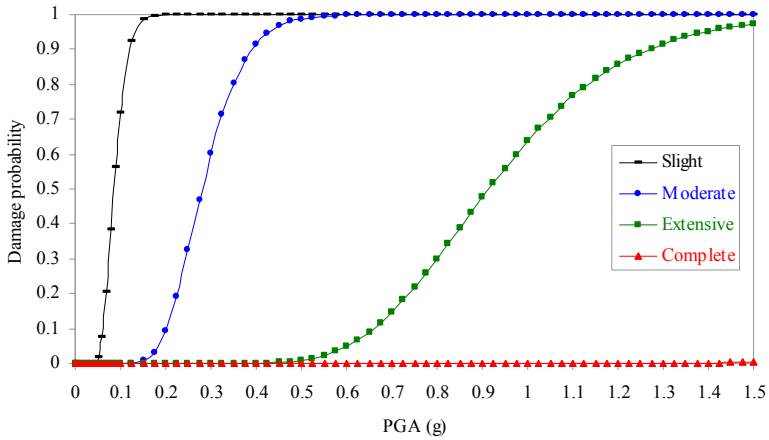

(a) MRF

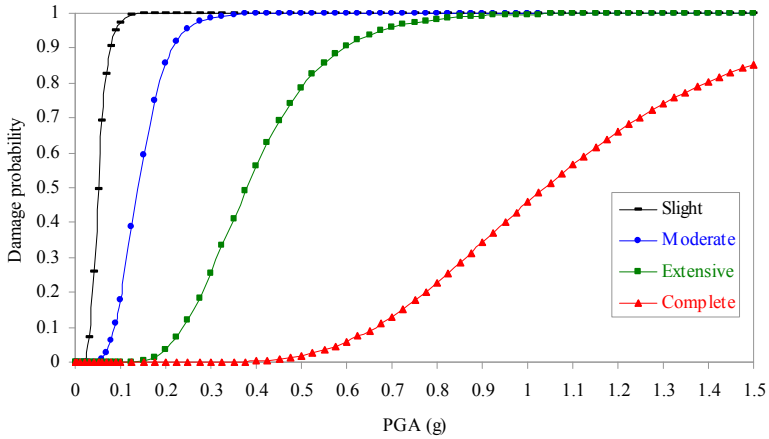

(b) GF-CSPSW

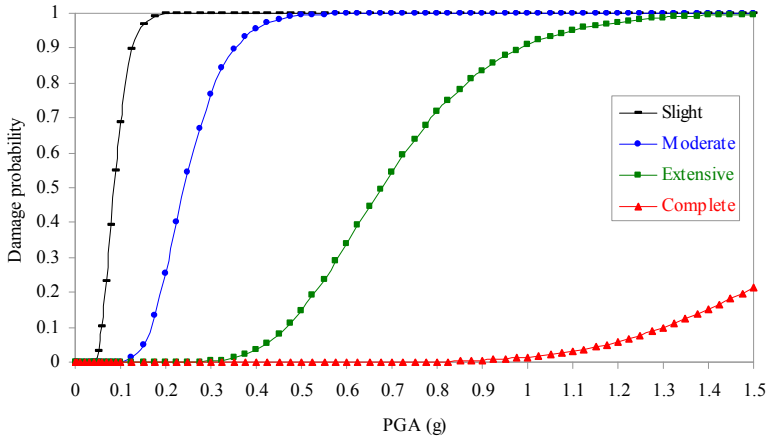

(c) GF-LYPSPSW2

Fig. 8.10 Fragility curves for predicting the probability of reaching or exceeding the nonstructural damage states for acceleration-sensitive components/contents of buildings

As it is seen in Fig. 8.8(a), structural fragility curves are developed for the Slight, Moderate, Extensive, and Complete damage states for the MRF model. In contrast, Figs. 8.8(b) and 8.8(c) plot the structural fragility curves generated for the four repair states, i.e. RS1, RS2, RS3, and RS5, for the two respective GF-CSPSW and GF-LYPSPSW2 models. The nonstructural drift and acceleration fragility curves developed for the Slight, Moderate, Extensive, and Complete damage states for the three considered structural models are also plotted in Figs. 8.9 and 8.10, respectively.

8.5 Discussion of Results

Quantitative assessment of risk to a structure from earthquakes is a multi-disciplinary and challenging problem which involves quantification of the shaking that a structure might experience at its base, quantification of the structural response and resulting damage, and also cost estimation to help determine the social and economic consequences of the damage. By considering the uncertainties present in many aspects of this problem, it is important for any assessment to be made in terms of probabilities (Baker and Cornell, 2006). In this chapter, the seismic response and retrofit of structures with conventional and LYP steel infill plates are investigated using the multi-stage process developed by the Pacific Earthquake Engineering Research (PEER) Center, as illustrated in Fig. 8.11.

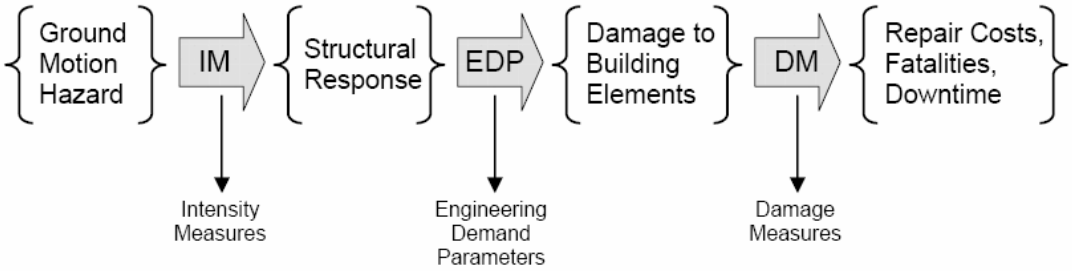

Fig. 8.11 Schematic illustration of the PEER-developed performance-based earthquake engineering methodology adopted in this study (Baker and Cornell, 2006)

It is believed that the adopted probabilistic methodology can provide a significant insight into the problem and result in a further efficient and robust assessment of seismic response and retrofit of structures using SPSW systems and LYP steel material.

After determination of the appropriate intermediate variables including the *IM*, *EDP*, and *DM* according to the process shown in Fig. 8.11, and then development of structural and nonstructural fragility curves by considering specific damage and repair states for the structural models, the seismic performance and effectiveness of retrofit of structures employing SPSW systems and LYP steel material are evaluated in this section. Assessments are made by comparing the median (50th percentile) PGA values of the fragility curves for all damage/repair states of the MRF, GF-CSPSW, and GF-LYPSPSW2 models. In fact, determination of the median values of probability of exceedance for the structural models and damage/repair states allows the comparison of vulnerability of the structural models, given that the variations are similar for different structural models.

The median values of PGA obtained from the structural fragility curves (Fig. 8.8) for the damage/repair states of the MRF and SPSW systems are shown in Fig. 8.12.

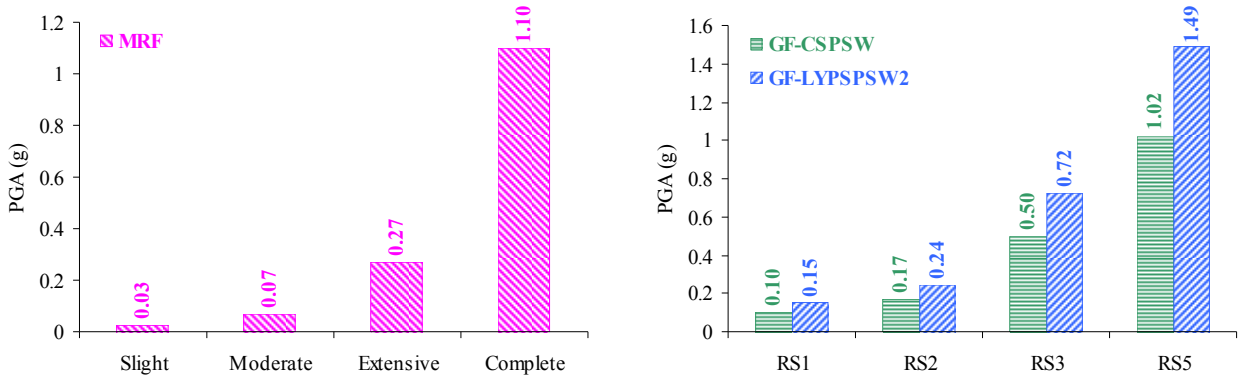

(a) MRF system, damage states

(b) SPSW systems, repair states

Fig. 8.12 Median values of PGA from the fragility curves for the damage/repair states of structural systems

Consideration of different criteria, i.e. damage and repair states, in developing the fragility curves for the MRF and the two SPSW systems does not allow to evaluate the seismic vulnerability of these lateral force-resisting systems in a comparative manner. Fig. 8.12(a) demonstrates that the median PGA values for the MRF model increase remarkably by moving from Slight to Complete damage states. Such a trend in general indicates that the structure will experience major damages at higher levels of earthquake ground shaking. Comparison of the median PGA values for the two SPSW systems shown in Fig. 8.12(b), on the other hand, demonstrates that the GF-CSPSW model is more vulnerable relative to the GF-LYPSPSW2 model, since the larger median values of PGA in case of the GF-LYPSPSW2 model are indicative of better seismic performance and reduction in system vulnerability.

The median PGA values from the nonstructural drift fragility curves (Fig. 8.9) for the Slight, Moderate, Extensive, and Complete damage states of the three structural models are shown in Fig. 8.13.

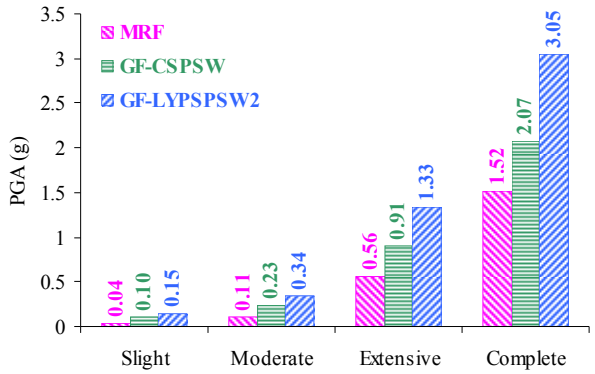

Fig. 8.13 Median values of PGA from the fragility curves for the damage states of nonstructural drift-sensitive components

As it is observed in Fig. 8.13, the MRF and GF-LYPSPSW2 models possess the smallest and the largest median PGA values, respectively, consistent with all four damage states. These

findings indicate that the MRF model is the most vulnerable and the GF-LYPSPSW2 model is the least vulnerable model among the three models. On this basis, it can be concluded that the GF-LYPSPSW2 model exhibits a better performance compared to the GF-CSPSW model, and the MRF model is expected to exhibit the weakest performance by experiencing damages at lower levels of ground shaking.

In addition, Fig. 8.14 shows the median values of PGA captured from the nonstructural acceleration fragility curves (Fig. 8.10) for the four damage states of the MRF, GF-CSPSW, and GF-LYPSPSW2 models.

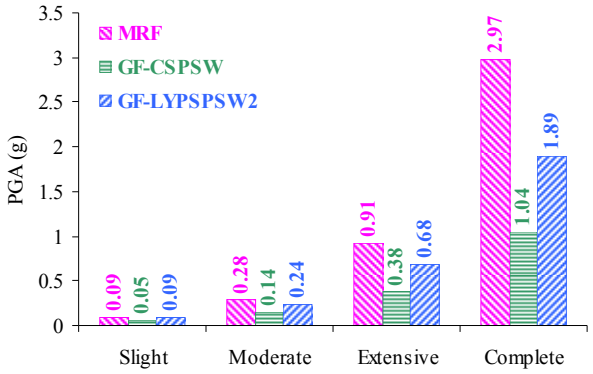

Fig. 8.14 Median values of PGA from the fragility curves for the damage states of nonstructural acceleration-sensitive components/contents

From the figure, it is found that the MRF model possesses the largest median values of PGA in cases of all damage states in comparison with the median values of the two GF-CSPSW and GF-LYPSPSW2 models. This does not necessarily indicate the better seismic performance of the MRF model, since from Fig. 8.2 it is quite evident that in spite of the favorable acceleration response, the MRF model shows the lowest drift performance due to its flexibility compared to the SPSW models. It is also found that retrofitting of the GF-CSPSW model with LYP steel infill plates of double thickness appears to be effective in terms of reducing the probability of damage

to the nonstructural acceleration-sensitive components and contents. The larger median PGA values of the GF-LYPSPSW2 model compared to those of the GF-CSPSW model in cases of all four damage states are indeed indicative of superior seismic performance of the GF-LYPSPSW2 model, since for a given damage state, the GF-LYPSPSW2 model is required to undergo higher levels of ground shaking in order to experience the same amount of damage as experienced by the GF-CSPSW model.

In summary, the results of the probabilistic methodology adopted in this study show that SPSW systems in general and LYP steel shear walls in particular are high-performing and efficient lateral force-resisting systems which can be effectively used in controlling the seismic response of structures. Application of LYP steel in lieu of the conventional structural steel is found to be quite effective in improving the buckling stability and seismic performance of SPSW systems, and consequently reducing the seismic vulnerability of buildings employing such lateral force-resisting and energy dissipating systems.

8.6 Concluding Remarks

The fragility function method was used in this chapter in order to evaluate the seismic performance and vulnerability of structures employing SPSW systems and LYP steel material. In spite of importance of fragility methodology in performance-based earthquake engineering, a search of the literature reveals that little steps have been taken towards application of this methodology in analysis, design, and retrofit of SPSW systems. On this basis, the main objective of this study was to take an effective step towards addressing this need by developing appropriate fragility functions and evaluating the seismic performance and vulnerability of code-designed and retrofitted SPSW systems through fragility analysis.

Nonlinear time-history analyses were performed in order to determine the peak interstory drift and peak floor acceleration responses of a moment-resisting and two code-designed and retrofitted SPSW frames, i.e. the MRF, GF-CSPSW, and GF-LYPSPSW2 models, subjected to a suite of thirty earthquake ground motions representing 50/50, 10/50, and 2/50 hazard levels. Evaluation of seismic performances of the structural models revealed that retrofitting of the code-designed and conventional steel SPSW frame with LYP steel infill plates of double thickness improves the drift and acceleration performances of the system through limiting the seismic responses in an effective manner.

Attempts were made in order to determine the most appropriate engineering demand parameter (EDP) and intensity measure (IM) pairs for optimal probabilistic seismic demand models (PSDMs) with lower degrees of scatter. Through consideration of a proper variability measure and regression analyses, the peak interstory drift ratio (PIDR) and peak floor acceleration (PFA) demand parameters were shown to have a good linear correlation with the PGA intensity measure. Accordingly, PFA-PGA and PIDR-PGA pairs were selected to generate fragility curves for the purpose of this study.

The probabilistic seismic demand analysis (PSDA) method was used in order to develop structural, nonstructural drift, and nonstructural acceleration fragility curves of the structural models by considering code-specified damage and some proposed repair states. The seismic performance and vulnerability of the structural models were then evaluated by comparing the median (50th percentile) values of PGA obtained from the fragility curves for all considered damage and repair states.

Based on the results of this study, SPSW systems in general appear to be more effective in controlling the seismic response and reducing the vulnerability of buildings compared to the

moment-resisting frames. It was shown that the retrofitted GF-LYPSPSW2 model with LYP steel infill plates of double thickness is less vulnerable compared to the original code-designed and conventional steel GF-CSPSW model. These findings indicate that retrofitting of SPSW systems with LYP steel infill plates of double thickness reduces the damage probability of SPSWs and results in a smaller damage potential and better seismic performance. Ultimately, it is quite important to note that such an improvement in structural behavior and seismic performance of SPSW systems is directly related to the application of LYP steel with superb material properties beneficial for seismic hazard mitigation of structures.

9. SUMMARY, CONCLUSIONS, AND FUTURE WORK

9.1 Summary

SPSWs are relatively new and efficient lateral force-resisting systems which have been designed and used with either stiffened and stocky or unstiffened and slender web plates based on disparate structural and economical considerations. Application of LYP steel material essentially developed for seismic control devices provides the possibility to design cost-effective and high-performing SPSW systems. Considering the novelty of SPSW systems and their recent introduction into the design codes, on one hand, and growth in development as well as use of LYP steel material, on the other hand, detailed and systematic investigations are required for confident and prevalent application of LYP steel material is seismic design and retrofit of SPSW systems. This research aims at taking effective steps towards addressing this need through comprehensive and systematic investigations on structural behavior and seismic performance of SPSWs employing LYP steel infill plates.

A general introduction and background of the SPSW systems along with the scope and objectives of this research were initially provided in Chapter 1. A summary of the past theoretical and experimental research works along with most recent developments on the analysis, design, and application of SPSW systems as well as LYP steel material were presented in Chapter 2. In Chapter 3, the fundamental mechanics, codified design provisions based on capacity-design requirements, and improvements made toward the performance-based seismic design of SPSW systems were discussed. The various advantages of application of LYP steel material in seismic design and retrofit of SPSW systems were shown through detailed and systematic analytical and numerical studies in the subsequent chapters.

The accurate determination of the limiting plate thickness corresponding to simultaneous buckling and yielding, which can serve as an effective parameter in seismic design of LYP steel shear wall systems was addressed through element-level investigations in Chapter 4. The structural characteristics of unstiffened LYP steel shear walls with slender, moderate, and stocky infill plates were then identified using nonlinear pushover and cyclic analyses through component-level investigations in Chapters 5 and 6, and a modified PFI method was proposed for predicting and characterizing the behavior of LYP steel shear walls with low yielding and high buckling capacities. In addition, the effectiveness of some AISC 341-10 (2010) code-specified design requirements and considerations was evaluated in Chapter 6, and proper recommendations were made for efficient analysis and design of LYP steel shear wall systems. The seismic performances of code-designed and retrofitted SPSW frames with conventional and LYP steel infill plates were evaluated using nonlinear dynamic analyses in Chapter 7, and the effectiveness of use of LYP steel material in improving the seismic response and performance of SPSW systems was demonstrated through system-level investigations. Finally, the effectiveness of design and retrofit of structures using SPSW systems and LYP steel material was verified in Chapter 8, through development of appropriate fragility functions and detailed probabilistic assessments. Overall, based on the findings of this comprehensive research work and results of the other published studies, it can be concluded that application of LYP steel with superb material properties suitable for seismic applications, can efficiently improve the structural behavior, seismic performance, and serviceability of SPSW systems in both new and retrofit construction.

9.2 Conclusions

The various advantages and characteristics of application of LYP steel material in seismic design and retrofit of SPSW systems were demonstrated and evaluated in this research through comprehensive element-, component-, and system-level investigations as well as probabilistic approaches. The major findings of this research work are provided in this section.

The following conclusions are drawn from the element-level investigations:

- Application of LYP steel with relatively low yield stress compared to the conventional steel can considerably reduce the required limiting plate thickness corresponding to concurrent geometrical-material bifurcation. Smaller limiting infill plate thickness can result in early yielding, absorption of more input energy, and consequently improved seismic performance of the system. Hence, accurate determination of the limiting plate thickness is important in seismic design of LYP steel shear wall systems.

- In practice, consideration of clamped support condition can provide reliable estimates for the limiting plate thickness in SPSWs, given that the boundary frame members are properly designed.

- Larger plate length-to-height ratios can unfavorably result in larger limiting plate thicknesses. Accordingly, as a design consideration, selection of optimal plate length-to-height ratios can result in desirable seismic performance of the SPSW systems.

- According to element-level investigations, beam-attached infill plates in SPSW systems can exhibit relatively weak cyclic performance as a result of excessive out-of-plane deformations due to the presence of two unrestrained edges, if not stiffened properly.

The following conclusions are drawn from the component-level investigations:

- Application of LYP steel infill plates in SPSWs can facilitate the design of such systems by setting a desirable plate-frame yielding sequence. This can also result in reduced forces imposed on the boundary frame members as compared to the conventional steel infill plates.

- Based on a detailed case study, application of LYP steel material offers the possibility of retrofit of existing conventional steel SPSWs with LYP steel infill plates of double thickness in a desirable and efficient manner. In fact, such a retrofit strategy can improve the initial stiffness and buckling as well as energy dissipation capacities of the SPSW system and also alleviate the high stiffness and over-strength concerns.

- Properly-designed SPSWs with unstiffened LYP steel infill plates can possess desirable stiffening and damping performances, i.e. improved initial stiffness, strength, and energy absorption capacity, which is indicative of superior lateral force-resisting and energy dissipating capabilities of such structural systems.

- Increasing of the panel aspect ratio can favorably increase the initial stiffness, strength, and energy absorption capacity of SPSWs. However, as the aspect ratio increases and especially gets larger than unity, relatively heavier HBE and VBE sections may be needed to meet the design requirements due to relatively larger thicknesses of LYP steel infill plates, which in turn may impose additional construction costs. Thus, selection of an optimal panel aspect ratio in design process can be quite effective in adjusting the construction costs and designing high-performing LYP steel shear wall systems.

- Evaluation of performances of RBS connections and panel zones as well as effectiveness of lateral bracing of frame members in the code-designed SPSW models revealed that behaviors of the frame components in LYP steel shear walls is somewhat influenced by the panel aspect ratio parameter, which necessitates the re-assessment of some respective design requirements.

- The modified PFI model, proposed in this research, can be effectively used for predicting and characterizing the behavior of LYP steel shear walls with moderate and stocky infill plates of different aspect ratios. In addition, this analytical model can serve as effective and simple design tool in structural design of LYP steel shear walls with relatively low yielding and high buckling capacities.

The following conclusions are drawn from the system-level investigations:

- The ASCE 7-10 (2010) code-specified formula underestimates the fundamental periods of SPSW frames. Consideration of more efficient approaches and/or proper modification of this formula is believed to result in further optimal designs.

- The "interstory" drift ratio is found to be more controlling than the "story" drift ratio in seismic design of structures, and SPSW frames have been demonstrated to be quite efficacious in limiting the drift demands.

- Retrofitting of the code-designed and conventional steel SPSW frame with LYP steel infill plates of relatively larger thicknesses is shown to be quite effective in improving the drift and acceleration responses of the structure. The LYP steel shear wall frames, also,

exhibit better performance in reducing the base shear, base moment, and VBE axial load demands compared to the conventional steel SPSW frame. Nonetheless, employment of overly thick LYP steel plates in retrofit of the code-designed SPSW frame with conventional steel infill plates is found to be disadvantageous which may result in undesirable performance of the structure.

- According to the findings of the system-level investigations, employment of LYP steel infill plates of double thickness is considered to be the most desirable and optimal option for retrofitting of the code-designed and conventional steel SPSW frame, which also results in enhanced ductility and energy dissipation capability of the system. This finding is consistent with the results of the case study on the retrofit of the SPSW systems performed through component-level investigations.

The following conclusions are drawn from the fragility analyses of the structural systems:

- A search of the most appropriate EDP-IM pairs for optimal PSDMs with lower variation degrees showed that PIDR (peak interstory drift ratio) and PFA (peak floor acceleration) parameters had a good linear correlation with the PGA (peak ground acceleration) intensity measure, and hence PIDR-PGA and PFA-PGA pairs were chosen for generating fragility functions in this research.

- Comparison of the median PGA values of the fragility curves, obtained for different structural models as well as damage/repair states, in this research, demonstrates the relative superiority of SPSW systems in controlling the seismic response and reducing the vulnerability of buildings.

- Fragility analyses also show that the retrofitted SPSW frame with LYP steel infill plates of double thickness is less vulnerable compared to the original code-designed and conventional steel SPSW frame. Accordingly, such a retrofit strategy lowers the damage potential and results in better seismic performance of the structure.

9.3 Recommendations for Future Work

Through the findings of this research program, a number of high-impact areas related to the design and application of SPSW systems in general and LYP steel shear walls in particular have been identified which need further attention and investigation in future studies. The research needs presented below are believed to make this promising lateral force-resisting system easier to design, more economical, and structurally more efficient. Recommendations for future research directions are as follows:

- From various strategies proposed to reduce column demands in SPSWs, application of LYP steel shear walls with RBS connections and beam-attached infill plates seems to have promising potential towards lowering the overall system demand on the vertical and horizontal boundary members. However, detailed investigations are required for development of cost-effective and structurally sound systems by effective limiting of the infill plate out-of-plane deformations through strategic placement of optimal stiffeners.

- Experimental investigations are required to further substantiate the findings of this research on analytical determination of the limiting web-plate thickness in SPSWs with LYP steel infill plates and also to identify and establish the structural characteristics of SPSWs with slender, moderate, and stocky LYP steel infill plates.

- Further experimental research is also required in order to verify the effectiveness of the proposed PFI model in predicting the behaviors of SPSWs with moderate and stocky infill plates. In particular, study on quantification of the shear and bending deformation contributions to the overall response of the SPSW system and its incorporation into the modified PFI model can improve the accuracy of this analytical model.

- Panel aspect ratio parameter has been shown to be effective on the limiting plate thickness magnitude as well as structural and seismic behaviors of unstiffened LYP steel shear wall systems. Further investigations on the effectiveness of this design parameter on structural and economical considerations, and development of practical design recommendations can result in design of high-performing and cost-effective structures.

- Based on the findings of this research, the effectiveness of the AISC 341-10 (2010) code-specified requirements on the stiffness and lateral bracing of frame members needs to be examined through further experimental and numerical investigations.

- In this research, the dynamic behaviors of 9-story and 5-bay structures subjected to a number of earthquake ground motions were studied though system-level investigations. For a further comprehensive seismic response and performance evaluation, it is suggested to consider multi-story structures with various numbers of stories and bays as well as span length-to-story height aspect ratios subjected to a large number of ground motions representing a wide range of hazard levels. This will develop a vast knowledge on the design, retrofit, and application of SPSW systems employed in low-, mid-, and high-rise buildings.

- This research, along with a few reported studies in the literature, has taken the initial steps towards the performance-based seismic design of SPSW systems. However, much research work is still required in this regard. Effective application of the fragility methodology relies on development and analysis of more experimental data, generation and codification of SPSW-specific damage and/or repair states, and studies on the selection of more efficient EDP and IM parameters in order for developing appropriate fragility functions for probabilistic seismic response and vulnerability assessment of SPSW systems in an efficient manner. Moreover, effective combination of different types of fragility curves for developing the overall fragility of the structure is an important subject which needs to be considered in the future work.

References

AISC 341-05 (2005). Seismic Provisions for Structural Steel Buildings. American Institute of Steel Construction, Chicago, IL.

AISC 341-10 (2010). Seismic Provisions for Structural Steel Buildings. American Institute of Steel Construction, Chicago, IL.

AISC 360-10 (2010). Specification for Structural Steel Buildings. American Institute of Steel Construction, Chicago, IL.

Akkar S., Sucuoğlu H. and Yakut A. (2005). "Displacement-based fragility functions for low- and mid-rise ordinary concrete buildings", *Earthquake Spectra*, 21(4), 901-927.

Alinia M.M. and Dastfan M. (2006). "Behaviour of thin steel plate shear walls regarding frame members", *Journal of Constructional Steel Research*, 62(7), 730-738.

Alinia M.M., Gheitasi A. and Erfani S. (2009). "Plastic shear buckling of unstiffened stocky plates", *Journal of Constructional Steel Research*, 65(8-9) 1631-1643.

Alinia M.M. and Sarraf Shirazi R. (2009). "On the design of stiffeners in steel plate shear walls", *Journal of Constructional Steel Research*, 65, 2069-2077.

ANSYS 11.0 (2007). ANSYS 11.0 documentation, ANSYS Inc.

ANSYS 14.0 (2011). ANSYS 14.0 documentation, ANSYS Inc.

ASCE 7-10 (2010). Minimum Design Loads for Buildings and Other Structures. American Society of Civil Engineers, Reston, VA.

Astaneh-Asl A. (2000). Seismic Behavior and Design of Steel Shear Walls. *Steel TIPS Report*, Structural Steel Educational Council, Moraga, CA.

Astaneh-Asl A. (2002). Seismic Behavior and Design of Composite Steel Plate Shear Walls. *Steel TIPS Report*, Structural Steel Educational Council, Moraga, CA.

Baker J.W. and Cornell C.A. (2006). Vector-Valued Ground Motion Intensity Measures for Probabilistic Seismic Demand Analysis. *PEER Report 2006/08*, Pacific Earthquake Engineering Research Center, College of Engineering, University of California, Berkeley.

Baldvins N.M., Berman J.W., Lowes L.N., Janes T.M. and Low N.A. (2012). "Fragility functions for steel plate shear walls", *Earthquake Spectra*, 28(2), 405-426.

Basler K. (1961). "Strength of plate girders in shear", *Journal of the Structural Division*, ASCE,

87(7), 150-180.

Bayat M.R. (2010). Performance-Based Plastic Design of Earthquake Resistant Steel Structures: Concentrically Braced frames, Tall Moment Frames, Plate Shear Wall Frames. *Ph.D. Dissertation*, The Faculty of Graduate School, The University of Texas at Arlington.

Behbahanifard M.R., Grondin G.Y. and Elwi A.E. (2003). Experimental and Numerical Investigation of Steel Plate Shear Wall. *Structural Engineering Report 254*, Department of Civil and Environmental Engineering, University of Alberta, Canada.

Berman J.W. (2011). "Seismic behavior of code designed steel plate shear walls", *Engineering Structures*, 33(1), 230-244.

Berman J.W. and Bruneau M. (2003). Experimental Investigation of Light-Gauge Steel Plate Shear Walls for the Seismic Retrofit of Buildings. *Technical Report MCEER-03-0001*, Multidisciplinary Center for Earthquake Engineering Research, Buffalo, NY.

Berman J.W. and Bruneau M. (2004). "Steel plate shear walls are not plate girders", *Engineering Journal*, AISC, 41(3), 95-106.

Berman J.W. and Bruneau M. (2005). "Experimental investigation of light-gauge steel plate shear walls", *Journal of Structural Engineering*, ASCE, 131(2), 259-267.

Berman J.W., Lowes L.N., Baldvins N.M., Low N.A. and Janes T.N. (2010). "Performance based design tools for steel plate shear walls", *Structures Congress*, ASCE, 3443-3454.

Berman J.W., Lowes L.N., Okazaki T., Bruneau M., Tsai K.C., Driver R.G. and Sabelli R. (2008). "Research needs and future directions for steel plate shear walls", *Structures Congress*, Vancouver, Canada.

Bhowmick A.K. (2009a). Seismic Analysis and Design of Steel Plate Shear Walls. *Ph.D. Dissertation*, Department of Civil and Environmental Engineering, University of Alberta.

Bhowmick A.K., Driver R.G. and Grondin G.Y. (2009b). "Seismic analysis of steel plate shear walls considering strain rate and *P*-delta effects", *Journal of Constructional Steel Research*, 65(5), 1149-1159.

Bhowmick A.K., Grondin G.Y. and Driver R.G. (2011). "Estimating fundamental periods of steel plate shear walls", *Engineering Structures*, 33(6), 1883-1893.

Bruneau M. and Bhagwagar T. (2002). "Seismic retrofit of flexible steel frames using thin infill panels", *Engineering Structures*, 24, 443-453.

Brush D.O. and Almroth B.O. (1975). Buckling of Bars, Plates and Shells. McGraw-Hill, New York.

Caccese V., Elgaaly M. and Chen R. (1993). "Experimental study of thin steel-plate shear walls under cyclic load", *Journal of Structural Engineering*, ASCE, 119(2), 573-587.

CAN/CSA S16-01 (2001). Limit States Design of Steel Structures. Canadian Standards Association, Toronto, Ontario, Canada.

Çelebi M. (1997). "Response of Olive View Hospital to Northridge and Whittier earthquakes", *Journal of Structural Engineering*, ASCE, 123(4), 389-396.

Chen S.J. and Jhang C. (2006). "Cyclic behavior of low yield point steel shear walls", *Thin-Walled Structures*, 44(7), 730-738.

Chen S.J. and Jhang C. (2011). "Experimental study of low-yield-point steel plate shear wall under in-plane load", *Journal of Constructional Steel Research*, 67(6), 977-985.

Chen W.F. and Lui E.M. (2006). Earthquake Engineering for Structural Design. CRC Press, Taylor & Francis Group, LLC.

Chen W.F., Yoshiaki G. and Liew J.Y.R. (1996). Stability Design of Semi-Rigid Frames. Vol. 1, John Wiley & Sons, Inc.

Chen Y.Z., Lee Y.Y., Li Q.S. and Guo Y.J. (2009). "Concise formula for the critical buckling stresses of an elastic plate under biaxial compression and shear", *Journal of Constructional Steel Research*, 65(7), 1507-1510.

Dastfan M. and Driver R.G. (2008). "Flexural stiffness limits for frame members of steel plate shear wall systems", *Proceedings of Annual Stability Conference*, Nashville, Structural Stability Research Council, Rolla, MO.

De Matteis G., Landolfo R. and Mazzolani F.M. (2003). "Seismic response of MR steel frames with low-yield steel shear panels", *Engineering Structures*, 25(2), 155-168.

Driver R.G., Kulak G.L., Kennedy D.J. L. and Elwi A.E. (1997). Seismic Behaviour of Steel Plate Shear Walls. *Structural Engineering Report No. 215*, Department of Civil and Environmental Engineering, University of Alberta, Edmonton, Alberta, Canada.

Dung P.N. (2011). Seismically Retrofitting Reinforced Concrete Moment Resisting Frames by Using Expanded Metal Panels. *Ph.D. Dissertation*, Structural Engineering Sector, Department of Architecture, Geology, Environment and Constructions, Faculty of Applied Sciences, University of Liege.

Eatherton M. (2006). "Design and construction of steel plate shear walls", *Proceedings of the 8th U.S. National Conference on Earthquake Engineering*, Paper No. 588, San Francisco, California, U.S.A.

Elgaaly M., Caccese V. and Du C. (1993). "Post-buckling behavior of steel-plate shear walls

under cyclic loads", *Journal of Structural Engineering*, ASCE, 119(2), 588-605.

FEMA 355C (2000). State of the Art Report on Systems Performance of Steel Moment Frames Subject to Earthquake Ground Shaking. Prepared by the SAC Joint Venture for the Federal Emergency Management Agency, Washington, D.C.

FEMA 445 (2006). Next-Generation Performance-Based Seismic Design Guidelines: Program Plan For New And Existing Buildings. Prepared by the Applied Technology Council for the Federal Emergency Management Agency, Washington, D.C.

FEMA 450 (2004). NEHRP Recommended Provisions for Seismic Regulations for New Buildings and Other Structures. Prepared by the Building Seismic Safety Council for the Federal Emergency Management Agency, Washington, D.C.

Gheitasi A. and Alinia M.M. (2010). "Slenderness classification of unstiffened metal plates under shear loading", *Thin-Walled Structures*, 48(7), 508-518.

Ghosh S., Adam F. and Das A. (2009). "Design of steel plate shear walls considering inelastic drift demand", *Journal of Constructional Steel Research*, 65, 1431-1437.

Ghosh S. and Kharmale S.B. (2010). Research on Steel Plate Shear Wall: Past, Present and Future. Structural Steel and Castings, Chapter 2, Nova Science Publishers, Inc., 57-106.

Gould N.C. (2003). Performance Based Seismic Design. International Risk Management Institute Online Articles, October.(http://www.irmi.com/expert/articles/2003/gould10.aspx)

Gupta A. and Krawinkler H. (1999). Seismic Demands for Performance Evaluation of Steel Moment Resisting Frame Structures. *Report No. 132*, The John A. Blume Earthquake Engineering Center, Department of Civil and Environmental Engineering, Stanford University.

Habashi H.R. and Alinia M.M. (2010). "Characteristics of the wall-frame interaction in steel plate shear walls", *Journal of Constructional Steel Research*, 66(2), 150-158.

HAZUS-MH MR5 (2010). Earthquake Loss Estimation Methodology. Technical and User's Manual, Department of Homeland Security, Federal Emergency Management Agency, Mitigation Division, Washington, D.C.

Hitaka T. and Matsui C. (2003). "Experimental study on steel shear wall with slits", *Journal of Structural Engineering*, ASCE, 129(5), 586-595.

Jahanpour A., Jönsson J. and Moharrami H. (2012). "Seismic behavior of semi-supported steel shear walls", *Journal of Constructional Steel Research*, 74, July, 118-133.

Janković S. and Stojadinović B. (2004). "Probabilistic performance-based seismic demand model for R/C frame buildings", *Proceedings of the 13th World Conference on Earthquake*

Engineering, Paper No. 1547, Vancouver, B.C., Canada.

Kharrazi M.H.K. (2005). Rational Method for Analysis and Design of Steel Plate Walls. *Ph.D. Dissertation*, The Faculty of Graduate Studies (Civil Engineering), The University of British Columbia, Canada.

Kulak G.L., Kennedy D.J.L., Driver R.G. and Medhekar M. (2001). "Steel plate shear walls - An overview", *Engineering Journal*, AISC, First Quarter, 50-62.

Kurata M., Leon R.T., DesRoches R. and Nakashima M. (2012). "Steel plate shear wall with tension-bracing for seismic rehabilitation of steel frames", *Journal of Constructional Steel Research*, 71, April, 92-103.

Kurban C.O. (2009a). A numerical study on response factors for steel plate shear wall systems. *M.Sc. Thesis*, The Graduate School of Natural and Applied Sciences, Middle East Technical University.

Kurban C.O. and Topkaya C. (2009b). "A numerical study on response modification, overstrength, and displacement amplification factors for steel plate shear wall systems", *Earthquake Engineering and Structural Dynamics*, 38, 497-516.

Lashgari M. (2009). "Finite element analysis of thin steel plate shear walls", *World Academy of Science*, *Engineering and Technology*, 58, 436-440.

Lowes L.N. and Li J. (2009). "Fragility curves for reinforced concrete moment frames", *Proceedings of the 2009 ATC & SEI Conference on Improving the Seismic Performance of Existing Buildings and Other Structures*, San Francisco, California, 403-414.

Lubell A.S. (1997). Performance of Unstiffened Steel Plate Shear Walls Under Cyclic Quasi-Static Loading. *M.A.Sc. Thesis*, Department of Civil Engineering, University of British Columbia, Canada.

Lubell A.S., Prion H.G.L., Ventura C.E. and Rezai M. (2000). "Unstiffened steel plate shear wall performance under cyclic loading", *Journal of Structural Engineering*, ASCE, 126(4), 453-460.

Mackie K. and Stojadinović B. (2001). "Probabilistic seismic demand model for California highway bridges", *Journal of Bridge Engineering*, ASCE, 6(6), 468-481.

Mahtab M. and Zahedi M. (2008). "Seismic retrofit of steel frames using steel plate shear walls", *Asian Journal of Applied Sciences*, 1(4), 316-326.

Massey C. (1963). "Elastic and inelastic lateral instability of I-beams", *The Engineer*, 216, 672-674.

Mimura H. and Akiyama H. (1977). "Load-deflection relationship of earthquake-resistant steel

shear walls with a developed diagonal tension field", *Transactions of the Architectural Institute of Japan*, 260, 109-114.

Mistakidis E. (2010). "Numerical study of low-yield point steel shear walls used for seismic applications", *Engineering Computations: International Journal for Computer-Aided Engineering and Software*, 27(2), 257-279.

Mistakidis E.S., De Matteis G. and Formisano A. (2007). "Low yield metal shear panels as an alternative for the seismic upgrading of concrete structures", *Advances in Engineering Software*, 38(8-9), 626-636.

Mo Y.L. and Perng S.F. (2000). "Seismic performance of framed shear walls made of corrugated steel", *Proceedings of the 6th ASCCS International Conference on Steel Concrete Composite Structures*, Los Angeles, CA, 1057-1064.

Moslehi Tabar A. and Deylami A. (2005). "Instability of beams with reduced beam section moment connections emphasizing the effect of column panel zone ductility", *Journal of Constructional Steel Research*, 61(11), 1475-1491.

Nakagawa S., Kihara H., Torii S., Nakata Y., Iwata M., Fujisawa K. and Fukuda K. (1996). "Hysteretic behavior of low yield strength steel panel shear wall - experimental investigation", *Proceedings of the 11th World Conference on Earthquake Engineering*, Paper No. 171.

Nakashima M. (1995a). "Strain-hardening behavior of shear panels made of low-yield steel. I: Test", *Journal of Structural Engineering*, ASCE, 121(12), 1742-1749.

Nakashima M., Akazawa T. and Tsuji B. (1995b). "Strain-hardening behavior of shear panels made of low-yield steel. II: Model", *Journal of Structural Engineering*, ASCE, 121(12), 1750-1757.

Park H.G., Kwack J.H., Jeon S.W., Kim W.K. and Choi I.R. (2007). "Framed steel plate wall behavior under cyclic lateral loading", *Journal of Structural Engineering*, ASCE, 133(3), 378-388.

Pirmoz A. (2010). "Beam-attached steel plate shear walls", *The Structural Design of Tall and Special Buildings*. doi: 10.1002/tal.651.

Rezai M. (1999). Seismic Behaviour of Steel Plate Shear Walls by Shake Table Testing. *Ph.D. Dissertation*, Department of Civil Engineering, The University of British Columbia, Vancouver, Canada.

Roberts T.M. and Sabouri-Ghomi S. (1992). "Hysteretic characteristics of unstiffened perforated steel plate shear walls", *Thin-Walled Structures*, 14(2), 139-151.

Sabelli R. and Bruneau M. (2006). Steel Plate Shear Walls. Steel Design Guide 20, American

Institute of Steel Construction, Chicago, IL.

Sabelli R., Bruneau M. and Driver R.G. (2008). "Steel plate shear walls in the upcoming 2010 AISC seismic provisions and 2009 Canadian Standard S16", *Structures Congress*, Vancouver, Canada.

Sabouri-Ghomi S. and Roberts T.M. (1992). "Nonlinear dynamic analysis of steel plate shear walls including shear and bending deformations", *Engineering Structures*, 14(5), 309-317.

Sabouri-Ghomi S., Ventura C.E. and Kharrazi M.H.K. (2005). "Shear analysis and design of ductile steel plate walls", *Journal of Structural Engineering*, ASCE, 131(6), 878-889.

Saeki E., Sugisawa M., Yamaguchi T. and Wada A. (1998). "Mechanical properties of low-yield point steels", *Journal of Materials in Civil Engineering*, ASCE, 10(3), 143-152.

Seilie I.F. and Hooper J.D. (2005). "Steel plate shear walls: Practical design and construction", *North American Steel Construction Conference*, Modern Steel Construction, April.

Shishkin J.J., Driver R.G. and Grondin G.Y. (2005). Analysis of Steel Plate Shear Walls Using the Modified Strip Model. *Structural Engineering Report No. 261*, Department of Civil and Environmental Engineering, University of Alberta, Edmonton, Alberta, Canada.

Shishkin J.J., Driver R.G. and Grondin G.Y. (2009). "Analysis of steel plate shear walls using the modified strip model", *Journal of Structural Engineering*, ASCE, 135(11), 1357-1366.

Southwell R.V. (1932). "On the analysis of experimental observations in problems of elastic stability", *Proceedings of the Royal Society of London*, Series A, 135(828), 601-616.

Takahashi Y., Takemoto Y., Takeda T. and Takagi M. (1973). "Experimental study on thin steel shear walls and particular bracings under alternative horizontal load", *Preliminary Report*, *IABSE Symposium on Resistance and Ultimate Deformability of Structures Acted on by Well-Defined Repeated Loads*, Lisbon, Portugal, 185-191.

Thorburn L.J., Kulak G.L. and Montgomery C.J. (1983). Analysis of Steel Plate Shear Walls. *Structural Engineering Report No. 107*, Department of Civil Engineering, University of Alberta, Edmonton, Alberta, Canada.

Timler P.A. and Kulak G.L. (1983). Experimental Study of Steel Plate Shear Walls. *Structural Engineering Report No. 114*, Department of Civil Engineering, University of Alberta, Edmonton, Alberta, Canada.

Timoshenko S.P. and Gere J.M. (1961). Theory of Elastic Stability. McGraw-Hill, New York.

Topkaya C. and Atasoy M. (2009). "Lateral stiffness of steel plate shear wall systems", *Thin-Walled Structures*, 47(8-9), 827-835.

Topkaya C. and Kurban C.O. (2009). "Natural periods of steel plate shear wall systems", *Journal of Constructional Steel Research*, 65(3), 542-551.

Torii S., Teramoto T., Kihara H. and Kitamura H. (1996). "The response control design of high-rise building with low yield steel wall", *Proceedings of the 11th World Conference on Earthquake Engineering*, Paper No. 97.

Trahair N.S. (1969). "Deformations of geometrically imperfect beams", *Journal of the Structural Division*, ASCE, 95(7), 1475-1496.

Tsai K.C. and Lin Y.C. (2005). "Seismic performance of steel plate shear wall frames", *Proceedings of the 4th International Conference on Advances in Steel Structures*, 13-15 June, Shanghai, China.

Vian D. and Bruneau M. (2004). "Testing of special LYS steel plate shear walls", *Proceedings of the 13th World Conference on Earthquake Engineering*, August 1-6, Vancouver, B.C., Canada.

Vian D., Bruneau M. and Purba R. (2009a). "Special perforated steel plate shear walls with reduced beam section anchor beams. II: Analysis and design recommendations", *Journal of Structural Engineering*, ASCE, 135(3), 221-228.

Vian D., Bruneau M., Tsai K.C. and Lin Y.C. (2009b). "Special perforated steel plate shear walls with reduced beam section anchor beams. I: Experimental investigation", *Journal of Structural Engineering*, ASCE, 135(3), 211-220.

Wagner H. (1931). Flat Sheet Metal Girders with Very Thin Webs, Part I - General Theories and Assumptions. *Technical Memorandum No. 604*, National Advisory Committee for Aeronautics, Washington, DC.

Xue M. and Lu L.W. (1994). "Interaction of infilled steel shear wall panels with surrounding frame members", *Proceedings of the Structural Stability Research Council Annual Technical Session*, Bethlehem, PA, 339-354.

Yakut A. and Yilmaz H. (2008). "Correlation of deformation demands with ground motion intensity", *Journal of Structural Engineering*, ASCE, 134(12), 1818-1828.

Yamaguchi T., Nakata Y., Takeuchi T., Ikebe T., Nagao T., Minami A. and Suzuki T. (1998). Seismic Control Devices Using Low-Yield-Point Steel. *Nippon Steel Technical Report No. 77, 78* July, 65-72.

Zhang J. and Huo Y. (2009). "Evaluating effectiveness and optimum design of isolation devices for highway bridges using the fragility function method", *Engineering Structures*, 31(8), 1648-1660.

Zhao Q. and Astaneh-Asl A. (2004). "Cyclic behavior of traditional and innovative composite

shear walls", *Journal of Structural Engineering*, ASCE, 130(2), 271-284.

Zirakian T. (2008). "Lateral-distortional buckling of I-beams and the extrapolation techniques", *Journal of Constructional Steel Research*, 64(1), 1-11.

Zirakian T. (2010). "On the application of the extrapolation techniques in elastic buckling", *Journal of Constructional Steel Research*, 66(3), 335-341.

Zoruba S. and Liddy W. (2007). "Steelwise: Structural steel materials update", *Modern Steel Construction Magazine*, AISC, March issue.